Crashworthiness Characterisation of the Car Front Bumper System Based on FEA Analysis

Xiyuan Zhang

Doctor of Philosophy 2019

Supervisors:
Dr Yiling Lu
Dr Dani Harmanto

Table of Contents

List of Figures

List of Tables

List of Abbreviations

CAD	Computer-Aided Design.
CAE	Computer-aided engineering
Cm	Centimetres
CFE	Crush force efficiency
CFL	Courant-Frederick-Levy
DM	Deutsche Mark
Euro-NCAP	European-New Car assessment programme
ESV	Experiment of safer vehicle
E.C.E	United Nations Economic Commission for Europe
FAA	Federal aviation administration
FEA	Element Analysis
Ft	Feet
Ft/s	Feet per second
FEA	Element Analysis
GMT	Glass mated thermoplastic
GHG	Greenhouse gases
IIHS	Insurance Institute of Highway safety
Indy 500	Indianapolis 500 race
IPF	Initial peak force
Km	Kilometres
Km/h	Kilometres per hour
MPH	Miles per hour
MSTRP	Motorsports safety technology research program
mm	Millimetre
MIL-STD-1290	Military-Standard-XXXX
M/s	Meters per second
NEDC	New European Driving Cycle
NHTSA	National highway transportation safety administration
SLR	Sport leicht rennsport
SMC	Sheet moulding compound
SEA	Specific energy absorption

UHSS	Ultra high strength steel
WHO	World health organisation

List of symbols

X_i	Nodal Displacement
f_i	Force applied to the nodes
b_i	body acceleration
ε_j	Strain
ε_i	Stress
τ_{ij}	Shear stress
C_{ij}	Stiffness matrix
h	Thickness of the macroscale specimen
σ_{ij}	Stress tensor
E	Young's modulus of elasticity
Δt	Time step
h	Smallest element size,
c	Element wave speed
f	Safety factor
ρ	Material density
p	Pressure
M	Material mass
V	Element volume
C_{ii}	Material stiffness
σ_y	Yield stress
v	Poisson ratio
E_a	Energy absorption
E_s	Energy absorption to its unit mass
t	Thickness of the tube wall

h Height of the tubes

θ Taper angle

F_{mean} Average force

F_{peak} Peak of the force

Author's declaration

At no time during the registration for the degree of Doctor of Philosophy has the author been registered for any other University Award.
Work submitted for this research degree at the University of Derby is the authors' work and has not formed part of any other University degrees.
None conflict of interest declared.

Author's signature

……

Acknowledgement

In the past four years of my search period, I have enjoyed interacting with many people within the engineering department, as well as IT and PGR office. The Derby university provided appropriate research facilities for me to conduct my research, laboratory experiment, library sources and contact from other experienced personnel to the name of few.

Particularly, I would like to express my gratitude to both my first supervisor Dr Yiling LU and Dr Dani Harmanto. Dr Lu invested the vast majority of his time and effort into the project the ensure it follows the correct path. Dr Lu inspired and encouraged me to solve problems rather than been gave direct answers. He also offered many background knowledges that enabled me to achieve a deeper understanding of the project.

I would like to thank the help from another related personal from the same department, Dr. Mazena Pawlik offered her insight on the material used. IT department supported the installation and operation of both hardware and software.

I would also like to express my appreciation and respect to the wife Mrs Ran Li. It is hard enough and very struggled to go through a PhD research process without any distraction, but not as hard as raising a child along the way. This thesis will not progress as much as expected without her involving many hours with our son. Salute to those tired hours during the day, and sleepless hours during the night.

Abstract

This thesis investigated different designs and material selections of vehicle front bumper system to improve the vehicle crashworthiness during the low impact speed (impact velocity=15km/h, 9.32mph) via FEA simulations. The primary purpose is to identify the most important parameters directly related to the improvement of crashworthiness using numerical parametric study. It is found the cross-section profile, curvature shape, material of the bumper beam, together with the connection to the crash box have been all identified that directly influence the crashworthiness performance of the front bumper system.

The bumper system, including the sub-components such as bumper beam, crash box, and the connection methods were carried all the parameters, including a number of folds, curvature shapes and spot welds were in-built while creating them into the CAD models using Solidworks. The final assembled complete bumper system is then imported into the ANSYS for further geometry checks and adjustment. Solver Autodyn is used to perform the FEA simulation, and numbers of results files were generated. Results files such as force reaction, plastic work, and equivalent stress, normal stress was all exported it into the Excel for parametric analysis and discussions.

Cross-section Profile-Out of proposed Single fold (fold 1) and Triple fold(fold 3) bumper beam profiles, Double fold (fold 2) bumper beam profile presented the best results of force reaction on both smoothness and force value, while the plastic work remained almost identical to profile fold 1 and 3 gained. Fold 2 profile is considered as a good performer since this profile regulated the deformation behaviour of the beam resulted in a smooth increasing force reaction curve. Where the force reaction curve on both fold 1 and fold 3 were fluctuated dramatically due to catastrophic structural failure.

Material-In between structural steel and aluminium alloy used in the bumper beam, while the structural steel made bumper beam achieved good force reaction and plastic work. Switched to aluminium can achieve similar force reaction trend and rate with Cross-section neglectable amount of plastic work reduced. Particularly the weight of the bumper beam is dropped down to 5.357 kg while maintaining similar crashworthiness performance to the structural steel.

Crash box connection- The bonded connection is considered as an ideal scenario and was

favoured in much other literature due to it simplifies the connection setting in the FEA environment since it automatically considers it as perfect contact. Three alternative connection methods were therefore proposed to simulate the more realistic scenario. It defined as welding connection that is constituted by a number of spot welds at left, right, top and bottom of the crash box. Since the bonded method contains no spot welds, a method of weld L+R was indicated by totally 4 spot welds appeared at both left and right side of the crash box. On top of this, 4 additional spot welds were added to the top and bottom of the crash box. Totally 4 spot welds were added only to both the top and bottom of the crash box to extend the comparison. While both bonded and weld L+R methods suffered from buckling effect to the crash box, particularly concentrated at the left and right side with high equivalent and normal stresses.

It is discovered weld full method provided promising results by reducing the buckling effect to both left and right faces of the crash box, and also managed to lower the equivalent stress down to 336.48MPa and normal stress on the connection surface down to 66MPa. Weld T+B also observed similar performance when compared with both bonded and weld L+R methods. While registered with very small amount of equivalent and normal stresses, the buckling effect is significantly reduced.

This thesis contributed the knowledge to the improvement of vehicle front bumper system. Particularly to the failure mode of both bumper beam and crash box, and offered the related optimisation.

Chapter 1. Literature Review

This research develops a novel intelligent framework for the vehicle crashworthiness test. Traditional physical tests require a prototype model to be produced, assembled, and then physical crashed for post-impact data analysis. This destructive method costs a significant amount of time and money. However, simulating the crash process via 3D Computer-Aided Design (CAD) models is considered a feasible alternative. Finite Element Analysis (FEA) simulation can perform repetitive iterations to achieve better test results with lower costs. The FEA simulated crashworthiness tests iterations can output "critical parameters": parameters that have a direct impact on the overall safety of the model. Changes to these parameters may result in safety improvements. This framework could be used on various vehicle models to achieve efficient product optimization and production.

1.1 Introduction to the Research project

The concept of crashworthiness is to determine the level of protection which a vehicle can achieve. Crashworthiness types, conditions, and parameters were developed by car manufacturers to primarily reduce the likelihood of damage to the vehicle itself, reduce the passenger injuries, as well as to satisfy the vehicle safety standards. In order to acquire post-impact behaviour and its related data, it is ideal to perform physical crashworthiness test to improve based on the original design. This means a destructive method that involves a prototype vehicle is propelled towards a fixed impact object, such as a concrete wall or a pole. The impact process generates crash footages and related data for the engineers to evaluate and further improve the safety of the vehicle. Due to the complexity of the crashworthiness process, preparation for each crash test is expensive, time-consuming, and the data is useful for only one specific category (frontal, rear, or side). In order to fine-tune the crashworthiness performance of a vehicle, multiple crashworthiness tests are needed to understand the comprehensive post-crash behaviour for vehicles, and it is necessary to conduct the tests in other categories, such as rear and side as well to achieve comprehensive safety purpose. As a result, it is inevitable the prototypes are subjected to partial, or complete destruction during the test are scrapped and many more prototypes are needed for any further tests. This will raise the costs and time needed during the development process; hence the crashworthiness test is very costly.

When compared the high-speed crash test, the crash test speed range such as low, or medium speed occurred more often than the high-speed scenario. A bumper system is therefore fitted to the front of the vehicle specifically to mitigate this problem. The bumper system is designated to be sacrificed in order to at least partially consume the impact energy without passing a significant amount to the rest of the vehicle and leads to more damage. Because such a system is located at very front of the vehicle, and most likely in contact with the impact object regardless of the impact type and speed. Thus, it is essential to have good crashworthiness performance on a bumper system.

1.2 Problem Outline

It has been over 100 years since the first fossil-fuelled vehicles were developed (Karl Benz, 1886), aspects such as electrification, metallurgy and aesthetic have contributed many improvements to the vehicle's design and production. Despite the evolution of technologies, it appears safety as a quantitative measure has evolved comparatively slower, and indeed has only matured in recent decades.

“Content removed due to copyright reasons”

Figure 1.1 Road Traffic Deaths by Type of Road User by WHO Region (WHO, 2015).

Figure 1.1 indicated that in 2015 car occupants accounted for the highest proportion of road traffic death when compared with cyclists, pedestrians, and motorcyclists globally. Vehicle

manufactures shall direct more attention to improving passenger safety, and should be continuously improved (WHO, 2015).

The first crashworthiness experiment was conducted by the US military in the early 1940s, on the topic of "Human tolerance" under the usage of military aircraft. Instead of improving the crashworthiness for a road vehicle, those experiments were addressing the safety design problems for military aircraft (Stanley, 2004). Nevertheless, the actual car crashworthiness tests were formally established much later by the United States Department of Transport at the early 1970s. A concept of the experiment of a safer vehicle (ESV) was formed specifically to conduct crashworthiness test to tackle vehicle safety-related issues. Many other countries were enrolled as well after its establishments, such as Japan, Germany, France and the UK. Later at the 1980s, E.C.E (United Nations Economic Commission for Europe) began to research on front and side crashworthiness for the region of European Union (Yang, 2009).

After the establishment of legal authorities at the early 1970s, the world's major car manufacturers were researching means of improving vehicle crashworthiness and seeking a method to standardize, and to evaluate the crashworthiness severity, eventually resulting in compulsory requirements introduced as laws. U. S. A., Japan, and most of the European countries have their own crashworthiness standards established over an extended period during the late 1980s. In 1998, the European Union had created and legislated the car crashworthiness standard. This crashworthiness standard required vehicles to satisfy the 56km/h frontal impact with 40% overlap area. Approximately in the same period, the USA and Japan also developed its legislation in which the car must satisfy the legal requirement before it can be sold on the market (Yang, 2009).

While the manufacturers still rely on the physical crashworthiness test to achieve safety improvements, it requires fully-assembled prototype vehicles, semi-structures or subsystem to participate. In compare with the traditional physical crashworthiness test, the popularity of computer-based crashworthiness simulation has increased in recent decades. Using computer-based software to numerically simulate the vehicle crashworthiness test requires the assistant of both Finite Element Analysis (FEA) and Computer-Aided Design (CAD). CAD is a large focus on replicating the vehicle's components into 3D(3-dimensional) parts that contain exact overall dimensions and local details, to create a "life-like" models and impact objects. On the other hand, FEA primarily aims to create a crashworthiness environment. Upon received the

replicated parts from the CAD software, it then assigns the connection between the parts, material properties and usage along with the boundary conditions. This re-creation of the crash environment allows infinite types of the real-world scenario impact event. It is worth for mention that some of the parts are subject to crashworthiness improvement, either on the dimensions of the part, or crash environments. Both CAD and FEA will allow an infinite number of changes to the parts and iterative simulations until the intended crashworthiness improvement is satisfied. Both CAD and FEA seamlessly work together to predict most accurate mechanical responses from the prototype models while saving the costs, time and labour during the design period.

1.3 Crashworthiness-military application

To further elaborate on the earlier section 1.2, as well as to realise its importance compared with other design factors, it is necessary to examine the evolution of how crashworthiness consideration was implemented to address the safety concerns during the design and manufactures. As previously mentioned, the origin or crashworthiness was to increase the survival rate of military aircraft, particularly helicopter crashes. Early safety-related equipment includes helmets for head protection, leather jacket for bruises to the body, and seatbelts were all quickly evolved into standard safety requirements. That on-board safety equipment did not progress significantly until the 1940s, where the researchers and designers realised the contribution of total safety concept which were focusing on the crash survivability (Dehaven, 1969).

It is stated the US army extensively focused on how to increase the occupants' survival rate, via re-design and test safety features to satisfy higher crashworthiness performance during the 1960s and 1970s. As a result, this decreased number of casualties, material losses, but an increase in mission effectiveness. It also pointed out that mission types such as low-altitude and low air-speed flying missions became more commonplace during the studied period, this allocates less time for rescue and rescue services. The Shifting between the flying types highlighted the importance of helicopters crashworthiness design and features. Because of the highly adaptive crashworthiness features and awareness for all mission types, fatalities and injuries of Crew members has reduced significantly (Carper, 1983). Because of the early establishment of crashworthiness awareness, and all related improvements and features. Based on the experiences after the improvement in the crashworthiness design on the

helicopter, he explicitly mentioned it is considered an insufficient method to prevent the accident, in order to permanently resolve the problems of casualties and material losses, but the problems were invariably taken place due to human, or operational errors (Carper, 1983).

Table 1.1 Army helicopter incident history 1972-1982 (Carper, 1983).

ACFT	NO. OF ACCID	NO. OF PSNL	NO. OF INJURIES MINOR	NO. OF INJURIES MAJOR	NO. OF FATAL-ITIES	COST-$M (MEN & MATL)	% ACCID WITH SURVIVORS	% FATAL IN ACCID WITH SURVIVORS
UH-1	426	1852	300	210	229	132	82	34
OH-58	235	533	97	76	59	28	86	25
AH-1	156	301	51	37	35	52	88	26
OH-6	72	160	44	19	9	5	93	22
CH-47	32	277	36	9	100	44	78	10
TOTAL ACFT	921	3123	528	351	432	261	85	26

However, the cost was still the main obstacle for essential onboard safety equipment upgrades, along with helicopter repair and replacement were the 3 main budget problems (Carper, 1983). Soon it found retrofitting, or to upgrade all the safety equipment into the non-crashworthy aircraft was an ideal solution and identified following areas that cannot be resolved by retro-fitting:

- The main structural collapse will cause loss of occupant's survival space because both roof and floor were deformed.

- Penetration wound to occupant's upper torso, such as head and chest area was sustained due to the sharp edges created via Structural frames bend inward to the cabin.

- Floor deformation caused the seat to dismount and relocation resulted in the occupants being ejected from the helicopter.

- Fire hazard presented by the landing gear penetration.

Due to the above issues found, it concluded that the concept of crashworthiness needs to be considered fundamentally during the design and production process. Retro-fitting into the

existing aircraft was unable to satisfy the safety needs during flying missions. Instead, a radical but viable approach must be established on the parameters of crashworthiness design. Retrofitting method has gradually evolved into crashworthiness focused design and development after many years. There were few crashworthiness parameters discovered along with the development of each newer generation of aircraft, particularly such as human tolerance, energy absorption, lightweight material, occupants' restraint system, impact characteristic. As a result, a world-first joint experiment on crashworthiness experiment was conducted in 1974 between the government and the industry. Formed guidance to focus on the crashworthiness improvement on to the lightweight fixed rotary-wing aircraft, and was later formulated into military standard, namely: "MIL-STD-1290". This standard primarily emphasised crashworthiness performance of overall structural integrity of a fuselage. The structure must have the strength and stiffness to maintain an acceptable survival space for any occupants on-board, as well as the seats, remained attached to the cabin. This standard also indicated that the heavy objects, such as the engine, and transmission will neither be detached from the body of the helicopter nor penetrate through the cabin area.

Furthermore, occupant safety was detailed in two separate sections of the requirement. Section 1 was dedicated to the impact load management, such as the aircraft fuselage must provide a certain amount of energy absorption in order to reduce the impact force applied to the occupants. Assembles, or components such as landing gears, seats, interior panels could all benefit from crushable materials and structure design, which helps the occupants to sustain from the minimum amount of acceleration force. Section 2 is focused on the occupant environment hazards, which including occupants' restrain systems, extra padding etc., in order to reduce the probability of failing. In an additional two points above, "MIL-STD-1290" standard also regulates the behaviour of how aircraft reacts to post-crash hazards, particularly to fire hazard due to oil and fluid leaks. From the summary of the above discussions, it is interpreted the crashworthiness design must be considered and embedded from the very beginning of the structure design, and it must serve the following purposes:

1. To secure the occupants inside the aircraft during, and after the impact event to reduce injury rate.

2. Maintain overall structural integrity without sacrifice the living space for its occupants.

3. Suitable deployment of deformable materials or structures to deliberately deform to absorb the impact energy, without passing further which increases the risk of occupants' injuries during, and after the impact took place.

"Content removed due to copyright reasons"

Figure 1.2 Energy management system (Carper, 1983).

It can be observed from the above-stated points, there are mainly focused on the helicopter structure. It explicitly expected that the onboard structural features like showed in figure 1.2, such as the landing gears, the seating frame inside the cabin, and the bottom fuselage area must work together as a crumple zone in order to deform and absorb excessive impact energy, and the rest of the structure must have acceptable level of strength to hold its integrity during the impact process.

1.3.1 Seat Design-The above points were all essential factors that contribute the foundation of good crashworthiness performance, and it approved this idea and specifically indicated the potential severe hazard presented to its occupants because the occupants were not appropriately restrained on their seats. Occupants will be started to receive the impact load via fixed seating structure after the fuselage touches the ground, the impact load will apply to the occupants immediately via the seat structure since it is directly bolted to the floor. This violated the occupant's safety concept since the mounting method can cause seat structure dislocation. Seat dislocation also leads to contact injury with interior parts, or possibly at the worst-case scenario,

eject out of the aircraft. During the newer aircraft models' crashworthiness design and improvement, human tolerance factors were heavily considered to minimise the occupants' injury rate, and to maximise the energy absorption capabilities on other onboard crashworthiness features (Carper, 1983).

The crashworthiness complied seat is mounted to the airframe, and similar to the landing gears, the structure optimisation efficiently increased the energy absorption which preventing the any additional impact energy passes on to the occupants via airframe, particularly at the vertical impact, which is the major cause of spinal compression fracture, which occurs between 25G to 30G of acceleration with the effected age group of young, to middle-aged adults. Sadly, there is a very small chance of survival when the acceleration rate is over 30G, hence it is necessary that the seat mechanism should absorb the excessive impact energy to prevent this type of injury, since the spinal compression will cause irreversible damage to the human body, and most of all will result in paralysis.

On the top of the crashworthiness capability of the seat itself showed in figure 1.2, the mounting position of the seat has also been investigated, results showed during the medium impact speed, the common spinal fractures sustained was caused by inappropriate seat mounting location, such as mounted on rigid surface, such as interior structure, impact load then directly transfer to the occupant via the rigid connection. Some extreme cases, where a poorly designed seat caused spinal injury with impact load between 8 to 10G. It is therefore recommended, the average crush load from vertical impact shall not exceed 14-15G for the military helicopter, and 11-12G for civil helicopters (Coltman, Van Ingen, and smith, 1986; Shanahan, 1991; Singley, 1981). Considered that the helicopter may have experience multi-direction impact that results in the impact load applied to the occupants from all axis, still, the structure of the seat that offers multi-direction protection has not been proofed as effective as plain vertical impact despite that few multi-direction protection seat solution offered by some manufacturers. Nevertheless, such crashworthiness complied seat featured additional fixture between the seat and the airframe, hence the occupants will not be ejected away due to seat detachment. Figure 1.3 below indicated the seat subjected to post-crash behaviour which fitted to the UH-60. A velocity of 15.2m/s (50ft/s) was approximated during the vertical impact. This resulted in the seat mechanism compressed 35.6cm (14 inches) when the acceleration reached to 14.5G. This crashworthy seat design saved the pilot to sustain from any spinal injury (Melvin *et al*., 1985).

“Content removed due to copyright reasons”

Figure 1.3 post-crash of the interior seat of the UH-60 helicopter (Carper, 1983).

“Content removed due to copyright reasons”

Figure 1.4 Severe crash accident of a UH-60 Blackhawk helicopter. (Carper, 1983)

Another case is shown in both figure 1.3 and 1.4, a very severe accident of UH-60 Blackhawk helicopter, the main container of both cockpit and cabin was dislocated away where only the bottom half of the airframe, few body panels were still intact, this level of damage presented

less chance of survival considered the severity of this accident. Nevertheless, the pilot received serious injuries but survived mainly due to the pilot has been restrained in the energy absorption seat. During the previous discussion of achievable high human body tolerance, up to 40G of acceleration is expected if the occupant is restrained correctly.

1.3.2 Occupants restraint system-Occupant restraint system serves the purposes of both restraining the occupant at appropriate seating position without excessive body movement, and enabling the controllable deceleration to absorb residual impact force from the fuselage deformation. It explained the military standard "MIL-5-58093" was especially initiated for this purpose since 1971. It required the aircraft must be equipped with 5 points safety belts which are demonstrated in figure 1.4, which includes the main lap belts, two shoulder belts. An additional strap to further secure the occupant which prevent it to slide underneath the lap belt when the aircraft is subjected to negative accelerations.

"Content removed due to copyright reasons"

Figure 1.5 Crashworthy seat design (Carper, 1983).

Figure 1.4 showed a first-ever specific crashworthiness test was performed in 1979 to verify the effectiveness of such design that potentially benefit both pilots. 95th percentile standard human-sized dummy was used with seven prototypes of crashworthiness designs to determine the most appropriate combination under dynamic loading conditions. Varies crashworthiness

design such as negative acceleration strap, belts pre-tensioners, deformable seats, and particularly, the inflatable head and body restraint system were also the first time to perform its practicality during this test. This test was intending to replicate the real-world crash scenario, with the functional human-sized dummy to generate realistic data.

Except for the multi belts system, the inflatable restraint system was also built into the prototype to determine the crashworthiness performance. It is found the belt system restrained both pilots on their seat without touching any interior parts, and the inflatable system aided the reduction of deceleration of the pilot's upper torso by keeps inflation for additional 1.5 seconds. The deceleration of the pilots' body was also discovered evenly distributed over the inflated cushion area. This resulted in additional protection to the head and neck as well. However, like demonstrated in figure 1.5, to avoid the sensor has been triggered in case of flying and combat vibration and manoeuvring, the calibration of the set off level to the sensor requires individual adjustment to each aircraft.

Figure 1.6 correct cushion inflation chart (Carper, 1983).

1.3.3 Landing gear design-During axial load conditions, such as the helicopter is subject to vertical deceleration due to sudden engine power loses, the landing gear would most likely to make the first contact with any objects. To avoid the landing gear penetrating into the cabin, it must be designed with high retractability that could consume a large amount of impact force.

Past years' accident statistics and mean loss data collected by the US army force safety canter revealed, it is beneficial to implement this crashworthiness landing gear design into the manufacturing of newer AH-64 helicopter, which allowed the impact force to be fully consumed at maximum level of 20ft per second (6.1m/s) during vertical drop condition of the aircraft.

"Content removed due to copyright reasons"

Figure 1.7 crashworthy landing gear of UH-60A (Carper, 1983).

Like the figure 1.6 displayed, the crashworthiness design will consume the impact load within the landing gear without damaging the bottom fuselage of the aircraft, which could lead to additional damage. The conventional landing gear mechanism found on older AH-1, UH-1 and OH-58 are less capable of absorbing the impact energy when subject to the same drop height. This crashworthiness landing gear design could potentially reduce the accident rate of 14% if it can be fitted to the rest of entire fleet of 500 helicopters, and this also corresponded to 570 million dollars of the repair bill, as well as 20 years additional fleet service life.

1.3.4 Fuselage Structure-Once the impact force is greater than the landing gear can reduce in the cases where the aircraft is subjected to higher impact velocity, the fuselage area is most likely to contact with impact objects after the landing gear, it is another critical area subjected to crashworthiness design. A radical approach was achieved via stages of design, prototype test

and analysis. It was suggested via the previously mentioned military standard (MIL-STD-1290) that the ideal target of the impact speed shall be 30ft per second without any occupants sustaining any injuries, prior to the approximated 30% impact force has already been consumed via the landing gears.

Figure 1.7 below proposed re-designed crashworthiness complied cabin. It was divided into three sections, namely

1: The middle section for occupants,

2: The fuel section behind the occupants and

3: A mechanical component section located on the top contains an engine and gearbox.

Figure 1.8 Crashworthiness cabin design (Carper, 1983)

It is worth to mention that a designated deformation section located below both sections of occupants and fuels. The interior structure within the deformation section will aid the deceleration into a stable trend that is appeared in a controllable manner, and the deformation folds outward to avoid floor penetration.

Except for the very established knowledge on the occupants’ restraint system in section 1.3.2, a further enhancement to the on-board features was discussed via both point 2 and 3. The importance of having a good structural design. Such as the landing gears, the cabin seating

frame, and the bottom fuselage area must work together as a designated deformation zone to manage the impact force effectively, either via deformable design, or stronger overall structure. This allows the fuselage to subject to pre-determined deformation behaviour, and to pass little to non-impact load to any other area or occupant. From the above discussion, it is concluded it closely focused on the development, as well as material selection to create a safe airframe for occupant, the results it is not just to comply with crashworthiness in place during the aircraft development and to reduce the injury rate, but also to save the financial costs and time involved for both healing the soldiers, as well as aircraft's downtime for the repair work. Further examining the crashworthiness optimization and involvement, alternative literature suggested crashworthiness can be improved from similar factors (Carper, 1983).

1.3.5 Fuel Tank-In a post-crash environment, occupants are most likely to experience the hazards, such as a fire caused by leaking fluid and fuel, burning fumes caused by combustible interior parts.

"Content removed due to copyright reasons"

Figure 1.9 Fire proofed self-sealed fuel tank (Carper, 1983)

Related solutions have all been provided such as demonstrated at the above figure, a non-survivable crash of Apache helicopter resulted the self-sealed fuel tank has been dis-located away from the airframe, without present any fire hazards. This function is relatively convenient

to retro-fit into the existing fleet models since 1970s and showed very effective of preventing any fire hazards. Unfortunately, the progress and retro-fitting this fireproof tank system was only forced by the Army regulation, and surprisingly that the newer models still unable to equipped with this function and require to be retro-fitted, after the standard design caused as high as 42 per cent deaths due to newer aircraft produced without this system. Consequently, the lack of regulation enforces on to the manufactures was the main cause despite that the certain manufactures offered this system as an optional extra, whereas left only a few manufacturers offered as included. This situation was finally improved since 1990, where the FAA (Federal aviation administration) issued a revision to have such system as standard with every new airframe produced.

1.3.6 Injury types identification-Shanahan (1993) summarised the above-discussed crashworthiness design and its overall achievements. Similar to the Carper's analysis, it categorises the crashworthiness into types, severities, and the effects after the implementation of crashworthiness improvements in 1993. It is admitted that the importance is since the establishment of the crashworthiness concept, structural integrity of the aircraft appeared more important in maximising the occupants' survivability than other factors.

Despite that, the concept was developed decades ago with many tests and design improvements, but still, the implementation progress of the crashworthiness features into the newly-built aircraft was much slower than anticipated, despite the promoting progress and the proved benefits and advantages, whereas except only minor amount of agricultural aircraft have been implemented.

This situation later was improved while the U.S army was destined to research and to improve the survivability of the aircraft. This accelerates the crashworthiness features available to more and more aircraft that have been built and complied with crashworthiness standard and yielded an improving the aircraft survival rate. It also focused on the most important design factors that contributed most to the increases in the survival rate (department of the army, 1989). This design guide has iterated over time and came into a comprehensive, standardised and mandatory requirement that considered as the primary source to reference any safety-related design and parameters for any new aircraft. Particularly, the UH-60 black hawk and AH-64 Apache helicopter fleets have been selected to perform any new crashworthiness design and this has become the standard production procedure for any other military aircraft design and

manufacture. (Carnell, 1978). This guide quickly gained high effectiveness on increasing the survival rate, as well as protecting the occupants from the injury in the first place. (Shananhan, 1991; Shananhan, 1989).

The situation was further analysed many older models of the used helicopter in the military, and he found apart from the repair of the aircraft after the impact, it is inevitable that certain degree of personal injury will occur almost all the time during the impact Shananhan (1991). Particularly, 90 per cent of the occupant's injuries sustained that is force related, and it can be effectively mitigated via adequate structural optimisation to the existing designs, such as airframe, or the personal restraint system. (Bezreh, 1963; Haley, 1971; Haley and hicks, 1975; Hicks, Adams, Shanahan, 1982). And because of this, he identified both traumatic injury and environmental injury are the main factors.

1.3.7 Traumatic and Environmental Injury-Traumatic injury was mainly caused by the external mechanical force that applies to the occupants, such as the impact load travels through the seat, the control joystick and interior panels. This external force exhibits high-speed accelerations with excessive vibrations. Environmental injury is caused slightly different, it was by the surrounding environments that helicopter experiences, such as drowning because of a water landing, heat and fumes because of burning material. All are which eventually lead to respiratory problem. Despite both injuries, categories were unavoidable and largely involved in a certain body location that in contact with impact object, it is agreed to prevent the occupants' injury in the first place shall be considered as a priority target. Structural integrity Optimisation is a viable method, similar to Carper mentioned at an earlier paragraph, designated collapsible bottom floor and frame, energy-absorbing landing gears, and compressible occupant's seat. Personal restraint system was also designed and fitted to the cabin which provides an appropriate anchor point for the occupants, such as acceleration strap, 5 points safety belts.

All the above Both Hudson and Carper reviewed the benefits of the availability of crashworthiness features, and this implementation successfully achieved the reduction of occupants' injury and death rate. This means an unnecessary cost for healing the soldiers and repair cost for helicopters were all saved. Because the benefits gained during this integration process, Shanahan further emphasised the importance, and established the basic principles of

the crashworthiness design shall follow as the container where contains the occupants, and it shall restrain the occupants correctly, without any significant structural collapse, while absorbing the impact energy, and maintain the structural integrity after the crash.

1.3.8 Results comparison-Similar to the crashworthiness implements by Carper in the earlier paragraph, Shanahan emphasizes on the structural optimisation from a more realistic perspective, by comparing the older and newer model to reflect the effectiveness of crashworthiness.

It indicated that the structural optimisation was to maximise the controlled collapse to achieve both maximum energy absorption and minimum interior intrusion. Meanwhile, to provide enough living space during, and after the impact. The container where occupants located provides the basic carrying and operating function of the aircraft, such as the cockpit at the front of the aircraft, and the cabin area with seats. During the impact, the cabin is most likely subject a vertical impact, and the cockpit is subject to axial impact since the aircraft may be experiencing forward motion as well. A good survivable space is expected where the cabin structure shall take most of the impact without any significant collapse caused by the engine and gearbox on the top, or sharp intrusion caused by designated deformable floor, and other exterior detail been intruded into the cabin, such as rotor blade or the landing gear. Shanahan repeatedly emphasized on this point that it is critical to maintaining the overall structural integrity since it acted as a safety cell, while effectively consume the impact load via designated crush area.

A clearly poor crashworthiness design showed in figure 1.9 below. It revealed the post-crash behaviour of the cabin design allowed the almost complete collapse of the roof structure which did not provide a survivable space for the occupants, this presented the occupants may experience the second impact with interior parts and could lead to severe personal injuries.

“Content removed due to copyright reasons”

Figure 1.10 Collapsed roof structure at post-crash behaviour. (Carper, 1983)

Despite the poor post-crash behaviour, one out of two pilots survived from the crash because of the energy absorption seat which was mounted to the roof.

“Content removed due to copyright reasons”

Figure 1.11 Rotor intrusion into the occupied spaces. (Carper, 1983)

Another example of the above figure showed a typical example of main rotor intrusion which damaged the cockpit windscreen as well as doors for the occupants entering and exiting the aircraft. The overall structural integrity remained intact and there was no obvious intrusion of both landing gears and main powertrain, however, the rotor damage to the exterior of the airframe suggested it could cause a much worse hazard.

Further analysis of this crash event, except the cabin structure, shall be improved, the inertial created via engine and gearbox also presented a serious problem. The heavy mass located on the top of the airframe should be considered to rigidly fix to the airframe without detachment during the impact. Surrounding structures shall consume the heavy mass acceleration without further passing to the cabin. The nose corn of the cockpit shall still design with a certain amount of strength to avoid any severe deceleration, such as nose corn scooped into the ground, which could cause the aircraft to flip over violently, instead of gliding through the ground and slow down gradually. It is can be understood that the total deformation of the airframe shall not exceed 15% of its total original size. (Shanahan, 1993)

As per figure 1.11 indicated below, newer UH-60 model carried the improved design to the main rotor system. The rotor blade deliberately breaks away from the main occupant's compartment without any intrusion which leaves a suitable amount of survivable space, as well as without presented any secondary injury to its occupants. (Shanahan, 1993)

"Content removed due to copyright reasons"

Figure 1.12 breakable rotor design to the newer UH-60 model
(Carper, 1983)

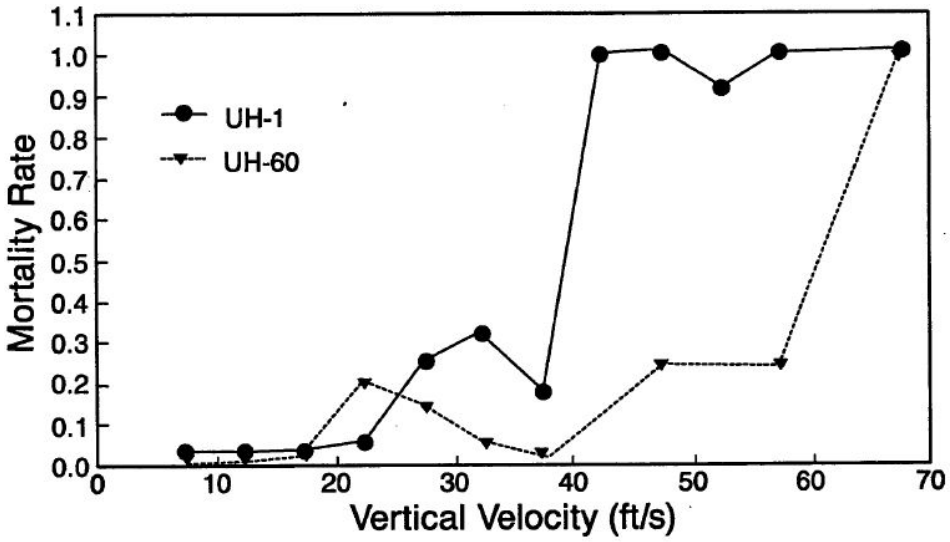

Figure 1.13 Mortality rate versus Vertical velocity (Shanahan,1992)

Figure 1.13 above clearly showed base on the 5ft/s frequency, the correlation was generated between the mortality rate and its corresponded to its vertical velocity for the aircraft model of older UH-1 and newer UH-60. The cumulative frequency between UH-1 and UH-60 were shared generally the same correlation before the impact velocity of 20ft/s. A conventional design UH-1 has less crashworthiness consideration, and therefore performed poorly. The mortality remained generally low which was between 0 to 0.2 before the velocity reached to 40 ft/s. Once the vertical impact velocity increased over 40ft/s, the mortality rate rocked from 0.1 to 1.0 and stayed deadly high throughout (Shanahan, 1992).

On the case of UH-60, crashworthiness improvements made it relatively low mortality rate within the impact velocity up to 60ft/s and performed the same as deadly as 1.0 after. This comparison between older and newer model aircraft appropriately demonstrated, crashworthiness implemented design can keep the mortality low, by stretching the corresponded maximum allowed impact velocity from 40ft/s to 60ft/s. And this 50% increases illustrated the newer UH-60 offers better occupants' safety in far higher impact velocity, that would otherwise be considered to be deadlier when flying in UH-1 counterpart.

To conclude this comparison, it shall be emphasised that as technology progresses, advanced material, production and design were gradually available for both military and civil market, although lack of commitment to resolving actual problems, and also the utilization to all available resources. If the helicopter related injuries and costs shall be analysed extensively

and realistically, the results should point that crashworthiness implementation will be considered as more cost-effective from long term perspective.

The further investigation examined the relationship between human tolerance and crash survivability under the topic of crashworthiness, and reached to a conclusion that the number of both aircraft and motor vehicle-related crash events will continue to increase, regardless of all efforts to prevent the crash happening in the first place. Sadly, except the injury or death happened to its occupants, there are many post-crash consequences involved as well (Shanahan, 2004). It estimated that it is confident that up to 85% of aircraft related injuries or death rate could be categorised as survivable, without to sustain a significant injury. The reason for such a high percentage of occupants' injuries or death rate it is because they lack crashworthiness design. It is critical to understand that the design of aircraft will require the concept of crashworthiness in place in order for the main structure to hold its integrity, this will make sure the impact forces do not exceed the maximum level of human tolerance allowed during the impact. It continued to investigate the importance of having crashworthiness design in place and found to satisfy the reduction the rate of occupants injury or death in order to achieve good crashworthiness performance, the impact force during the crash is less than a human can withstand, and the structure which contains the occupants must remain an acceptable space during the impact taken a place Shanahan (2004). However, it still found numbers of causes related to serious injury or death can be achieved with only survived with minor injuries, largely because the crashworthiness design isn't acceptable, hence offers less protection than a good crashworthiness alternative provides. Crashes which caused serious injury or death represents the airframe, seats and occupant's restraint system were incapable to protect its occupants that could have been received with only minor injuries. Consequently, it identified the concept of crashworthiness is equally important to helicopter design, but in the meantime to the vehicle design and manufactures as well (Shanahan, 2004).

However, it specifically indicated that there are many settlements during the design, and manufacturing process to achieve good crashworthiness product. And it further explained this concept and stated it is possible to build an aircraft with heavy steel which gives total confident and safety to its occupants, but it would be impossible to fly. Modern crashworthiness design requires few trade-offs in order to satisfy the good crashworthiness performance, which this

requirement directly pointed to the satisfactory on both material and finance. Heavier gauged material will result in good occupant's protection, but surely also leads to high fuel consumption due to additional weight carried, hence reducing the combat radius. Alternatively, a lightweight material, with advanced crashworthiness design is an ideal choice, but with higher costs as well. Consequently, a correct determination of good crashworthiness performance must be considered to reach an acceptable breakeven point between good crashworthiness design, lightweight material, and financial viability. In addition to this, it continued pointed out that the crashworthiness design will also need to comply with local or regional legislations before, either aircraft or vehicle can be sold to the relative market. This compulsory requirement could bring more restrictions to the original design, since the manufacturers have to follow, and considered this is the minimum requirement for their product before it can be sold on this market. It also mentioned about the crash environment where an aircraft or a vehicle is likely to involve, such as crash speed, angle, this is directly influenced to how the manufactures design in order to satisfy the crashworthiness need. It carried on pointed out that the force generated during the crash process can be quantified as the magnitude and also from varies directions, consequently, there are few essential factors involved during the impact process.

1.3.9 Summary of military application- all previously mentioned points were focusing on the relationship between the acceleration to the human factors and together could affect the level of survivability during the crash event. Excepted the factors mentioned above, other has suggested the survivability is also heavily related to the surrounding environment, such as the interior or exterior structure of an aircraft, or a vehicle that travels. Structural integrity has been very well examined and emphasized in the earlier paragraph (Carper, 1983; Shanahan, 2004).

Shanahan concluded main areas which are closely linked to the level of crash survivability. Firstly, the main passenger compartment will need to remain its integrity, without significantly deformed, collapsed, or even penetrated. Secondly, the capabilities of the restraint system to the onboard passengers, as this will avoid the passenger to sustain from secondary injuries. In an addition to the previous two points, at a particular case where the crash load is significant due to the scale of the impact, and the acceleration magnitude is dramatically increased within a very short period of time, hence it is critical to channel the impact away from the passenger compartment. A crashworthy structure can be created with correct type, and amount of energy absorption materials implemented. It creates the sacrificial section at a critical location. Where significant hardware damage is avoidable a minor crash case, and the aircraft does not lose any

ability to remain during the flying mission, or carrying occupants. But the occupants will sustain from minimum injuries during the severe impact conditions as the sacrificial section will deform and crumple to follow the design where safety consume the crash load. It also explained that in order to improve the crashworthiness a vehicle, automobile designer places optimized structures at both front and back of the vehicle, and this crush zones will protect its own occupants in the event of the crash happened. However, Shanahan still indicated there are hazards still presented after the aircraft has crashed. Hazards such as pierced fuel line may lead to leakage and fire. Crash-landed on a water surface also displayed a problem where occupants may trap inside the cabin because of the malfunctioned restraint system, or airframe penetrated inside the cabin which prevents occupants to escape (Shananhan, 2001).

Shanahan summarised all the above findings and stated all crashes were involved with personal injuries, regardless of its minor or major, civil or military, should be thoroughly investigated and documented for further records. Because the documented results were precious due to people been injured or dead. All the collectively, historical data shall be submitted to relative authorities to promote the importance of having crashworthiness in place, as well as to improve the crashworthiness performance on future models. The authorities including government bodies, or manufactures who is producing aircraft or vehicles, since each individual case were created. Despite the accident or crash is inevitably reoccurring constantly and resulted occupants' injuries or sometimes even death, literature was suggested it is therefore very important to understand the importance of having crashworthiness in place in order to reduce the numbers of casualties (Carper, 1983; Shanahan, 2004)

The fact that indeed where the military was valued both their soldiers' life and because of this, varies crashworthiness design has been adopted to newer aircrafts production. Particularly to the investigation explicitly emphasized the case of using the crash-proof fuel system. The military discovered that approximately 40 per cent of the fatal injuries are due to fire hazards during the Vietnam War, because of the fuel system was leaking after the impact. Later developed revised fuel system which will contain all the fuel within the system even after the aircraft is subjected to impact, also retro-fitted this crash proofed fuel system to older aircraft which was previously manufactured.

A costs involvement has been reviewed and suggested aircraft retro-fitting cost $7517 based on the model UH1 at the 1970s. Of course, this came with the compromises of reduction on

both loading capacity of 160 pounds, as well as 11 gallons of fuel. Nevertheless, the results were significantly effective, achieved only a few thermal related injuries were documented, and this proves Crash proof fuel system is indeed very effective. However, compared with the military inefficiently of implementing such a system into the new aircraft production, the numbers of civilian helicopters equipped with such a system were near to non-existence. Similar crashworthiness design, such as energy absorption airframe, landing gears and seat mechanism have all been slowly adopted into the civilian applications ever since. Shanahan criticized this rather slow progress of crashworthiness adoption and implementation was largely due to the regulators weren't serious enough about to change the regulations. This reluctant attitude has directly affected the manufactures to adopt to this safer design as well, where only a few offered as optional extra but rarely as standard equipment. Consequently, without the correct influence from the industries and government regulators whether it's compulsorily or voluntarily, consumers who purchased the product were less willingly favoured to add the safety features fitted (Shananhan, 2001).

To summarise the above findings, human can tolerance significant amount of crash load that based on providing good crashworthiness structure and occupants restraint. It is suggested the crashworthiness design shall focus on considered in advance regarding an appropriate impact load management. The impact load needs to be completely, or at least partly consumed with the deformation of energy absorption, and residue load shall continue to be channelled around the cabin, and transfer to other locations, such as to reinforce the surrounding cabin structures, hence, to avoid passenger compartment collapse, as well as to minimise both exterior and interior parts. Instead of focusing on passively restrain the passengers within the seating area. And because of the crashworthiness indeed contributed to higher occupant's survivability rate within the military applications due to the implementation of varies types of crashworthiness concepts and optimisations, Shanahan further recommended that the similar crashworthiness designs shall be adapted to the manufacturing of civilian aircraft, or even road vehicles as well.

1.4 Crashworthiness-Motorsport application

Without a doubt, similar crashworthiness infrastructures have been adapted and implemented on the road vehicle design and production. Particularly, in the motorsport sector was the pioneer sector that was seriously implemented such infrastructure. A precedent case was to use the on-board recording device (a black box) to the actual moving vehicle to record its acceleration,

deceleration, wheel speed, steering angle etc. in order to find the relationship between the safety features to drivers' survivability.

Literature conducted using motorsport racing event as a potential case study due to the realistic and scale. It believed that crashworthiness concept can achieve higher survivability due to many precedent cases in earlier military applications, such concept was implemented into the historical Indy 500 (Indianapolis 500 race) motorsport event that all candidate vehicles were consistently driven over 155mph, hence it is considered as a suitable opportunity to determine the vehicle's crashworthiness are critical (Melvin *et* al, 1998). A data logging device was fitted to each individual race vehicle and it records all on-board data while the vehicle is driving on the track. This specific device utilises varies sensors and specific mounting location to achieve comprehensive data logging to reflect the precise movement and behaviour of both race car and its driver on the track while it subjected to collision. The primary reason for having such a system fitted to the actual race car it is because the data generated on the moving vehicle are more representative in compare with the much simpler crash test conducted in the laboratory. And this method indeed reflected what the actual driver was experiencing while the race car is subject to the crash event. While this investigation was ongoing, a relationship between the impact behaviour of the racing vehicle and the human tolerance was established in order to determine the appropriate, and specific protection method to the race vehicle itself, which can offer a higher level of safety protection under the impact condition. Road vehicle design and construction can also be benefited to this investigation when the knowledge is fully discovered.

The nature of the Indy 500 motorsport competition was largely involved in the vehicle that constantly driving at any speed above 100km/h, car racing event will inevitably be causing an accident during the races, whether it is multi-vehicle involved, or it's against the wall.

“Content removed due to copyright reasons”

Figure 1.14 Typical Indy 500 racing car setup and driver position (Melvin *et al*, 1998)

The form of Motorsports safety technology research program (MSTRP) was specifically created by General motors at 1991 to dress varies crashworthiness related questions. Despite the racing car event shares fewer similarities with normal road vehicles, such as the seating position of the driver, the vehicle construction and configuration, driving speed to the name of few, but both road and racing use are looking for to achieve the same goal, which is to get the occupants from location to another without sustaining any harm. Particularly, the MSTRP selected the factor of acceleration and deceleration to its driver as a determining factor which measured very close to its own vehicle’s behaviour. A comprehensive understanding to the movement, behaviour, and injury of the driver during the impact can be considered as very effective parameters that could later be beneficial to the road car’s development and production of the road vehicle.

Despite that safety is the ultimate goal for both racing and road use, there is a fundamental difference between both types of vehicle usage. The Indy 500 racing event has a universal standardised safety regulation. To further extend this point, firstly, the driver’s seat is tight fitted

into the narrow tunnel at steeply reclined at 45° from vertical. Paddings were very little due to the tightly fitted seat offers. Six points belts restraint system has also been fitted to the seat structure. This system consists of two 75 mm wide shoulder belts that connected to another pair of 75 mm lap belts. An additional pair of straps were also included within the system that prevents the driver from slips down from the impact. In addition to this, a head restraint is fixed to an anchor that is part of the chassis structure to avoid the drivers head experiencing excessive movement during the impact. The side of the driver's seat is designed to be higher than the shoulder of the driver. The racing vehicle is built embedded with crashworthiness features as well. There are pre-defined three main impact zones, which are front, side and the rear. A tapered cone-shaped nose structure absorbs impact energy via controlled deformation when the race car is subject to axial head-on crash. The side of the race car is constructed with composite shall, as it provides space to fit the cooling system, as well as other auxiliary components. They both shall composite side structures are also satisfying the aerodynamic purpose that creating the downforce for the car. For, more importantly, the composite built shall structure absorbs impact energy via structure deformation during the impact. Due to the seating configuration allows only one driver located in the middle of the car, hence the deformation of both side composite material will maximise the energy absorption during the impact and therefore offers higher crashworthiness performance. The recording device is rigidly mounted to the floor of the car, which is very close to the driver, meanwhile, it still remains accessible in case the unit requires repair or data logging. Both gearbox and engine are fitted to the rear of the car which has no crashworthiness structures, or any other protection implemented.

1.4.1 Accident observation and definition-The race car drivers on the oval-shaped race circuit for a certain number of laps, and sometimes the race car loses control and crashes with the wall or collide with another race car. It appeared to be very dangerous for audience observation that seen a race car travelling at over 200 mph (300km/h) and impacts with other objects. It is clear that any collision under this velocity will predominately cause death. However, the actual impact velocity appeared to be much less than the travelling speed during the impact. MSTRP took advantage of the on-board recording box and successfully captured and analysed two high-speed accident. The results showed the centre of the mass of a race car shall be the appropriate factor to estimate the impact process. In addition to this discovery, it also suggested the deformation of the nosecone shall be included as well to assist the impact estimation accurately.

To define the severity of the accident, the velocity difference during the impact process of a race car that results in varies the level of deceleration. The velocity difference does not reflect how fast the race car travels, but it represents how the impact affects the direction and the impact process of the race car. Similarly, the deceleration created at varies direction that caused by the impact is decided by the impact behaviour of the race car. It is worth to noticed that, not like a road car accident, race car travels in excessive of 170 mph (280km/h), but the canter of the mass of the race car normally pointed less angled towards to the wall. Considered the side wall stays stationary during the race car's impact process, the kinetic energy that bounces the race car away represents the changing of impact velocity that equals the canter of mass which perpendicular to the wall. The reason for such phenomenon it is because the composite made structures will crumple accordingly that to achieve permanent deformation with little to non-structural recovery due to elastic energy. At the worst-case scenario where the race crashes head-on towards to the wall, the centre of mass will be a shift from the perpendicular at the initial impact position, gradually transferred into the gliding motion that paralleled to the wall along the impact process. This observation demonstrated the relationship between the impact angle to the velocity changes to a race car and provided a discovery that the shallow impact angle will result from the velocity variation to a race car that much lower than the actual travelling speed.

1.4.2 Results and categorisation-It is worth to notice that the total numbers of incidents were 477, but the actual numbers of recording were only 262. There are a few reasons were contributing to this difference. Primarily due to the initial device installation time did not start until the mid of the racing season, hence the only handful of race cars were implemented. The completion of devices installation to all race cars was in 1994. For more importantly, most of the incidents were classified as a minor issue where this did not trigger the device. The recording device itself malfunctioned and failed to record the incidents were also presented within this consideration, it was due to the components fatigue failure, but it was quickly rectified thereafter. During the course of this experiment, the deceleration rate higher than 20G was considered and therefore yielded 202 cases as documented. On the top of this, 33 cases were categorised as multiple impacts where the race car collided with another car, or the wall more than once, and of course 17 of those 33 cases were demonstrating a race car were also subjected to deceleration in multiple directions as well, this generated 3 times more peak value.

Figure 1.15 Case distribution of peak decelerations In Frontal Impact (Melvin *et al*, 1998).

Figure 1.16 Changes of total velocity in Frontal impact (Melvin *et al*, 1998).

Frontal impact has only 3.1% out of many other impact locations on the race car and its grouped per above figures illustrated, where case number distribution showed more than 50% of the decelerations were exceeded 40G, and the mean peak deceleration for the 13 cases were 50.7G, and other 4 case groups were also exceeded the decelerations of 60G.

Figure 1.17 Case distribution of Peak Decelerations in Side-Impact (Melvin *et al*, 1998).

Figure 1.18 Changes in Total velocity in a Side impact (Melvin *et al*, 1998).

The above figures 1.17 and 1.18 both displayed for how the side impact cases were accumulated. 105 cases were recorded as side impact with the peak decelerations above 40G, and with 41 cases reached to 60G, and with 7 cases that exceeded 100G. The mean peak deceleration was 53.3G.

Figure 1.19 Case distribution of Peak deceleration in Rear impact (Melvin *et al*, 1998).

Figure 1.20 Changes in total velocity in Rear Impact (Melvin *et al*, 1998).

On the rear impact scenario, the case distribution represented that there were 30 cases contributed to peak decelerations above 40G, and 17 other cases demonstrated above 60G of decelerations, and 6 more severe cases suggested that excessive 80G of decelerations were reached. This yielded the means velocity changed of 11.6m/sec. In addition to this, 4 more cases that have yielded deceleration rate of over 60G resulted from 15.2m/sec of total velocity changes.

1.4.3 Injury analysis-despite that most of the crashes resulted from the peak deceleration above 40G, however, due to the excellent energy absorption design to both front, and side of the race car, all 202 recorded impact cases did not produce any significant injury to its drivers. To further analysing that the relationship between the race car offers, and to its driver's injury severity, it is worth to mention that, based on the crashworthiness considered and designed, with the introduction and implementation of energy-absorbing nose cone and chassis extension by 1993, there were no further low torso related injury sustained to the drivers reported. However, a frontal impact case still managed to make an exception of which yielded an over 80G of the peak deceleration. This particular case resulted in the driver sustained low torso fracture that surgical treatment was not necessary. The main reason which contributed to this particular case, was where the drivers' leg was subjected to an excessive amount of acceleration due to the frontal impact, and this inertial induced type of load that caused the driver's leg to collide with the pedals. There were few other low torso injury-related accidents have been recorded as well, and largely caused by the cabin intrusion during the flexural impact. Many of the suspension components, such as alloy wheels, suspension arms and others were penetrating into the cockpit and therefore created damage to both race cars and its drivers.

The deadliest accident recorded was reached to 105.6G of peak deceleration. Later medical treatment revealed that the driver sustained a low torso joint fracture as well as pulmonary contusion, fortunately, the driver survived after. It is impossible to measure an exact number of decelerations to the driver because of the intrusion; hence it is very difficult and inaccurate to make the chassis deceleration rate to represent the drivers' acceleration. It is analysed that the average deceleration rate of 53G was estimated during the impact while the chassis is deforming.

It is realised that the nosecone located at the front of the race car is extremely effective in control the deceleration speed. It consumes and transfers little to none of the residual impact force further to the driver. Because of these findings, in 1993, the Indy 500 regulation amended the design of the nosecone that in order to achieve specified impact load and also extended the chassis with additional 12.7 cm for the driver's feet. There are no further cases reported that the driver sustains low torso injury such as legs and feet, or an intrusion injury during the frontal impact.

1.5 Crashworthiness-domestic application

As the previous section described, safety-related features were populated within the motorsport application to protect its drivers. The motorsport field requires advancement to all aspects of the vehicle, which requires not only the powerful drivetrain and good aerodynamics, is but also equipped with safety features, both active and passive. However, the implementation of those safety features, particularly the bumper system was somewhat very slow.

"Content removed due to copyright reasons"

Figure 1.21 Five mph damage-free bumper beam design (Automobile-catalog, 2010).

Needless to say, the main function of the vehicle bumper beam is to protect the body of the vehicle during the minor impact, such as manoeuvre in and out of the tight parking spot. At the beginning of the 1900s, automotive manufacturers start to fit the bumpers on vehicles. They were commonly sold as accessories for the customer who is going to purchase the vehicle. It was more of ornamental purpose and less of safety concern if the vehicle is subject it to crash. In the end, the bumper beam has to serve the purposes of aesthetics, aerodynamics, and safety. Figure 1.20 showed historical vehicle safety design: the chromed metal bumper was made in a convex shape, and mounted away from the vehicle to achieve energy absorption during the impact. This also served to reduce the repair or replacement costs due to damaging much more

expensive parts behind the bumper beam, such as headlight, grille and bonnet. Over the years that regulations, environmental concerns, material development and aesthetic evolved significantly which shifted the manufacturers to focus the emphasis on reducing the fuel consumption and increasing the safety and aesthetics. In the early of history of vehicle manufacturing, due to the limited knowledge to produce the bumper beam and fascia with plastic-based material, as well as different aesthetic and public appreciation purpose with less consideration to the safety factor, the bumper beam was designed and fitted to the outside of the main vehicle's body and normally does not come with the car. Vehicle owners have the free will whether it is decided to retrofit the bumpers back on to their cars after they have purchased them.

A pioneering Czech automobile maker was the first-ever fitted the bumper to their manufactured vehicle as early as 1897. The build quality of those fitted bumpers was badly enough only to emphasize the cosmetic without any safety concerns. Other owners use longer spring bolts to replace the short factory fitted bolts, or sometimes to drill additional holes of all, which enabled them to retrofit the bumper. Apart from the complicated installation process, vehicle owners have also a number of problems to deal with after. Such as metal made bumper started to rust after a post-installation period., bumpers rattle while the vehicle is on the road, poor overall mechanical practice made it offers little to no energy absorption capability. G.D. Fisher registered a patent - made the installation much more convenient by produced a mounting bracket that reduces the complexity of the installation process (Beecroft, 1924; Timothy, 2016).

During the mid-1910s, while the retrofitting the bumper to a car is a popular trend, while large numbers of manufacturers still offered either not available, or as an optional to fit the bumper to the car. Very few automobile manufacturers were started to fit the bumper as standard equipment by the factory, but only with a simple strip of metal either located at the front or the back of the vehicle (Davis, 2010).

Later at the 1920s, factory fitted bumper has finally reached a common practice where most of manufacturers offering the front and back bumpers to be fitted to their vehicle as standard equipment. Manufacturers gradually started shifting the focus from the aesthetics towards functionalities, which made the vehicle design considerably more complex. Over the many

years of vehicle production, the vehicle's bumper still didn't evolve itself from being basic horizontal steel bars fitted either front or back, with a slight curvature to follow the front-end structure of the vehicle.

"Content removed due to copyright reasons"

Figure 1.22 Aesthetic polished metal bumper bar (Timothy, 2016)

Until the 1950s, bumper appeared as chromed to show its presence as many manufacturers started to use other chromed parts, together with chromed wheels, windscreen bezels and mirrors to suits for the consumer's taste as showed in figure 1.22. This was to address the purpose of sportiness, as well as aesthetics.

"Content removed due to copyright reasons"

Figure 1.23 Common 1970s vehicles with chromed oriented parts (Timothy, 2016).

The manufacturers overemphasized the exterior design and style. Consequently, the repair or replacement costs increased when the vehicle was involved with the crash event, and still performed poorly in the event of a crash. The vehicle bumpers safety did not receive equal attention when compared with the factor of aesthetic until 1971s, where the USA officially initialled vehicle bumper regulation which explicitly required the amount of protection that a bumper has to provide. According to the United States Federal motor vehicle safety (FMVS) No.215, it is compulsory that the front and rear bumpers fit the automobile manufactured after the model year 1973, which is made compulsory to pass some specified bumper crash tests. Specifically, during the test speed to 5 miles per hour(mph) (~ 8 km/h) for the front bumper, and 2.5 miles per hour(mph) (4 km/h) for the rear bumper, both must prevent the headlights, taillights, fuel system components and other safety equipment from damage during impact.

Manufacturers were quickly shifted their focus into making the bumper to satisfy regulations. As indicated in Figure 1.24, Chevrolet made the model Corvette fitted with rear plastic bumper cover to hide the metal bumper inside to satisfy all needs (i.e. aesthetic, aerodynamic, as well as crash safety).

Figure 1.24 1974 Chevrolet rear plastic bumper cover (Timothy, 2016).

The regulation No.215 by FMVS was revised at 1974s. No damage to the above-mentioned parts while crash test impact from any angle became legal requirement.

“Content removed due to copyright reasons”

Figure 1.25 Bumper revision from 1971(left) to 1974(right) for the safety purpose (NHTSA, 1997).

Regulation No.215 became more stringent where it has been updated once again at the later year of 1979. This time all body panels on the vehicle must be intact with same impact speed, and angle rather than just exterior details, such as lights and grills. In the manufacture year of 1940 onwards, bumper allows to sustain a certain amount of damage, but any other safety equipment, such as headlight, taillight, fuel system and body panels should receive no damage.

The revised regulation has an dramatic effect on how manufacturers design their bumper system (see Figure 1.24). The red vehicle was a 1971 model produced by Chrysler, front chrome metal bumper was integrated into the front-end design, and rear metal bumper contained the taillight inside. Such a design has the front and rear bumpers integrated into the body of the vehicle which enhanced the aesthetics. This however will lead to large damage where bumper did not satisfy the primary function-to absorb the impact energy, and to protect other nearby safety components. Consequently, headlight and bonnet are more likely to be damaged, as well as rear taillight which will be deformed due to it located inside the rear bumper. These types of bumpers fitted to the model year 1974 was generally re-designed. Both front and rear bumpers were further extruded away from the vehicle body to further enhance

its energy absorption capabilities. The rear taillight has been re-located to the top of the bumper, and hence to satisfies the minimum repair costs.

“Content removed due to copyright reasons”

Figure 1.26 1974 Safety bumper design offered by Fiat(left) and Ford (right) (Timothy, 2016).

In order to satisfy the revised vehicle safety regulation at 1974s, manufacturers were increased the size of the bumper size in order to increase the contact area. Figure 1.25 illustrated two main streams of how manufacturers were adapting the new regulation. Left picture was 1974 model Fiat which featured the actual bumper was mounted further away from the rear of the car body. A metal bumper shall with plastic made corner protection piece was mounted with shock absorbers. Emphasis the energy absorption capability had been pursued while maintaining the body panels with no damage. In addition to this, the right-hand picture indicated that Ford LTD II model year between 1977 to 1979 equipped with enlarged front and rear metal bumper cover. The wider bumper than the body of the car was designed to avoid damaging the body panels. At this point, the factors such as lightweight, fuel-efficient, and aerodynamic are slowly receiving the attention from the manufacturers. During the 1980s where some manufacturers were researching the possibilities of using plastic material as the exterior cover to hide the metal bumper inside.

“Content removed due to copyright reasons”

Figure 1.27 1980s model Mercedes crashworthiness bumper system (Timothy, 2016).

The government established the vehicle safety regulation to emphasize heavily on the safety factor during the aftermath of the oil crisis from 1973 to 1979. The vehicle manufacturers were driven to look for a better design of bumper that shall achieve good aerodynamic stability, lightweight made to save the fuel, as well as safety. Figure 1.26 showed the 1980 Mercedes was testing the new plastic made front and rear bumpers fitted to its s-class with the design aims of better aerodynamic and safety. This design still required a layer of the metal part to strengthen to maintain the rigidity of the bumpers. The advantage of fitted plastic bumpers was quickly adapted by the manufacturers, as the chrome metal bumpers were gradually phased out of history which still appeared in modern SUV models. Having a plastic bumper cover allows manufacturers to develop better aerodynamic performance, as well as to improve the aesthetic to suits their individual needs. For the safety aspect, metal bumper has been hidden inside the bumper cover to provide additional support. It can be made with lighter and stronger material, such as aluminium or composite. Aluminium bumper beam product was common with no filling material inside, but with polystyrene foam or honeycomb structure in between the cover and beam can help absorb the impact energy.

1.6 Bumper system Construction

However, this report believes regardless the number of safety features equipped by manufacturers or how well does the bumper system iterated, during most of the crash events, the car's front and the rear bumper system are first to impact in the majority of cases (Davoodi, 2011). Rather than a simple rubber or plastic cover in the past many years, the modern bumper system consisted of many sub-components.

Figure 1.27 below showed a modern car's bumper system assembly located at the front and rear of the car. Undertray (1) and bumper fascia (2) both made from polyurethane material were to serve the purpose of providing better aerodynamics. The foam insert is made from polystyrene (3) which inserted into the back of the bumper fascia absorbs the most of the impact energy during the low-speed impact. Both of them will absorb further high impact energy dissipation that it structural steel made cross-member (4) and energy absorber (5) located behind it. Mainframe (6) is made of ultra high strength steel (UHSS) and serves as a force induction channel which diverges excessive amount of impact force to the compartment. Nevertheless, it also provides a mounting point for engine or gearbox and further joint by chassis frame member.

“Content removed due to copyright reasons”

Figure 1.28 Vehicle exterior, front, main bumper components (EPC, 2010).

It is expected the crashworthiness performance of entier bumper system regardless of the impact speed. The front end of a car will need to be robust enough where foam insert and bumper fascia will absorb the small amount of energy under low-speed impact without causing any further damage to the vital components located behind, such as Radiator, Intercooler, and condenser, etc. Whereas in the case of high-speed impact, the foam insert and fascia will direct the impact force around the bumper, where cross member and energy absorber must also be capable of deforming completely to dissipate the significant amount of impact energy during the event of the crash. This led to believe that there are plenty of improvements on how to design a bumper car system. This theory is proved by many past types of research, such as uses the composite material to replace the conventional metal bumper part to achieve both improved crashworthiness and lightweight (Belingardi *et al.,* 2015). Shape optimisation of the bumper beam profile (Belingardi *et al.,* 2013). In addition to all the above investigation, frame member behind the bumper beam and energy absorber was also investigated as well for a possible hybrid material replacement for crashworthiness improvement (Zhou, *et al*., 2011).

1.7 Legislations and guidance

Crashworthiness tests are conducted before the car starts to sale. While complying with all the enforced crashworthiness tests required by local legislation. However, particularly in European countries, implementing a new law is costly and time-consuming due to the scale of European countries, and many amendments and final agreement are required; therefore, it reduces the flexibility of the legislation, this leads to no further incentive to improve. The third-party such as Euro-NCAP or IIHS is adapting any newer changes to provide a continuous improvement by regularly enhancing its assessment procedures to stimulate further improvement in vehicle safety (Brain, 2011).

1.7.1 Euro-NCAP crashworthiness test guidance

"Content removed due to copyright reasons"

Figure 1.29 Types of Crashes conducted by Euro-NCAP (Euro-NCAP, 2010).

Regional Institute such as in the European countries, Euro-NCAP was established to perform crashworthiness tests independently and publish the results. Euro-NCAP has a very comprehensive assessment method to ensure the best knowledge learned, full data acquired during all impact tests while is concentrated into their rating system. Figure 1.28 above displayed the Euro-NCAP uses six types of crashworthiness tests; all the test results then will be concentrated in a rather simple, a five-star rating system which is to represent the level of protection.

1.7.2 IIHS crashworthiness test

Similarly, in the U.S.A, for the purpose of scientific and educational use, Insurance Institutes for Highway Safety (IIHS) was formed in 1959 where it's an independent, non-profit organization dedicated to reducing the on-road injuries, deaths and property damage from car crashes. The purpose of this institute establishment is to research on both accident avoidance and vehicle crashworthiness. IIHS has evolved four types of crashworthiness test to determine the level of safety to a car.

Figure 1.29 demonstrates four crashworthiness categories offered by IIHS. Results scores are added together, and the vehicle is categorized into Good, Acceptable, Marginal, and Poor.

Figure 1.30 all types of Crash test conducted by IIHS (IIHS, 2010).

Despite both E.C.E and NHTSA was the legal requirement, instead, Euro-NCAP and IIHS tests are much more comprehensive and stringent when compared with. Both Euro-NCAP and IIHS tests are not compulsory, and therefore, it's not required for the car to be sold on the market. Brain argued the third-party organization acts to supervise the vehicle manufacturers from the positive way. By doing so, regular test results releases will either benefit the consumers to shop for safer cars and pursuing manufacturers to produce safer cars as well. However, the Euro-NCAP is concerned at the best possible crashworthiness outcome which it has the testing speed

of 64km/h when compared with E.C.E standard, which has the minimum legal requirement at a speed of 56km/h (Brain, 2011).

This responsibility is a key factor that drives manufacturers to design better structures, implement new and lightweight material, advanced technologies on to their cars altogether to minimise the chance of onboard passengers' injury rate and hence to achieve highest possible safety standard. Nevertheless, IIHS claimed they had reached this goal since the establishment of an institute, where the number of people killed on roads in the United States remained relatively high. Nevertheless, since 1979, despite the population and some miles travelled this trend has fallen each year gradually, mainly it is contributed by the improvement of the road conditions and also safer vehicles (IIHS, 2016). This report is partly agreed with this point yet, in recent years, the car safety-related technologies and inventions have all been progressed significantly. This report partially agrees that the current trend of car safety, where manufacturers do not want to be limited by passive safety. Such as the presence of seat belts and airbag, but the presence of more active safety equipment on-board enhanced the car safety further, and recent inventions include lane departure warning system, automatic brake system, active radar cruise control, and night vision (Euro-NCAP, 2016; IIHS, 2016). Nevertheless, a real car accident could be a lot more serious when compared with test results in the laboratory. Therefore, both tests offered by Euro-NCAP and IIHS are most useful in comparing cars, rather than proving an absolute car safety value, thereby aiding the customer in determining the relative safety of each vehicle.

1.8 Crashworthiness Test-Dynamic

The crashworthiness of bumper test is widely dominated by either Physical crashworthiness analysis or computer-aided Finite element crash test simulation. Before the advent of computer simulation, material crashworthiness tests were the only option. Material tests are a straightforward and objective crash test for cars during the research and design phases. To perform a real crash test, manufacturers will require designated crash environments. An empty runway provides sufficient acceleration; different type of impact targets with different weight. Meanwhile, special equipment is necessary since the car will need to be either towed or pushed towards the impact object at a certain speed or, at a different angle. On top of this, electronic devices such as sensors, computers, and others are essential to measuring all correct readings from the car after the impact of post-crashworthiness analysis, re-design and further improvements. The manufacturer will consider many scenarios where the car will crash with,

the parts or the assemblies also need to be produced in quantity and to be tested repetitively determine the best combination. Parts or assemblies can be therefore optimized in this way to find the most optimized combination. In physical crashworthiness test, test car can only be used once every time. The test sample such as parts, assemblies or complete cars will be destroyed after the test. Therefore, test samples will lose its economic value. The Development cycle of which, crash test, re-design and re-test again will take the significant extended period of time and costs as well. Consequently, physical crashworthiness appears less efficient considered from the time, cost and labour perspective.

1.9 Crashworthiness Test-FEA simulation

Computer-Aided Design (CAE) and Finite Element Analysis (FEA) has been used to an assisted car manufacturer. During the early development of Computer-Aided Simulation for crashworthiness test, the simulation results were limited due to the low computational capabilities. Also, lack of progress to the core theory, consequently, to simulate complete car simulation were tough to perform, sometimes almost impossible were only a few less complicated simulations to local design were able to perform, and the speed and the accuracy of the simulating process were therefore affected. Consequently, the overall advantages of CAE and FEA simulation have not been fully explored and demonstrated, therefore, didn't meet the manufacturer's needs. Because the computer science progressed vastly that the hardware and software capabilities have all been increased dramatically in the recent decade, this rising trend made CAE and FEA simulation widely used, accepted and became the very feasible solution to the car crashworthiness test within the automotive industry.

CAE and FEA simulation method have many advantages when compared with the conventional physical test. Primarily, model computer drawing replicates the models involved during the crash test at 1:1 scale. The material, historical detail is also produced and further manipulated as well to suit individual needs based on the design parameters. Secondly, it does not require any physical equipment to be presented and therefore saves time and costs. Thirdly, the new product lead time can be shortened significantly because all aspects of test-related will perform at the earlier stage of the development period. It benefits the design team to achieve comprehensive background knowledge without producing significant numbers of prototypes. Consequently, the end product quality is expected. Furthermore, simulation progress is repeatable since all parameters are highly customisable, a design team can repeatedly fine-tune the specific parameters until it satisfies the design purpose.

“Content removed due to copyright reasons”

Figure 1.31 Possible Probe deployment (Costas, 2014)

Moreover, the physical crash test where cameras and sensors have physical limitations. For example, at Figure 1.30, the stress limit of the frame member during the impact process, or, the deformation behaviour of energy absorber is all located in the tight engine bay. Such data is critical for frontal crashworthiness optimisation, where FEA simulation enables the design team to deploy probes or sensors right in the middle of the material to give a very accurate result.

1.10 Challenges of the current bumper system

The primary function of the bumper system is to absorb impact energy within the intended designed speed range. The previous section demonstrates the location and the main components within the bumper system integration as well. The manufacturers take the advantages of advanced plastic injection moulding and metallurgy to make an integrated bumper system. To achieve both aesthetic (appearance) and functionality (aerodynamic and impact-resistant etc.), the integration of the bumper system has been revised for many generations, from the original heavy metal exposed and fitted to the outside of the vehicle, and plastic bumper used on Mercedes S-class for both aerodynamic and impact-resistant, until the very recently well-integrated bumper system.

Due to the currency inflation, raw material shortage, and increasing cost of labour, it gets more and more expensive to develop and produce the bumper system (Muhamad, 2008). He argued because the aesthetic and legislation purposes, manufacturer has to design and integrate the bumper system. This will fully explore the integration and every single component within the

bumper system work together harmoniously to achieve maximum energy absorption during crash process. This substantially increased the working effect between each component and resulted in an unavoidable collateral damage. Furthermore, Muhamad (2008) specifically criticized that higher development costs indeed perform well in the legal crash tests and real-world crashworthiness scenario. But the damage repair is very painful and very awkward to accept for the vehicle owner in the likelihood of a crash event.

Other similar concepts have been investigated and tested, whereas the integrated bumper system includes few transversely fitted bumper beam, crash box and impact-absorbing foam. This system was made lightweight for better fuel economy. Increasing the thickness, width or the length of the metallic made beam will increase the weight and dimension of the bumper system, but also costs more to produce during the manufacturing process, and to repair or replace after the vehicle is subjected to crash event. Nevertheless, the bumper beam is the main component undergoing deformation as soon as the vehicle collides with another object. It is an ideal scenario to maintain the same crashworthiness performance and to explore the possibilities of using alternative lightweight material (Belingardi *et* al., 2014).

Throughout every generation of improvement, the manufacturers intend to gain more energy absorption rate during the crashworthiness test process, while saving the weight to achieve better fuel consumption. It is inevitable to require placing additional material at the increased thickness then manufacturing into crash purposeful shape. Consequently, the integration process gained additional weight and exterior size that may not be able to satisfy the fuel consumption and exterior appearance. However, to compensate this gained additional system's weight, lighter metallic material can be deployed to achieve similar impact-resistant performance. Furthermore, the internal shape and cross-section of the bumper beam, as well as the urethane foams will need to be re-designed and re-located to satisfy needs of appearance as well as aerodynamic requirement. Nevertheless, when material replacement and re-design satisfied both needs for aesthetic and functionalities, it usually incurred with additional labour hours. This will ultimately increase the costs of the model development and may delay the development process. Therefore, it is not surprising that the good bumper system design is an acceptable trade-off between without the increases of weight, which resulted by placing more material, with increased thickness, meanwhile, satisfies the functionalities of aerodynamic and crashworthiness, still aesthetically pleased to look.

1.11 Alternative design of bumper beam

The challenges in the bumper system design can be roughly categorised into two main areas, weight reduction, and crashworthiness performance. Previous displayed bumper system assembly (Figure 1.27) has identified the location and the importance of the bumper system, more investigation shall focus on the benefit of weight reduction to the bumper system and factors dictating the crashworthiness performance.

1.11.1-Weight reduction the weight of the vehicle will exert a negative impact on vehicle performance, such as fuel economy, fuel range and acceleration. Yamane and Furuhama (1998) particularly focused on the fuel type as impact factor, and included petrol, electric and hydrogen into the comparison. It was found that electric vehicle suffered the most because the 300 kg of fuel module carried on-board (i.e., only travels 55km distance). Hydrogen vehicle with liquid hydrogen module achieved approximately 400km of driving range despite the fact that its hydrogen tank is 100 kg **(**Yamane and Furuhama, 1998)

Table 1.2 Weight comparison to hydrogen and battery equivalent of 30L petrol (Yamane and Furuhama, 1998).

Fuel type	Fuel		Tank wt (kg)	Total wt (kg)	Reference
	Vol. (l)	Wt (kg)			
Gasoline	30	22	5	27	[6]
Hydrogen					
Liquid H_2	115	8.2	65	73	[6]
Metal hydrides		8.2	764	772	[6]
Light high pres. container	348	8.2	265	273	[7]
Battery*			1360		[6]

* Assumption: The energy density is 40 Wh/kg and the power conversion efficiency is 5 times as large as that of gasoline

The first observation from this table is that the weight of the fuel and fuel tank was the primary reason for the reduction in fuel economy. The economy is reduced by 6% when the total weight of both fuel and tank is 100 kg. This economy figure is further lowered by 32% when the total weight of both fuel and tanks is increased to 700 kg. A significant 48% of the economy is lost when the weight is increased to 1400 kg. This reflected 73 kg of liquid hydrogen tank has less impact on the driving range than the metal hydride and battery module. In terms of driving range, it is found the storage methods is the main factor.

A battery-driven vehicle can practically only take 300 kg worth of battery, which only yielded 55km of a range that is similar to the city driving scenario at a period of 8 hours. It is less practical if the driving range of 100 km is needed, a rather heavy 650 kg worth of battery. This made battery-driven vehicle less competitive and attractive to both manufacturer and customer. Slightly better metal hydride storage vehicle can achieve 100km of range equipped with 300 kg metal hydride battery. Doubled range of 200 km resulted from 770 kg of metal hydride battery-equipped as this reached to 50% weight of the vehicle. Liquid hydrogen, however, can achieve comfortably 400 km of the driving range with 100 kg of hydrogen and tank combined.

The combined weight of fuel and tank largely effect on both vehicles acceleration. It is found weight significantly reduced the vehicles acceleration ability. When uses 2nd, 3rd and 4th gear as a starting point, the total weight of 100 kg, 700 kg and 1400 kg all yielded lowered acceleration rate at 22%, 28% and 31% each other individually. The acceleration time under the same total weight configuration at the same shifting gear is 8.45 seconds, 5.26 seconds and 3.89 seconds respectively. Generally, it is acceptable for a vehicle takes 5 seconds to accelerate from 80km/h to 100 km/h. Under this factor, vehicle configured with 100 kg and 700 kg of total weight are recommended to use to 2nd gear to start the shift. If higher shifting point, such as 3rd gear is required to complete the acceleration within 5 seconds, it is suggested that the total weight of 100 kg is the maximum limit.

The main concern of the above study was focused on the driveability of a vehicle due to the weight reduction, others have looked into the crashworthiness perspective. Because the bumper beam is the key components from the entire bumper system, and it absorbs impact energy during the crash, it is proposed to further enhance its energy absorption capability as well as weight reduction. It is worth mentioning that the weight reduction should be based on the precondition of vehicle safety and crashworthiness. Therefore, any design of front bumper system must be thoroughly investigated before proceed to the manufacturing stage (Feng and Feng 2002).

With development of composite material, it has been increasingly proposed as alternative to conventional steel counterpart. From the literature, the conventional metallic made bumper is always tested first to establish the baseline performance. Similar literature by and utilised the

advantage of composite material instead of conventional metallic counterpart. It explained specified thickness to the bumper beam did not fail during the pre-determined impact condition, with additional weight gained during the production gave the clear reason that the traditional metallic material was not considered since it increased the total bumper system weight by 500% when compared with its composite made bumper beam. It indicated both GMT (glass mated thermoplastic) and SMC (sheet moulding compound) are the ideal candidate to make the bumper beam from the perspectives of manufacturing easiness, economical, weight reduction and improved impact behaviour (Marzbanard *et al*., 2009). To confirm composite made beam is indeed valid bumper material, a 4.0 km/h impact test was performed with 3 metallic reference material, namely steel, magnesium and aluminium. They are assigned to the bumper beam to establish the baseline crashworthiness performance.

Figure 1.32 Crashworthiness results from proposed material, Magnesium (top left), Steel (bottom left), Aluminium (top right), force reaction (bottom right) (Mazabanard *et* al., 2009).

Metallic bumper results showed among of all 3 metallic material, aluminium made bumper yielded higher deformation area since it has lower stiffness. The impact velocities of aluminium made bumper appeared in higher value than both counterparts made of steel and magnesium. Because of this, aluminium made bumper beam has more contact area with the impactor and appears to deform more than the steel and magnesium. It is also observed from the force chart, while both steel and magnesium were very similar during the impact process, aluminium

achieved less peak force value, and the force curve lasted slightly longer than the other two materials. This means less force peak will help the vehicle to achieve better deceleration, and fewer components will experience violent deceleration and potentially getting damaged. Alternatively, both GMT (glass-mated thermoplastic) and SMC (sheet moulding compound) made bumper from short glass fibres which sized from 12-25 mm were proposed and tested.

Table 1.3 Material properties of GMT and SMC composites (Mazabanard *et al*., 2009).

Material	$E(GPa)$	ν	$S_y(MPa)$	$\rho\ (kg/m^3)$
GMT	12	0.41	230	1280
SMC	20	0.33	309	1830

It is found 3.0 mm GMT made bumper beam with strengthening rib failed during the test, it is later decided the ribs were removed but increased the beam thickness to 5.0 mm to prevent the structural yield.

Figure 1.33 Von-Mises distribution on the GMT made beam (Mazabanard *et al*., 2009).

The above contour map showed the Von-Mises stress distribution in the centre section after the beam thickness was increased. Most high stress was concentrated in the middle of the beam. It yielded a maximum value of 220.78 MPa, which did not exceed the maximum material yield strength of 230 MPa. A similar situation was repeated in SMC made beam, a thickness of 3.0 mm of a beam with strengthening ribs failed during the test due to the failure stress was higher than the maximum yield strength. Accordingly, all strengthen ribs were removed but the beam thickness was increased to 4.0 mm, the peak von-Mises stress peaked at a value of 306.04 MPa,

which did not exceed 309 MPa of maximum material yield strength. The GMT, Modified GMT and Modified SMC achieved 2.89 kg, 3.16 kg and 2.83 kg each other respectively. In comparison with other metal counterparts, composite bumper beam saved weight. The removal of strengthening ribs did not affect the crashworthiness performance of the bumper beam, where 4km/h impact test results showed the Von-Mises stress levels of both GMT and SMC made bumper beams were within the material limit and therefore satisfied both lightweight and improved crashworthiness (Marzbanrad *et al*., 2009).

Instead of focusing on the weight reduction and crashworthiness improvement to the bumper system at the local scale, other had investigated within the range of metallic materials only at the scale of the entire vehicle to determine whether it is possible to achieve both lightweight and crashworthiness need. It mentioned that the weight reduction as an important factor should be considered at the scale of the whole vehicle instead of only at the bumper system. The use of correct material combinations has a positive effect on both lightweight as well as crashworthiness. It looked into the issue of growing numbers of concern to the pollution caused by increasing numbers of automobiles on the road, and this has a direct effect to the manufacturers to produce greener vehicle in the near future. It considered weight reduction is the most effective method to overcome this problem, particularly 0.09 to 0.21km per litre fuel economy is achievable for every 57 kg of materials is saved (Han and Clark, 1995).

Weight reduction can benefit both fuel consumption as well as vehicle performance. It is usually speculated that there is a conflict between reducing the weight of a vehicle while increasing the passenger comfort and safety-related equipment on-board. Despite difficulties to satisfy both needs, the progress of optimising the conventional steel structure of a vehicle has come a long way and indeed achieved some improvements. New weight reduction method seemed to be always found for newer vehicle development. Evolved meteorology and emerging technologies helped manufacturer to fully utilise the benefit of high strength metallic material and sometimes, composite material.

Either to re-deploy or to replace existing metallic material or to use alternative composite material, they have all contributed to vehicle weight reduction significantly. Under the current development and progress, further improvement is achievable of using custom material and

material deployment. E.g. a sports model produced by Daimler-Benz is made from aluminium and die-cast magnesium. This lightweight design improved the handling of the vehicle but also saved the fuel cost and CO2 emission. To further analyse exactly how weight reduction can benefit the owner, a life-cycle vehicle energy consumption was displayed below.

Figure 1.34 Weight effect on fuel consumption and its distribution (Jambo and Beyer, 1997).

NEDC (New European Driving Cycle) fuel consumption cycle test showed in Figure 1.34 above revealed up to 54% of the fuel were used to move the vehicle. Clearly, the weight factor contributed more than 50% of total fuel consumption than other factors, such as aerodynamic rolling and others less important and attractive. In the earlier section1.5: Crashworthiness-domestic application, one of the reasons during the bumper beam design iteration intends to achieve better aerodynamic feature. Less drag is expected as a result of less fuel is used. However, based on the Figure 1.33 indicated, overall, the weight reduction shall be considered as priority factor since it contributed more than 50% of the total fuel consumption when compared with other factors (Jambo and Beyer, 1997). Figure 1.33 also suggested the body of the vehicle takes up to 27% in total material distribution when compared with other factors, such as suspension, interior and drivetrain are 27%, 21% and 25% each other respectively. Regardless of either to use different metallic material or the material re-deployment, the dependence on the metallic material will somehow reach its limit that further weight reduction will incur higher costs. Any optimisation process almost started from full steel body shell to establish a benchmark for further weight reduction target. During the body-in-white stage, minor or partly steel replacement can save up to 7% of the weight. To continue the weight improvement, most of the part are made of aluminium and can sometimes reduce 30% to 50% weight in bodyshell when compared with full steel counterpart. As emerging manufacturing

techniques and material advancement, it is possible to use fibre reinforced composite material. To further emphasize the relationship between the weight optimisation with correspondent costs, Figure 1.34 below clearly showed for each desired weight reduction tier into the bodyshell design, there is a correlated price increase. Hence it is important to find an acceptable point of between the price and the material usage which is the main concern to the manufacturer.

Figure 1.35 Design concept of weight reduction VS cost matrix (Jambo and Beyer, 1997).

Since the costs reflect on the usage of lightweight material, newly developed material and production methods can be implemented to improve safety requirement as well as to lower the costs. It used model's development as for an example and demonstrated which part of the vehicle is suitable for lightweight material, and the availability on both materials and manufacturing techniques.

“Content removed due to copyright reasons”

Figure 1.36 Lightweight material application on the roof and seat construction (Jambo and Beyer, 1997).

The lightweight aluminium usage on the SLR (Sport leicht rennsport) model, particularly the removable rooftop has achieved 52% weight reduction but incurred additional 30 DM (Deutsche Mark) per kg of reduced weight compared to steel model since the full-aluminium design also incurred significantly higher costs. Magnesium was also used to make seat frame shown on the right side in Figure 1.36. As a result, each frame yielded remarkable 8 kg of weight without sacrificing any safety requirement. The seat restraint system requires strict impact requirement and it has to maintain high stiffness throughout the crashworthiness test.

“Content removed due to copyright reasons”

Figure 1.37 Roof construction of SL model sports car (Jambo and Beyer, 1997).

Figure 1.36 displayed the weight difference when produced with varies material types. While the standard steel part was the heaviest at 6.7 kg, direct replaced with aluminium reduced this figure to 4.0 kg. Although the same panel can be only 3.0 kg if it's made from aluminium-foam, which is a 50% weight saving than the steel counterpart, the production still admitted the higher cost and accepted the magnesium as a suitable candidate for production.

"Content removed due to copyright reasons"

Figure 1.38 Production methods of C-class (Jambo and Beyer, 1997).

Different production methods can also influence the weight of the door assembly during the production process for the C-class. As shown in Figure 1.38, the production method was switched to die-casting only gained 0.6 kg of weight. All the above-elaborated features focused on the relationship between the weight reduction and its correspondent cost. The manufacturer did not just consider heavily the lightweight concept but implemented extensively as well. Production method also appeared with certain limitations, such as a thickness limits to casting the thin-walled parts that between 1 to 1.5mm, a die-casting method is, therefore needed. Die-casting method can achieve high integration with less joint needed and fewer costs, but it requires an auxiliary heating process to the magnesium sheet prior to the casting process, and this indeed comes with additional costs as well. It further mentioned corrosion can occur if the magnesium in contact with other metallic material, it resulted in a layer of plastic film or hard coating is necessary.

1.11.2 Frame rail material Except the weight saving, vehicle safety must also be satisfied during the weight optimisation process. It is noted that the weight optimisation must consider the crashworthiness requirements, and design closely to meet the crash test. It explained from the picture showed below:

Figure 1.39 Curved and straight front frame rail of A-class (Jambo and Beyer, 1997).

To fully utilise the potential of new lightweight material, a cross-section of Mercedes A-class was used to demonstrate the crashworthiness results for both profiles of the front frame rail. The curved profile, which was commonly fitted to other vehicles, yielded higher strength due to the bending motion when the frontal area was subjected to impact. Either thicker material is required, or additional strengthen piece is needed in order to compensate this natural disadvantage. On the other hand, a straight profile frame showed promising result when compared with a curved profile, when only sustain both tensile and compressive stresses during the impact process. Further experimental work focused on the possibility of substituting the aluminium with composite material was performed especially for crashworthiness purposes.

Figure 1.40 Curved and straight front frame rail of A-class (Jambo and Beyer, 1997).

Axial impact test result revealed while the aluminium has positive advantage on energy absorption structure over the steel, composite material, both SMC (sheet moulding compound) and reinforced plastic with oriented fibres, in this case, have demonstrated twice much of the energy absorption over the aluminium as a good performer. With the fact of 50% of weight reduction on the top of the doubled energy absorption made metallic material less competitive. The unique material property provided the composite has very high specific stiffness and strength than its metal counterparts, hence made it a potential candidate from both weight reduction as well as crashworthiness performance on some of the critical area during the vehicle development phase (Jambo and Beyer, 1997).

While many of the vehicle parts are made from a metallic material, alternatively, composite materials used for vehicle production were also extensively discussed and studied. It reported glass mat thermoplastic (GMT) material is a promising material since it has good mechanical behaviour as well as energy-absorbing capability, and there are increasing numbers of attention focused on to use such material as a metallic substitute (Marzbanrad *et al*., 2009).

1.11.3 Energy Triggering mechanism The advantages of controlled structural deformation were demonstrated and highlighted briefly in the previous paragraph. Underlying triggering mechanism was studied in other literature (Khalid and Qrimli, 2016). The main reason to build the energy triggering mechanism into the geometry is to induce the impact load via the plastic work of the geometry's deformation. This is very important when the vehicle is subjected to severe axial impact load. This energy inducing profile is built to deliberately reduce the structural integrity of the geometry, to ensure the geometry collapse into a controllable manner. The smoother of this process exhibits, the less violent of the deceleration rate will be.

"Content removed due to copyright reasons"

Figure 1.41 Bi-metallic rectangular thin wall tube under different trigger mechanisms (Khalid and Qrimli, 2016).

A 54.0 km/h axial crash test was performed via FEA simulation. This work indicated a few important parameters to evaluate whether the geometries has good crashworthiness performance. Those parameters include overall geometry deformation behaviour, Force reaction, crush force efficiency (CFE), failure modes throughout every stage of the FEA simulation. Some purposely built geometries can achieve good energy absorption rate as well as deformation behaviour, Figure 1.41 illustrated 4 types of proposed initiators that were implemented into the FEA simulations. The deformation process of the geometry converted the kinetic energy via plastic deformation, which is initiated by its energy triggering mechanism. Hence it is necessary to build the geometry with a suitable triggering profile to ensure a very smooth energy absorption process without any significant fluctuations.

Table 1.4 Different initiator types of crashworthiness parameters values (Khalid and Qrimli, 2016).

Trigger types	Absorbed Energy (kJ)	Peak Load (kN)	Crash force efficiency
Without trigger	24429	226	0.466
Bead trigger	21280	222	0.489
Ellipse trigger	23753	214	0.491
Circular trigger	23269	225	0.475
Triangle Trigger	24073	224	0.479

“Content removed due to copyright reasons”

Figure 1.42 Load VS displacement curves for all initiators (Khalid and Qrimli, 2016).

“Content removed due to copyright reasons”

Figure 1.43 Initial peak load values of the four initiators type (Khalid and Qrimli, 2016).

Figure 1.44 Crash force efficiency values of the four initiator types
(Khalid and Qrimli, 2016).

Figure 1.45 Energy absorption values of the four initiator types
(Khalid and Qrimli, 2016)

Figures 1.40 showed 4 types of energy initiators, namely 1: Bead, 2: Elliptical, 3: circular and 4: triangular. They are all tested under the loading conditions then compared against the parameters whether to determine the suitability of acceptable energy triggering mechanism. A baseline geometry was also created and tested to establish the benchmark. Figure 1.41 and 1.42

demonstrated the reaction force over the geometry displacement. For all 4 triggering profiles, circular types achieved the lowest peak load value (i.e. 214 kN), and also circular type appeared to be a smoother trend throughout the crushing displacement. The other 3 types response were fluctuated. Figure 1.43 showed the crash force efficiency of all 4 types of profiles design, which was an indication of the deformation process stability throughout the simulation. Circular profile achieved the highest efficiency, which was 0.50, where elliptical profile came slightly lower at 0.49. Triangle profile achieved similar efficiency when compared with no triggering profile inbuilt around which was around 0.48. Bead been the worst profile only reached 0.47 among the lowest efficiency when compared with all others. Finally, Figure 1.44 showed the energy absorption of all 4 profiles. Without any doubt that the bead profile achieved the lowest energy absorption rate where only 21kJ. Other Profiles such as elliptical, circular, triangle have all reached similar values without any significant difference when compared with no initiator inbuilt.

Similar research conducted both static and dynamic axial crush tests were investigated based on the square column (Ghani and Hassan, 2013). Some critical parameters focused to determine the crush performance such as Initial peak force (IPF), crush force efficiency (CFE) and specific energy absorption (SEA) were carefully examined. Again, this study had implemented implement such a trigger mechanism built into the geometries for axial crush so that failure was induced in a controlled manner. This resulted in a much more desirable deformation behaviour and this led to less pressure to its occupants. This study selected the square column as test sample it is because the material is relatively continence to acquire and fabricate and its excellent potential energy absorption rate. This potential can be optimized by adding the energy trigger mechanism as well as the selection of making the column, hence by going to a progressive buckling and deformation process, the trigger mechanism with these particular geometries will achieve good impact results and could be incorporated into automobile production. A tapered plunger impact head was proposed and fitted to the top (or front) of the square column.

“Content removed due to copyright reasons”

Figure 1.46 External plunger design on axial impact tube (Ghani and Hssan, 2013).

The above pictures compared with a plain square column to the alternative tapered plunger fitted to the top. The tapered plunger has been modified into 20^0, 30^0, 40^0 and 50^0 respectively, and all geometries have been simulated to obtain the results. Both models were subjected to FEA simulation under the drop mass of 28 kg at speed of 4.4m/s. To evaluate the simulation results, critical parameters, such as the specific energy absorption was formulated as:

$$\text{Specific energy absorption: } E_s = \frac{W}{V_\rho}$$

where $E_s$is the energy absorption to its unit mass, W total energy absorbed, V the volume of sample and ρ is material density. Crush force efficiency is, however, to determine the collapse force uniformly happening over the deformation period. The perfect efficiency value should be close to 100% as possible. However due to the design factors, materials, and production costs, at most axial crush will yield approximately 30% to 50% and it can be formulated as:

$$\text{Crush force efficiency: } \eta_c = \frac{F_{mean}}{F_{peak}}$$

where η_c represents the efficiency of the force, F_{mean} average force, and F_{peak} the peak of the force. Along with both parameters discussed above, the Initial peak force also shares the same importance as the peak force.

“Content removed due to copyright reasons”

Figure 1.47 Force and displacement of varies plungers’ angle (Ghani and Hssan, 2013).

“Content removed due to copyright reasons”

Figure 1.48 Deformation behaviour of all tube profiles (Ghani and Hssan, 2013).

Force over displacement results of all 5 tapered profiles showed that all profiles have higher initial peak load regardless of the angle of the taper, but soon followed with fluctuated force reactions throughout the simulations. All tapered profiles shared the similarity of initial fluctuated before reaching to their peak load except that the plain column profile had immediate peak load. Most proceeded further into steady structural collapse. Despite that the plain profile has very high initial peak load and quickly dropped back to similar force level compared with other tapered profile, the force reaction appeared uprising while all other tapered profile was declining until the displacement reached to 0.05m.

All 5 tests above demonstrated the geometry’s failure mode under the given load condition. In Figure 1.50 generally all 5 tests achieved progressive failure, where all initiated from the column started to bend inward, and gradually folded downwards as the plunger pressed

gradually. However, except the plain column, the tapered angle of the plunger influenced the folding behaviour. The folding initiated from the middle section with a plain column and progressing downwards of the column without any obvious uniformity.

In the dynamic crash test Figure 1.48 showed the IPF (initial peak force) obtained by plain profile column earned highest peak force which was almost 60,000N. Various other tapered column profiles achieved lower peak force value: the 20^0 taper profile brought slight improvement just below plain profile, while 30^0, 40^0 and 50^0 all yielded much lower initial peak force each other respectively. Those results indicated that the initial peak force reduces corresponding to the increases of the taper angle.

Crush force efficiency of the plain column has achieved just above 30%, whereas the 20^0 tapered profile yielded an even worse result which was below 30%. On the other hand, angle profile 30^0, 40^0 and 50^0 achieved relatively higher efficiency which was around 40%. Particularly the 50^0 profile achieved the highest efficiency of 43%. For the result of specific energy absorption, the plain column profile once achieved the highest value which is 11680 j/kg, while the taper profile of 20^0, 30^o and 40^0 all absorbed approximately around 11600 j/kg of energy. The lowest energy absorption (11550 J/kg) occurred to the 50^0 taper profile.

Figure 1.49 Initial peak force at various plunger taper angle (Ghani and Hssan, 2013)

“Content removed due to copyright reasons”

Figure 1.50 Crush force efficiency at various plunger taper angle (Ghani and Hssan, 2013).

“Content removed due to copyright reasons”

Figure 1.51 Specific energy absorption at varies plunger taper angle (Ghani and Hssan, 2013).

Table 1.5 Results of IPF, CFE and SEA at varies plunger taper angle (Ghani and Hssan, 2013)

	Plain Column	% change			
		20°	30°	40°	50°
IPF (N)	58610	-4.3	-33.8	-24.4	-27.4
CFE (%)	32.2	-9	+27	+19.3	+29.5
SEA (J/kg)	11684	-0.006	-0.005	-0.006	-1.1

By comparing the plain column with the tapered column, the above table 1.5 demonstrated that 30^0 profile made 33.8% improvement over the plain column. As for the CFE value, both 30^0 and 50^0 profiles have achieved much-closed improvement, which was 27% and 29.5% respectively. The SEA tests revealed that tapered angles apparently reduced negligible amounts of energy absorption which was between 0.005% to 1.1%. Based on the above all the results showed above, it can be concluded that using energy triggering mechanism will indeed improve the crashworthiness performance of tube geometry when subject to axial crash load. Considering the improvement made on both IPF and CFE overall 4 tapered profiles, the minor difference of SEA value can be ignored, and the 30^0 profile achieved all-round best performer out of all 5 test runs, which reduced 33.8% of IPF, and also successfully increased the crush force efficiency at 29.5%, hence the 30^0 tapered profile was the most suitable energy triggering mechanism to apply to squared column geometry if the design element considered it for axial impact load.

The energy triggering mechanism has also been investigated with the triggering mechanism inbuilt to achieve improved crashworthiness results for the helicopter. When the helicopter is subjected to vertical crush load, it is expected that the helicopter's fuselage to enter a steady deformation process in order to reduce the acceleration rate, hence created a less harmful environment for the occupant without sustaining any serious personal injuries. Kindervater and Deletombe (2000) focused on how to improve the crashworthiness by appropriately consuming and releasing the impact load brought to the fuselage. The primary contact areas, such as landing gears, the bottom of the fuselage were considered to be the sacrificial design to deliberately for crashworthiness purposes.

From the figure 1.54, the fuselage and the landing gears situated at most extremities of the main body of the helicopter, which are more likely to contact with the impact object during the contact. In this case, the bottom of the fuselage, the main structure of the helicopter has been selected to further enhance the energy absorption design. The diagram showed the energy-absorbing beam has been added to the main structure, and the subfloor was crossed joined in a boxed shape. In addition to this, two shapes of cruciform joints method have been created for the crashworthiness comparison.

“Content removed due to copyright reasons”

Figure 1.52 Crashworthy construction of helicopters Sub-floor (Kindervater and Deletombe, 2000)

It can be seen from figure 1.52 that the intersection of the cruciform made into two profiles, a squared centre on the left, as well as the conical-shaped on the right. Both samples were subjected to axial pressing with a rigid plate, at the velocity of 10 m/s. The deformation process of an intersection element design showed below. In figure 1.53, the bottom of the joint started to deform at around of 5 ms, the centre rounded design acted as energy triggering mechanism to initiate the impact process, followed with the further deformation at the upper half of the centre joint around 15 ms,.

“Content removed due to copyright reasons”

Figure 1.53 Embedded energy triggering mechanism (Kindervater and Deletombe, 2000).

“Content removed due to copyright reasons”

Figure 1.54 Embedded energy triggering mechanism (Kindervater and Deletombe, 2000).

“Content removed due to copyright reasons”

Figure 1.55 Force reaction versus deformation at varies samples
(Kindervater and Deletombe, 2000).

The force versus deformation result (Figure 1.55) showed the simulation results of the energy absorption process. The blue represents the rigid centre joint, and the red represents the conical centre joint with 10° pitch angle. In the presence of the rigid joint, the force incurred during the entire deformation length was stopped before 90mm, initial peak load over 40 kN happened at early 10 mm of deformation. On the other hand, the 10° conical joint intersection maintained the energy absorption until the deformation reached to 120 mm without any significant fluctuations. The conical joint also produced peak load similar to the rigid joint but came in later deformation process, almost 30 mm. Based on the above observations, the rigid joint intersection design can’t absorb enough energy throughout the entire deformation process, which means the rigid intersection experienced with geometry fracture and led to uncontrolled

deformation behaviour. Since the geometry didn't deform as the design intended to, it almost lost the ability to absorb energy towards the end of the simulation. Whereas the conical joint, which was equipped with energy triggering mechanism, still produced an initial peak load upon the initial contact. This aided the deformation process, by regulating the deformation behaviour which allowed absorbing impact energy after 80 mm and carried on at a relatively steady trend. Due to the energy triggering mechanism is benefiting the local intersection joint when is subject to axial impact, it also has been implemented into the sub-flooring joint design as well.

Figure 1.56 Embedded crashworthy energy triggering sub-floor (Kindervater and Deletombe, 2000).

Figure 1.57 Contour plot of crashworthy sub-floor (Kindervater and Deletombe, 2000)

The test sample showed in figure 1.56 above illustrated, at each intersection of the subfloor

section, a conical shaped energy triggering mechanism was placed and interconnected with waved longitudinal plate to simulate one section of the subfloor. This geometry subjected to drop test with the mass of 501 kg added and velocity at 9.2 m/s. It can be observed that both side longitudinal waved plates were bending towards outside after the impact, while the top and bottom waved plates have experienced the deformation, but mostly exhibited concentrating at the bottom of the plates. Compared with the FEA simulation of the quarter section of the subfloor showed in Figure 1.57 Under the same loading conditions, the simulated quarter floor section exhibited similar deformation behaviour is compared with the physical drop test. The contour demonstrated the stress distribution on every single meshed element and appeared all concentrated at the bottom of the connecting plate and it showed similar damage results to the physical test (Kindervater and Deletombe, 2000).

1.11.4 Axial Impact test – The above investigation demonstrated of the introduction of energy triggering mechanism can increase the crashworthiness performance, particularly reducing the peak load, and increasing the energy absorption, and to aid smooth crushing process and therefore to achieve progressive deformation. It will be beneficial to integrate some energy triggering mechanism into the existing structure. Hu *et* al. (2016) looked into the case of how to improve the helicopter's survivability on both civil and military fields via the appropriate modification to the floor joint with energy absorption unit. The helicopter is largely involving in low altitude flying scenario, and more likely to expose to low altitude interference, such as high-level ground objects, such as power cable, bird strike, buildings. On the military use, low altitude flying mission also means the helicopter has higher probabilities of getting attacked via ground force. While to maintain the combat capabilities, the safety aspect of the onboard occupants shall also be well looked after as well. Most situations were most likely to involve the emergency landing, and possibly causes serious injuries or even death. However, this can be reduced to a minimum, if the aircraft overall structure is designed with good crashworthiness concept. Good crashworthiness aircraft will appropriately take the damage and absorb via structural deformation during the crash landing without passes it on to its occupants and this has become the main requirement for the helicopter design and construction. (Hu *et al*., 2009; Hu *et al*., 2016).

“Content removed due to copyright reasons”

Figure 1.58 Energy absorption unit (Hu *et al.,* 2016).

Figure 1.58 above illustrated the sub floor’s layout, as well as its construction. It identified the bottom of the helicopter is an ideal sacrificial area which can be modified to fit the cylindrical energy absorption joint within the subfloor construction in order to increase the crashworthiness performance. In addition to this, the energy triggering mechanism located on the top of the unit to ensure a progressive failure during the crash. The impact test was performed 5 times with the fibre orientation from 15 mm, 30 mm, 45 mm, and 60 mm and 75 mm, with a chamfered trigger at 45^0 for all samples, tube length of the tube remains same throughout the experiment at 125 mm.

“Content removed due to copyright reasons”

Figure 1.59 Results of all 5 profiles composite tube (Hu *et al*, 2016)

Figure 1.58 showed the impact test results of all 5 types of fibre orientations. The first diagram indicated the value of crush force efficiency (CFL) – the ratio between mean crush load (P_{mean}) over the maximum crush load (P_{max}),

$$\text{Crush force efficiency (CFL)} = \frac{P_{mean}}{P_{max}}$$

CFL ratio measures the effectiveness of energy absorption during the impact process and ideally shall be close to 100% where possible (Kim *et al.,* 2010). In reality, the general efficiency ratio was showing at an increasing trend which corresponded to the fibre degree increases. Where fibre orientation $\theta = 60°$ achieved the highest efficiency and the CFL ratio dropped when the fibre orientation reached to $\theta = 70°$. This indicated the sample with fibre orientation $\theta = 0°$ and $\theta = 15°$ were more likely to experience significant failure. The SEA diagram represented the specific energy absorption (SEA) of all tested samples. All 5 fibre orientations profiles achieved relatively good SEA value from 47.9J/g to 82J/g, regardless of its fibre orientations profiles. Peak load (P_{max}) indicated the deceleration rate of the impactor-based on the geometry. Peak load is is strongly related to how occupants can withstand the impact force. From the human tolerance perspective, this value shall be carefully controlled to avoid the serious injuries sustained by its occupants. It can be observed fibre orientation θ has a direct effect on the peak load value, where peak load dropped while the "θ" angle is increased. The $\theta = 45^{o}$ case achieved the lowest peak load. The overall energy absorption performance can be evaluated via the parameter of mean load (P_{mean}) and all fibre orientation profiles achieved good P_{mean} value excepted the $\theta = 45^{o}$ had the lowest value. This different was however not significant when compared with other 4 profiles.

Nagel and Thambirantnam (2005) also found the tapered thin-walled structure will benefit when it's subjected to axial impact process. A computer-based simulation was performed to determine whether it is appropriate to add the taper as energy triggering mechanism during the impact of thin-walled rectangular tubes. Particular attention was paid to the stability of the crushing process as well as deformation responses. It utilised variables such as wall thickness, taper angle, and the number of tapered sides. A standard tube was also simulated to establish the baseline. This research firstly identified the benefit of using the purpose-built energy absorber which had a positive effect on to its structure. The impact energy was largely consumed and left little to no damage to the rest structures. This concept was particularly interesting for the automobile industries which was largely adapted to the production process.

Any designated crumple zones will absorb impact energy when the vehicle is subjected to various types of impact, and avoid further transferring to the rest structure or even passengers. It is therefore essential to have such energy absorption structure built-in. This study largely focused on a square, or circular cross-section profiled thin-walled tubes as ideal test subjects, due to the immediate material availability and relatively low cost. Despite that thin-walled tube structure is an ideal candidate for axial impact load condition, it appears with some limitations as: high in initial peak load, no significant amount of energy absorption and non-uniform deformation behaviour. A tapered thin-walled tube has been proposed for a suitable alternative construction. It features the modified tube end where several taper angles were examined. In addition to this, taper featured tube also performed well under the oblique impact condition as it provided a consistent crush load during the tube deformation. Furthermore, due to the tapered end design, it triggered the deformation process and avoided global buckling reduction, which is an undesirable failure mode during the axial impact test.

It is found very limited studies of comparison between standard tubes and tapered tubes, however, few experimental tests focused on the relationship between the load to its deflection as well as failure mode and response between the standard and tapered circular tubes. On top of this, it further discovered the comparison between rectangular and square tapered tubes were also limited. Nevertheless, it looked into the effect of both static and dynamic crush to the tapered sheet metal tubes of rectangular cross-section. It determined the results of mean crush-load deflection under the analytical model with experimental validation (Nagel and Thambirantnam, 2005; Reid and Reddy, 1986).

It is summarized that, in general, few studies focused on the energy absorption behaviour and characteristics of tapered think-walled rectangular tubes. However, to determine the deformation behaviour, computer-based simulation shall perform in order to find out the correspondent energy absorption rate, as well as the failure of the tapered beam. FE element model was created to replicate the actual taper as well as the thin-walled tubes. Meanwhile, parameters such as wall thickness, taper angle, and a number of the taper sides can all be included within the boundary conditions. It is expected the outcome of this study is to find the energy absorption and deformation behaviour of the tapered end think-walled tubes, and whether it is an alternative suitable energy absorber when compared with standard thin-walled tubes. It built both model profiles of standard straight tubes, as well as tampered tubes.

Figure 1.60 Different proposed tube profiles (Nagel and Thambirantnam, 2005).

Figure 1.61 Mesh and boundary conditions (Nagel and Thambirantnam, 2005).

Figure 1.60 demonstrated the overall exterior dimensions of proposed 4 different samples, while the first is a straight tube, other tapered tubes with 3 profiles at the double taper, triple taper and four tapers were also created (Nagel and Thambirantnam, 2005). Figure 1.61 detailed how FE models replicate the detail of the tube construction. Boundary conditions of the simulation were also included. Since the test is set as static axial, for both straight and tapered geometries, a rigid top plate is press downwards to the base rigid plate, where the geometries are fully constrained to it without any movement. Since the geometries were fixed to the base plate, the contact between the top rigid plate to both straight and double tapered tube were frictionless. Meanwhile, the Coulomb friction coefficient of 0.02 was defined to all contact surfaces during the four tapered static tests. Additionally, due to other previous published works

done during 2004, mild steel was selected largely because it has suitable ductility for the deformation, as well as good energy absorption characteristic, with material properties at yielded strength of σ_y = 304.6 MPa, Young's modulus of E = 205 GPa, Poisson ratio of v = 0.3, and the density of ρ = 7700 kg/m^3 (Nagel and Thambiratnam, 2004).

As described in the early paragraph, this study will use standard straight built rectangular tubes to establish the baseline performance. On top of this, tapered rectangular tubes with 3 different taper angle profiles also created to see this will resulted in energy absorption, as well as deformation behaviour improvement. This study included few input parameters during the design phase, such as the height of the tubes as "*h"*, number of the taper as *"n"*, the thickness of the tube wall as "*t*", and the taper angle of the geometry as "*θ"*. As results of few output parameters in correspondent, which includes Initial peak load as "F_{bs}", mean load value as F_{ms}, energy absorption value as "E_s". The intended purpose of this study is to alter the key parameters such as the number and the angle of the taper as well as the wall thickness gave the fixed tube height, in order to improve the energy absorption via plastic deformation, or to yielded higher mean crush load during the deformation process. Nagel and Thambirantnam (2005) fixed some of the parameters to create a valid result. Parameters such as the height of the tube are maintained at 300 mm throughout, the cross-section of the tube is fixed to 100x50 mm, finally, the material assigned to the tube is the same for all 4 tube profiles. This parametric study allowed the results to reveal the effect or the benefit achieved after the simulation when one or more parameters are altered to identify either it yielded a positive or negative impact.

Figure 1.62 Deformation process of all proposed tube profiles (Nagel and Thambirantnam, 2005).

Figure 1.63 Effect on to the initial peak load on various of wall thickness, taper angle, and taper number (Nagel and Thambirantnam, 2005).

Figure 1.62 and 1.63 both showed the effect on the initial peak load under varies of parameters during the simulation. It found that as per wall thickness increases, the peak load increases as well. Meanwhile, as per taper angle increases, the peak load decreases. Despite both wall thickness and taper angle have a greater effect on the initial peak load, both parameters have less effect on the double tapered tube.

Figure 1.64 effect on to the initial peak load on various of taper angle (Nagel and Thambiratnam, 2005).

According to Figure 1.64 above, adding the tapered design to the tube reduced the initial peak load, it appeared all 4 tube profiles. Also, an increased taper angle from 5^{o} to 15^{o} will also result in a reduction of the initial peak load as well. This study indicated that it is critically important to keep the initial peak load low. High initial peak load means higher acceleration that experienced by both the structure of the vehicle as well as its occupants. Hence the lower the value of the initial peak load, the less deceleration will experience via the vehicle and the passengers. In addition to the above finding, the initial peak load result also revealed frusta (four taper tubes) achieved a generally lower initial peak load when compared with other profiles particularly.

Figure 1.65 Effect on to the mean load on various wall thickness and taper number (Nagel and Thambiratnam, 2005).

Figure 1.66 Effect on to the energy absorption on various wall thickness and taper number (Nagel and Thambiratnam, 2005).

This study also extracted both mean load and energy absorption trend of all 4 tube profiles which showed in both Figures 1.65 and 1.66 above. Primarily, the mean load chart illustrated the mean load value was closely related to the wall thickness when compared with taper angle and taper number, which appeared have less effect. However, as per wall thickness increases, the taper number appeared to effect more on the mean load as well. For the energy absorption diagram, once again, wall thickness increases resulted in varies levels of gained energy absorption. This increasing trend was also related to increasing numbers of taper.

“Content removed due to copyright reasons”

Figure 1.67 Effect on to the average crush force efficiency on various parameters (Nagel and Thambiratnam, 2005).

The above diagram summarized the effect to the average crush force efficiency under the various wall thickness, angle and number of tapers. It stated an important concept, that the relationship between the mean load to the initial peak load, as F_{ms}/F_{bs} is considered as form factor, also known as crush force efficiency. It emphasized that any modification or optimization of the energy absorption structure should aim for higher crush force efficiency, the lower of the initial peak load and the higher mean crush load will lead to better structural performance. The above diagram demonstrated that the crush force efficiency in this study that can be increased via to increase the wall thickness, or to increase the taper angle. However, the diagram also suggested as per number and angle of the taper increases will result in the increases in average crush force efficiency, but the influence of the wall thickness appeared less effective. Furthermore, look into the h-θ group that suggested that wall thickness has a more positive influence to increase the crush force efficiency than to increase the taper angle. This means that the wall thickness is much more efficient when comes to higher crush force efficiency while the taper angle at a higher value.

“Content removed due to copyright reasons”

Figure 1.68 Effect on to the average crush force efficiency on a tapered angle (Nagel and Thambiratnam, 2005)

On the top of the overall effect to the crush force efficiency by all parameters at the previous paragraph, the above diagram was focused on particularly on the effect of changing the taper angle will influence in crush force efficiency under the wall thickness fixed at 1.5 mm. Once again, the tapered tube showed higher crush force efficiency when compared with a standard straight tube, where the frusta tapered tube showed significant of high efficiency as the taper angle increases over the standard straight tube. This huge improvement suggested that either adding the taper to the plain tube, or to increase the taper angle will both yielded very good crashworthiness behaviour, and it demonstrated good performance for both of the worlds, which are low initial peak load, and higher mean load.

The above analysis was based on using the crush force efficiency as a performance factor; however, the primary purpose of the energy absorption structure is to absorb impact energy via deformation. This means Ideally, the bigger size or dimension of the structure, the more energy can be absorbed. However, this is not the case when implementing this technique into the real world scenario, where usually the amount of available space for energy absorption area is relatively limited. This is often the case and particularly occurs on to the vehicle design and production within the automobile industry, where more conditions have to meet, such as aesthetic for aerodynamic, drivetrain package for the overall design, lighter material for cost-saving. Hence Nagel and Thambiratnam further analysed the results by using both energy

absorption per unit crush length, and energy absorption per unit mass as another two performance factor to see if the tapered tube will still satisfy the purpose.

Figure 1.69 Effect on to the average energy absorption measured by per crush length (Nagel and Thambiratnam, 2005).

The above result was categorized into parameter groups of the wall thickness of h, angle of the taper of θ, and combined h-θ. Given the tube, the length was fixed throughout the simulation, and the data collection was ended when the tube deformation reached to 200 mm. Obviously, increase the wall thickness achieved a significant amount of energy absorption increases. This was largely due to the tube has additional material after increased the wall thickness, hence more plastic deformation was expected. However, this is not the case to the taper angle.

Figure 1.70 Effect on to the average energy absorption measured by per unit mass (Nagel and Thambiratnam, 2005).

It appeared triple taper tube absorbed most of the energy when compared with other tube profiles. This means after increase the wall thickness, within the same dimension and size of the designated energy impact zone, tripled tapered would have the highest amount of energy absorption and also highest efficiency. Similarly, to the available length of the energy absorption structure, the above diagram described the average crush force efficiency when measured by per unit mass. This performance factor is closely related to the weight of the vehicle. It is ideal that designated energy absorption area shall be built with ductile metallic material which inherently capable of absorbing more impact energy. However, this is a contradictory condition that totally against the modern vehicle production within the automobile industry, where manufacturing is trying hard to research into alternative material, that is convenient to produce and assemble, weigh less after been mounted on to the vehicle. This leads to fuel saving, CO2 reduction and even can be re-cycled and re-used again. Consequently, a lighter material that has excellent energy absorption capability is ideal in this scenario where weight reduction is crucial. Unit per mass provides a comparison between all 4 tube profiles to determine which tube geometry offers higher energy absorption efficiency per geometry weight. Total deformation length is fixed at 200 mm for all 4 tube profiles, and results showed both wall thickness and taper angle have very little influence on the energy absorption efficiency, where only double tapered tube responded this test well. In general, it can be understood that as the wall thickness increases, so does the energy absorption per unit mass increases as well. On the other hand, energy absorption actual decreased as per taper angle increases which caused by additional gained weight. Furthermore, the h-θ group indicated varying the wall thickness resulted in very little difference in the energy absorption per unit mass. Surprisingly, given the unit per mass, straight tube absorbed most energy, followed with the tripled tapered tube, double-tapered tube and frusta tube were came to last. This suggested as per the number of the taper increases, so does the weight gain during the process. This led to less energy absorption rate achieved, as per the number of taper increases, despite this actually increase the energy absorption.

Although the energy absorption performance was reduced in terms of the unit per mass, changing the geometry will have a positive impact to the overall performance and an inevitable amount of material will be also added along the process. This reflected that the study overlooked the material characteristics despite it proved changing the geometry will generally improve the energy absorption capability. Since many of those geometries and structure are more likely to appear in energy absorption application in high-speed cases, such as vehicle or

train. Particularly in the automotive industry, where the crashworthiness perspective of which a structure should ideally yield a low initial peak load to avoid sudden deceleration, and continued to absorb as much as possible impact load via higher mean load and energy absorption that will leave little for the rest of the vehicle or its passenger to experience. This will then achieve the ultimate goal of providing better protection in the event of a crash.

1.11.5 Flexural impact test – All the above cases were focusing on how thin-walled structure behaves while under the axial load condition, and all appeared yielded good results in regard to their individual parameter changes, alternative material replacement, or a structural optimization. However, other studies have appeared more interests in the structure's response under the flexural impact condition. The investigation of improvement on to the local energy absorption structure by numerical simulation was conducted. A study however, in this case, investigated the crash response of the vehicle bumper beam when subjected to frontal impact. It stated bumper beam belongs to the bumper subsystem, which normally fitted to both fronts and the rear of the vehicle. It is considered as designated crumple zone where the main purpose is to absorb the impact energy via deformation, in case of the vehicle is involved in a collision (Belingardi *et al*., 2013).

Generally, the bumper system includes the transverse beam that hidden behind the bumper fascia. Crash boxes on both the left and right side, and frame rail. The mounting and fastening methods vary to manufactures where its mixed type between welding or screw and bolt, but the transverse bumper beam was located at very front of the bumper system regardless, hence it is more likely to get in contact with the object upon the initial impact. Meanwhile, it is, therefore, the bumper beam remained a certain degree of strength in order to resist, or a partially deform during the low-speed impact that without further damaging the surrounding components or even pedestrians. On the other hand, fully deformation is expected during the medium or high speed, this will ensure that primarily, maximum deformation is reached, and the impact related damage is very well contained within the designated energy absorption area, without further experienced by either the vehicle structure or its passengers. Consequently, it emphasized it is critical to have a suitable bumper beam design, and it is challenging task to acquire a good combination between a good deformation behaviour with the correct material characteristic in order to satisfy both low speed and high-speed impact performance (Belingardi *et al*., 2013).

During this investigation, it found that except the existing metallic material made transverse bumper beam, the composite material has evolved itself into an alternative metallic replacement. It considered from the manufacturing perspective as a convenience to manufacture and assembly. Particularly for the pultruded composite bumper beam has the characteristic of high fibre alignment and content, hence high compression strength. This leads to a potential candidate to replace the traditional metallic made beam. Other researches have concluded pultruded composite products retained the characteristic of the metallic bumper beam when subject to flexural deformation, that the composite has higher energy absorption rate, as result of been assigned to safety structures such as bumper beam and crash boxes during the numerical simulation on another study.

However, due to the composite material has a different failure response when subject to the impact. The factors that contribute to this including the type and matrix of the fibre, the exterior dimension of the geometry, impact speed and impact object. It is different than metallic material absorbs energy via deformation, and to manipulate the parameters such as beams shape, thickness and material leads to improved deformation behaviour without any other unexpected types of failure. Not like the metallic material offers ductility that allows progressive failure mode, composite structure, however, appeared in a different failure mode due to it has higher stiffness, but to go to large fragmentation while under the impact. It aimed to replace the traditional metallic material with more modern and higher energy absorption capability, but this involves potential modification to the bumper beam geometry due to different failure mode appeared.

It is criticized that the characteristic of the composite material behaves must be taking into the consideration of existing geometry, which is widely assigned with metallic properties may not perform as expected during the numerical simulation. Hence it is undesirable to Solely replace the material without taking into the consideration of the energy absorption process. A research was conducted on the deformation behaviour of composite made tubes when subject to quasi-static transverse load condition (Charoenphan *et al*., 2004).

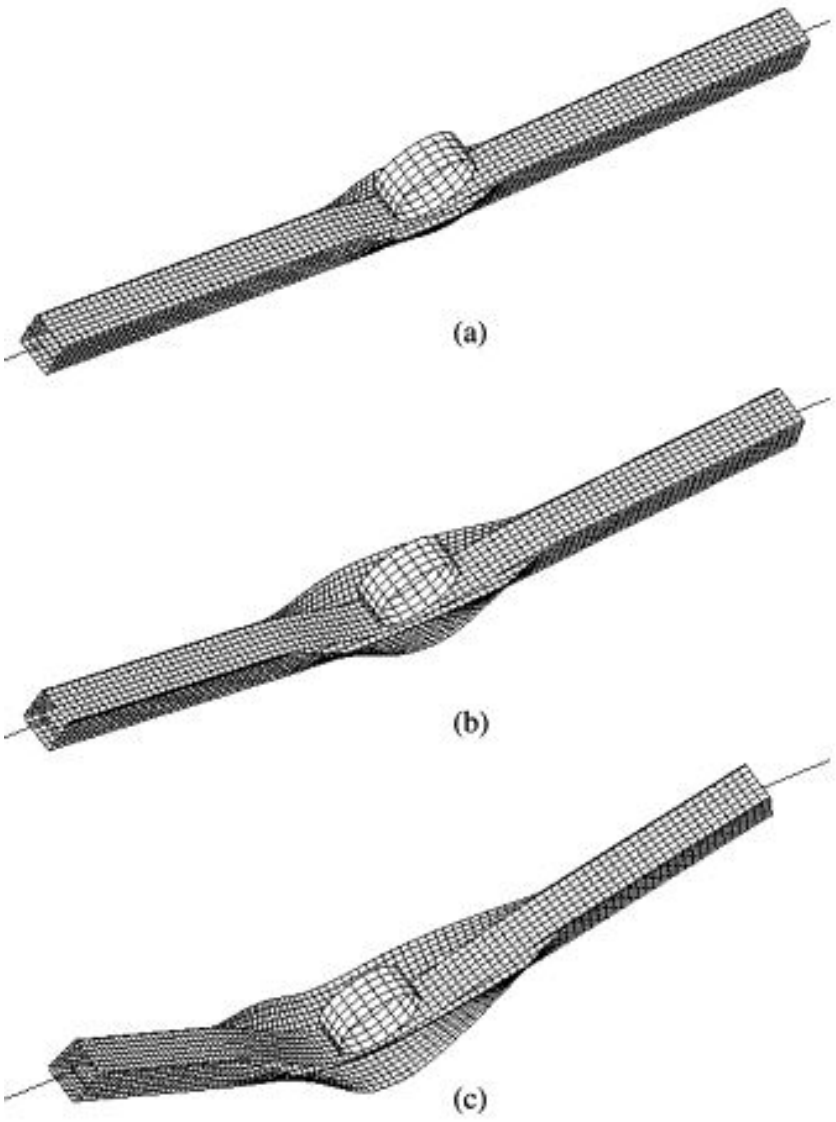

Figure 1.71 Detected Progressive failure of the composite made beam (Charoenphan *et al*., 2004).

Results showed the composite beam appeared progressive failure while the rigid roller is pressing downward against the beam. Similar research also suggested the progressive failure mode was anticipated during the composite made bumper beam impact test. Such as other literature discovered to modify the existing bumper beam into varies shape, in order to suit the characteristic of composite material failure. As a result of this, Standard beam geometry has been modified into further 7 different cross-section profiles showed below (Davoodi *et al*., 2011; Charoenphan *et al*., 2004).

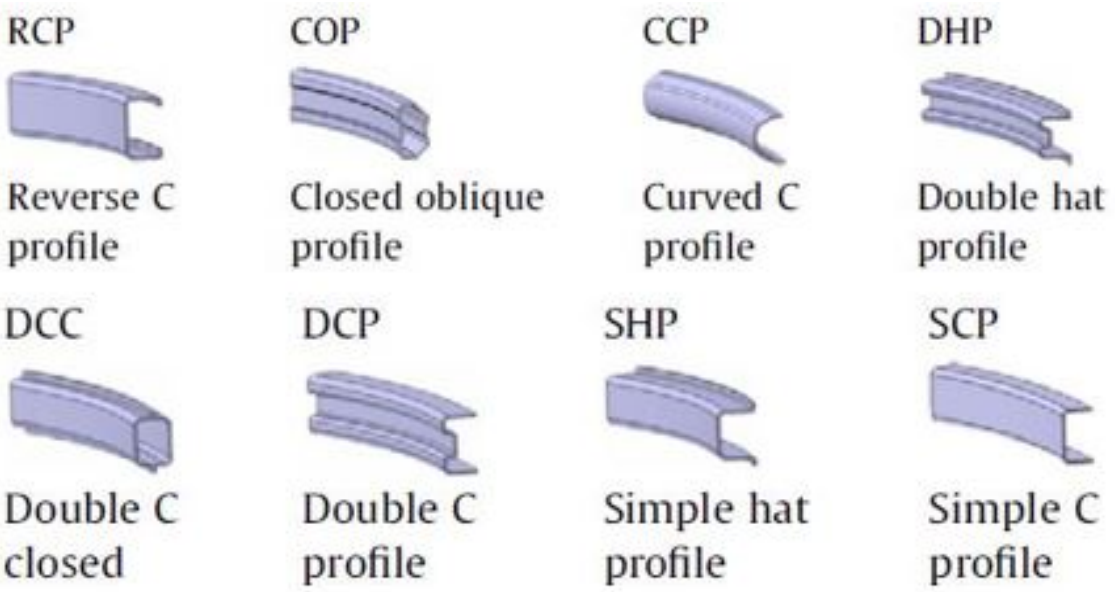

Figure 1.72 Eight bumper beam cross-section modifications (Davoodi, 2011).

All the modified cross-section profiles represented standard reverse "C" profile, as well as other 7 different cross-section types. Later simulation results indicated that some of the profiles have fully utilized the unique cross-section and indeed provided additional energy support, also interpreted that rather than large plastic deformation given by the conventional metallic made beam, a composite made beam, however, presented a progressive failure mode.

Consequently, both the Davoodi and Saiphon investigations revealed that when using the composite as an alternative option for bumper beam production, it is considered a certain degree of beam geometry modification is necessary to adapt the composite material which to fully explorer the high energy absorption characteristic and lightweight. Nevertheless, most of the composite made geometries were subjected to an axial impact load.

Instead, a study focused on the composite structural optimization subjected to flexural impact scenario. Since the geometry requires modification, after obtained the failure mode from above-mentioned studies conducted by others, this study purposed 8 different bumper beam cross-section profiles, while utilized the pultruded fibreglass like material (Belingardi *et al*., 2013)

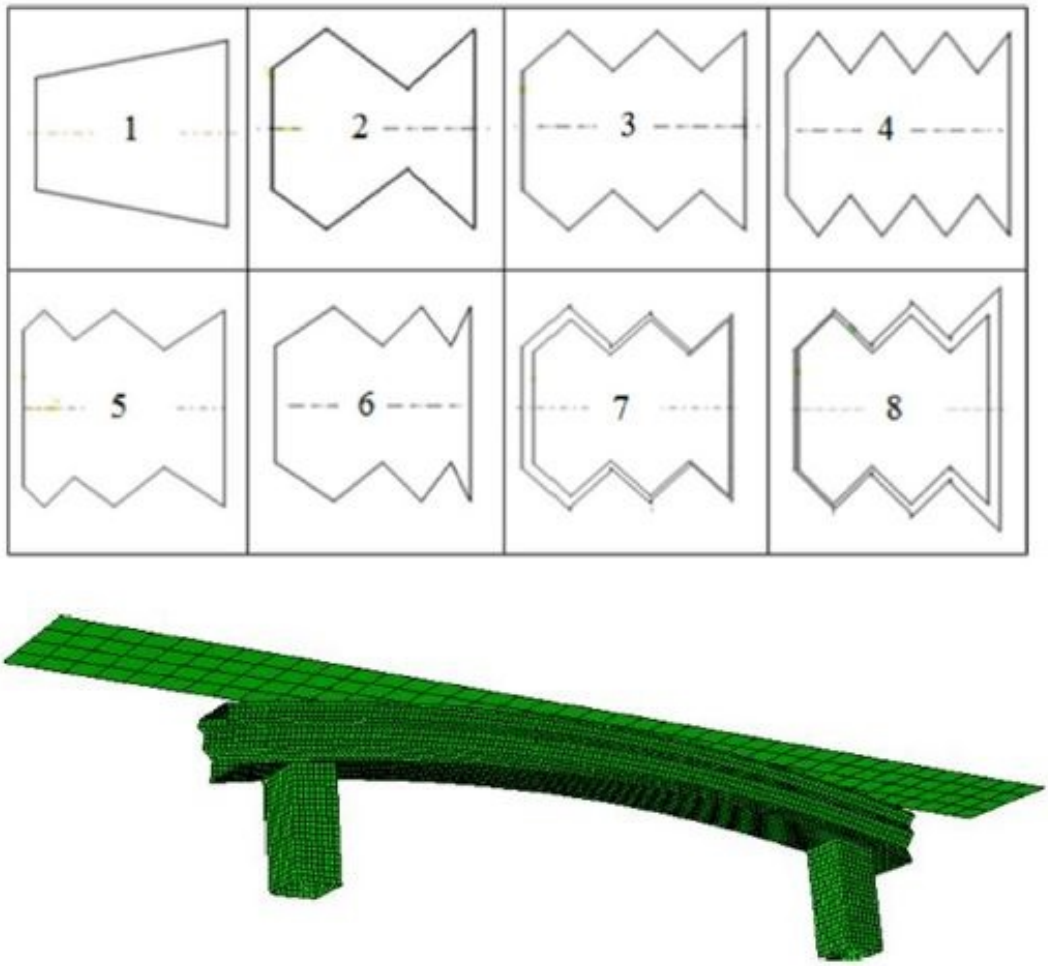

Figure 1.73 Purposed cross-section profiles performance (Belingardi *et al*., 2013).

As per Figure 1.72 indicated, modified cross-section profiles were purposed and an FEA geometry has been imputed into the simulation. It can be seen from the above Figure that the profile 1 represented common cross-section used widely on vehicle production as its relatively easy to manufacture and to assemble.

It expressed the main concern of when using composite as an alternative option which the failure mode of the composite tube, as well as few works of literature, stated previous, normally via fragmentation. As soon as either axial or flexural compression starts, the stress generated by the impact force will be concentrated at contact area that cannot be disbursed gradually, this stress concentration eventually increased to a certain level which leads to catastrophic failure of the entire structure, such as crack, bend or tear. Those types of undesirable Localized failure results in overall structural integrity no longer be able to retain its original shape to carry on with further deformation, and causes interfered deformation process, hence the structure no

longer offers any continues energy absorption. To tackle this stress concentration problem, IT introduced a failure triggering cross-section. It initiates the stress and induces the deformation while the stress is increased at a localized area. In this example, the fold profiles, that defined as designated stress concentration area is built into 7 other profiles which potentially to help the composite beam to retain its original shape while under the impact force. Primary it allows the force to concentrate between the fold without sacrificing to cause catastrophic failure. Also, it induces the impact of energy to compress the fold. This stress concentration area or the fold structure will compress as impact lasts, to create a consistent deformation were ideally to yield a progressive failure mode. To achieve the desired results, parameters, material and thickness and impact velocity were fixed, while the parameters of cross-section profile and beam bending curvature were variable to see if improvement can be achieved (Belingardi *et al*., 2013).

The simulation was to test the feasibility of alternative composite made tube is valid to be considered as using energy absorption structure and therefore can be integrated into the vehicle production subject to low-speed impact scenario. This was contributed via few satisfactory conditions that it explained, primarily, based on the above diagram showed the assembled structure against the impact wall, the first parameter was obviously the impact velocity which determined at 15km/h. This rise the question that there are many speed rating standards for legislation related vehicle impact speed, as well as due to the research purpose of third party test. Under the USA scenario, such as IIHS (Insurance Institute of Highway safety) as the third party guidance that specializing in researching the very specific category of high injury and death related crash type and speed, and consequently referencing while rating their test speed. This resulted from IIHS rated the speed of moderate frontal impact at 40mph (or, 64km/h), whereas NHTSA (National highway traffic safety administration) is rated their speed at 35mph (or, 56km/h). The speed rating in European area is similar but it uses Euro-NCAP as equivalent test standard, it rated the speed of 40% overlap frontal impact at 40mph (or 64km/h), and 31mph(or 50km/h) for 100% overlap frontal impact, whereas the European legislation requires slightly lower 56km/h at frontal impact Test.

This literature emphasized that this study mainly investigates how the failure occurs while the beam is under the low-speed impact, and particularly IIHS provided, and rated 10km/h and 5km/h for full-frontal and corner only bumper test, same speed rating is also applied when testing the rear of the vehicle as well. However, it criticized that the results after the simulation are not to satisfy specific legislations. But since the work is to determine the suitability of

composite is alternative replacement when manufactured as energy absorption bumper beam, and at given optimized geometry to see any performance increases, hence the impact speed was determined to be slightly higher than the IIHS bumper test standard, at 15km/h. Other parameters such as failure mode, displacement and peak load values are all within the considerations of whether to determine the earlier purposed cross-section profiles will work with new composite material. As mentioned at earlier paragraph, the composite material mainly consists of fibre mixture that gave this type of material a progressive failure mode, the desired outcome after replace the metallic material is the grooves between folds that built into the geometry acts as energy triggering mechanism that allows the stress concentration deliberately focused at those locations, and induce the composite beam into a stable failure mode without causing any fragmentation which inevitably leads to catastrophic structure failure. It explicitly indicated that a number of folds increases will help to consume the stress via the formation of crack and aid the beam enter into a progressive failure. Nevertheless, the number of folds will exceed the physical limit of the beam and eventually causes strength reduction, the fold is no longer acts as energy triggering mechanism, but instead to create localized failure, and predominantly leads to decreases of energy absorption as well as undesirable deformation behaviour (Belingardi *et al*., 2013).

1.11.6 Frame rail impact test – So far, all the above studies used composite material as a suitable alternative for structural optimization to achieve both better energy absorption and reduction of force reaction. Nagel and Thambiratnam used a specific energy absorption as their parameter to quantify the improvement. It heavily addressed the importance of maximizing the energy absorption per unit mass on the bumper system and indeed they have achieved this. However, it appeared they ignored maximising the energy absorption per unit mass also means less unit mass required to carry onboard which could save the weight of the bumper system. Consequently, while increasing the specific absorption per mass yielded positive impact to the overall structural performance, but the energy absorption from a unit mass perspective without considering the weight reduction is less comprehensive since reducing the system's weight will have a direct effect to the fuel consumption to the vehicle. However, it indeed mentioned the weight saved when replaced the traditional metallic material with composite. A specific study did not consider the composite as an alternative lightweight material but still focused on metals when looking to improve crashworthiness and lightening of vehicles S-frame. Some combination of metallic material was found to achieve better crashworthiness performance. A

study was previously mentioned indicated that the weight of the vehicle had a negative impact on the vehicle performance, such as accelerations, decelerations and fuel economy. Lighter material replaced the heavy metallic material, which will result in both better crashworthiness and reduce the system's weight. Hence this work focused on the crashworthiness performance of s-frame on the passenger vehicle and found the s-frame located at the front of the vehicle that allows drivetrain components to be mounted on the top. It consists of welded thin-walled tubes and bent to certain exterior dimension depends on the manufacturer's specification. Generally, the bumper system will be fitted to the front of the s-frame to complete the front end looks of the vehicle, also gave varies mounting space for auxiliary components, such as radiators, pipework, and headlights. It appears to use lighter material can certainly benefit the s-frame, both weight reduction and increase the crashworthiness performance. In order to serve the weight reduction, it considered a few alternative metallic materials, such as aluminium, magnesium or advanced high strength steel. Without further investigating the possibility of using composite material, it selected the hybrid method, which was combined with a section of mild steel due to its high stiffness, and another section of Aluminium because of its energy absorption capability and lightweight characteristic (Tehrani and Nikahd, 2006; Yamane and Furuhama, 1998).

It can be observed from the above-mentioned results, the peak load curve indicated the deceleration of the structure that the lower of the force reaction, less acceleration is expected. Pultruded composite beam provided low peak load on both initial contact and throughout the impact process, this means pultruded beam offered mild deceleration while subjected to impact with the rigid wall, while the impact behaviour of metallic made beam appeared more aggressive. This is a very important factor to determine whether the vehicle or passenger safety has been satisfied or not. Other literature also dressed the importance of keeping the peak load trend as it’s closely related to passenger’s safety. It explicitly indicated peak load is closely related to the occupant’s risk, because force reaction represented the deceleration rate during the impact, hence less peak load results in less deceleration, this will aid both passengers and rest of the vehicle structure to slow down gradually without performing a harmful severe declaration (Beyene *et al*., 2014).

So far, some of the above studies used composite material as a suitable alternative for structural optimization to achieve both better energy absorption and reduction of force reaction. Some study used a specific energy absorption as their parameter to quantify the improvement. It

heavily addressed the importance of maximizing the energy absorption per unit mass on the bumper system and indeed they have achieved this. However, it appeared they ignored maximising the energy absorption per unit mass also means less unit mass required to carry onboard which could save the weight of the bumper system. Consequently, while increasing the specific absorption per mass yielded positive impact to the overall structural performance, but the energy absorption from a unit mass perspective without considering the weight reduction is less comprehensive since reducing the system's weight will have a direct effect to the fuel consumption to the vehicle. However indeed mentioned about the weight saved when replaced the traditional metallic material with composite (Nagel and Thambiratnam, 2005; Berlingardi *et al*., 2013)

Somewhat other study did not consider the composite as an alternative lightweight material but still focused on metals when looking to improve crashworthiness and lightening of vehicles S-frame. Some combination of metallic material was found to achieve better crashworthiness performance. A similar study has also indicated that the weight of the vehicle had a negative impact on the vehicle performance, such as accelerations, decelerations and fuel economy. Lighter material replaced the heavy metallic material, which will result in both better crashworthiness and reduce the system's weight hence this study still focused on the crashworthiness performance of s-frame on the passenger vehicle and found the s-frame located at the front of the vehicle that allows drivetrain components to be mounted on the top. It consists of welded thin-walled tubes and bent to certain exterior dimension depending on the manufacturer's specification. Generally, the bumper system will be fitted to the front of the s-frame to complete the front end looks of the vehicle, also gave various mounting space for auxiliary components, such as radiators, pipework, and headlights. Lighter material appear to benefit the s-frame by reducing weigh and increasing the crashworthiness performance. In order to serve the weight reduction, it considered a few alternative metallic materials, such as aluminium, magnesium or advanced high strength steel. Without further investigating the possibility of using composite material, it selected the hybrid method, which was combined with a section of mild steel due to its high stiffness, and another section of aluminium because of its energy absorption capability and lightweight characteristic (Yamane and Furuhama, 1998; Tehrani and Nikahd, 2006). 3D models have been created by adopting some cross-sectional profiles (Belingardi *et* al., 2013). This work also included various cross-sections of the S frame to make the comparison.

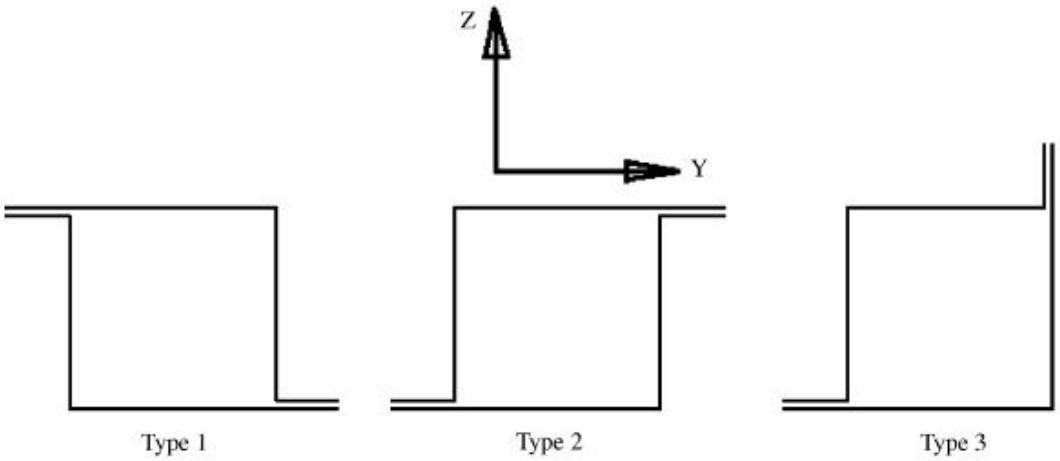

Figure 1.74 Proposed frame cross-sections (Tehrani and Nikahd, 2006).

“Content removed due to copyright reasons”

Figure 1.75 Proposed Frame model and boundary condition (Tehrani and Nikahd, 2006).

Both above diagram 1.73 and 1.74 showed the overall model of the s-frame and adopted cross-section profiles of the frame. In the simulation setup as shown in Figure 1.74, the frame was fixed at one end, and the load was applied at the other end. A mixture degree of bending, compression and tensile was expected since the frame existed in three-dimension form. The

property of the mild steel assigned to this model listed as Young's modulus of $E = 2.07 \times 10^5$ N/mm^2, the initial yield stress is σ_y = 335.47 N/mm^2, and Poisson's ratio is v = 0.3. Since the joint between the steel and aluminium is treated as welded, hence the welding material is considered as same as steel and the welding pitch is 30 mm with 550 N/mm^2 of yield point.

Table 1.6 Comparison of maximum energy absorption of proposed cross-section profiles (Tehrani and Nikahd, 2006).

Type	Weight (kg)	Wall thickness (mm)	Max energy absorption (J)
1	5.794	1.6	4014.09
2	5.794	1.6	4586.74
3	5.784	1.6	4738.48

Out of all proposed cross-sectional profiles, type 3 is more capable of absorbing impact energy over the type 1 and 2. This became the baseline crashworthiness performance of the frame design and type 3 was therefore selected to carry forward for further optimization. After the type 3 cross-section was selected, the next optimization focused on how welding joint affects the crashworthiness performance.

Figure 1.76 Model #1 welding joint of S frame (Tehrani and Nikahd, 2006).

“Content removed due to copyright reasons”

Figure 1.77 Model #2 welding joint of S frame (Tehrani and Nikahd, 2006).

“Content removed due to copyright reasons”

Figure 1.78 Welding differences between two models (Tehrani and Nikahd, 2006).

A hybrid frame was designed to combine both steel and aluminium, and both models of welding joints were also created. Both metallic frame parts used an identical thickness (1.6 mm). After FEA simulations, both Figures 1.78 and 1.79 indicated the effect on to both force reaction as well as energy absorption compared between baseline and proposed welding joints. It is very obvious that hybrid frame design achieved significant lowering of initial peak force, both remained around 10 kN upon the initial contact. Baseline frame, however, yielded much higher force value which was over 60 kN. This means the hybrid frame design would reduce the possibility of severe injury for passengers to receive, on the other hand, energy absorption revealed that the absorption increased very little that can be considered as not a significant improvement regardless welding joints is presented or types of joints. It can be summarized that mixed between both metallic materials is true can reduce the injury rate of the passengers, while retained almost the same amount of energy absorption with welding joint presented onboard.

Figure 1.79 Effect on different welding joint to force (Tehrani and Nikahd, 2006).

Figure 1.80 Effect on different welding joint to energy absorption (Tehrani and Nikahd, 2006).

Figure 1.81 Thickness effect on welding model #1 to force (Tehrani and Nikahd, 2006).

Figure 1.82 Thickness Effect on welding model #1 to energy absorption (Tehrani and Nikahd, 2006).

Figure 1.83 Thickness effect on welding model #2 to force (Tehrani and Nikahd, 2006).

Figure 1.84 Thickness effect on welding model #2 to energy absorption (Tehrani and Nikahd, 2006).

To further enhance the crashworthiness performance of the newly designed hybrid frame, this study modified the thickness of both types of material onboard which was originally tested at 1.6 mm. Aluminium was considered to receive varies thickness to see any improvement on both energy absorption as well as force reaction. Welding joint was determined was not influence the energy absorption during the impact, hence in this thickness optimization stage, welding models #1 and #2 was selected as a fixed parameter to see whether to vary the Aluminium thickness will yield crashworthiness improvement.

It can be seen from both Figures 1.80 and 1.81, under the welding joint model #1, the initial force reaction behaved differently in response to the thickness variations. As the baseline used the same mild steel entirely for the frame design, it yielded the highest force reaction upon the initial contact, all 3 types of hybrid frames achieved lower force value. Both the initial peak force and force curve trend were lower as per thickness decreased. This indicated that force reaction was directly affected by the thickness of the material. Varying the thickness to the frame also gained positive improvement on the energy absorption rate, except that the 2.8 mm absorbed less energy than the baseline, both 3.1 mm and 3.4 mm gained 11 % and 33 % improvements over the baseline design. On the welding joint model #2, the force reaction curves were performed similarly to the model #1, where the thickness variation to the aluminium section of the frame yielded lower peak force upon the initial contact. It can be seen from the above Figures 1.82 and 1.83, various thickness applied to the aluminium achieved a significant amount of initial peak force regardless at any proposed thickness when compared with steel baseline model. Besides this, model #2 at a thickness of 3.4 mm achieved the lowest force reaction throughout the simulation. Both 3.1 mm and 3.4 mm of aluminium design absorbed higher amount of impact energy.

1.12 Aim and Objectives

This thesis focuses on model development for improving vehicle crashworthiness based on numerical simulation. It requires to analyses current solutions fitted to the vehicle, and extract critical parameters during the model development, and computer simulation, which will affect the crashworthiness performance, and discover possible optimizations. This project aims to develop a novel computer simulation model to improve vehicle crashworthiness and to enhance the bumper contribution towards the safety of the vehicle. The workflow uses 3D computer software to re-create the existing solution which widely fitted to the vehicle currently, this establishes the benchmark as baseline performance. Finite element analysis software will examine the replicated geometries via computer simulation, which enables this project to establish the benchmark of how current solution performs during the crashworthiness test. Once the performance of the current solution is fully understood, then the workflow will focus on building on an improved solution, and in the meantime, to identify the critical parameters which will ultimately affect the overall crashworthiness performance. Intensive simulations are expected for final crashworthiness improvement based on only a few important parameters to achieve desired results. To summaries all the above discussion, it can be interpreted that the objectives of this thesis are:

- To review previous studies of vehicle crashworthiness including the testing procedure and numerical simulation work.

- To review the car bumper design and crashworthiness studies including the bumper structure, bumper beam profile, materials in the bumper system.

- To design a bumper subsystem with detailed bumper beam profiles and to numerically investigate the effect of beam curvature on the crashworthiness.

- To conduct a parametric study on the beam of different cross-section profiles and to investigate the effect of materials for beam and the filler inside the beam to achieve better crashworthiness performance out of the current design.

- To investigate the influence of the crash box and its interaction with a bumper beam in the lower-speed crash simulation.

- To numerically predict the response of improved car bumper design in a several of loading scenarios.

Chapter 2 Methodology and Validations

This thesis focuses on the front bumper system of a four-door family car. The presence of occupants is not explicitly considered. The bumper beam and crash boxes located at the front of the car are subjected to extensive crashworthiness assessment. The following factors are focused on: various types and thickness of the material; different cross-section profiles and general shapes.

2.1 Creation of 3D models and FEA Solver

Each component within the front bumper system, such as bumper beam, beam filler and crash boxes, are all created and assembled into the complete bumper system via Dassault Solidworks. The resultant bumper beam maintains the same overall exterior geometry details and its characteristics, such as bending curvature, cross-sections, material types and thickness, and the connection between the bumper to the crash boxes. The assembled front bumper system is then transferred into the ANSYS workbench, and explicit dynamics module was used to conduct the crashworthiness simulations. All the mentioned characteristics remain unchanged during the transfer stage. In the explicit dynamics solver, the following options will be further explored in relation to this front bumper design and analysis.

1. Bumper beam material.
2. Bumper beam profile – Number of folds
3. Bumper beam shapes – curvature radius of Bending curvature
4. Bumper beam to crash boxes connection – Both number, and location of spot welds.

The Investigations covered from 1 to 4 were presented in the following chapters of 3, 4, 5, 6 and 7. Those investigations represented the step-by-step approach to improve the crashworthiness results of the front bumper system. During the vehicle crashworthiness test, the entire impact process generally lasts no more than a few seconds, from the front bumper system starts to engage the impact object until the vehicle comes to a stop. This critical impact process directly revealed the post-impact behaviour and which parameters can subject to adjustment in order to improve the crashworthiness performance. Explicit dynamics was purposely selected for this reason where it is suitable to re-create such an impact process. Very small-time steps while large model deformation is involved. This method was proved successful by some recent study where some extensively small integration time steps can be

used to achieve the acceptable results (Lee, 2014).

2.2 Basic formulation of explicit dynamics

In ANSYS FEA software, both Implicit and explicit methods are capable of performing dynamic simulations. Depends on the object velocity encountered in the scenario, one method may be more suitable than the other. While the implicit method performs better in dealing with static, or relatively slow impact case, medium or high-speed impact would require explicit dynamics to resolve.

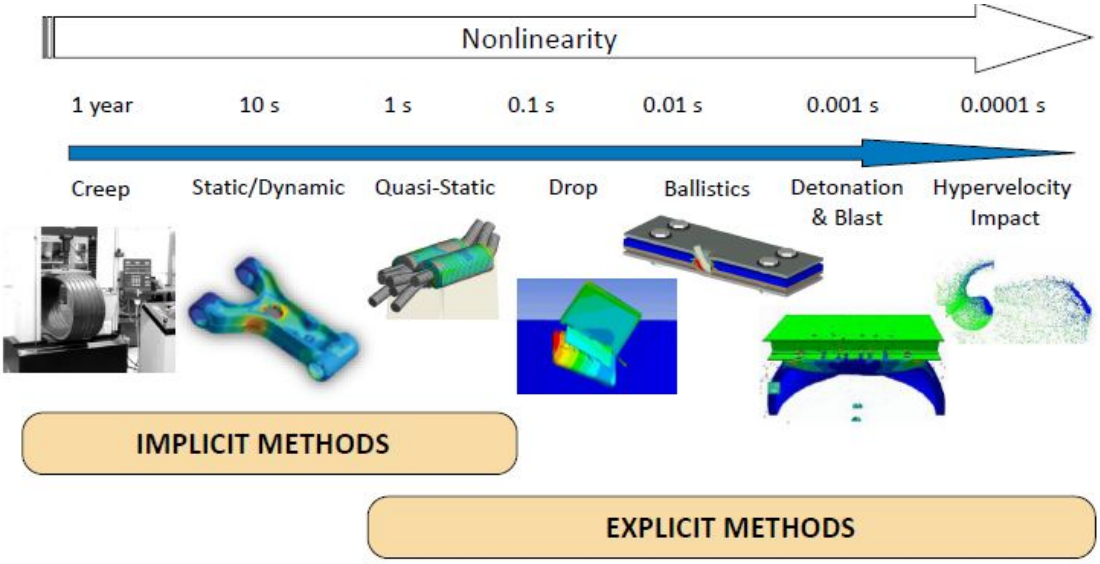

Figure 2.1 The comparison between Implicit and Explicit methods (ANSYS, Inc. 2016).

Figure 2.1 clearly indicated the impact scenarios range from a static situation which is located at the far left of the arrow to very fast impact velocity to the right side. This means the higher of the impact speed towards the right side, the impact event occurs more non-linearly. Explicit dynamics quantifies the amount of force and energy absorption occurred to the test sample or structure and captures a deformation process during the impact. This enables the designer to quickly pinpoint the problems and make an immediate improvement.

The basic solution of explicit method uses the central difference time integration scheme. When the simulation starts, the node on the element is subjected to many factors, such as internal/external stress, contact and boundary conditions. These nodal accelerations are described as:

$$\text{Nodal acceleration:} \quad \ddot{x}_i = \frac{F_i}{m} + b_i$$

where x_i equals the nodal displacement of the components (i = 1, 2, 3), f_i equals the force applied to the nodes, b_i equals to the components of body acceleration, and m means the mass of the node. Where the accelerations at the time of $n - \frac{1}{2}$ is determined, the velocities at the time of $n + \frac{1}{2}$ is then formulated as:

$$\text{Velocity at } n + \tfrac{1}{2}\text{:} \quad \dot{x}_i^{\,n+\frac{1}{2}} = \dot{x}_i^{\,n-\frac{1}{2}} + \ddot{x}_i \, \Delta t^n$$

The position of the node is updated based on time of $n + 1$, and integrating with the velocities:

$$\text{Updated position at time } n+1\text{:} \quad \dot{x}_i^{\,n+1} = \dot{x}_i^{\,n} + \dot{x}_i^{\,n+\frac{1}{2}} \, \Delta t^{n+\frac{1}{2}}$$

The basic integration equations display the conservation of mass, momentum and energy using the Lagrange coordinates, where the material constitutes the model once it has been assigned. Other simulation parameters, such as material properties, impact velocity and initial boundary conditions are all pre-defined in the explicit dynamics solver. When uses Lagrange formulations, it is necessary to generate the mesh to the models before it can subject to any simulations. Mesh allows the model to move and deform due to pre-defined simulation parameters, and this satisfies the conservation of mass is automatically. The partial differential equations which demonstrate the conservation of momentum is related to the acceleration to the stress tensor σ_{ij}:

$$\begin{aligned}
\rho\ddot{x} &= b_x + \frac{a\sigma_{xx}}{ax} + \frac{a\sigma_{xy}}{ay} + \frac{a\sigma_{xz}}{az} \\
\rho\ddot{y} &= b_y + \frac{a\sigma_{yx}}{ax} + \frac{a\sigma_{yy}}{ay} + \frac{a\sigma_{yz}}{az} \\
\rho\ddot{z} &= b_z + \frac{a\sigma_{zx}}{ax} + \frac{a\sigma_{zy}}{ay} + \frac{a\sigma_{zz}}{az}
\end{aligned}$$

The energy conservation is formulated as:

$$\dot{e} = \frac{1}{\rho}(\sigma_{xx}\dot{\varepsilon}_{xx} + \sigma_{yy}\dot{\varepsilon}_{yy} + \sigma_{zz}\dot{\varepsilon}_{zz} + 2\sigma_{xy}\dot{\varepsilon_{xy}} + 2\sigma_{yz}\dot{\varepsilon_{yz}} + 2\sigma_{xx}\dot{\varepsilon_{zx}})$$

2.3 Explicit dynamics cycle

For each time step elapses, there is a related calculation based on all the equations showed above that represent each element of the model after the mesh is generated. This calculation procedure is obtained from the calculated result from the end of the previous time step. This calculation starts with a pre-defined simulation environment and with meshed models.

The time integration will firstly update the location of all mesh nodes, this causes movement of the nodes which leads to displacement of the elements. Gradual node movement leads to element deformation, this then results in the changes to geometry volume. At the meantime, the strain rates are derived from this process. Stresses are then derived from the strain rates via constitutive laws. Stresses feedback will generate the nodal forces, in which external nodal forces are calculated from pre-defined boundary condition, and the nodal accelerations are also calculated from the total nodal forces that divide the nodal mass. These accelerations are integrated into the explicit process by time in order to produce new nodal velocities, it is then integrated into the explicit process by time to generate new nodal positions. The explicit dynamics is working on this repetitive cycle until the defined end time is reached.

2.4 Timestep

Sections 2.2 and 2.3 briefly introduced the concept of implicit dynamics. Meanwhile focused on the explicit dynamics closely on its methods and formulas. It utilised the working cycle to demonstrate the working principle and related calculations. Since the explicit can be resolved directly, iteration at each time integration is not necessary. This means explicit dynamics does not need to satisfy the convergence requirement. However, this also indicated the explicit dynamics can sometimes behave unstably. The problems such as large element distortion, energy error is all suggested there are no controlled parameters to monitor, or conditions to satisfy in order to determine the stability of after the solver completes each time integration. Hence the explicit solver requires an alternative parameter to monitor the stability during the simulation process. Instead, the principle of conservation of energy was used to track the simulation stability. Since the energy conservation must be satisfied, the solver will calculate the overall energy at each time step, and it shows the percentage of energy error during the simulation process. The simulation will stop when recorded energy error was deviated and reach a threshold (Courant *et al*, 1967). The stable time step calculation is formulated as:

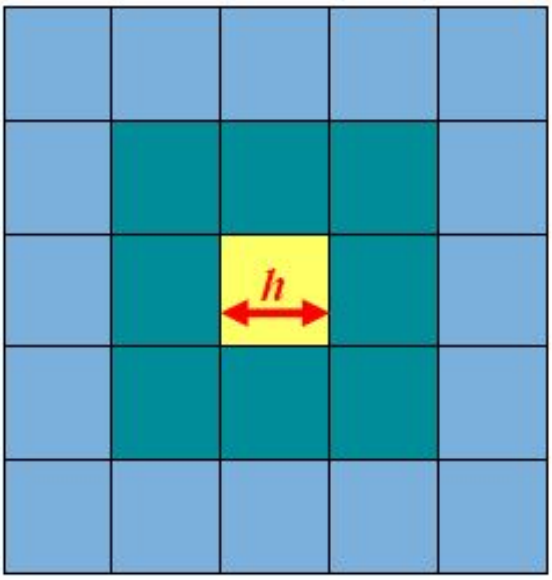

Figure 2.2 Example of the smallest time step (ANSYS, Inc. 2016).

$$\text{Time Step: } \Delta t \leq f \leq \left[\frac{h}{c}\right]_{\min}$$

Where the single time step Δt cannot passes further than the smallest element size after the geometry is assigned with material property and meshed. Where "h" is the smallest element size, "c" is the wave speed of the element. A safety factor "f" is used to represent the stability of the simulation. To further extend the wave speed "c", the material wave speed is given:

$$\text{Material wave speed: } \sigma = \sqrt{\frac{E}{\rho}}\text{, where Density: } \rho = \frac{m}{V}$$

Change fomular

Where "E" is Young's modulus, "ρ" is the density of the material, "m" is the mass of the material and "V" is the volume of an element. It is considered very important to select a suitable time step that should be small enough to capture details of the simulation but avoided to select smaller time step to increase the unnecessary calculation time.

2.5 Mass scaling (keep the formula consistent)

It is worth mentioning that the conservation of energy sometimes cannot be met and interfered, such as the component is severely deformed due to the material that assigned to the component showed at low stiffness. The lower stiffness can result in the element to distorts badly during the impact process which sometimes reaches to what the explicit dynamics solver cannot compensate even after suitably increased the simulation time steps. Because the time steps are

determined based on the minimum length of an element after the model was received the desired material. Manually increasing the mass of each element in order to increase the allowed time step is considered a valid alternative method without a sacrifice of simulation accuracy. Mass scaling can be enabled before the simulation starts, and it can vehicles as:

$$\text{Mass scaling:}\Delta t \propto \frac{1}{c} = \frac{1}{\sqrt{\frac{c_{ii}}{\rho}}} = \sqrt{\frac{m}{VC_{ii}}}$$

Where the C_{ii} represents the material stiffness (i=1, 2, 3), ρ indicates the density of the selected material, m indicates the material's mass, the V is the volume of the element. Manually adding the additional mass leads to larger time step been obtained, and this ultimate effect the reduction of the computational time.

2.6 Methodology

Earlier paragraph 2.1 proposed 4 parameters that concluded after reviewed numbers of the literature demonstrated in early chapter 1. To systematically analyse the effect to the crashworthiness of the frontal bumper system, the basic bumper system is featured at 4 general shapes, with 3 profiles, all listed below as:

Table 2.1 Shape and profile designation

Basic bumper Feature and Designation				
Shape & profile Designation	Shape Baseline	Shape 2	Shape 3	Shape 4
Fold 1	Straight beam	2000 mm	2400 mm	3000 mm
Fold 2	Straight beam	2000 mm	2400 mm	3000 mm
Fold 3	Straight beam	2000 mm	2400 mm	3000 mm

2.6.1 CAD drawing of the Bumper Beam

Table 2.2 Bumper Beam Specification – Fold 1

Bumper Beam Specification – Fold 1				
Profile	Depth (mm)	Height (mm)	Length (mm)	Weight(kg)
Fold 1	105	107.03	1394	5.31

Cross-section	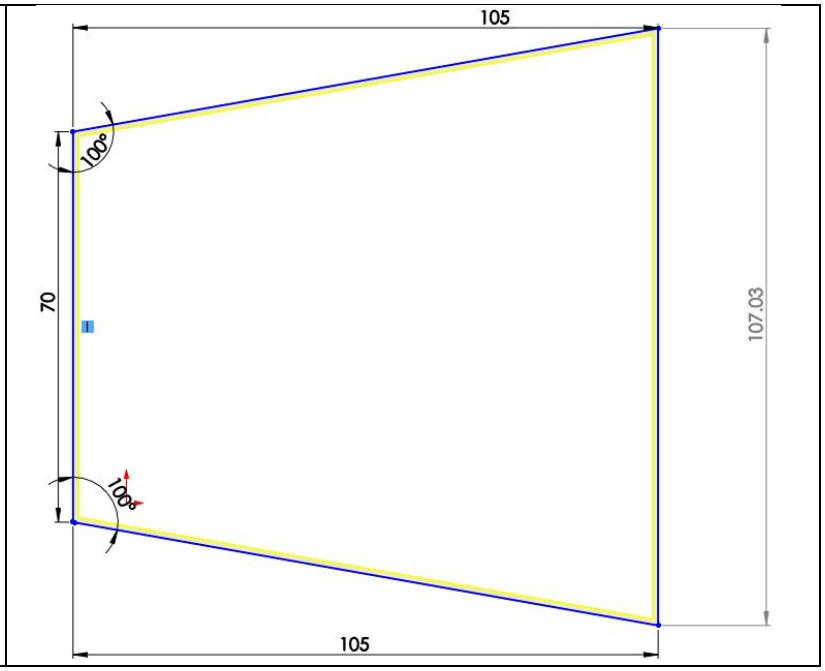

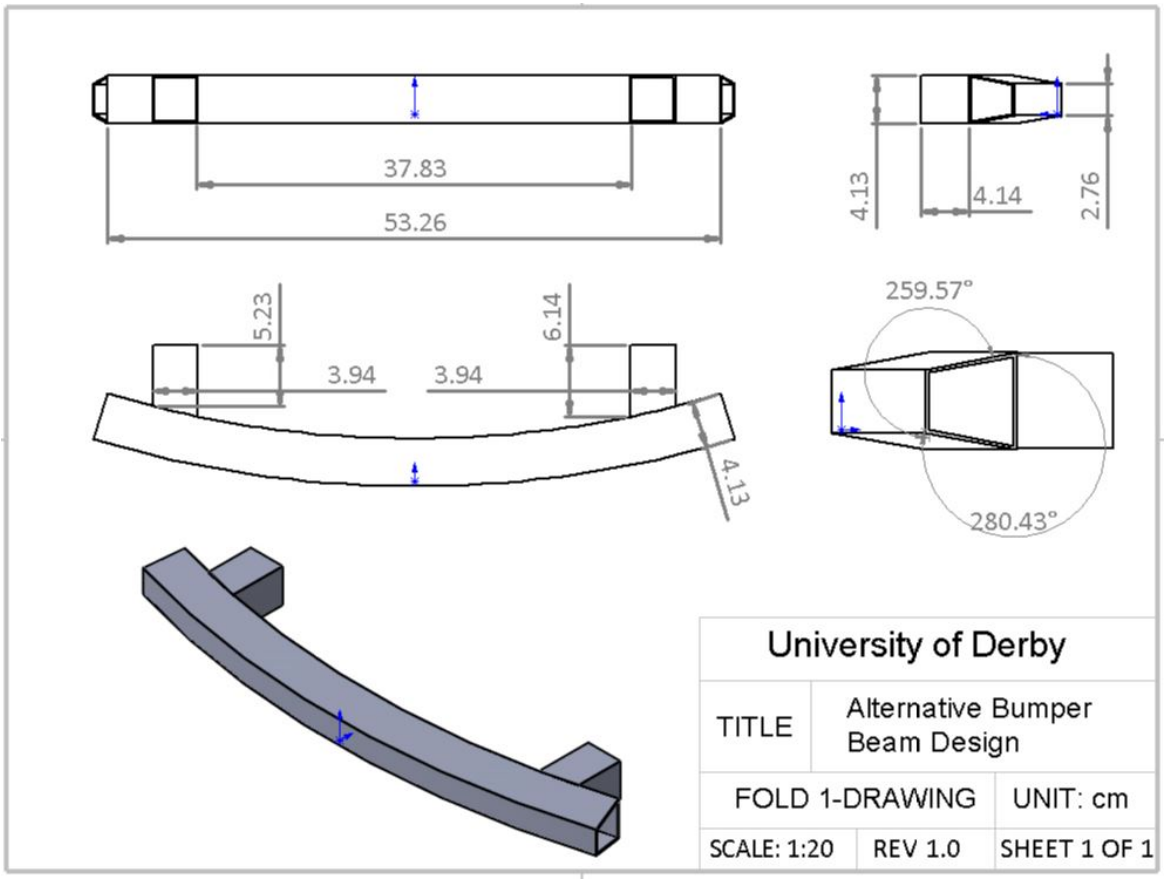

Figure 2.3 Fold 1 CAD drawing

Table 2.3 Bumper Beam Specification – Fold 2

Bumper Beam Specification – Fold 2				
Profile	Depth (mm)	Height (mm)	Length (mm)	Weight (kg)
Fold 2	116.34	109.33	1394	8.39

Cross-section	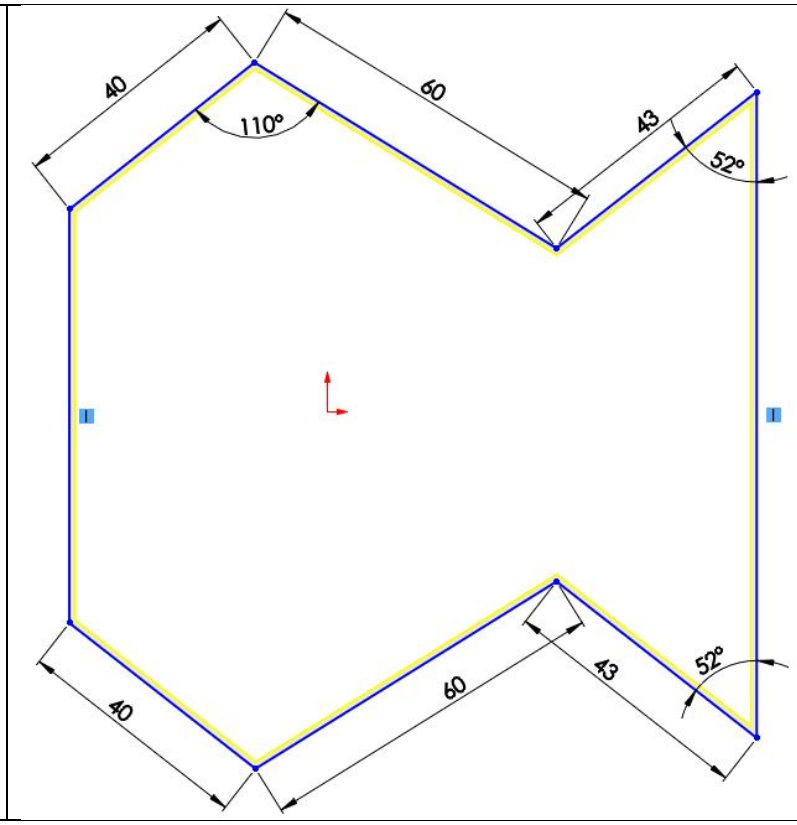

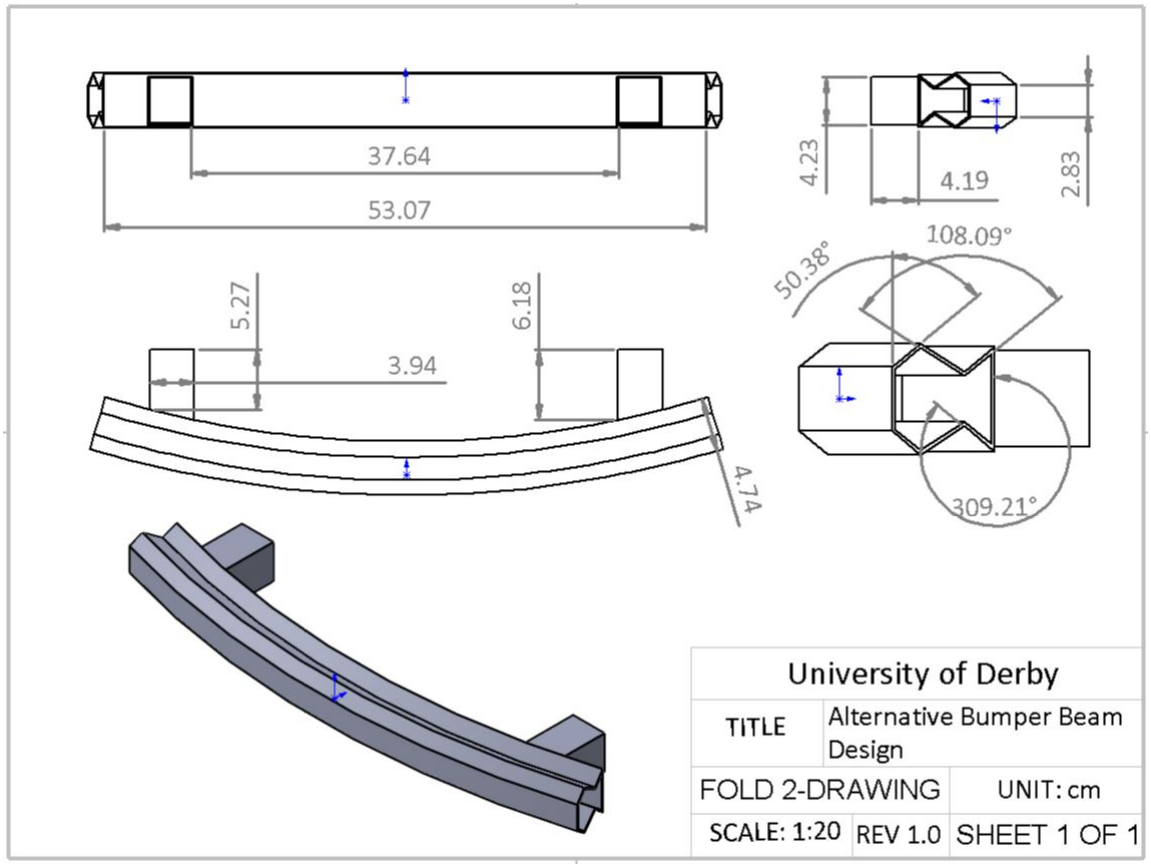

Figure 2.4 Fold 2 CAD drawing

Table 2.4 Bumper Beam Specification – Fold 3

Bumper Beam Specification – Fold 3				
Profile	Depth (mm)	Height (mm)	Length (mm)	Weight (kg)
Fold 2	123.74	119.50	1394	8.47
Cross-section	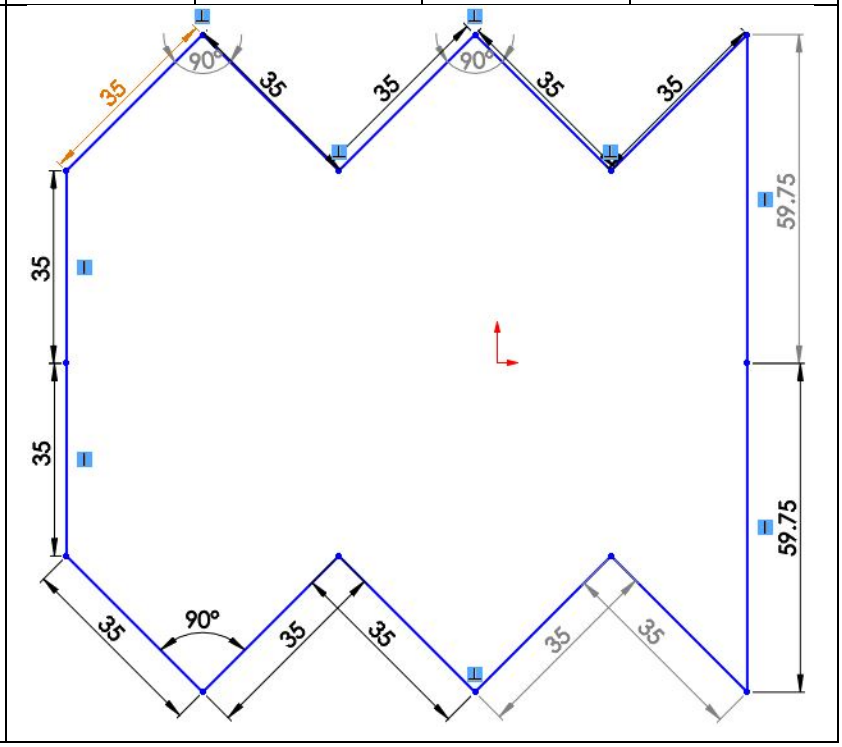			

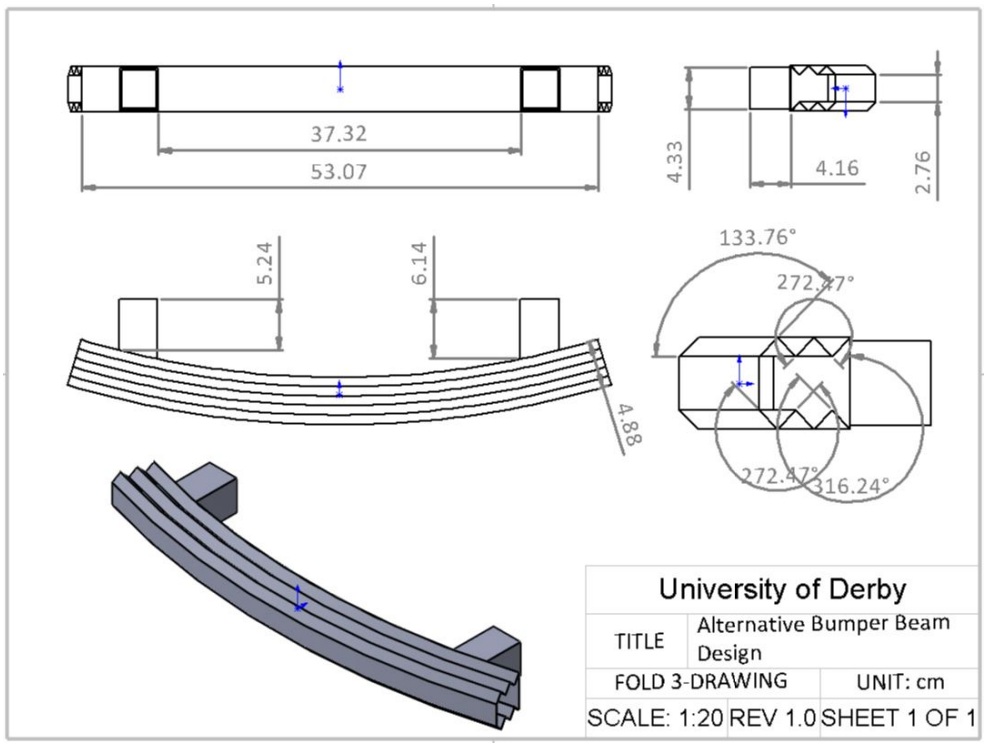

Figure 2.5 Fold 3 CAD drawing

The basic bumper beam shape was assigned with 4 different of curvature radius, each curvature

shape then further modified with 3 different cross-section profiles. Baseline shape was established that reflected as straight beam without any curvature. Followed with curvature shape of 2000 mm, 2400 mm and 3000 mm. Increasing the curvature to the bumper beam did not just increase the impact displacement and space, but also gained additional bumper system stability. The curvature also aids the distribution of the impact load where it regulates the impact force through the front bumper system. Because of this, an extra rigid connection was added between the bumper beam and crash boxes to enhance the energy absorption. (Osterman *et al*, 1992; Osterman *et al*, 1994; Sharpe *et al*, 2001; Pilkey *et al*, 2008; Hu *et al*, 2015)

It is demonstrated at the work conducted in the geometrical optimisation of the bumper beam, 5 beam shape was proposed at a minimum of 2400 mm, 2862 mm, 3200 mm and 2600 mm. This beam shape covered the range between 2400 mm to 3600 mm with 400 mm increases per shape change. Considered the 400 mm interval, it is also observed there was a big gap between straight beam to 2400 mm. This led to believe the result yielded if a beam curvature is built within this gap that may reveal some crashworthiness improvement which was overlooked. hence the selection of the beam shape of this research work will still use 400mm per shape change but assumed the range started from a minimum of 2000 mm, to capture the potential missing crashworthiness improvement that may have been overlooked. This resulted in the rest of the bumper beams shape which is 2400 mm and 2800 mm. Instead of selecting 3200 mm as it appeared in other literature, a shape at 3000 mm was selected alternatively selected with 200 mm radius increases and became the fourth shape. During the model beam construction, the overall shape is significantly bigger when the beam curvature was at 3200 mm. A few front bumper systems showed in chapter 3 indicated the bumper beam was generally in some degree of curvature. Some showed regular curvature cross the whole beam, others than carried some additional local geometrical features to enhance its crashworthiness capabilities. This research work was convinced 3200 mm beam curvature was a rare case where 3000 mm was the upper limit, and therefore 3000 mm was selected for the fourth shape. (Belingardi *et al*, 2013)

The results that were obtained from those pilot simulations run reflected the process of selecting the beam shape and found that the results are generally supported this assumption. When increased the curvature shape from 0 mm to 2000 mm, a considerable amount of force reaction value is reduced, and the overall deformation appeared in a smooth and self-regulated manner without any catastrophic or localised failure. where both force reaction and deformation process produced by the curvature shape at 1000 mm did not show significant

improvement. Literature mentioned the straight shape is found on some of the vehicles that fitted with such bumper beam shape, and still available to purchase on the market. Numbers of actual vehicle front bumper beam were shown in chapter 3 also proved this point. Hence the baseline shape was decided and built at straight beam without any curvature, although most of the energy-absorbing beam structure existed at a certain degree of curvature. A Pilot run results also indicated 2400 mm and 2800 mm have achieved some improvement over its predecessor. (Osterman *et al*, 1994; Sharpe *et al*, 2001; Pilkey *et al*, 2008; Fellers et al, 2002; Cheon et al, 1997)

The cross-section was also considered within this stage since the energy triggering mechanism as detailed in section 1.11.3. It stated the importance of energy triggering mechanism that was built into the metallic made structure, especially for energy absorption purposes. This will ultimately reduce the initial peak load of the structure upon the initial contact to the impact object, but also to regulate the deformation process instead to create any significant structural failure. Both of these benefits utilise as much as material available on the test bumper beam to participate in the impact process in order to maximise the amount of energy absorption.

Most of the energy triggering mechanism was used in the axial impact test where the test piece is subjected to vertical impact load. However, this is found to be difficult when the test piece is subjected to flexural impact, and specially made from composite material, and particularly to the case where the direct upgrade from metallic to composite. Non-like the isotropic property offered by the metallic material where the beam structure collapsed and compressed due to flexural type load, and the impact energy is absorbed plastically. The orthotropic material property of composite may present good strength in one direction, and weaker on the other two out of three-dimensional axis. As a result of this, composite structure shatters and fragments. Without any type of triggering mechanism to induce the impact and also to regulate the process, this will lead to composite fibre breakage. Surface crack almost happened shortly after the initial contact. This particular failure mode will inevitably proceed into an early stage catastrophic failure, where the beam unable to maintain its geometrical integrity during the early impact process and reduced the possibility of further absorbing impact energy.

In this scenario, the cross-section of the bumper beam is redesigned with a number of the fold grooves that act as a trigger mechanism and these grooves are designated as a fold profile. The profile contains numbers of folds were therefore created and built at fold 1, fold 2 and fold 3

each other individually, and detailed in later paragraph 2.7: CAD drawings. (Jones and Wierzbicki, 1993; Osterman *et al*, 1992; Palmer *et al*, 1997; Charoenphan *et al*, 2004; Pilkey *et al*, 2008)

To make sure the impact surface between the bumper beam to the rigid wall, the cross-section of all three profiles were symmetrical between the top and bottom half to make sure the deformation process happened without interference from poor model quality. Impact velocity and weight also appear ca influence the results during the stability test runs. Other parameters such as the material property and thickness that assigned to the beam, the impact velocity of the bumper system and other boundary conditions remain the same throughout the simulations.

Due to the number of parameters and variables involved, a few pilot simulations were performed prior to conduct the proper simulation to ensure the stability and the validity of the simulation. Excepted the validity of the simulation is going to perform in later paragraph 2.10: validation, early stability tests were specifically to verify the model features were correctly built, such as shapes and profiles. Other simulation related settings such as energy error, total run time and material properties were investigated as well.

2.6.2 Material, velocities and laden weight (specify steel type, consistent material property)

Table 2.5 Material properties

Properties Of all Materials						
Type	Density kg/m^3	Young's Modulus MPa	Poisson's Ratio	Yield strength MPa	Bulk modulus MPa	Shear Modulus MPa
AL6063 T6	2700	65,000	0.3	330	51,467	25,000
Steel	7850	210,000	0.3	250	166,670	76,923
Concrete	2300	30,000	0.18	28	15,625	12,712

Table 2.6 True stress-strain data

True stress-strain data						
AL6063-T6	E_p	0	0.02	0.04	0.06	0.08
	$\sigma(MPa)$	180	185	200	210	225
Structural Steel	E_p	0	0.0244	0.0485	0.0951	0.1384
	$\sigma(MPa)$	304.6	344.19	385.51	424.88	450.39

Structural steel and Aluminium alloy were used in chapter 3 and chapter 4. To justify the reason for this material usage, an investigation was conducted based on the crashworthiness performance on the bumper beam using both composite and metallic material, the structural steel was added as baseline performance, with Young's modulus E=20600 MPa, density ρ=7830 kg/m^3, Poisson ratio v=0.3 (Beyene *et al*., 2013). It then tested the bumper system at 15 km/h (9.3 mph). Other have suggested the bumper beam is made from aluminium conventionally and tested was performed at 15km/h, although the property of this aluminium material isn't available (Liu *et al*, 2016). A lightweight bumper system design made the comparison between the use of structural steel and aluminium 6061 to achieve the lightweight purpose, although the specific material property of this 6061 aluminium was not available (Wang *et al*, 2018). A particular work conducted on specifically to use the high strength steel to achieve lightweight and crashworthy car body. The sample of this high strength steel was provided by Bao steel corporation, and it has the yield stress of 220 MPa, with failure stress at 355 MPa. It did attach the laden weight of 1000 kg to the back of the bumper beam to a re-created more realistic scenario. Further foam filled bumper beam was also conducted using two types of steel which were labelled as B410 LA and B260 LYD. The mechanical properties of B410 LA are density ρ=7800 kg/m^3, Young's modulus E=21000 MPa, Poisson's ratio v=0.3, it has the initial yield stress of 443 MPa. B260 LYD shared the same properties above, but at less initial yield stress at 344 MPa. The impact was performed at a relatively slow velocity of 1m/s, with the laden weight assigned to the system at 1380 kg (Xiao *et al*, 2015). Integrated crash-box to the bumper beam was also tested at speed of 4 km/h and 8 km/h, with baseline material of mild steel, was selected, with the mechanical property of density ρ=7830 km/m^3, Young's modulus E=20600 MPa, Poisson ratio v=0.3. 1000 kg of laden weight is added to the back of this integrated bumper system.

An Axial crash test was performed on the square column to determine the SEA (specific energy Absorption), CFE (Crush force efficiency) and IPF (Initial peak force). The test sample was made from the aluminium 6063-T5, with the general properties of density ρ=2700 kg/m^3, Young's modulus E=65000 MPa, Poisson ratio v=0.3, yield strength at 180 MPa and the Ultimate tensile strength at 220 MPa (Ghai, *et al*, 2013). Other axial test used steel as model material, it is investigated the possibility of reducing the weight of the frame rail between types of materials, and also to increase the crashworthiness of the rail. It used the Steel with the properties of p=7800 kg/m^3, Young's modulus E=20700 MPa, Poisson ratio v=0.3, initial yield at 335.47 MPa. The total run time was 0.05 seconds with the impact velocity of 2.0 m/s. The

similar axial test was performed to determine whether the high strength steel is an ideal solution to replace the mild steel when comes to the side rail in the front. Both mild and high strength steel shared general properties, such as the density of ρ=7850 kg/m^3, Young's modulus E=21000 MPa, Poisson ratio v=0.3. The yield stress of σ_y 343 MPa made the high strength steel achieved better crashworthiness via RSM method, and the mild steel has 180.5 MPa was considered less favourable (Zhang *et al*, 2007).

The test velocities used in both IIHS (Insurance Institute of Highway Safety) and E.C.E (Economic Commission for European of the United Nations) are much less than the speed appeared in some of the literature works. Other works of literature than decided to use slightly higher impact velocities than the legally required impact velocities. Although the works of literature were used the legal test velocities are considered met the minimum standard, but in both cases were to select the same impact velocities as the legal requirement or higher, both perspectives are considered as compliance. However, the author of this research tends to agree with some pieces of literature were to conduct the bumper system impact at higher impact velocities than the minimum legal requirements. This considered as compliance with the legal requirement as to a minimum standard, but also achieve the intention to improve the crashworthiness of a bumper system. This is to ensure the bumper system will primarily satisfy any legal requirement and guidance, but also to perform better than other bumper system design. A similar reason to select higher impact velocity for better crashworthiness result, a 1000 kg of laden weight was also added to the bumper beam system to the simulation process was closer to what happened in the real world.

Material selection also largely affect the outcome of the simulations. The previous paragraph demonstrated mainly structural steel, or aluminium were used in varies pieces of literature, both gained good crashworthiness performance. It is noticed both flexural and axial tests investigated were all selected the steel as their baseline performance, and aluminium or composite as an alternative candidate. This showed the steel is the most favoured material and used in many cases. The author of this research tends to follow this method and using structural steel to establish baseline performance. Aluminium was selected as alternative material due to large numbers of works of literature used it to achieve a lightweight purpose. Since weight reduction is a parameter to determine crashworthiness performance.

2.7 Solver Environment

Explicit dynamic solver requires suitable settings for all parameters involved in each simulation. Bumper beam, crash box and a wall will be assembled into the assembly file and imported into the solver. It is noted the components included within the front bumper system were all made from thin-wall tubes instead of a solid piece to save the weight. However, in the FEA environment, the assembled front bumper system was defined as made from solid components. The component that as solid incur a significant amount of weight, and this means the computational time is increased correspondently as well. To ensure efficient and valid simulation results, all components included within the front bumper system is defined as the shell instead of solid.

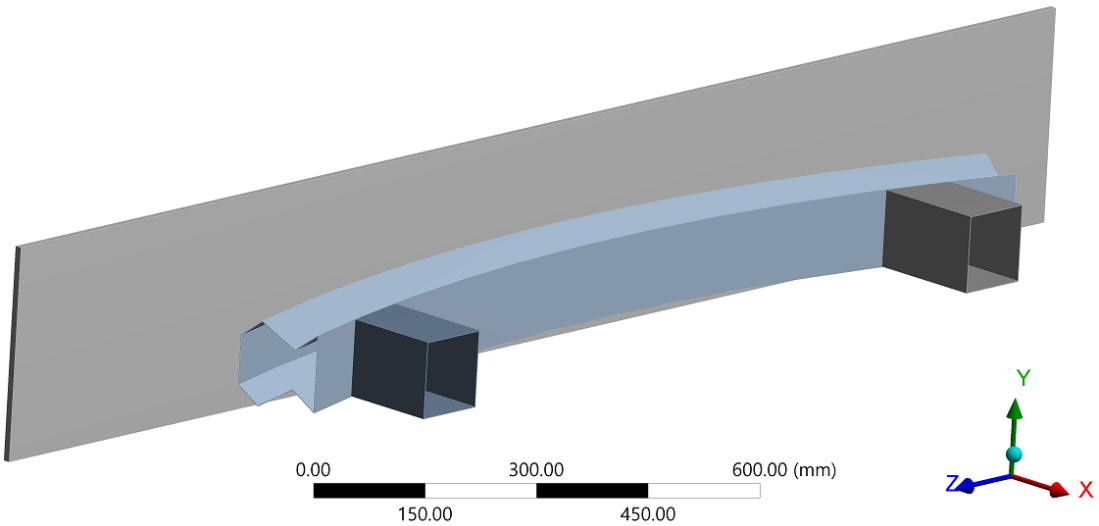

Figure 2.6 Ready to simulate assembly in Explicit dynamic.

Figure 2.6 showed the front bumper system assembly, and it is ready for simulating full frontal impact. The impact velocity of the bumper system was 4.2 m/s or 15 km/h. While the impact wall was set to rigid, Bumper beam is set to flexible and assigned with Structural steel, and later will be changed to Aluminium 6063-T6 for further investigation. Both crash boxes were rigidly attached to the back of the beam and had a total laden weight of 1000 kg combined to represent the realistic weight of a vehicle. Except that the beam profiles and curvature were available at varies profiles, impact velocity, types and system weight remained the same.

2.8 Validation

The front bumper system is presented at both flexural, and axial impact; hence two validation cases were performed based on the simulation types stated above. A flexural deformation was performed with the assembled bumper beam system was used under the impact velocity of 1

m/s.

2.8.1 Flexural Deformation – A validation case showed in Figure 2.6 based on the frontal bumper system impact was performed. An extremely closed front bumper system was created based on Figure 2.7, with correct material properties assigned. The boundary condition of and the simulation was also implemented, such as impact velocity, the thickness, the cross-section profiles and the bending curvature of the beam were all retained and satisfied in the validation run.

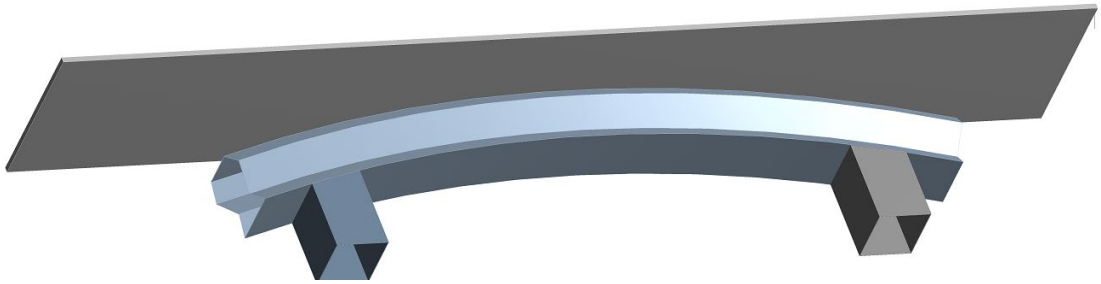

Figure 2.7 Validation model setup on simulation.

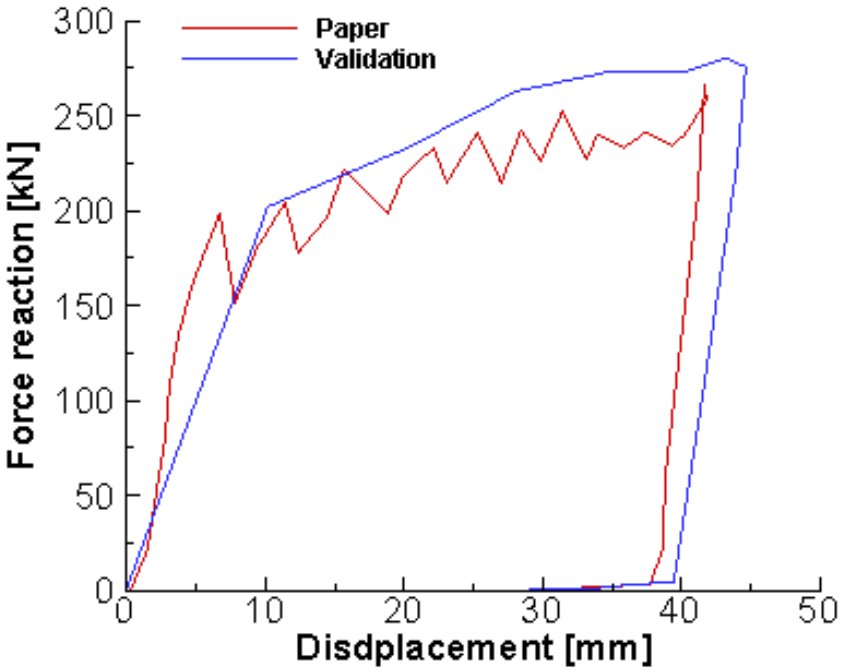

Figure 2.8 Validation of Flexural Deformation.

Figure 2.8 showed the difference between the literature and validation based on the same front bumper system. It is observed the literature yielded the initial peak force of 200 kN when the bumper system is displaced 5 mm, with fluctuated waved force trend, a slight increase resulted.

It reached a maximum of force value of 250 kN when the bumper system is displaced at 40 mm. Similarly, the validation run achieved slightly more peak force value just before the beam reached to 10 mm of its displacement. Despite the validation carried on this slight increasing trend which is similar to the literature paper, but without any curve fluctuation. Nevertheless, it reached to very similar peak force, and immediately dropped back down to 0 when both reached to 38 mm, and 40 mm of displacement each other respectively.

2.8.2 Axial Deformation – An axial load deformation was also included and validated. An investigation was conducted an axial load deformation on the vertical thin-walled tube. It was predicted base on the empty thin wall made tubes, adding the internal braces will achieve a positive impact on the force reaction. It featured circle geometry, with 3 types of internal brace fittings, and square geometry with 2 types of internal brace fittings. Empty circle tube will be validated using the same FEA set up to establish the baseline, and additional cross brace tube was also validated to see the coherent results in between (Song *et al*, 2012).

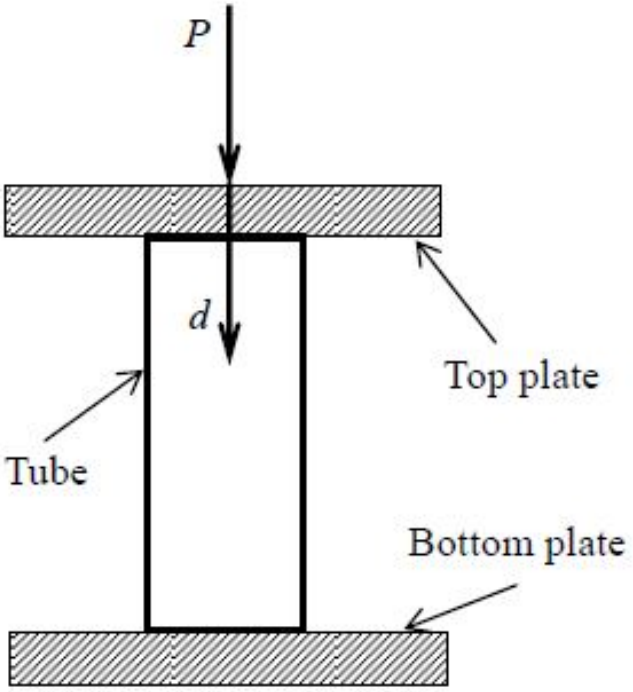

Figure 2.9 Experiment setup (Song *et al*, 2012).

Song, Chen and Lu also included an empty tube for both circle and square geometries to establish the baseline of the performance. The validation work used both empty and cross profiles for the circle geometry, and empty profile for the square tube for the validation purposes. While building the 3D models, the exact physical measurement of the tube was used.

For the circle geometry, tube overall length of 120 mm and the outer diameter of 59.9 mm resulted in the wall thickness of 1.8 mm was used for the empty profile. The cross profile, however, has 1.0 mm of tube thickness with tube length and outer diameter retained at the same value. On the other hand, for the square geometry, 1.1 mm thickness of the tube wall resulted in 40.3 mm of outer diameter. Tube length remained the same as the circle geometry for valid displacement. All test samples assigned with mild steel and same material properties which are: density ρ=7332.3 kg/m^3, E =190.5 GPa and Poisson's ratio v =0.3. The yield stress σ_y =287.9 MPa which generated via true stress and strain data showed as:

Table 2.7 True stress and strain data of mild steel (Song *et al*, 2012).

True stress and strain data of used material						
True stress (MPa)	287.91	335.43	385.38	425.38	476.66	506.93
Plastic strain	0	0.0319	0.0533	0.0793	0.137	0.205

Figure 2.10 Deformation behaviour of Circle tube between the literature and validation results. (Song *et al*, 2012).

It is worth to mention that the wall thickness at the test sample was slightly different. It is observed that the more brace added inside the tube, the less thickness of the wall thickness will be. The square geometry showed the same thickness to reduce the effect. To avoid this will have a negative impact on the simulation results, the weight of the geometry was altered slightly to ensure all test samples remained approximately the same (Song *et al*, 2012).

Chapter 3. Result and Discussion (SS)

This chapter focused on the results based on structural steel as candidate material. Both force reaction and energy absorption features were thoroughly investigated and reflected on the effect of the beam profiles. Excepted to the historical review of the bumper system's development and regulations in chapter 1, it is also important to examine current designs of the bumper system which are widely fitted to vehicles (E.C.E., 1994). Some important parameters were identified and used to make further improvements on the crashworthiness (Karagiozova *et al*, 2004; Wan *et al*, 2013).

Table 3.1 Various car bumper system design (obtained from google.co.uk)

"Content removed due to copyright reasons"

Table 3.1 showed various front bumper systems' beam profiles that are all currently fitted to the vehicle covering from the model year of 2001 onwards (Zhang *et al*, 2006). Most of the bumper beams featured curvature as well as cross-section profiles (Hashimoto *et al*, 2007). The prescription of the bumper beam shapes is also driven by aesthetic consideration, weight requirement and surrounding components (Langseth et al, 1999; Mamalis *et al*, 1997). The cross-section profile is usually non-uniform throughout the whole length of the beam (Reid *et al*, 1987). Some sharp bend and indentation are purposely built into the beam and crash boxes. These may serve as energy triggering mechanism to induce the crash load, or to regulate the impact by introducing a steady deformation process (Nagel *et al*, 2005; Przybylski, 2012; Davoodi *et al*, 2011)

3.1 Simulation Preparation

The basic beam was firstly created as shown in Figure 3.1 with 3 different cross-section profiles. The curvature shape was later added to this model. The crash boxes on both sides of the bumper beam are then extruded outwards of the beam. after the crash boxes extrusion operation in the Solidworks model, the “bend” command to create the curvature often initiated a geometrical error. This also caused a further issue when creating the foam, which will fit inside of the beam at later chapter. As a result, the entire bumper beam model had to create in a different way.

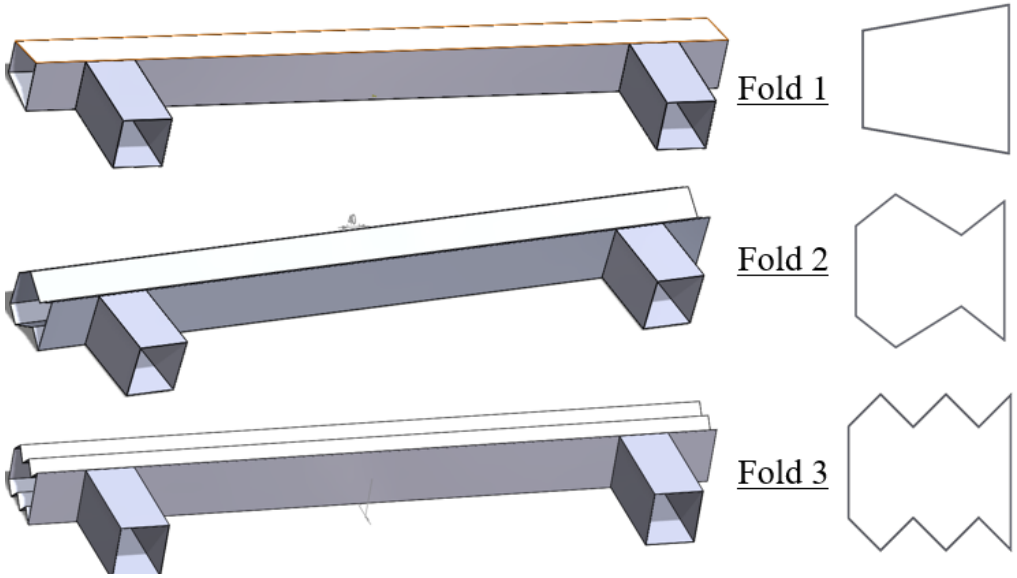

Figure 3.1 Fold beam with its cross-section profile from the Top, Middle and Bottom.

This error was first discovered during the surface interference inspection, where the edge of the crash-box interferes with the beam itself. This also affects the retro-fitting foam in the study of filler material for the beam (see Chapter 6) where interference warning persists after inserted the foam into the beam. The alternative “flex” command was used to define a curvature radius of curvature angle to define purposely showed Figure 3.2 resolved this problem. In the “flex” function, either the curvature radius of curvature angle can be defined to create correct curvature shape. In this case, a curvature radius was set 2400 mm and crash boxes were then successfully extruded to the beam surface.

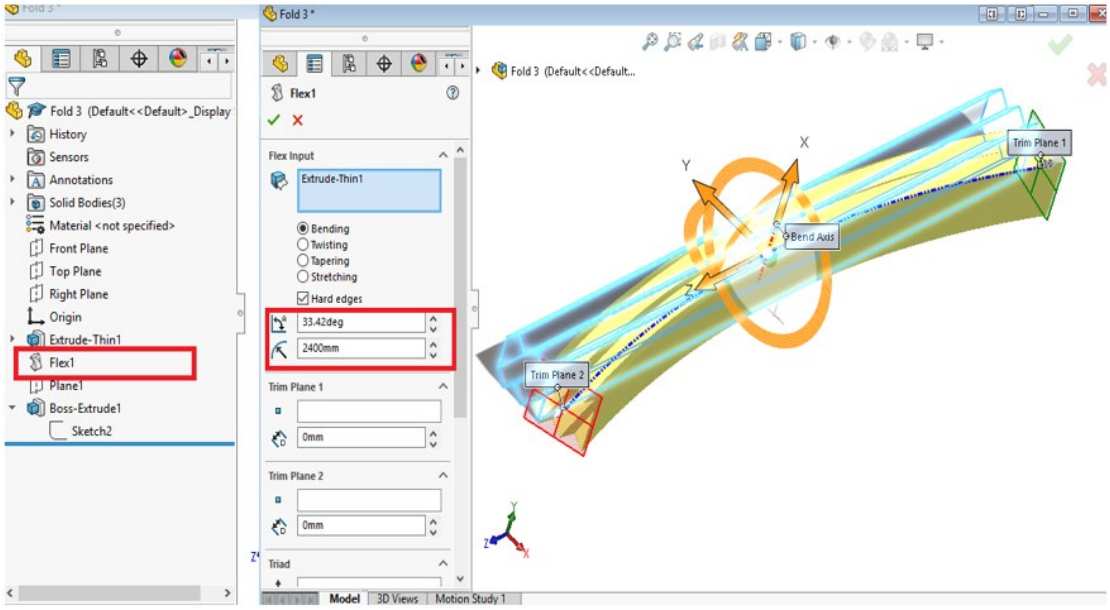

Figure 3.2 Flex function and its settings.

Once the correctly assembled bumper beam with crash-boxes was free from any geometrical faults, it then transferred into the Explicit dynamics and subjected to further prepare in an FEA environment. There are quite a few areas and parameters that require user input before the simulation. The bumper system assembled in Solidworks is created with the solid element. This incurred significant long simulation time. Where shell element is used alternatively to perform this type of simulation. This allows the thickness to be assigned to any components within the bumper system before or after each simulation to enhance the flexibility to suits individual optimisation requirement.

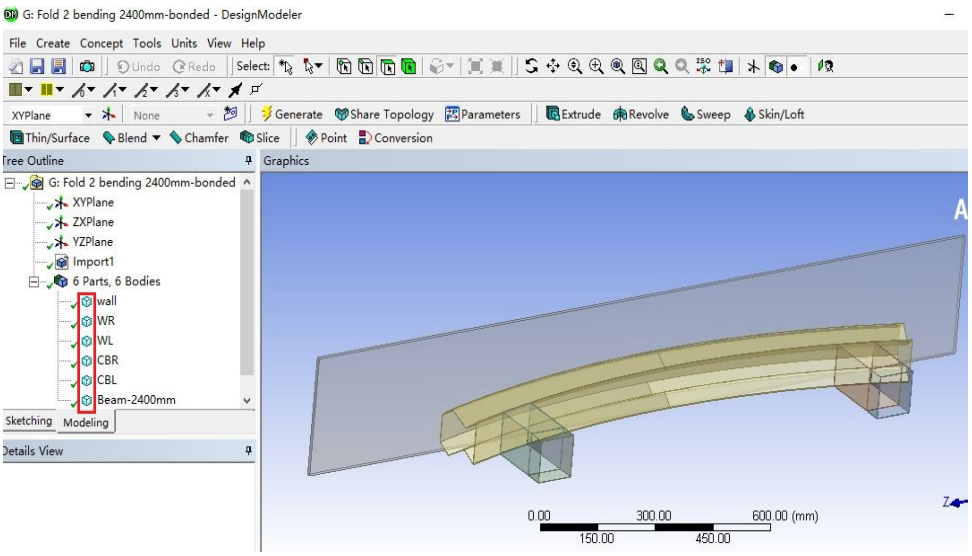

Figure 3.3 Bumper system assembly in Solid element.

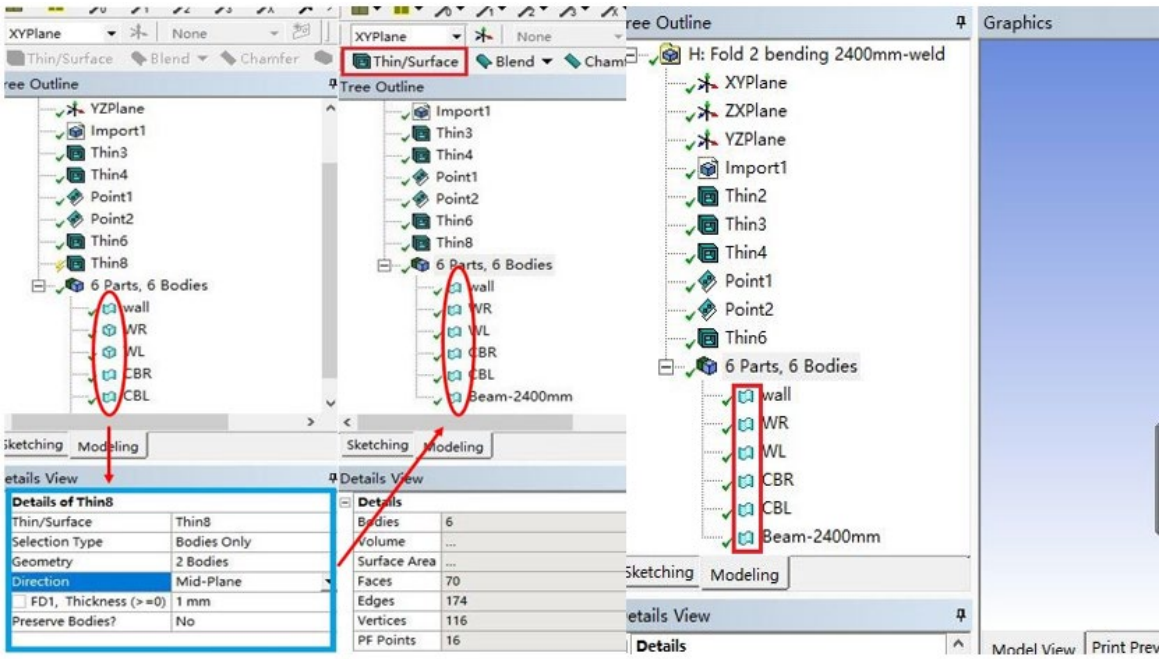

Figure 3.4 element alteration from Solid to Shell.

Design Modeller showed a clear difference between Figure 3.3 and 3.4, where the symbol in front of every component to the bumper system represented the solid element as before, and showed in shall element after it was converted. Noted the thickness appeared during the element conversion in Figure 3.4 allowed it to be defined as 0 mm where later in the explicit dynamics allows further input. Out of most bumper system designs, there were still small numbers of existing beam profiles that built with little, to no curvature at all.

A literature review investigated the curvature as an important parameter and found it can largely influence the outcome of the crashworthiness performance. It investigated the effect on to the crashworthiness performance given varies beam curvature radius profiles (Roopesh *et al*, 2015; Rimy and Faieza, 2010; Kumar *et al*, 2014). It proposed 4 cross-sections to the bumper beam and showed the deformation behaviour, force reaction and energy absorption value at the results.

As briefly illustrated in figure 1.72 at chapter 1, 8 cross section profiles were proposed and Subjected with 3 different cross-section profiles and different materials to evaluate the most suitable combination between those parameters.

Figure 3.5 Effect on to the mode of deformation for fold profile 1 to 4 (Belingardi *et al*., 2013).

Figure 3.6 Effect on reaction for and mode of deformation for fold profile 1 to 4 (Belingardi *et al*., 2013).

Figure 3.7 Effect on energy absorption for fold profile 1 to 4 (Belingardi *et al*., 2013).

The above figure showed all 4 profiles mode of the failure as well as their individual reaction force throughout the simulation. It can be clearly seen that fold 1 has slightly higher initial peak load around 0.01 second at the value of 150 kN, fold 2, 3 and 4 remained considerably lower range within 100 kN. Despite this obvious issue, fold 1, 2 and 3 offered a relatively smooth and consistent force reaction curve for the first 0.04 seconds. However, in general, fold 3 achieved overall good failure mode via a smoother force reaction curve when compared with fold 1, 2 and 3. This suggested that the deformation process of fold 3 remained within the expectation without any significant failure and hence yielded a progressive failure. This progressive failure mode did not carry over when the fold 4 was tested. It generally did not provide a progressive failure as fold 3 yielded but also showed a spike of force reaction

occurred just over the 0.04 seconds, this was due to the interference between the folds.

According to the Energy absorption chart at figure 3.7, it can be observed that all 4 profiles were achieved relatively smooth energy absorption process, but specifically profile 3 yielded better within the comparison, this is an indication of the fold 3 profile provides a stable failure mode that during the deformation, while maintained the energy absorption process. Smooth energy curve also means the fold 3 geometry deformed progressively without any significant catastrophic failure. All the above-analysed results concluded fourth fold is the under limit where beam showed undesirable results. Where the failure mode of fold 3 indicated the 3 fold design on the beam is appropriate for the stress to concentrate within the folding groove in order to aid the general deformation of the beam. The smooth and consistent force reaction curve of fold 3 reflected this. This study continued to conduct further optimization on both cross-section profile as well as the curvature of the beam. Based on the composite made fold 3 performed well on both energy absorption, failure behaviour and peak load, it is decided to further optimize the geometry for any potential energy absorption creases.

Figure 3.8 Two additional iterations from fold 3 (Belingardi *et al*., 2013).

It further modified the cross-section of fold 3, and iterated into profile 5 that featured a deeper length of a rear fold than the fold in the front, this resulted in strength reduction of profile 5. However, a completely opposite idea from profile 5 iterated into the profile 6, it featured deeper fold in the front.

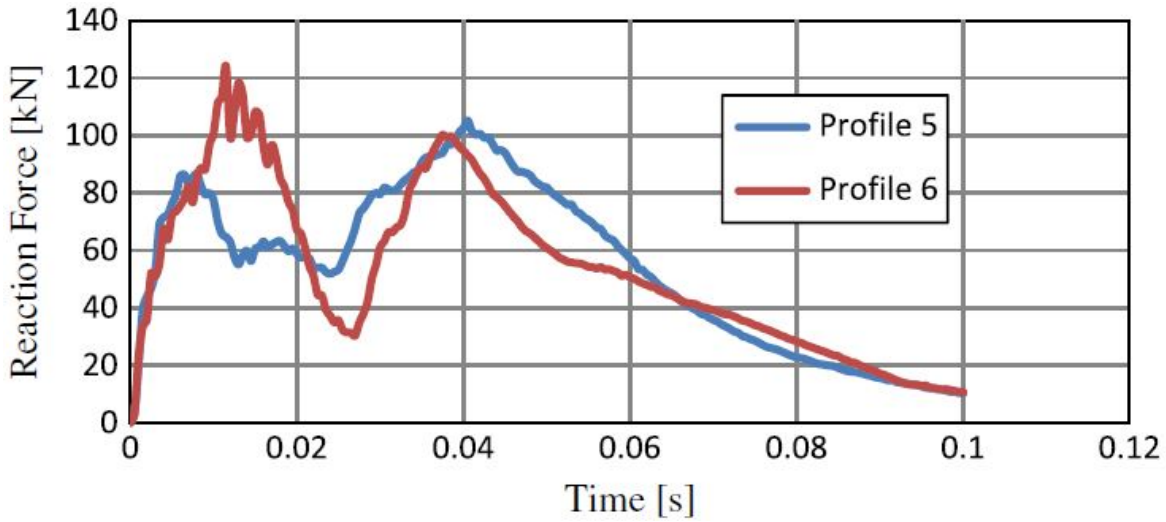

Figure 3.9 Effect of force reaction to the modified profile 5 and 6 cross-section profile (Belingardi *et al*., 2013).

Based on the failure behaviour from the figure 3.8. Fold 5 featured had deeper fold length at the rear of the beam achieved smooth deformation process, and the milder reaction force curve showed fold 5 generally satisfied the condition of smooth energy absorption throughout the simulation without any catastrophic failure. However, this is not the case of the fold 6. Deformation behaviour revealed that deeper fold length at front of the beam resulted in localized failure in the middle of the beam, and this particular profile gained higher force reaction when compared with the profile 5. It believed the thickness of the beam can also be an important factor that may have a positive impact to both deformation behaviour as well as energy absorption increases, consequently, using fold 3 as baseline reference, thickness iterations were constructed and became profile 7 and 8.

“Content removed due to copyright reasons”

Figure 3.10 Effect to the deformation behaviour of varies thickness beam profile (Belingardi *et al*., 2013).

“Content removed due to copyright reasons”

Figure 3.11 Effect to the deformation behaviour of varies thickness beam profile (Belingardi *et al*., 2013).

It is observed from both figure 1.78 and 1.79, the outer surface thickness of fold profile 7 a was increased followed the rest of the beam thickness remained the same. Fold 8 however is built complete opposite way, where the rear out surface thickness is increased but the front section of the beam remained the same. The results were quite the opposite as well. According to the figure above, profile 8 experienced a catastrophic failure where a localized structural failure occurred in the middle of the beam, and higher force reaction with spike value occurred in 0.04 seconds made believed that a localized failure is inevitable. When compared with profile 7, the peak load was generally smooth throughout the simulation without any spike on the force reaction. This suggested the deformation behaviour was better without any obvious undesired failure. Compare with all the results yielded by the profile 5,6, 7 and 8, it can be concluded that during the impact process, beam geometry built appeared in less strength in the first fold, deformation process appeared unstable, this represented by the localized structural failure that at some point of the simulation, it lost the capability to hold its relative original shape spike, such as the deformation behaviour of profile 6 and 8. On the other hand, when the first fold built at higher strength via either increase the thickness or reduce the angle of the fold, deformation process showed much more stable, and with noticeable low peak load, such as the case of profile 5 and 7.

And to conclude the improved made over the original profile 3, and iteration to the fold angle made to profile 5, and further thickness iteration done to the profile 7, both force reaction and energy absorption were all included within the comparison.

“Content removed due to copyright reasons”

Figure 3.12 Reaction force and energy absorption between profile 3, 5 and 7 (Belingardi *et al*., 2013).

It can be seen clearly, that based on already improved profile 3 out of the comparison with other profiles have the fold built into the beam geometry, alter the angle of the first fold, profile 5 achieved slightly better force reaction as well as deformation behaviour. Profile 7 showed added thickness at the first fold can also provide stable failure behaviour, and increase the energy absorption. However, increase the thickness will ultimately increase the peak load when compared with profile 3 and 5. This proportional relationship between the material thickness and peak load was coherently related to the earlier study (Nagel and Thambiratnam, 2005). The initial peak was just over 100 kN, but still higher than 90 kN and 80 kN yielded by profile 3 and 5 individually. And the overall trend of the force curve was higher than the other 2 profiles throughout the simulation. Nevertheless profile 7 achieved good energy absorption at a maximum of just below 10kJ while profile 3 and 5 only reached to just over 8kJ.

This literature took the third potential parameters that could have a positive impact on the performance, by constructing all the bumper beam into a curved shape, and with designated curvature of 2400 mm, 2862 mm, 2400 mm and 3600 mm. A 0 mm (straight beam) has also been included to establish the baseline to compare. Profile 7 in these cases was selected targeted test geometry which gave good energy absorption as well as the failure response during the simulation. Indeed, a straight bumper beam has also been added to the curvature comparison as baseline performance (Jones and Wierzbicki, 1993; Belingardi *et al*., 2015).

Figure 3.13 Reaction force VS time for different beam curvatures (Belingardi *et al*.,2013).

Figure 3.14 Reaction force VS time for different beam curvatures (Belingardi *et al*.,2013).

“Content removed due to copyright reasons”

Figure 3.15 Failure response at curvature a: 2400 mm, b: 3200 mm, c: straight beam (Belingardi *et al*.,2013).

Figure 3.13, 3.14 and 3.15 demonstrated the effect on to reaction force and energy absorption to the beam curvature increases. First to be noticed that the straight bumper beam with no curvature assigned, resulted force curve experienced a spiked over the chart limit at 400 kN after 0.02 seconds, the force curve indicated straight beam performed poorly due to unable to maintain its relative structure during the deformation process, and also caused by maximum contact area between the beam and impact wall. Further analysed other curvature profiles, it is realized when beam curvature was reduced below a certain level, such as profile a at 2400 mm in figure showed, the impact velocity promotes bending motion insufficiently.

Consequently, the stress concentration on to the outer surface of the first fold which in contact with the impact wall, since this stress cannot be sufficiently absorbed via the fold compression, this localized stress concentration led to catastrophic failure to the curvature less than 2800 mm. Based on this study, fold 3 geometry that equipped with profile 7 modification, with bending curvature at 3200 mm outperformed any other beam profiles. Despite that profile 7 indeed satisfied both high energy absorption, lower peak load, and lighter beam weight.

Table 3.2 Results of energy absorption and peak load for varies beam curvature profiles (Belingardi *et al*.,2013).

Radius (mm)	Energy absorption (kJ)	Peak load (kN)
2400	8.000	276.7
2862	9.852	109.4
3400	9.8585	156.6
3600	9.8491	381.1
Straight	9.852	1389.53

However, profile 7 still yielded a considerable high peak load rate at 0.05 seconds. Nevertheless, compared with 275 kN yielded by beam curvature of 2400 mm, 375 kN by beam curvature of 3600 mm, as well as the severely high of 1389 kN yielded by straight profile. To summaries the above findings, it is observed that from the force reaction perspective, introducing the curvature to the beam is indeed made improvement, but as the curvature radius is over certain level, in the case of this study, the upper limit is 2800 mm, started to show the sign of spike in force curve. It is a proportional relationship of higher of the curvature will lead to higher force reaction. On the energy absorption perspective, it is noticed the curvature radius either increases or decreases at a certain level contributed to the instability of the progressive failure of the beam, whereas the beam lost the capability to hold its relative original shape during the impact that appeared less linearity trend, hence resulted in reduced energy absorption rate.

For the interests of how failure occurs between the traditional metallic material, as well as an alternative composite material, some literature took a one step further based on already improved profile 7 with unidirectional but added bi-directional fibreglass to see if there are improvements. Additional structural steel has been added for this comparison as baseline performance. After added bi-directional composite material and structural steel, this final comparison answered the questions related to energy absorption structure, such as energy absorption ability and deformation behaviour between the traditional metallic material and composite material.

Figure 3.16 Effect on to the force reaction and energy of proposed material types (Belingardi *et al*., 2013).

Table 3.3 Results of Energy absorption and a peak load of proposed material types (Belingardi *et al*., 2013).

The above figure indicated both results of reaction and energy absorption based on the proposed 3 types of material. It is obvious that on the force reaction perspective, steel material gave higher initial peak load at 200 kN where other two composite types yielded much less at around 50 kN. However, on the energy absorption factor, despite all three proposed material types absorbed similar amount of energy, it is how each individual curve registered on the diagram separated between the metallic and composites, even between both types of composite. Firstly, the structural steel yielded approximately 40 mm of displacement while fabric composite reached to further 65 mm and pultruded at even further of 110 mm. This suggested the deformation process of steel made bumper beam completed the similar energy absorption with extremely short time, while fabric composite provided much smooth, elongated force trend with less concentrated failure process, pultruded achieved at most smooth energy curve and used twice much of the displacement. This means fabric offered generally better linearity when compared with steel beam, pultruded beam offered a huge improvement over both fabric and metal beam while still yielded the same energy absorption. To conclude all the above findings, it is clearly showed thickness, cross-section profile, and material replacement all have the positive impact of minimized the force reaction, as well as maximize the energy absorption. This experiment also criticized that in the case of complete material replacement for the bumper beam, it is essential to re-design the existing geometry, in order to adapt the different deformation characteristic.

It is summarised that both curvature radius and cross-section profile indeed achieved better force reaction as well as energy absorption. Despite this fact, it is noticed that manufacturers still produced their bumper beam with varies curvature and cross-section profiles to suits for individual requirement on aerodynamic, or aesthetic. Straight beam however performed poorly in this simulation test, but this does not mean it will also perform badly in a real-world scenario.

3.2 Force Reaction – Straight Beam

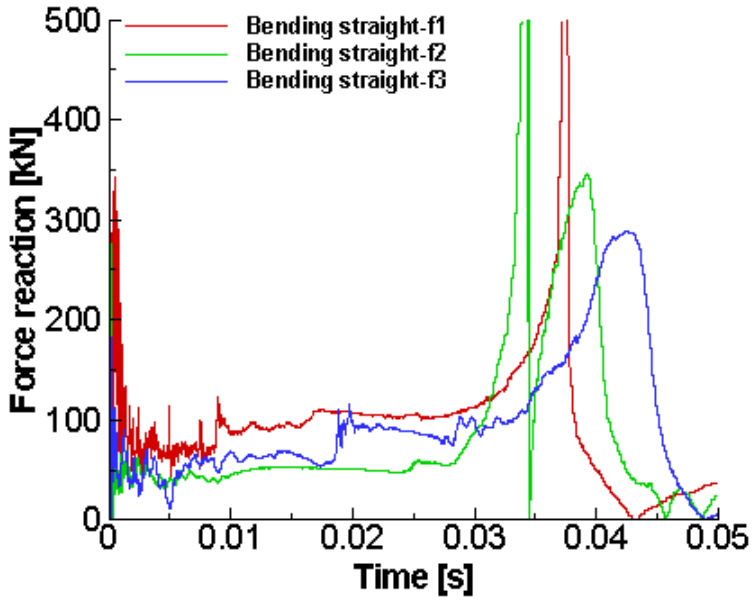

Figure 3.17 Curvature straight effects to the force reaction on all fold profiles.

Figure 3.17 showed the force reaction of all 3 types of fold profiles. All three fold profiles exhibited a very high initial peak load. Fold 1 and fold 2 peaked around 300 kN whereas fold 3 gained lower initial peak load, which was just below 200 kN. All 3 fold profiles experienced similar force drop back to range from below 100 KN and carried on relatively smooth until 0.03 seconds. Both fold 1 and fold 2 force curves increased dramatically that spiked over 500 kN (chart limit) then decreased back down in a considerably short period of time. Closer examination showed that the fold 1 reached the only force spike at approximately 0.037 seconds and fold 2 experienced twice at 0.033 and 0.035 seconds respectively. Both force curves on fold 1 and fold 2 eventually decayed to zero force value thereafter. Fold 3 behaved in a similar pattern after 0.03 seconds and gained force spike at 0.045 seconds, but the force value is significantly lower than the other 2 profiles.

Their force reaction curves can be explained from the deformation process as shown in Figure 3.17. The initial peak force was exceptionally high for all 3 fold profiles. The similarities of this initial peak load were purely attributed to the straight beam which has no curvature and caused numerical instability when the initial contact between beam and a rigid wall was numerically established. As results of this, 100 per cent overlap surface between the flat beam surface to the rigid wall was observed upon the initial contact. Because the force was calculated according to the stress sustained via the nodes on each element that is in contact with the rigid

wall. the higher number of the elements in contact with the wall due to straight beam design, the higher reaction force was yielded during the impact process. Any numerical instability in creating the contact will be greatly amplified by the large contact area. Particularly upon the initial contact moment, all 3 fold profiles sustained high peak load at the beginning of the simulation. However, the force curves of all 3 profiles dropped back and maintained to below 100 kN after the initial contact stage. This indicated that the absence of any curvature in the bumper beam will cause a very quick rise of reaction force which is passed to the folding groove. This enabled the beam deformation process steadily and provided constant energy absorption, which would otherwise present an absorption reduction due to unstable deformation and structural failure. This steady deformation behaviour reflected on the trend of force curve at all beam profiles until 0.03 seconds.

This trend did not last long. Instead, all force curve trend was dominated with violent force fluctuations after 0.03 seconds. This was due to the insufficient number of folds built in fold 1 and fold 2 for the straight beam. Both beam profiles did not effectively consume total resultant impact load before reached to the saturation stage, the residue impact load continued to drive the bumper beam assembly further into the wall that ultimately drew crash-boxes directly into the impact process and therefore created the force reaction to fluctuate violently. This inevitable issue was remedied a lot in fold 3, which has been improved significantly largely due to extra fold available (see Figure 3.14). The initial peak initial force reaction upon the impact was merely 180 kN, which is at considerably less than what the other profiles offered. The value and trend of force curve behaved much more desirable after 0.03 seconds.

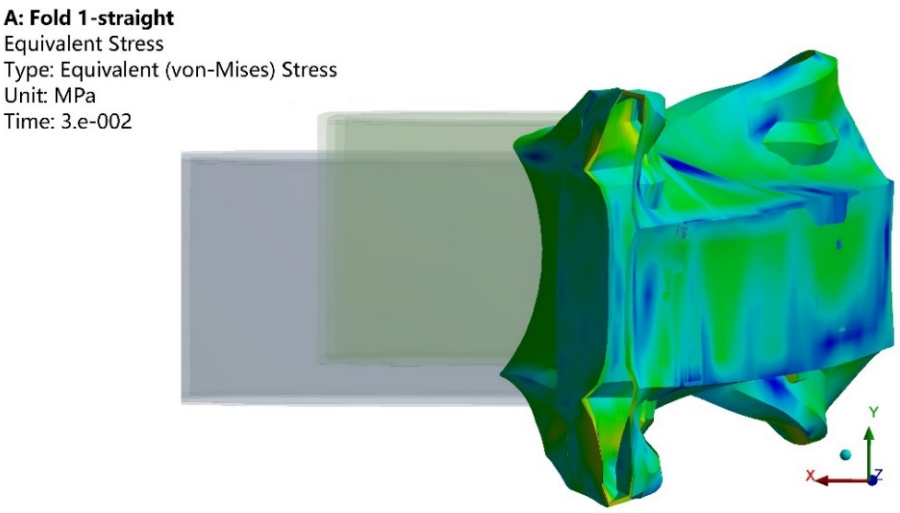

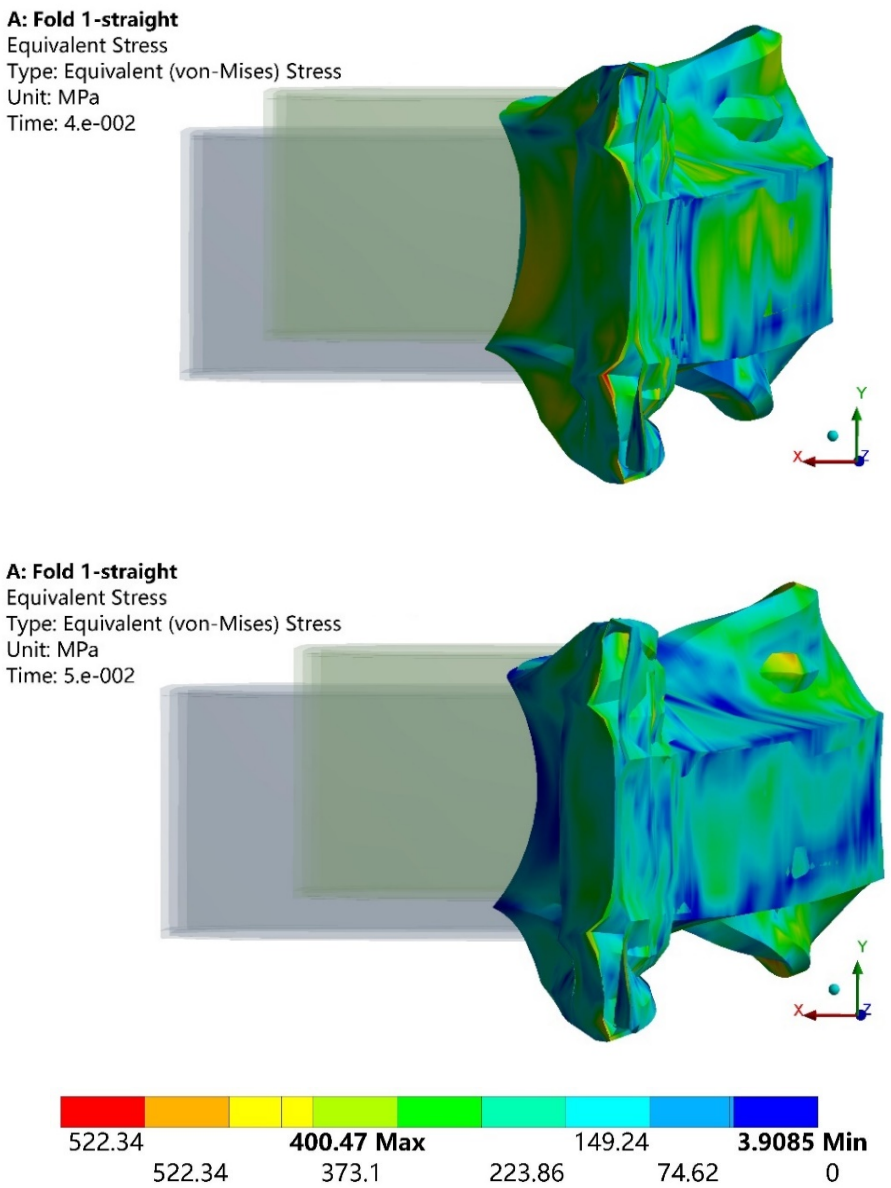

Figure 3.18 Von mises stress distribution of fold 1 from 0.03 to 0.05s.

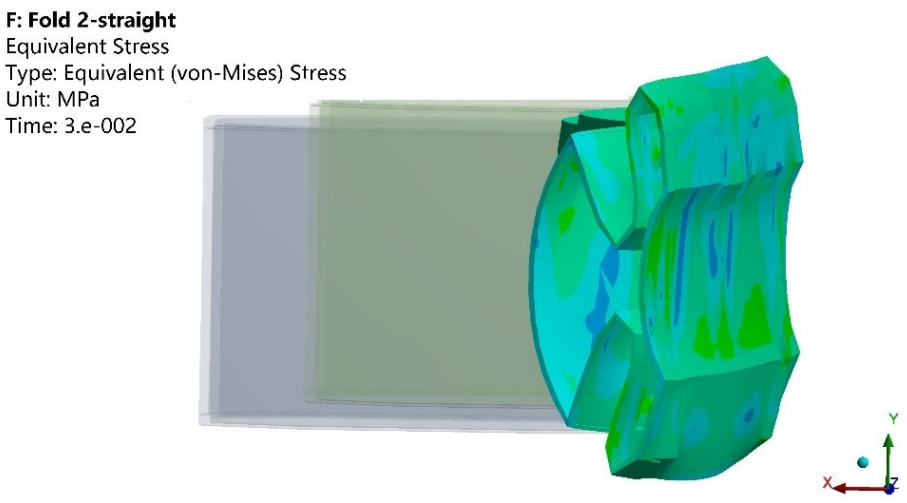

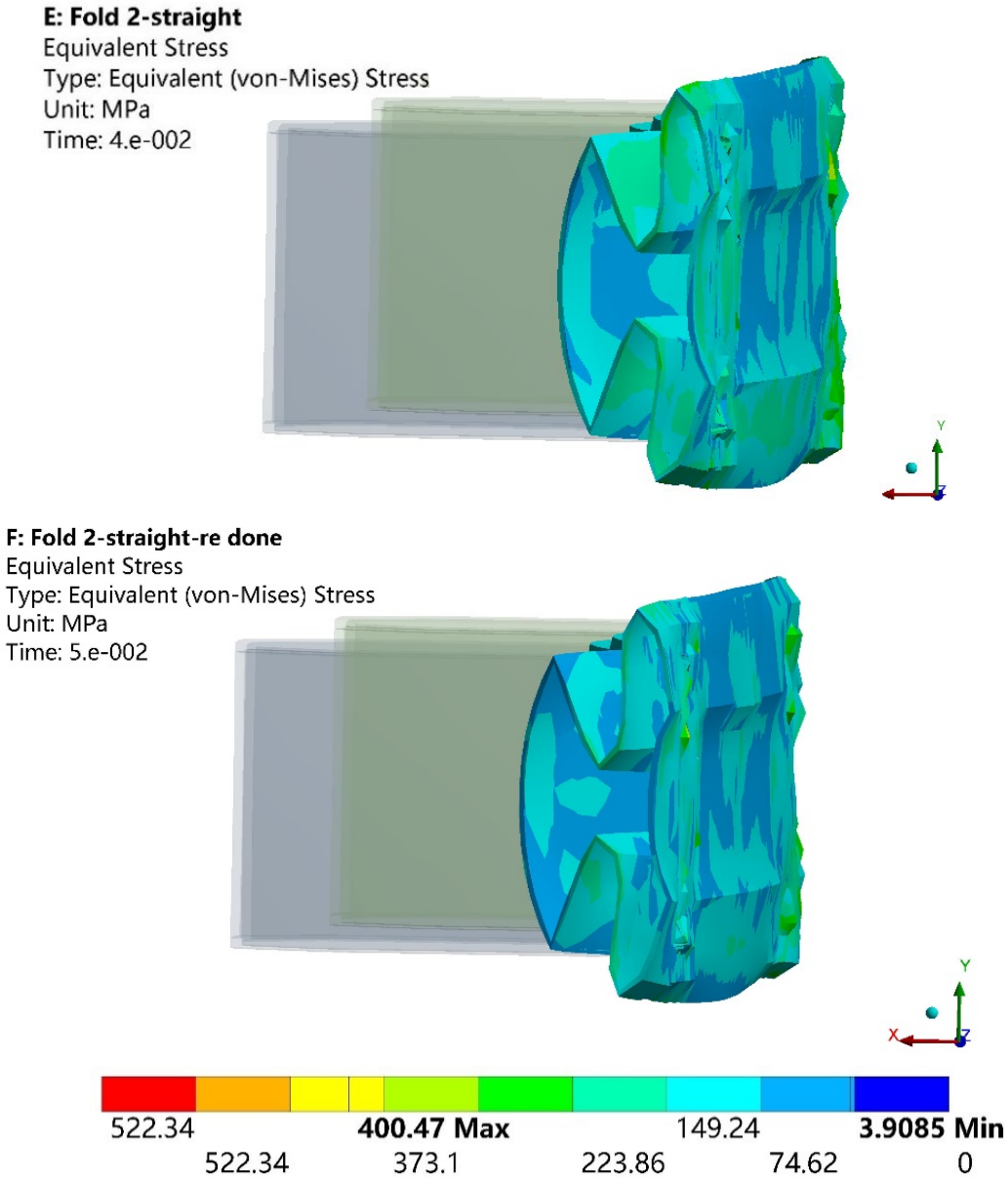

Figure 3.19 Deformation behaviour of fold profile 2 from 0.03 to 0.05s.

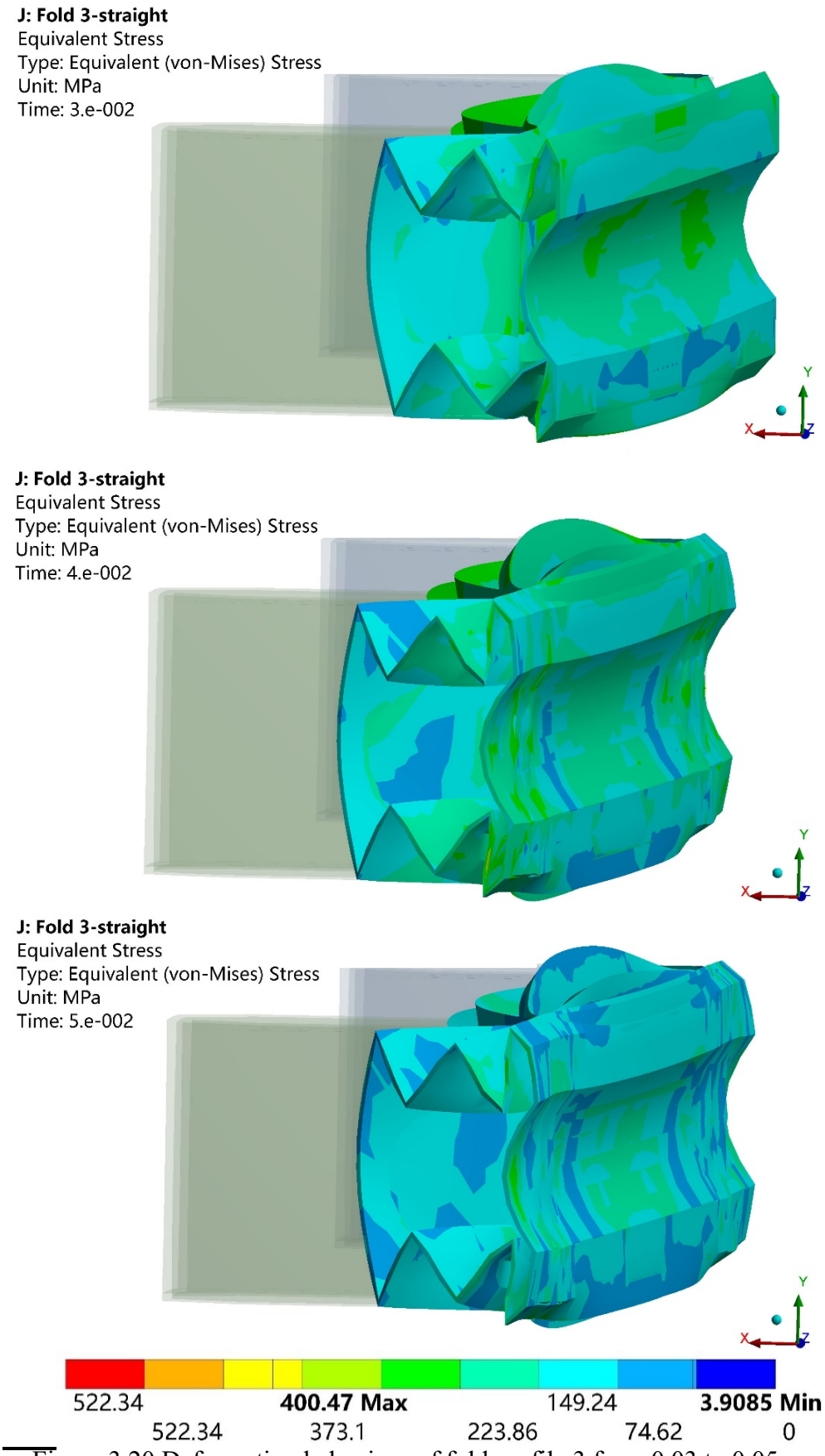

Figure 3.20 Deformation behaviour of fold profile 3 from 0.03 to 0.05s.

3.3 Force Reaction – Curvature 2000 mm

Curvature was purposely introduced the straight beam to suppress the initial high peak force. Figure 3.15 showed the effect on the force reaction after the bending curvature radius was set 2000 mm. The initial peak force for all fold profiles fell into a much lower range than the straight beam design. The initial peak force of fold 1 reached 90 kN while both fold 2 and fold 3 remained at a much lower value at 35 kN and 25 kN respectively. The force curve for fold 1 entered into the wave trend of between 65 and 90 kN, where this trend was generated per 0.005-second interval. This was followed by an increasing trend from 80 kN to 100 kN. The fold profile 2 presented a gentle increase after the initial peak phase at a value of 35 kN. It experienced a gentle drop to 45 kN before 0.02 seconds then stabilized at 60 kN towards the end of the simulation. Force curve of fold 3 initiated at even lower initial peak load at just 25 kN, and quickly climbed to 70 kN that was in the force range of fold 1. This reaction force curve ended with a gentle decline after showing a similar wave trend and value like fold 1 during the same period.

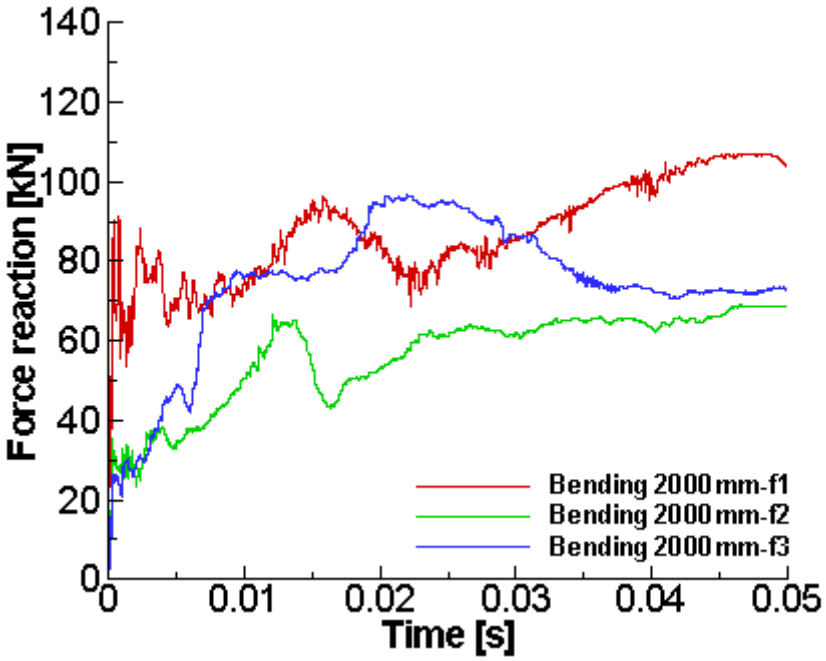

Figure 3.21 Curvature 2000 mm effects to the force reaction on all fold profiles.

Compared to straight beam (as shown in Figure 3.17), Figure 3.21 revealed that beam curvature reduced overall peak forces the beam experienced on all fold profiles. All fold profiles have recorded the initial peak force only 1/4 counterpart of the straight beam. The introduction of curvature radius 2000 mm improved the deformation process after the initial impact. But also

appeared less capable to regulate its deformation process. Increasing the beam curvature from 0 mm to 2000 mm has reduced the initial impact area with the wall, which this potential benefit to all fold profiles to achieve good overall force reaction results. It can also observe from Figure 3.21, the exhibition of increased force curves on all 3 profiles indicated the effectiveness of deformation engagement and to its energy absorption process.

The fold 1 increased the reaction force towards the end of the simulation, which was caused by limited compressing motion due to one folding in the beam profile. This led to the contact area between the beam and wall remaining the same during the deformation process. Consequently, the resultant reaction force continued increasing after the 0.03 seconds throughout the simulation. The fold 2 presented some gentle deceleration upon the initial contact which was illustrated by a low initial force value at 30 kN. Because of two folding structure, it effectively buckled upon the establishment of initial contact, the resultant force was less than fold 1 until 0.02 seconds. With the progress of beam compression occurrence after 0.02 seconds, the mid-section in the bumper beam bent and buckled inwards. It indicated the beam entered further deformation stage where the folding design was once again compressed further locally. It prevented the beam intruded backwards under the bending effect. Fold 3 recorded the force at a slightly lower value of 25 kN upon the initial contact then increased further to 0.02 seconds. Unlike the force drop at 0.02 seconds, then fold 3 effectively was compressed at all folding locally without a bending motion, the force curve increased further after 0.02 seconds. This demonstrated the fold 3 is capable to process the residue impact load without creating bending motion to the beam like showed in fold 2.

3.4 Force Reaction – curvature 2400 mm

Bending curvature increased to 2400 mm has resulted in fold 1 to yield a higher initial peak load of 80 kN, while the fold 2 and fold 3 have achieved at a much lower value at 30 kN and 10 kN each other respectively. Figure 3.16 displayed the fold1 yielded a different force curve after 0.02 seconds then the other profiles. It gained fluctuated range between 40 kN to 70 kN for the first 0.02 second, and started of experiencing a sudden force increases dramatically and remained this trend until it reached to 130 kN before it plunged back down to 5 0kN right before the simulation ends. Both fold 2 and 3 showed gradual increases after the initial contact with the wall and displayed similar force trend thereafter. While the fold curve on fold 2 entered into a gentle decrease, fold 3 carried on the previous gentle increases and entered into a steady-state until the end of the simulation.

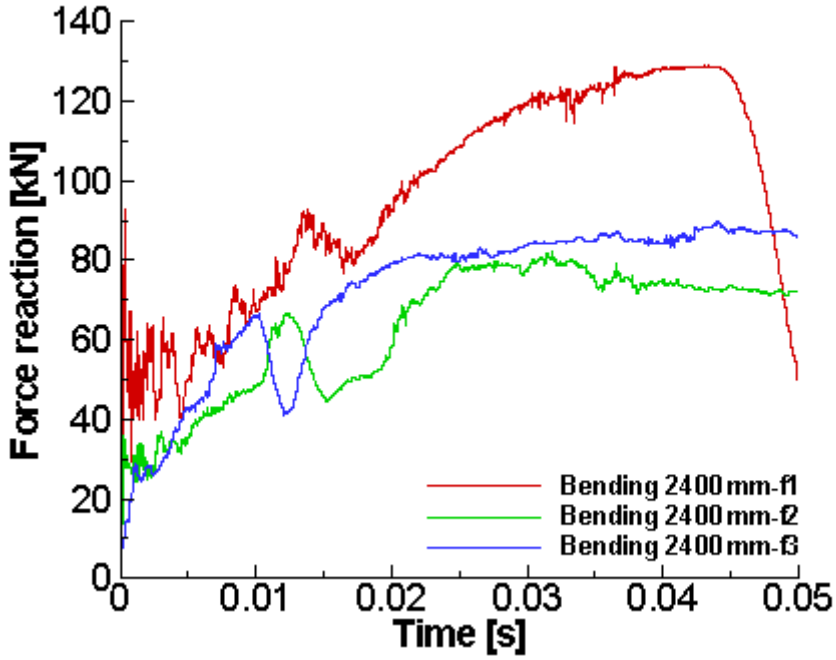

Figure 3.22 curvature 2400 mm effects to the force reaction on all fold profiles.

Despite that the curvature has been increased to 2400 mm, all profiles performed reasonably well on the initial peak force, while the fold 1 yielded similar initial force around 90 kN compared to the curvature at 2000 mm, both fold 2 and fold 3 remained noticeably low. There is a significant force increase occurred to fold 1 after 0.02 seconds due to the increased contact area between the beam and the wall. Due to the nature of the fold 1 that has less deformation capability, as the bumper beam is further driven towards to the wall, localised failure was presented such as buckle and expand as the crash-boxes started to engage the impact process. This ultimately demonstrated the fold 1 beam is less capable to regulate structural deformation, which resulted in greater force reaction detected.

While folding 2 and fold 3 performed better, both performed differently. Further increasing the curvature to 2400 mm did not affect the initial peak load of fold 2 but to its force trend. The force curve of fold 2 appeared a general increase towards to the middle of the simulation, and a quick drop indicated the first fold on the beam is came in self-contact, and increased again indicated after the first fold was fully compressed and closed, and the second fold started to receive further kinetic impact energy. The force curve of fold 3 behaved similarly to fold 2. An obvious curve drop indicated the transition from the fully compressed first fold to the second fold continued to engage further impact load. Steady gentle increases after the 0.02 seconds demonstrated a fold 3 was performed reasonably well until the end of the simulation. This

indicated the deformation process was in a good controllable manner where the overall beam shaped has maintained throughout the impact process.

3.5 Force Reaction – curvature 3000 mm

At the beam curvature of 3000 mm, initial force reaction value was at a very low rate of all 3 profiles like displayed in figure 3.17. While fold 2 and 3 remained at low force rate upon the initial contact, fold 1 has achieved both initial peak force reduction, from 90 kN down to 30kN, and also demonstrated a stable and regulated force increases throughout of the impact process. This also benefited the initial peak force of fold 2 where its only 10 kN, as well as its steady impact process which similar to the fold 1. Fold 3 displayed a similar force trend to both fold 1 and 2 but appeared in a significant increase than the other profiles. The force curve recorded in a steady trend at 110 kN throughout the rest of the simulation.

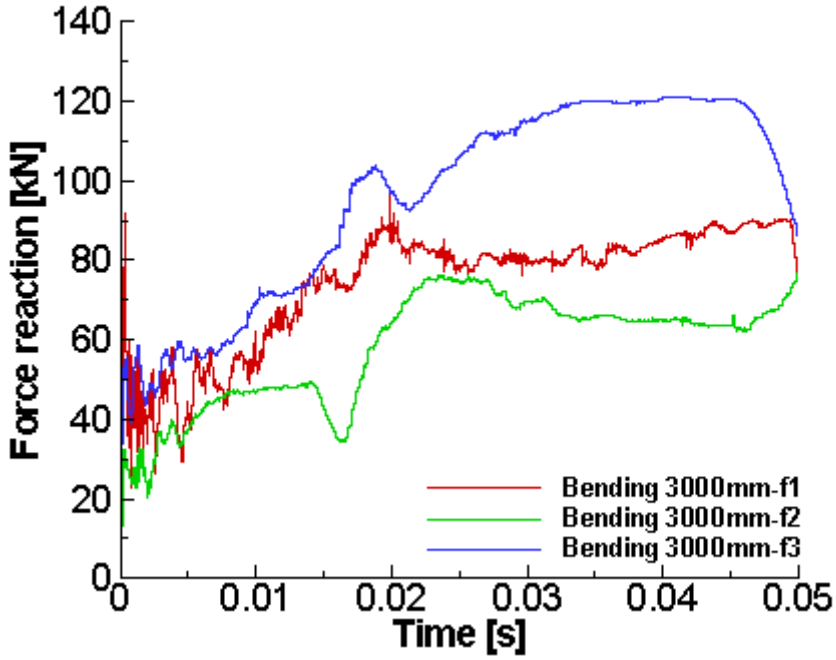

Figure 3.23 Curvature 3000 mm effects to the force reaction on all fold profiles.

The 3000 mm curvature radius did improve the initial force reaction. This means upon the initial contact; all beam profiles were able to decelerate the bumper system gently and smoothly without potentially damaging any nearby components. Continued to benefit all fold profiles with very low initial peak force.

Further observed the Figure 3.23 showed 3000 mm beam curvature allowed both fold 1 and 2 to deform gradually without any significant fluctuations, and this was indeed reflected at a

consistent force curves showed on both fold 1 and fold 2 force curves. However, a short force drop occurred to fold 2 before 0.02 second suggested the compression of the first fold was nearly completed and continued increasing force displayed the second fold started to engage at any residue impact load. On the other hand, the continued force curve increases on fold 1 indicated only one fold structure was consuming the impact load, and it had to work an extended period to further absorbing the impact energy.

Fold 3 entered gradual increases until the 0.02 seconds, indicated the deformation occurred in a consistent and regulated manner. This did not last long but replaced with large force increases. This phenomenon suggested due to the additional fold built into the fold 3 that allowed the beam to further engage the residue impact load, while the fold 1 and 2 were almost reached to a deformation saturation that folds on them approached into almost fully compression. The third fold was started to engage the residue impact load.

3.6 Plastic work – Straight Beam

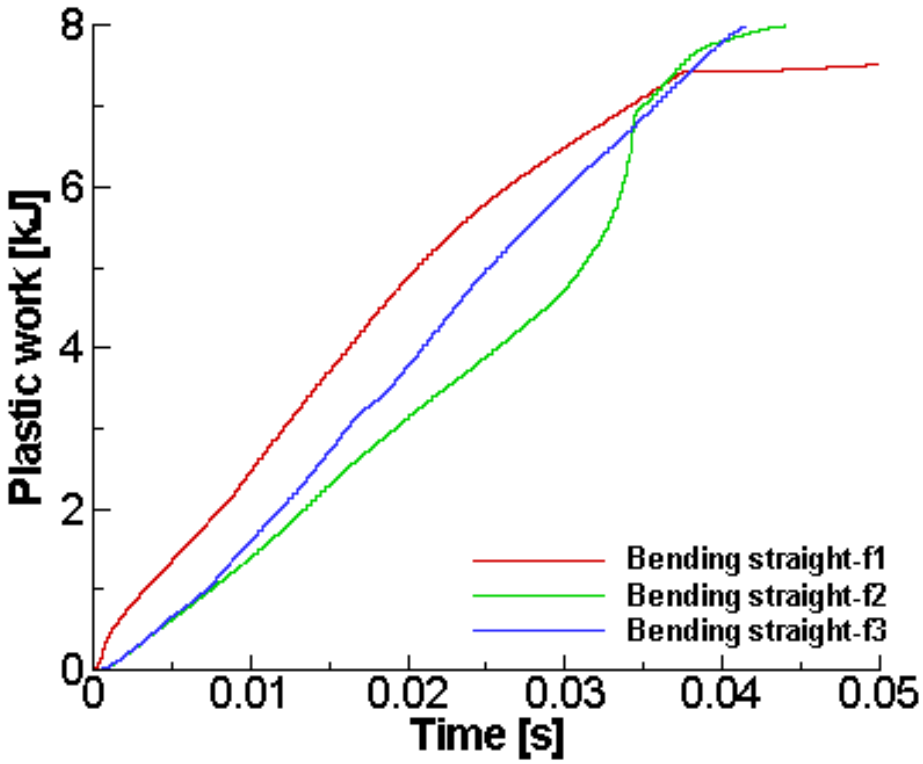

Figure 3.24 Curvature straight Effects to the plastic work on all fold profiles.

Description – Based on the information showed in Figure 3.24, fold 1 appeared at a slightly higher energy absorption rate until the 0.04 seconds. Initial absorption started at 0.5 kJ, which

was higher than both fold 1 and 2. It then maintained this higher but smooth absorption rate smoothly throughout. It reached to 7.52 kJ just before the end of the impact process. The energy curve on both fold 2 and fold 3 were initiated at a lower and almost identical absorption rate, until the 0.01 seconds compared to the fold 1, but proceeded further differently.

While fold 3 maintained at a steady absorption increases, fold 2 carried further at a reduced rate before 0.03 seconds but experienced a sudden incline from below 5 kJ to almost 7 kJ when reached to 0.04 seconds. It entered a slight incline until finally settled at 8.05 kJ. The absorption curve on fold 3 maintained a smooth absorption trend throughout the impact process, while both fold 1 proceeded higher and fold 2 proceeded lower. It reached to maximum absorption rate at 8.119 kJ.

Discussion – It is noticed that all 3 fold profiles performed relatively smooth for the first 0.035 seconds without any significant increases or decreases. Fold 1 displayed at higher absorption rate upon the initial contact while folding 2 and fold 3 remained in a gentle increase. This was caused by an insufficient number of folds on the beam. Without energy triggering mechanism provided by the multiple folds upon the initial contact, fold 1 immediately engaged the impact process as well as the rest of the deformation process thereafter. Interestingly this higher absorption rate stopped at 0.04 seconds and maintained almost flat until the end of the impact process. This is a clear indication of fold 1 was less capable to absorb complete impact energy. The only 1 fold deformed completely and sustained more deformation than the other profiles. And because of this, fold 1 profile reached to a saturation point quicker than the other profiles, and its energy absorption curve hardly registered any value after 0.04 seconds. Although fold 1 was recorded at a higher absorption rate, with the characteristic of smooth and consistent, it reflected it effectively held its own structural integrity throughout the impact process (Lee *et al*, 1996).

It is further observed fold 2 and 3 did not repeat this issue, both two profiles registered slightly higher absorption rate after 0.04 seconds. Despite the fold 2 reached to similar highest absorption rate to the fold 3, without any curvature presented to the beam, 2 folds design resulted in the outer surface of the beam bent inward during the impact process. Missing curvature further contributed negatively to the reduction of the contact area to the rigid wall, this reflected on the reduced absorption rate between 0.01 and 0.03 seconds as a result. This means the fold 2 did not effectively consume its impact energy and ultimately caused the crash-

box to collide with the wall and a sudden absorption increase was registered in Figure 3.18.

Additional fold built into the fold 3 appeared did not achieve a significant increase of energy absorption but aided the deformation behaviour of the beam. Without exhibiting either higher absorption rate like fold 1 or a fluctuated absorption rate like fold 2, it continued at a steady increasing rate towards to the end of the impact process. This smooth energy curve represented the deformation behaviour was relatively well-executed, where the compression motion is effective, and the collapse process from the first to third fold was well within the expectation. Interestingly without any curvature presented, fold 3 was benefited from regulated impact force transition between the fold suggested no sudden absorption curve movement that behaved like fold 1 and 2.

Parameters –

Table 3.4 Curvature straight Effects to the plastic work on all fold profiles.

Plastic work-Bending straight					
Profile	Weight (kg)	Total PW (kJ)	**SEA (kJ/kg)**	Avg PW (kJ)	**CFE (%)**
Fold 1	12.743	25.347	**19.892**	9.687	**38.22**
Fold 2	15.181	21.358	**14.066**	6.968	**32.62**
Fold 3	17.615	23.258	**13.205**	7.99	**34.35**

Out of all 3 fold profiles, weight increases in correspondence of adding each fold to the beam structure. Under the same loading conditions, it is expected that there should be accompanied by extra energy absorption (Xuan *et al*, 2003; Feng and Feng, 2002). This is not the case were under the straight beam design, fold 2 and 3 both have achieved reduced SEA (specific energy absorption) and CFE (Crush force efficiency) than the fold 1. Despite this reduced performance showed in fold 2, fold 3 however, showed improvement on both SEA and CFE. Despite that, the fold 2 absorbed 3.989 kJ less energy than the fold 1, but the SEA was offset heavily by 29% because of the added weight. The total energy absorption was reduced from 25.347 J with fold 1 to 21.358 J with fold 2. Fold 3 has further additional 2.429 kg weight on the beam due to the third fold added, but this did not affect both SEA and CFE performance. Additional energy absorption was expected as increased to 23.258 kJ.

It is observed that the fold 1 remained in a smooth absorption process upon the initial impact, but a clear converse curve showed between 0.01 seconds to 0.03 seconds. This was due to the only 1 fold engaged the deformation without any energy triggering process. This also caused

the absorption interrupted and stopped after 0.04 seconds, mainly due to rapid beam deformation without any further available geometry. Fold 2 appeared in a concaved curve during a similar period of 0.02 and 0.03 seconds. This was due to the beam contact surface buckled while the second fold was expanding. Fold 3 improved both SEA and CFE when compared to fold 2, mainly because of the third fold provided a stable deformation allowed for additional energy absorption during the process. It can be concluded that, fold 3 achieved overall a good deformation behaviour and increased energy absorption when compared to fold 2.

3.7 Plastic work – Curvature 2000 mm

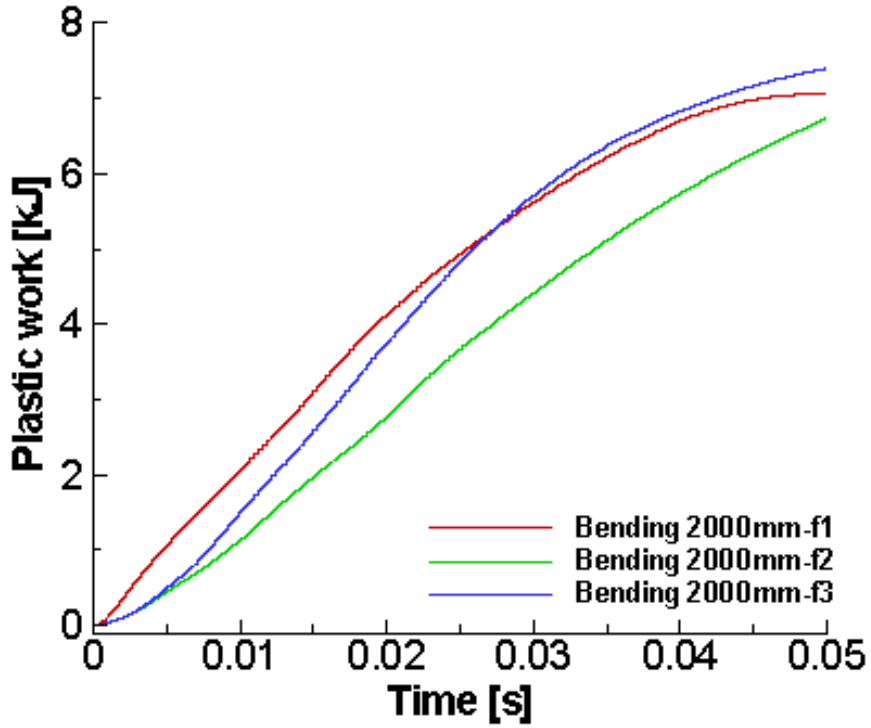

Figure 3.25 Curvature 2000 mm Effects to the plastic work on all fold profiles.

Description – According to Figure 3.25, fold 1 started with a higher absorption rate when compared to fold 2 and 3 upon the initial contact. It maintained this smooth trend and reached to the maximum energy absorption at 7.05 kJ. Fold 2 started with a similar rate when compared with fold 3 until 0.01 seconds but not thereafter. it appeared in slight increasing after, it maintained this energy absorption rate throughout the simulation, and finally reached to the maximum energy absorption value at 6.74 kJ. Fold 3 showed the different trend then fold 1 and 2. It shared a similar absorption rate to fold 2 until 0.01 seconds and entered into gradual

increases towards higher absorption level offer by fold 1 until the 0.03 seconds. It carried on at this higher absorption rate until reached to the 7.40 kJ of maximum energy absorption.

Discussion – Fold 1 achieved a higher energy absorption rate at the beginning of the chart then the fold 2 and 3. It maintained this smooth absorption rate for the first 0.03 seconds, where fold 2 and 3 are generally lower. This higher absorption rate suggested that fold 1 offered more plastic deformation while both fold 2 and 3 offered less. This smooth absorption rate carried on means the rest of the deformation process occurred in an orderly fashion without any significant fluctuations.

Fold 2 started at similar absorption rate to the fold 3 until just before 0.01 seconds. It then entered a steady absorption increases throughout the simulation. Although fold 3 offered similar deformation behaviour and plastic deformation until 0.01 seconds. Fold 3 entered a gradual increase in its absorption rate before 0.03 seconds and overtook what fold1 offered. This indicated that the fold 3 offered more plastic deformation for the first 0.03 seconds then the fold 2, and generally more than fold 1 achieved. It continued this trend towards the end of the simulation after overtook the fold 1 curve and reached to the end of the simulation at a higher absorption rate than both fold 1 and fold 2.

Parameters –

Table 3.5 Curvature 2000mm Effects to the plastic work on all fold profiles.

Plastic work-Bending 2000 mm					
Profile	Weight (kg)	Total PW (kJ)	**SEA (kJ/kg)**	Avg PW (kJ)	**CFE (%)**
Fold 1	12.743	22.17	**17.398**	8.054	**36.33**
Fold 2	15.181	17.418	**11.473**	5.661	**32.50**
Fold 3	17.615	21.426	**12.163**	7.219	**33.7**

Despite all 3 fold profiles performed differently during the deformation process in table 3.5, all 3 profiles showed similar results without significant difference under the beam curvature of 2000 mm. Fold 1 of being the lightest beam structure only weigh 12.743 kg when compared with 15.181 kg to the fold 2 and 17.615 kg to the fold 3. As a result of this, fold 1 achieved a higher crush force efficiency of 36.33%, followed with lower figures of 32.50% and 33.7% performed by fold 2 and fold 3 each other individually.

Realised there is only 1 fold built into the fold 1 profile, it fully compressed during the

deformation process and absorbed the highest amount of impact energy at 221,703 J. Having the lighter beam construction also gained higher specific energy absorption at 17.398 kJ/kg, when compared with 11.473 kJ/kg and 12.163 kJ/kg to the both fold 2 and 3 each other respectively. Although fold 1 performed better absorption rate at the beginning of the simulation compared with the fold 2 and 3, as well as towards the mid-range until the 0.03 seconds of the simulation. However, fold 3 outperformed on the energy absorption rate after this time. Fold 3 of being the heaviest beam construction that it carried 4.872 kg more than fold 1, the maximum plastic work appeared 0.35kJ higher than the fold 1 which is 7.05 kJ. However, this additional weight indeed reflected some negative impact on the performance. 2.63% of the crush force efficiency was reduced to 214,257 J when compared with 221,703 J achieved by fold 1, followed with a 7.2% drop of the crush force efficiency.

Nevertheless, both fold 1 and fold 3 were performed much closed, fold 2 came in behind of both fold 1 and 3. Fold 2 maintained did not appear obvious increase like the fold 3 after the 0.01 seconds, instead maintained a smooth energy absorption curve, throughout the simulation. This means the first and second fold have been compressed gradually via the impact force without any significant failure. Further observed from the chart, the energy absorption process of fold 3 is an increasing trend instead of a smooth trend like fold 1 and 2. This means the deformation behaviour of the fold 2 happened linearly where fold 1 appeared very slight increases after 0.01 second until 0.04 seconds. Furthermore, adding a second fold to the beam structure beans its 2.438 kg heavier than the fold 1, and brought negative impact to both totals absorb energy reduced to 104,506.04 J, as well as crush force efficiency has been lowered to 51.80%. Although fold 3 carried additional fold to the beam structure when compared with fold 2, this did not achieve a significant improvement over the parameters when compared with fold 2. Overall, fold 2 achieved 6.2% less crush force efficiency, and 0.8 kJ less mean plastic work value. And due to the Lower total energy absorption yielded, and hence a 6.88 kJ/kg of specific energy absorption rate is reached and appeared suffered 5.9% less value. Nevertheless, fold 2 performed better on the energy absorption process, by offering the deformation process linearly, and hence achieved a progressive failure overall.

3.8 Plastic work – Curvature 2400 mm

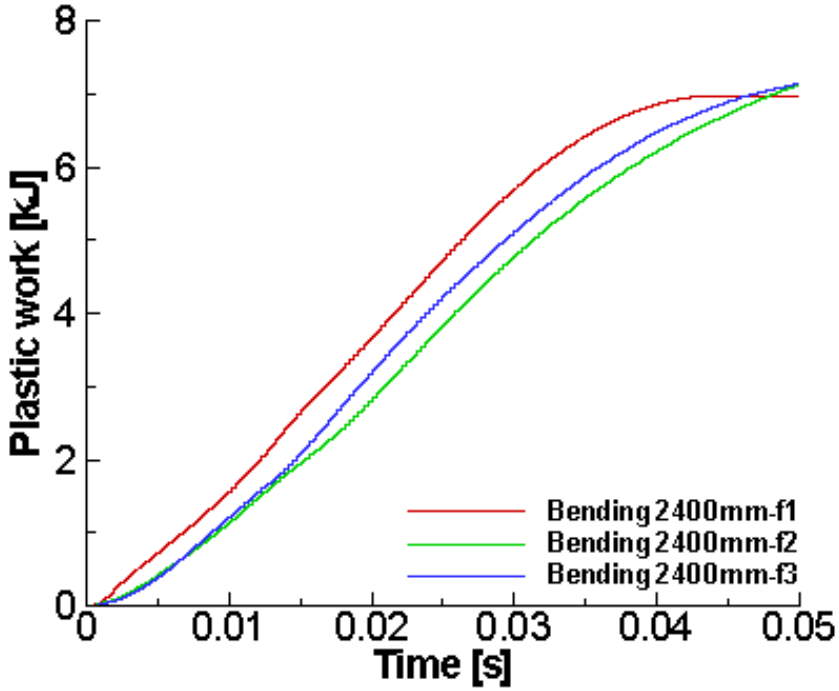

Figure 3.26 Curvature 2400 mm Effects to the plastic work on all fold profiles.

Description – Figure 3.20 showed at the curvature of 2400 mm, fold 1 started at slightly higher absorption rate when compared with fold 2 and 3 initially. It maintained this increasing trend throughout the simulation smoothly and reached to the peak value of 6.982 kJ before entered a steady absorption rate. Fold 2 started at less absorption rate, but the smooth increases of absorption rate proceeded further with a steady increasing trend for the first 0.02 seconds and maintained this trend throughout the impact process. Fold 3 showed similar absorption curve for the first 0.02 seconds but proceeded further with higher absorption after 0.02 seconds then the fold 2, but less than fold 1. It continued at this slightly higher absorption rate throughout the impact process and reached to identical maximum absorption rate than the fold 2.

Discussion – Generally, it is observed from the diagram that all 3 fold profiles have achieved good deformation behaviour because of the smooth energy absorption curves without fluctuations. However, all profiles performed slightly different from each other. Fold 1 started and maintained a slightly higher absorption rate when compared with the fold 1 and 2. This was due to fold 1 offered an immediate deformation response upon the initial impact to the wall, and the continuous engagement of deformation process led its absorption curve proceed

further higher than both fold 2 and 3.

This immediate deformation response did not last long where no further deformation is detected after 0.04 seconds, as the absorption curve reached to a peak absorption level and maintained flat whereas further deformation was detected on both fold 2 and fold 3. The energy absorption curves on both fold 2 and fold 3 were identical until 0.02 seconds. While fold 2 maintained its gradual increases, fold 3 proceeded further at higher absorption rate when compared with fold 2. This increasing amount of absorption means fold 3 offered similar deformation behaviour to the fold 2 for the first 0.015 seconds due to identical energy absorption rate. It then continually offered slightly more after this time.

Despite the fold 2 offered less absorption rate than the fold 3, the curve trend still showed smoothly and steadily throughout the rest of the impact process. This indicated the fold 2 behaved gentled during its deformation process, and still achieved identical maximum energy absorption.

Parameters –

Table 3.6 Bending effect on to the plastic work with proposed profiles.

Plastic work-Bending 2400 mm					
Profile	Weight (kg)	Total PW (kJ)	**SEA (kJ/kg)**	Avg PW (kJ)	**CFE (%)**
Fold 1	12.743	21.39	**16.784**	7.3599	**34.40%**
Fold 2	15.181	18.48	**12.174**	11.8452	**64.10%**
Fold 3	17.615	19.49	**11.065**	6.3588	**32.62%**

Under the beam curvature of 2400 mm, fold 1 performed better than fold 2 and 3, where it absorbed the total amount of the impact energy at 21.39 kJ. This was due to the advantage of single fold design that caused an immediate deformation engagement upon the initial contact, where the only fold had to work very hard under the impact load. This ended the deformation process early where it reached to maximum deformation at 0.04 seconds, while fold 2 and 3 carried on provided further energy absorption. The convex curve on the fold 1 indicated the deformation process of both fold 2 and 3 were gentler before the time elapsed to 0.02 seconds.

Although fold 2 progressed with lower absorption rate throughout the simulation then the fold 3, but this means it offered slightly more stable deformation behaviour during the impact and reduced absorption rate did not have significant impact to its energy absorption ability, as it

had identical maximum of energy absorption of 18.48 kJ when compared with 19.49 kJ yielded by fold 3. Additional fold benefited the fold 3 and improved both deformation behaviour, and increased the amount of impact energy. Located between both fold 1 and fold 3, the smooth energy absorption curve and steady increases suggested more desired deformation behaviour and indeed increased energy absorption after 0.015 seconds when compared with fold 2.

This reflected on to both average and maximum energy absorption, which was 6.3588 kJ then the 7.3599 kJ yielded by fold 1, and nearly similar maximum energy absorption, which was 19.49 kJ then 21.39 kJ yielded by fold 1. This means when compared with fold 2, fold 3 has higher efficiency to manage the deformation in correspondence of plastic work.

Despite all the results showed above, all 3 profiles offered good energy absorption via a smooth deformation without any unexpected structural failure. However, due to the inherent structural characteristic with fold 1 where no further energy absorption was observed after 0.04 seconds, fold 2 and fold 3 continued to offer additional structural deformation in order to achieve further impact energy absorption.

3.9 Plastic work – Curvature 3000 mm

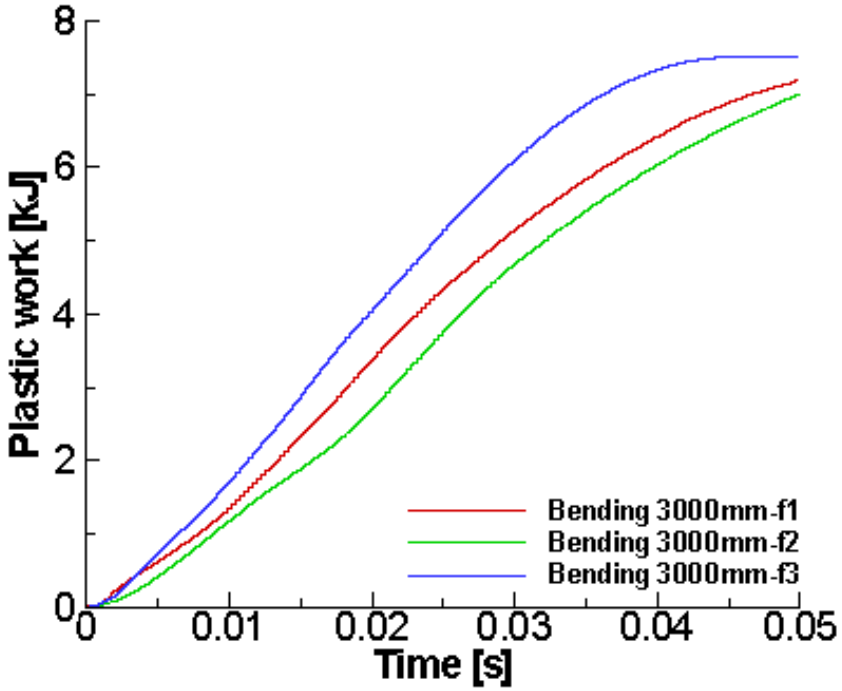

Figure 3.27 Curvature 3000 mm effects to the plastic work on all fold profiles.

Description – Figure 3.27 showed all 3 fold profiles offered a similar level of energy absorption rate when increased the beam curvature to 3000 mm. Both fold 1 and fold 3 showed higher plastic work after the initial contact with the wall when compared with fold 2 proceeded at reduced absorption rate. Fold 3 departed into step energy absorption after 0.01 second and reached a maximum absorption rate at 22.99 kJ. Fold 1 remained the same incline rate throughout the simulation and ended at less maximum absorption rate at 19.93 kJ. Fold 2 appeared with less energy absorption when compared with fold 1 and 3 overall. Fold 2 proceeded at this reduced absorption rate throughout the rest of the simulation before experienced a gentle drop around 0.02 seconds and yielded 18.03 kJ of maximum absorption.

Discussion – Fold 3 remained at higher absorption rate throughout the simulation when compared with both fold 1 and 2. Both fold 1 and 2 showed a very similar absorption behaviour upon the initial contact with the impact wall. This means curvature increases allowed fold 3 to deform faster until 0.04 seconds, but nearly no further absorption after this time. Fold 1 maintained its absorption rate throughout the simulation and resulted in a smooth absorption curve. This represented that the one fold beam had a steady energy absorption increases, so did the deformation process was linear. This smooth deformation process also applied to the fold 2 as well despite it showed a reduced energy absorption curve when compared with both fold 1 and 3. An absorption drop from 0.015 to 0.025 seconds was caused by the beam bent inwards, but the rate resumed shortly after.

After initiated at a similar level of absorption to the fold 1 and fold 2, fold 3 generally yielded higher energy absorption throughout the simulation process. Fold 3 soon entered into a steep absorption increases, by concentrating its absorption and showing between 0.015 seconds to 0.04 seconds. This deformation did not last until the end where the absorption has come to an end at 0.04 seconds since the absorption curve was almost flat after this time. This reflected the three folds indeed offered an extra energy absorption, as well as higher maximum absorption level. However, this caused a linearity issue to its absorption process and allowed most of the absorption took place before 0.04 seconds. Whereas continues deformation process occurred to both fold 1 and fold 2 throughout the impact process as more desirable choices.

Table 3.7 Bending effect on to the plastic work with proposed profiles.

Plastic work-Bending 3000 mm					
Profile	Weight (kg)	Total PW (kJ)	**SEA (kJ/kg)**	Avg PW (kJ)	**CFE (%)**
Fold 1	12.742	19.93	**15.644**	6.6729	**33.47**

Fold 2	15.181	18.03	**11.878**	5.1829	**32.23**
Fold 3	17.615	22.99	**13.056**	7.9181	**34.43**

Parameters – It is observed both fold 1 and 2 achieved approximately a similar trend with very little difference on both total and average absorption rate, which were reflected at the value of 19.93 kJ and 18.03 kJ, as well as average plastic work value at 6.6729 kJ and 5.1829 kJ.

In the essence of the performance of energy absorption rate, fold 1 and fold 2 came very close, but fold 2 performed slightly less than the fold 1. This means under the beam curvature of 3000 mm, instead of benefiting the CFE (crush force efficiency) increases, it added additional 2.439 kg weight on the fold 2, which directly affected the SEA (specific energy absorption) since it is calculated as per unit mass that the higher of the SEA, the lower of the weight.

On the case of fold 3, curvature increases aided both maximum and average energy absorption. The maximum energy absorption rate was achieved at 22.99 kJ, this was due to higher energy absorption because of the additional fold structure built-in. this also regulated the beam deformation and achieved average plastic work at 7.91KJ, which was 6.6729 kJ to the fold 1, and 7.9181 kJ yielded by fold 2. Both total and average energy absorption rate ultimately resulted in better crush force efficiency, 34.42 % was indeed at higher than fold 1 and fold 2.

However, the deformation process curve of fold 3 revealed it appeared more aggressive than both fold 1 and 2 between 0.015 to 0.04 seconds. This was due to much quicker fold compression that allowed more concentrated energy absorption from 0.015 seconds towards throughout the simulation. The main disadvantage revealed the fold 3 appeared less efficient to control its deformation behaviour. Where fold 1 and 2 demonstrated a seamless force transition during its deformation behaviour because both profiles demonstrated both folds were effectively compressed allowed smooth energy absorption, and abilities to distribute and controlled the energy absorption every stage of the impact process.

3.10 Analysis and recommendations

Both force reaction and plastic work of the bumper beam was made from structural steel at various curvature degrees and fold profiles.

Initial peak load – In the case of the straight beam, all fold profiles exhibited very high initial

peak loads, which presented a negative effect on crashworthiness during the impact process. The initial contact force between the bumper beam to the rigid wall was very violent. The initial peak force was found slightly less on fold 2 and fold 3, which amounts to no significant reduction in crashworthiness. This problem was alleviated by adding the curvature to the impact direction. The force reaction upon the initial contact was drastically reduced as soon as minimum 2000 mm beam curvature was added into the bumper beam. Increased the curvature further to 2400 mm and 3000 mm did not gain any more reduction on peak force reduction, but both curvatures maintained this good behaviour and showed generally lower value (Mamalis *et al*, 2000; Karnhari and Chao, 2003; Alghamdi, 2002;).

Crash-box interference – Adding the curvature to the bumper beam can regulate the impact process when compared with straight beam profiles. Compared with the straight beams, a significant amount of crash-box interference almost occurred to all the fold profiles, and particularly appeared more frequently after 0.03 seconds. This means that the straight beam resulted in the beam in 100 per cent overlap with the rigid wall, and the crash-box failure found on all fold profiles indicated without any curvature, the straight beam is an inefficient construction during the impact process, where the beam cannot effectively engage with the impact process. It is inevitable that those failures were reflected in the force reaction chart.

Effect of curvature effect overall force reaction – The increase of curvature radius can regulate the deformation process of the beam. When compared with the straight beam as a baseline, all fold profiles were showed more controllable and regulated at its own deformation despite some appeared in steep increases, other than in steady decreases. Fold 1 was the most difficult fold beam where due to lack of multiple folds available, the only fold had to work very hard during the deformation process. This was indeed reflected on to the initial peak force as well as the overall force distribution. While the initial peak force of both fold 2 and fold 3 showed between 20 kN to 40 kN as the curvature further increases, fold 1 was consistent at its range, which was almost always at 60 kN to 80 kN. This is a good indication of the only available fold had to engage the impact process very quickly regardless of the curvature presented on the beam. Further compare between the overall force reaction between the curvature of 2000 mm, 2400 mm and 3000 mm, the force curve appeared in an increasing trend. This means the fold 1 was offered continues beam deformation in order to keep absorbing the impact energy. However, the curvature of 2400 mm failed to regulate the beam deformation after 0.02 seconds, it caused a significant amount of force fluctuation, whereas, on curvature

2000 mm and 3000 mm, the force increased steadily and regulated.
Fold 2 and fold 3 behaved steadier when compared with that of fold 1. The curvature radius of the beam did not yield much force fluctuations on the fold 2, where it was self-regulated through all curvatures and all reached to both high reaction and energy absorption. Fold 3 in these cases only has been benefited from curvature 2000 mm and 2400 mm, but experienced a steep force increases after 0.02 seconds when increased the curvature to 3000 mm. The curvature increases negatively contributed to the overall force trend on fold 3 where a concentrated deformation was formed and caused the energy absorption to end early as well.

Fold effect overall force reaction – The benefit to building multiple folds into the beam is that the impact energy can be consumed via fold compression gradually without causing any unstable deformation, and the benefit of doing so is immediately reflected on the results in the straight bumper beam. Fold 1 suffered from the most where only available fold showed the design intend purpose of providing consistent deformation. This was reflected in the steady increases by 0.035 seconds. However, lack of multiple fold design and to its available material made the fold 1 less capable to process any residue impact load and caused the force spiked over the chart limit.

A similar issue was repeated on the fold 2 beam even with two folds were available. The force spiked twice towards the end of the impact process suggested fold 2 was less effective to manage its residue impact load. Despite the energy absorption of fold 2 carried on further absorption after 0.035 seconds, this was caused by the crash-box interference as the beam was further forced into the wall. Fold 3 largely resolved this problem because the force no long spiked. An obvious force increases occurred at 0.0425 seconds suggested minimum crash-box interference was received, but without any force, spikes showed in fold 1 and fold 2. Instead, fold 3 yielded a relatively steady increasing force trend for the first 0.04 seconds.

Further compared the results between the curvatures of 2000 mm, 2400 mm and 3000 mm, fold design once again confirmed its positivity towards the deformation process. Despite that the force reaction increased dramatically in the curvature of 2400 mm chart after 0.02 seconds, the force curves recorded via the curvatures of 2000 mm and 3000 mm behaved as a relatively steady increasing trend. This showed fold 1 was able to manage its deformation efficiently. However, the forced ending of in all curvatures was at the reduced trend. Particularly to the curvature of 2400 mm where a significant amount of energy absorption increases to 120 kN

was recorded from 0.02 seconds towards the end of the impact process. It then immediately plunged down to less than 60 kN near the end showed at the curvature of 2400 mm, fold 1 lost its structural integrity and started with localised failure that caused significant amount of force increases was detected. Correlated energy absorption process also displayed the same issue. The energy absorption was maintained higher, and particularly before 0.04 seconds than the other fold profiles. As a result, the absorption dropped significantly after no more structure available to process further deformation. As the opposite of this issue, fold 2 and fold 3 behaved in much more desired results. The force reaction on both showed overall good deformation process excepted fold 3 experienced a similar issue when increased the curvature to 3000 mm. sudden force increases mean multiple folds did not regulate the deformation of fold 3, where the compression of the beam faster. And because of this, the energy absorption stopped as soon as the force started to drop, where both fold 2 and 3 were in a very stable increasing force trend as well as its energy absorption.

Recommendations – Based on all the results analysed above, the introduction of curvature into the bumper beam can reduce the initial contact force and stabilise the deformation process thereafter. In the presence of the curvature radius of 2000 mm, all 3 fold profiles behaved relatively acceptable without significant reaction force fluctuations. When the curvature radius of the beam to 2400 mm, folds profiles 2 and 3 continued to exhibit a smooth reaction force throughout the impact process, but this resulted in a sudden increase in the force indicating structural instability to fold 1. When the curvature radius was increased further to 3000 mm, the folded profile 3 turns unstable during the impact process which was reflected by a sudden force increase after 0.02 seconds.

Interestingly, during the impact process of any structural failure, all affect energy absorption is greatly affected by its deformation behaviour. This means the bumper beam would be able to hold its structural integrity during the impact with the help from correct curvature and number of folds in the cross-section profile. Cases such all fold profiles in straight, fold 1 in all curvature, fold 3 in curvature 3000 mm always reflected on its energy absorption chart, where there are always with a stopped energy absorption that accompanied with its correspondent force drop (Das, 2001; Busch, 2000; Belingardi *et al*., 2013)

Chapter 4. Result and Discussion (Aluminium)

Chapter 4 investigated the crashworthiness benefit gained using aluminium instead of structural steel, which was tested in chapter 3. This was primarily due to the material property, where commonly, the density of aluminium is around 2700 kg/m^3 to 2770 kg/m^3, where the structural steel counterpart is around 7000 kg/m^3 to 7800 kg/m^3. This contributed significantly towards the weight saving where potentially 30% to 50% is achievable than the structural steel made components. The second benefit was the raw material production. The life cycle assessment revealed during the raw material acquirement, GHG (greenhouse gases) is largely saved when the production is switched to aluminium. Aluminium also helps the vehicle to achieve better road performance, since the aluminium mad components reduced the load of the axle. Furthermore, the amount of weight saved when switched to aluminium made components can either benefit the fuel consumption to a vehicle or, allows to accommodate any other performance or comfort related functions. The third benefit is realised when the vehicle is subjected to accident repair, where an effective bumper system can maximise its crashworthiness and minimise the cost to replace any components then it is necessary. Both customers can enjoy a safer vehicle, and the insurance provider faces at low compensation payout (AAM, 2013; Baccouche *et al*, 2007; Farkas *et al*, 2012; Hirsch, 2011).

Known the advantages of using aluminium, an investigation work was conducted on the design of a lightweight body-in-white structure that based on the new material indices of thin-walled beams under the consideration of crashworthiness. It indicated current body-in-white construction uses a single material, such as steel ort aluminium. An alternative multi-material construction method is considered for its ability to optimise the combination between different materials that ultimately can achieve performance on both weight reduction as well as low production cost.

The optimisation of vehicle body-in-white requires novel material performance index which is a decisive method on the material selection since the advantages and disadvantages were presented all together. The core concept of this optimisation is based on the suitable type of material used at the correct location since the performance is considered as a whole vehicle instead of regional improvement, a material selection method was proposed based on the contribution from the material, as well as the usage of this material. It emphasized the material

may be presented with many characteristics, but in the real-world scenario design demand that it requires to satisfy certain criteria, such as less density with good strength, higher corrosion resistance together with medium acquirement cost. It concluded that the range of materials shall be categorised into a performance index, where the final desired material selection shall follow its actual location and needs in order to overlap with the material can satisfy this is particularly benefited simpler body structure, such as body panels. This method appeared less effective when dealing with a more complicated structure, such as a bumper system, frame rail, and pillars, which constitutes the main body of a vehicle (Ashby, 2000).

Other have indeed studied the performance of material substitute without sacrifice the stiffness of the structures. And particularly, multi-purpose optimisation was conducted primarily to find the cause of weight reduction effects to the material substitution and the viability of maintaining the stiffness of structures. It stated direct material replacement was studied extensively in the past years. And it has been long established aluminium made component is significantly lighter than the conventional steel components and for its constant stiffness. Since both aluminium and magnesium are both considered as lightweight alternative options, their specific modules are very similar to the steel, and this presented challenge to achieve weight reduction while retaining the constant stiffness (Patton *et al*, 2004).

The optimisation intended to achieve two purposes, lightweight and inexpensive. Figure 4.1 showed an FE model has represented the test vehicle and it was based on the standard 4 door family sedan. The main structural members that could benefit from the optimisation were categorised into table 4.1, and the potential candidate materials and their properties were also displayed in Figure 4.2.

Figure 4.1 FE model of body-in-white (NHTSA, 2000).

Table 4.1 Areas that subjected to crashworthiness improvement (Cui *et al*, 2011)

“Content removed due to copyright reasons”

Table 4.2 Potential candidate material and its properties. (Cui *et al*, 2011)

“Content removed due to copyright reasons”

To satisfy both crashworthiness as well as the stiffness of the frontal area, an explicit simulation was performed at the velocity of 48 km/h and conducted by LS-DYNA. Another static analysis simulation was also performed with MSC/NASTRAN. 1000 N of loads were assigned to both front and rear seats of the car, and the rear shock absorber mount was constrained at all direction where front shock absorber mount was only constrained at the vertical direction.

“Content removed due to copyright reasons”

Figure 4.2 Absorbed energy comparison between original and improved designs (Cui *et al*, 2011).

“Content removed due to copyright reasons”

Figure 4.3 Acceleration comparison between original and improved designs (Cui *et al*, 2011).

Table 4.3 Material involvement before and after the optimization (Cui *et al*, 2011).

“Content removed due to copyright reasons”

Based on the results showed in Figures 4.2, 4.3 and table 4.3, optimised material selection is

far better than the original design. The new material combination has little impact on the crashworthiness and bending stiffness. Table 4.3 indicated the optimal design has only able to reduce 0.0009 mm of thickness but reduced 30.6 kg of the weight. This means less amount of material is used with only $14.3 increases. The production cost of the entire body is ultimately reduced to $32. Interestingly noticed that the worst design has achieved 64.3 kg weight reduction when compared with the original design, and 33.7 kg weight reduction if compared with the optimal design. The reason for such lightweight achievement was due to the extensive usage of aluminium. Obviously, this presented a costs problem, where it costs $35.4 more than the original design and $68 more than the optimal design. Nevertheless, this prospect may be completely different if the product is aimed at the different tier of customers where the economy is no longer a concern.

4.1 Simulation Preparation

Figure 4.4 Adding new material in the engineering data source in explicit dynamics. (ANSYS, 2016)

The engineering data showed in Figure 4.4 provided the control for material properties, particularly to this chapter where the aluminium alloy was selected and must be entered manually to replace structural steel which was previously created and used. It is further observed from this Figure, drag and drops the "engineering data" from the components system toolbox, and right mouse click allows it to be entered manually.

“Content removed due to copyright reasons”

Figure 4.5 material selection process. Top: Engineering data layout; Middle: B: Material selection; bottom: individual adjustment (ANSYS, 2016)

Once the new project was created showed in Figure 4.4, engineering data is available to check in the top Figure showed in 4.5. All main functions to the material properties are shown within the layout. In this case, aluminium alloy is decided, and can be selected in the material library: "General materials". Clicked the "+" mark at the front to add it into the selection. Once the material is added to the selection, some of the parameters will need manual entry. Like showed in the bottom graph in Figure 4.5, the unit can be displayed as values as defined, or values in project units. This allows the unit to be defined during the manual entry or can be readjusted again later during the simulation to achieve maximum flexibility.

4.2 Force reaction – straight beam

According to Figure 4.6, fold 1 yielded approximately 100 kN of peak load upon the initial contact to the wall but stepped down after a very short force fluctuation as the simulation carries on. It maintained the force value with a slightly increasing trend towards to the 0.03 seconds, then encountered a violent force at both 0.0325 seconds and 0.0375 seconds. Fold 2 appeared in similar peak load value to the fold 1 upon the initial impact, it also proceeded further at a similar trend as well. Violent force fluctuation was repeated itself again on the fold 2 which fold 1 previously experienced. Fold 3 shared similar peak load as well as the force trend thereafter. The violent force trend still existed towards the end of the impact process. The violent force fluctuation still occurred at fold 3, but at much later time elapses and happened just below 450 kN.

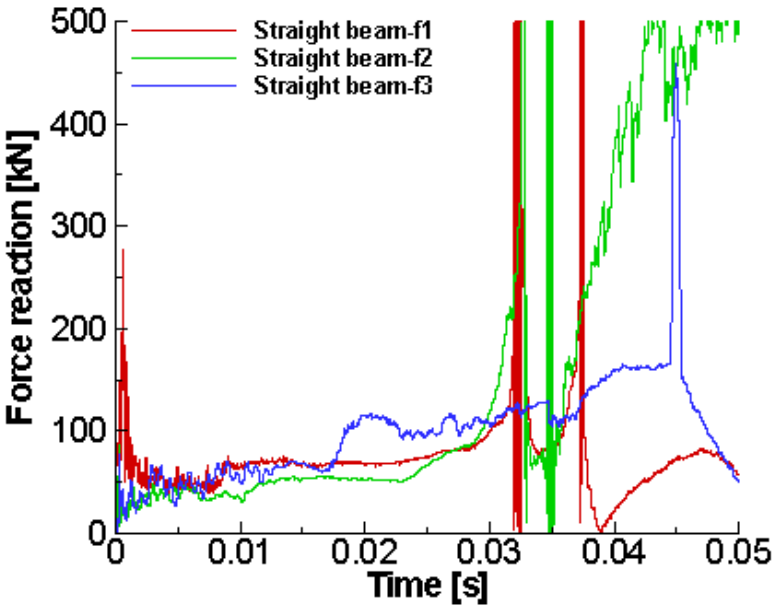

Figure 4.6 Curvature straight Effects of force reaction to all fold profiles.

The above Figure reflected the effect to the force reaction when the bumper beam was built at straight under 3-fold profiles with Aluminium Alloy. This resulted in all the fold profiles beam reached 100 per cent overlap with the impact wall and led to a high initial peak load. The straight beam made the fold 1 suffered the most on the force reaction upon the initial contact with the wall when compared to fold 2 and fold 3. Although the initial peak load happened in a very short period of time, as the fold structure compressed further away, the force settled down and proceeded steadily until 0.03 seconds. Violent force fluctuation that spiked off the chart appeared twice after this time before it reached the end of the simulation.

This was due to the impact load cannot be fully consumed during the deformation process until 0.03 seconds, where the only one-fold available had to engage completely. The Smooth force increases before 0.03 seconds indicated the deformation engagement of fold 1 was effective and it generally maintained its structural integrity without any failure. Further violent force fluctuations mean the fold 1 beam is inherent lack of ability to provide any further deformation due to limited numbers of fold available. As a result, the residue impact load further pushed the beam until the rigid crash-boxes started to interfere with the rigid wall. This crash-boxes interference represented a structural problem, which reflected the fold 1 is insufficient to handle all the impact force, where the structural compression was finished before the simulation reached to the end.

Fold 2 managed to improve the initial impact force just below 50 kN where the fold 1 yielded over 100 kN because of additional fold available. Further steady increases until 0.03 seconds mean the deformation process was efficient and the forced transition from the first to the second fold was smooth. This did not last throughout the impact process, where violent force fluctuation still folds on to the fold 2 design suggested lack of multiple fold structure available on the beam.

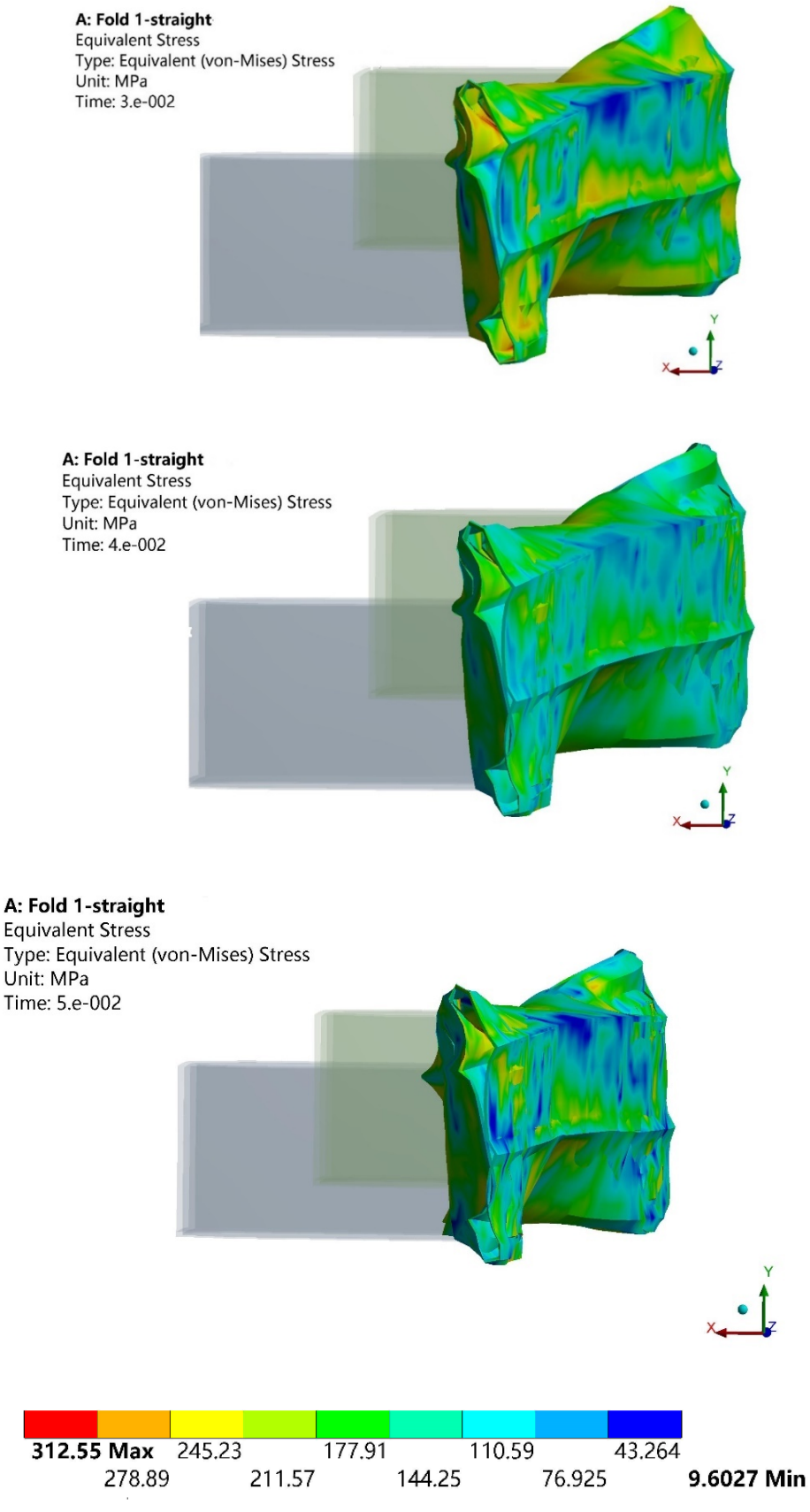

Figure 4.7 Von mises stress distribution of fold 1 from 0.03 to 0.05s.

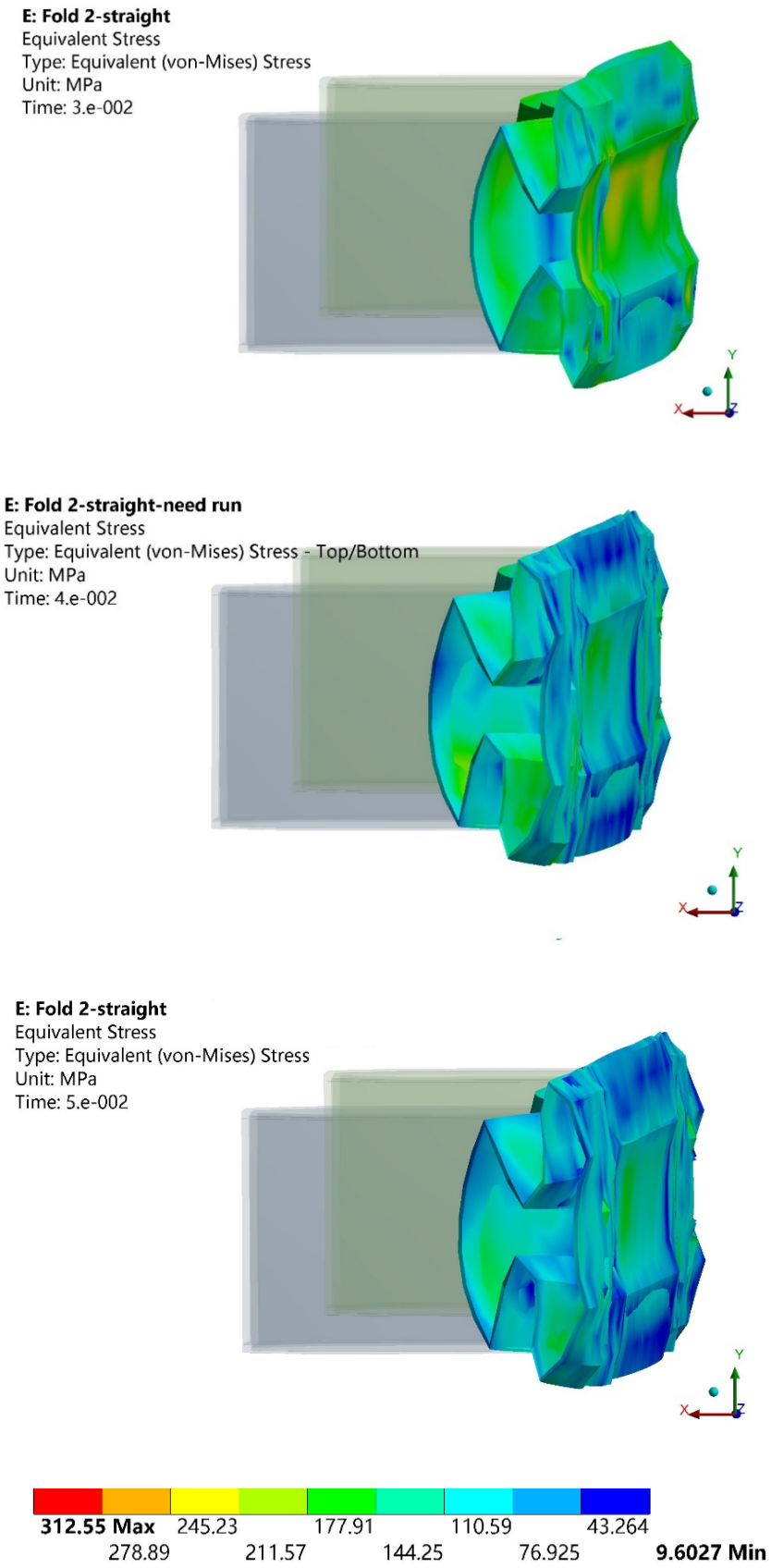

Figure 4.8 Von mises stress distribution of fold 2 from 0.03 to 0.05s.

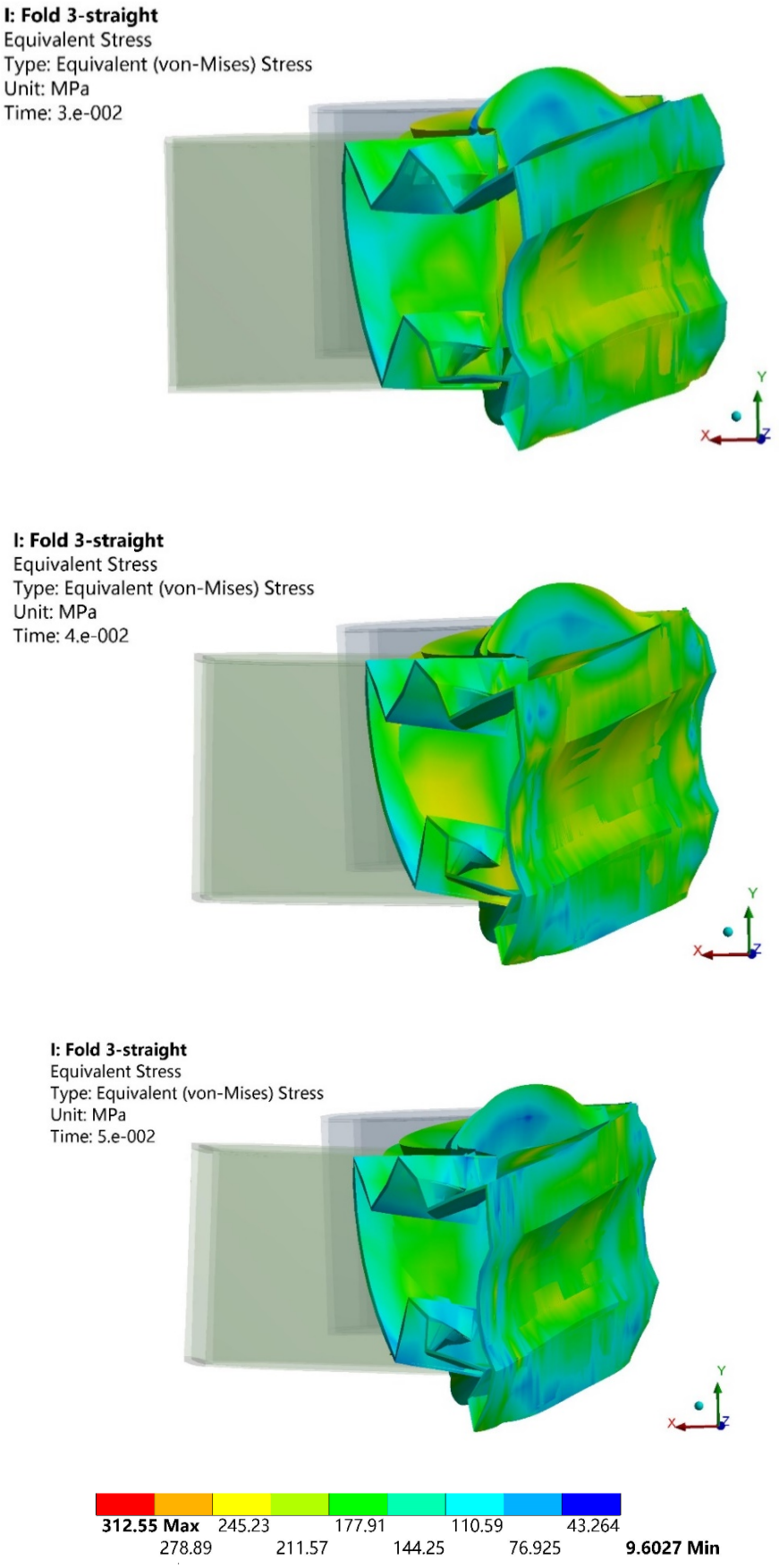

Figure 4.9 Von mises stress distribution of fold 3 from 0.03 to 0.05s.

As a result, the crash-box interference occurred after 0.03 seconds. Figures 4.7, 4.8 and 4.9 described the crash-box interference process during the impact process at 0.03, 0.04 and 0.05 seconds. It is realised due to lack of multiple folds available to both fold 1 and fold 2, the relative position of crash-boxes changed as the simulation progressed further while the crash-boxes started to interfere the beam deformation, and it is inevitable that the force reaction curves spiked off the chart number of times after 0.03 seconds.

In this case, much more desirable force response is observed from the fold 3. Low initial peak force and force trend thereafter suggested the initial engagement between the beam to the rigid wall was effective, and the steady force increases thereafter mean the deformation process of the beam was regulated without significant structural failure. Fold 3 only experience the force spike 450 kN towards to the end of the impact process. The crash-box interference for fold 3 is still much less due to the third fold built into the fold profile and made additional deformation possible. It is worth to mention that while the folds 1 and 2 suffered from crash box interference, they both lost the abilities to offer further structural deformation after 0.03 seconds. While fold 3 behaved more appropriately via continued increases to its force curve. Despite the force spike was still sustained, there is still a considerable amount of residue impact force existed, this already made a vast improvement over the folds 1 and 2.

4.3 Force Reaction – Curvature 2000 mm

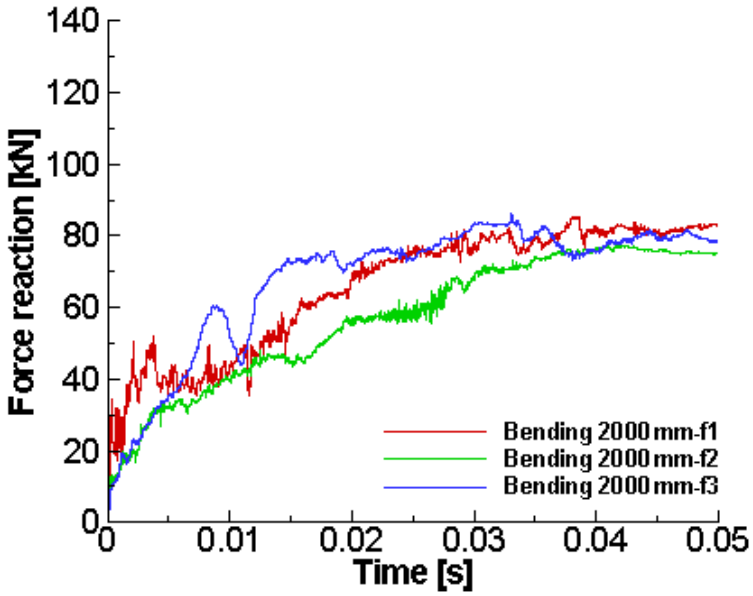

Figure 4.10 curvature 2000mm Effects of force reaction to all fold profiles.

Description-Figure 4.10 showed the effect of the force reaction after introduced the curvature at 2000 mm to all 3 fold profiles. Upon the initial contact, fold 1 yielded 20 kN of initial peak load and entered a gradual increase stage, and thee force curve behaved generally well without any significant fluctuation. This reaction force increased up to 80 kN then maintained within this range throughout the simulation. Fold 2 started with very low initial peak load – just below 10 kN and proceeded further with a similar increasing trend as fold 1. It maintained this increasing trend towards to the end of the simulation without any fluctuation, then reduced slightly after 0.04 seconds, finally ended at 75 kN. Fold 3 also began with significantly low force reaction value which was less than 5 kN upon the initial contact. It proceeded further with a gradual increase throughout the impact process excepted a force drop. It quickly regained its increasing trend and carried on this increase towards the end of the simulation.

Discussion - Compared to the previous beam that was constructed without any curvature, all 3 fold profiles were benefited after the introduction of the curvature 2000 mm to the beam. Without the issue of crash-box interference, all 3 fold profiles experienced a smooth gradual increase in the reaction force throughout the simulation. The curvature immediately aided the fold 1 and yielded a considerably low force reaction upon the initial contact, which was 20 kN. It further proceeded at a gradual increase towards the end of the impact process. This was due to immediate engagement to the deformation process offered by the only fold available. Increased curvature also provided stable deformation behaviour, which was reflected on steady force increases that were carried throughout the rest of the simulation.

The initial peak load on fold 2 was less than 10 kN. Without the abrupt increase in initial peak force shown in fold 1, the first fold on the fold 2 beam started to compress then followed by compression of the second fold. As a result, it proceeded throughout the impact process with a steadily increasing curve. This indicated the fold 2 achieved a gentle initial contact with the rigid wall, and the first fold 1 provided a good compression during the deformation. Further smooth force increases also suggested the force transition from the first fold to the second fold was also stable and regulated. This also suggested added second fold can regulate the deformation behaviour by effectively held its structural integrity.

After obtaining a very low initial peak load that was similar to fold 2, fold 3 proceeded at a gradual increase thereafter. However, add the third fold to the beam seems disrupted the

deformation process where a force drop was observed at 0.0125 seconds, although the force was quickly regained its increasing trend and continued at its trend towards to the end of the impact process.

Despite the fold 3 has achieved overall reasonable force trend with very low initial peak load, the force disruption caused by the third fold presented on the beam means it reduced the structural integrity of the beam, where the force cannot transfer smoothly from the compression of the first fold into where the seconds fold started to compress.

4.4 Force reaction – curvature 2400 mm

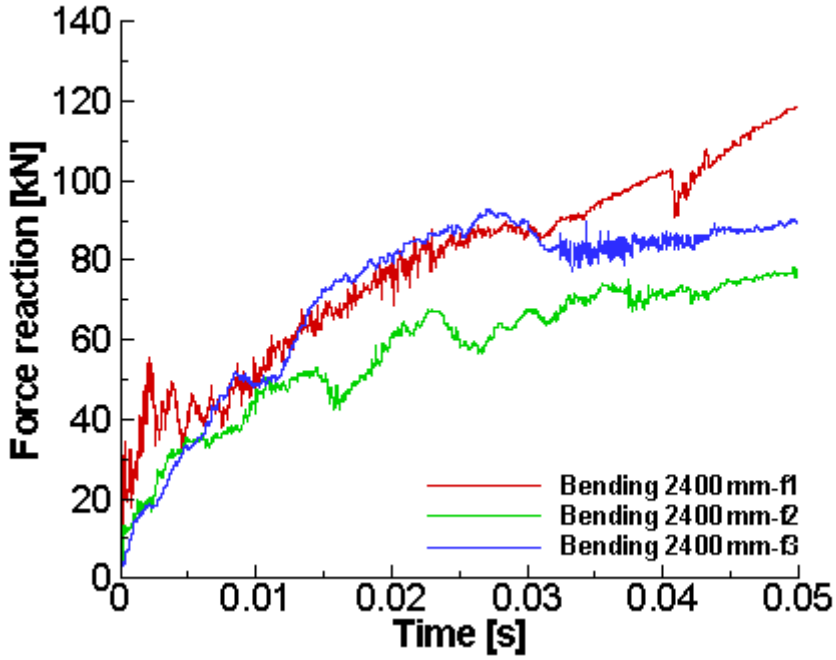

Figure 4.11 Curvature 2400 mm effects to force reaction on all fold profiles.

Description-It is observed from Figure 4.11, all fold profiles were still benefited from the curvature increases in terms of both initial peak load and the deformation process throughout the impact process. Fold 1 started from 20 kN of initial force load upon the initial contact and quickly experienced a steep force increases until 0.01 second before settled into a gradual increase, with a further climbing after 0.03 seconds, it carried this increasing trend throughout and ended at 120 kN.

Fold 2 obtained very low 10 kN of force value upon the initial contact and followed with gradual increases. The increase was maintained throughout the simulation and ended at 70 kN.

Fold 3 appeared in a similar initial peak load to fold 2, but its reaction force increased at a slightly higher rate until 0.03 seconds. It dropped slightly but quickly regained the gently increasing trend towards the end of the simulation.

Discussion – Increasing the beam curvature to 2400 mm is of benefit to all fold profiles, where the initial peak load force stayed at a lower range. Fold 1 achieved very low initial force load at only 20 kN and quickly entered into a gradual increase until 0.03 seconds. It then entered into a steep force increases thereafter towards the end of the impact process. This was due to there is only one fold presented on the beam which immediately started to deform upon the initial contact. Gradual increases suggested the deformation was very wall regulated. And the sudden increases suggested curvature of 2400 mm allowed fold 1 for further deformation after 0.03 seconds.

Despite both fold 2 and fold 3 were built with multiple folds on the bumper beam, both initial peak loads were very low, and the force reaction process was relatively stable throughout the impact process. After fold 2 started with a very low of force 10 kN upon the initial contact, gentle increases towards 0.015 seconds suggested the first fold was engaged with the deformation well and the fold compression is regulated. An obvious force drops before 0.02 seconds indicated that the force transition from the first fold to the second fold was disrupted. Despite this, fold 2 still maintained the stable deformation behaviour during the compression of the second fold throughout the impact without any significant interruption.

Started with a significantly low initial force which was only 5 kN, fold 3 displayed a smooth trend that similar to the fold 2 until 0.01 seconds. This means the first fold offered a gentle fold compression during the engagement to the impact wall. It is worth to mention that fold 3 shared the force drop that also found on fold 2. This phenomenon represented the first fold was fully compressed and it triggered the second fold into the deformation process. With further stabilised force trend towards the end of the impact process. This suggested the compression of the second fold was completely and triggered the third fold into further deformation.

Generally observed from the diagram, when increased the beam curvature to 2400 mm, fold 2 achieved the lowest force trend when compared with both fold 1 and fold 3. On the other hand, due to the physical geometry limit of the fold 1, the only available fold had to work completely to disburse all impact load, hence it showed the force subjected to quick increases after the

initial contact due to more aggressive deformation while fold 2 and 3 were considerably lower.

This also caused the fold 1 to maintain a marginally higher force trend throughout the impact process when compared with fold 2 and 3. The force curve further increased after 0.03 seconds indicated the fold 1 experienced further deformation to disburse any residue impact load.

Whereas both fold 2 and 3 were benefited from multiple fold compressions upon until the 0.03 seconds, hence both of their force trends were relatively smooth throughout the rest of the simulation. Because an additional fold was available to the fold 3, it achieved slightly higher force value to fold 2, where it overtook the fold 2 force curve after 0.015 second and able to maintain this higher force trend. However, it dropped slightly after 0.03 seconds suggested increased the curvature from 2000 mm to 2400 mm made the deformation of fold 3 unstable, where it cannot maintain its structural integrity particularly after 0.03 seconds and caused this force drop issue. It all suggested fold 2 was the appropriate fold profile under this curvature since both 0.01 seconds to the fold 1, and after 0.03 seconds for fold 3 showed unstable deformation that caused the force to fluctuate.

4.5 Force reaction – curvature 3000 mm

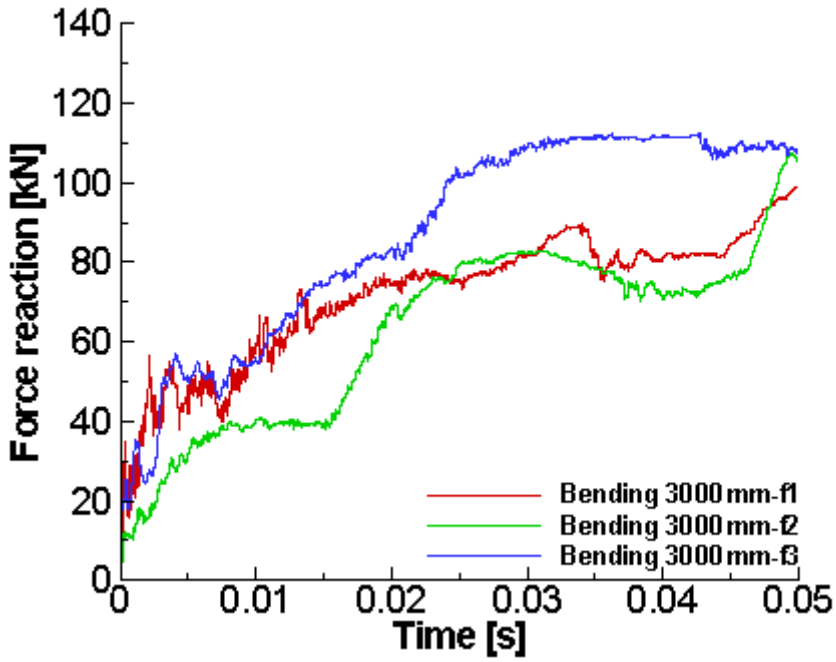

Figure 4.12 Curvature 3000 mm effects to force reaction on all fold profiles.

Description – Figure 4.12 indicated the effect to force reaction after beam curvature was increased to 3000 mm. This benefited the fold 1 to achieve very low 20 kN of force upon the initial contact. It then entered into a gradual increase and carried this trend throughout the simulation.

Fold 2 also achieved very low initial force at 10 kN upon the contact with the rigid wall, and also entered into a smooth curve increases towards the 0.02 seconds. It then experienced sharp increases twice that occurred just before 0.02 seconds, as well as after 0.045 seconds. Fold 3 achieved a slightly higher initial force reaction at 20 kN but shared a similar trend to fold 1 until 0.02 seconds. It further increased into much higher force range at 110 kN after 0.02 seconds, whereas both fold 1 and fold 2 and were yielded much less during the same time.

Discussion – Increase the beam curvature to 3000 mm benefited the fold 1 to achieve low initial peak force, but it also aided the deformation behaviour after the initial contact. Fold 1 showed relatively smooth increases throughout the simulation without any significant fluctuations presented. This suggested the fold 1 was able to maintain its relative structural integrity without any catastrophic failure. The smooth force increases after the initial contact also suggested the fold 1 subjected to complete compression during the impact process.

Fold 2 initiated the impact smoothly via the good compression behaviour of the first fold, and the second fold was also compressed within the expectation. Increased the curvature to 3000mm resolved the force drop that was indicated in the previous curvature of 2400 mm, where the force was interrupted from the first fold to the second fold. After gaining 20 kN of force reaction upon the initial impact, fold 3 entered into the force trend that was similar to fold 1, and further increased after 0.03 seconds. This indicated that the first and second folds were engaging the deformation very well without any fluctuations. However, the transition from the second fold to the third fold was not smooth.

The steep increases occurred after 0.02 seconds indicated the fold 3 unable to hold its original structure and the force started to interrupt the compression of the third fold and eventually caused this steep increase. This also means while increased the curvature benefited the initial peak load as well as first 0.025 seconds of the deformation process provided by the first and the second folds, the compression of the fold 3 was not stable.

4.6 Plastic Work – Straight beam

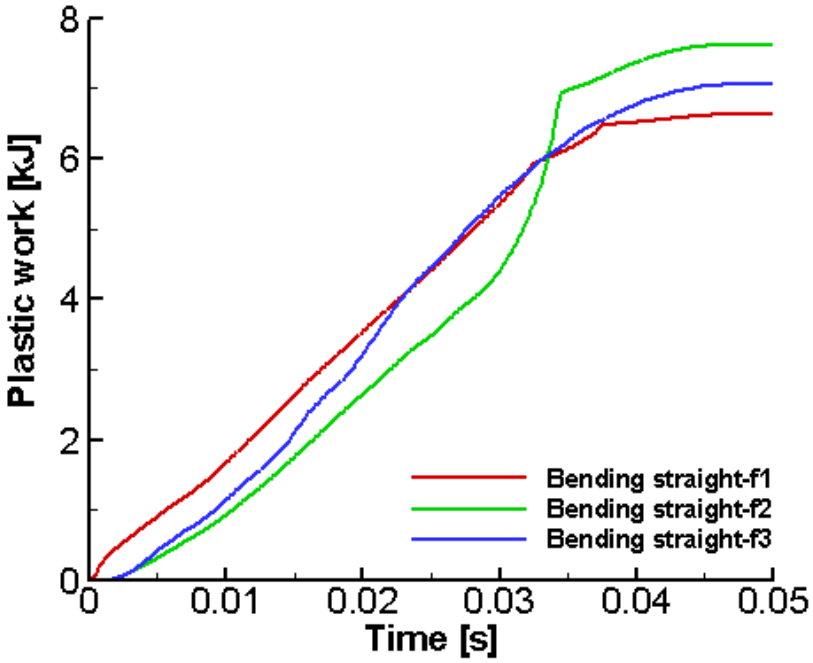

Figure 4.13 Curvature straight Effect to the plastic work on all fold profiles.

Description – Fold 1 appeared at a slightly higher energy absorption rate at the beginning, and it was maintained until 0.02 seconds, then overtaken by the fold 3. It carried on at this rate of incline further and reached a steady increase after 0.04 seconds and end of the simulation. Fold 3 started at lower absorption rate when compared to fold 1, but reached the same rate towards the 0.02 seconds. After overlapped with fold 1, the absorption rate maintained this rate throughout the impact process. Fold 2 initiated at lower absorption rate compared to both fold 1 and 3. It started to absorb a significant amount of energy after experienced a steady absorption increases at 0.03 seconds. It reached a steady increase of 0.035 seconds and carried this trend throughout the impact process.

Discussion – It is observed fold 1 started at a higher absorption rate than both fold 2 and fold 3 for the first 0.025 seconds. This was due to the only one fold presented on the beam and it engaged the deformation process immediately upon the initial contact to the wall. The absorption rate was lower on the fold 2 and 3, this was due to the fold compression interacted each other and caused reduced absorption rate.

Fold 2 did not appear in any higher absorption process but progressed at steady increases and

experienced a steep increase thereafter. This was due to a straight beam design did not allow any progressivity of the failure to the beam. This negatively impacted the deformation behaviour of the fold 2 that cannot absorb most of the impact energy, where residue force still pushed the bumper beam towards the wall. This demonstrated that without any curvature, straight beam design is lack of promoting and regulating the deformation of the beam and hence effected the energy absorption. This issue was also found on the fold 1, but with severe absorption increases that were caused by the crash-box that interfered the deformation process.

For the same reason, fold 3 was benefited from multiple fold construction. It is found behaved at much smoother absorption curve when compared with fold 1 and 2 where the multiple folds design promoted progressive deformation, allowed the force to compress the first fold, and gradually transferred to the next available fold one throughout the simulation. The smooth inline curve of the fold 3 indicated the energy absorption process was smooth throughout and did not stop until the end of the impact process. Where both fold 1 and fold 2 were experienced a clear interruption to their absorption curve.

Parameter Analysis –

Table 4.4 Curvature straight to the plastic work on all fold profiles.

Plastic work-Bending straight beam					
Profile	Weight (kg)	Total PW (kJ)	**SEA (kJ/kg)**	Avg PW (kJ)	**CFE (%)**
Fold 1	4.496	20.643	**45.914**	7.4193	**35.94%**
Fold 2	5.357	19.526	**36.442**	6.0112	**30.79%**
Fold 3	6.216	20.183	**32.474**	6.9378	**34.37%**

With straight beam curvature, fold 1 was immediately started the fold compression and resulted a higher energy absorption was achieved for the first 0.02 seconds and reached to the total amount of energy absorption at 20.643 kJ. Due to the natural advantage of the weight, when compared to fold 2 and fold 3, it achieved 45.914 kJ/kg of SEA which is largely improved then the other two profiles. It maintained higher energy absorption for the first 0.02 seconds and did not leave behind when the fold 3 reached a similar absorption rate until 0.04 seconds, it achieved an average absorption rate of 7.4193 kJ. This led to a crushing force efficiency of 35.94%. When compared with fold 2 that had additional fold built into the beam and expected to absorb more impact energy, this is not the case where the energy absorption rate on the fold 2 remained at a lower value just before the 0.04 seconds. Despite it overtook the curve of both

fold 1 and fold 3, it reached to slightly lower 19.526 kJ of total absorbed energy. It also resulted in 36.442 kJ/kg of specific energy absorption.

Fold 3 had most of the folds presented on the beam and inevitably gained more weight. Despite it yielded similar maximum energy absorption of 20.183 kJ, it gained 32.474 kJ/kg of specific energy absorption, which is lower than both folds 1 and 2. The energy absorption curve reached to the range of fold 1, and shared similar absorption rate until 0.04 seconds, and overtook it further until the simulation was ended. As results of this, multiple folds construction helped the fold 3 absorbed average 6.9378 kJ of impact energy. This aided the fold 3 achieved 34.37% of crush force efficiency.

4.7 Plastic work – curvature 2000 mm

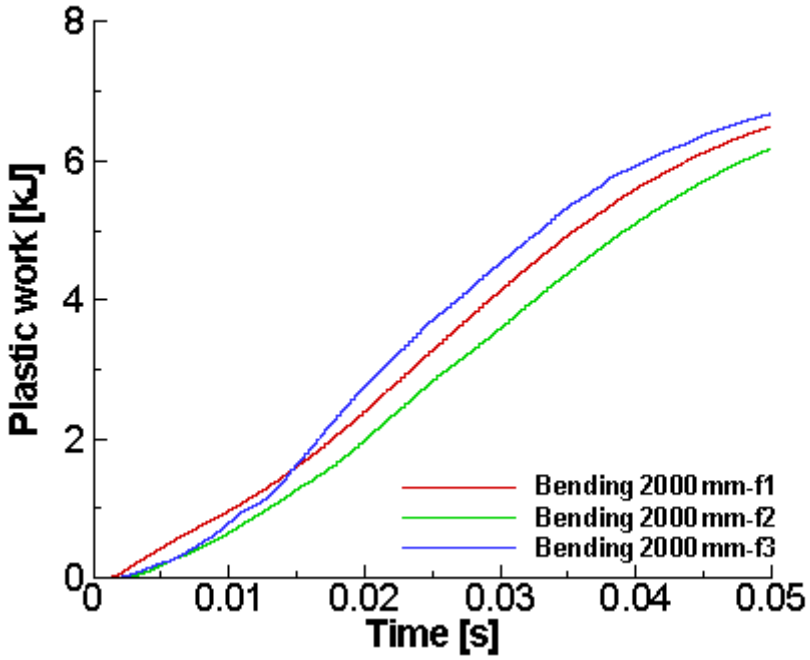

Figure 4.14 Curvature 2000 mm effects to the plastic work on all fold profiles.

Description – The above diagram indicated effect to the plastic work when increased the curvature radius to 2000 mm. Fold 1 started with a slightly higher absorption rate until the 0.01 second, and maintained this smooth absorption rate throughout the simulation without any fluctuation, it reached around 6.5 kJ of energy absorption at the end. Folds 2 and 3 were at slightly lower force rate during the same period where fold 3 increased its absorption further higher than the fold 1 after 0.015 seconds. Fold 2 however carried further energy absorption at less rate than both fold 1 and 3. Both fold 2 and fold 3 were maintained its smooth absorption

curve throughout the simulation and reached to maximum absorption rate at approximately 6 kJ in the end. Fold 3 continued at its increased absorption after 0.015 seconds and maintained this higher absorption rate throughout and reached to a maximum of 6.5 kJ of absorption rate at the end of the simulation.

Discussion – Fold 1 achieved slightly higher energy absorption until the 0.01 second. This was caused by the immediate engagement to the deformation process via the only fold available. While fold 2 and 3 remained lower rate suggested multiple folds regulated the deformation behaviour and both fold 2 and 3 showed gentle deformation process upon the initial contact, allowed the force to transfer seamlessly after existing fold is fully compressed.

Fold 2 achieved slightly lower energy absorption rate throughout the simulation when compared with both fold 1 and 3. Despite it built with additional fold then the fold 1, this did not improve the energy absorption. Fold 3 started at a similar amount of absorption rate to fold 2 for the first 0.01 second. It then entered into a gradual increase and managed to overtake the absorption of fold 1 after 0.015 seconds. A third fold presented on the bumper beam means additional available material, and it is inevitably going to absorb more impact energy compared to fold 1 and 2.

Parameter Analysis –

Table 4.5 Curvature 2000 mm effects to the plastic work on all fold profiles.

Plastic work-Bending straight beam					
Profile	Weight (kg)	Total PW (kJ)	**SEA (kJ/kg)**	Avg PW (kJ)	**CFE (%)**
Fold 1	4.496	16.329	**36.320**	5.204	**31.90%**
Fold 2	5.357	14.373	**26.831**	4.299	**29.90%**
Fold 3	6.216	17.256	**27.760**	5.361	**31.10%**

Increased the beam curvature to 2000 mm benefited the fold 1, particularly to its initial peak force as well as its smooth energy absorption process during the impact process. Due to its immediate engagement to the impact wall and smooth absorption process, it yielded total 16.329 kJ of impact energy, and because only one fold available on the beam, it achieved highest SEA (specific energy absorption) rate, which was 36.320 kJ/kg. Due to multiple folds design, fold 3 absorbed more energy after 0.015 seconds, and this reflected on the total energy absorption of 17.526 kJ. This, however, reduced its specific energy absorption when compared

with lighter fold 1, it yielded 27.760 kJ/kg. Fold 2 did not utilise the curvature increases effectively and achieved overall reduced energy absorption, which was 14.373 kJ. However, fold 2 provided a good overall deformation process when observed from its force reaction, with slightly less total energy absorption and average energy absorption, it achieved 29.90 % of the crush force efficiency which was very close to what fold 3 offered.

4.8 Plastic work – curvature 2400 mm

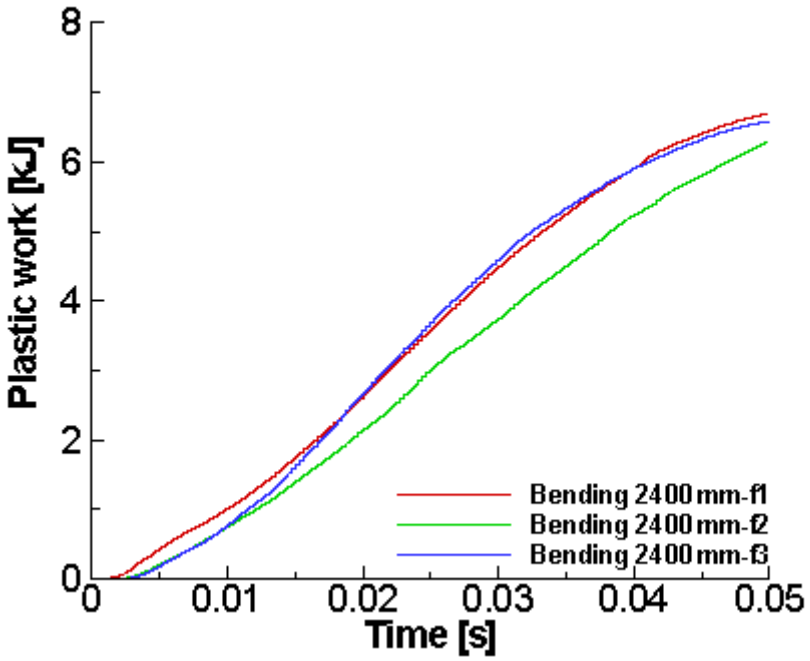

Figure 4.15 Curvature 2400 mm effects to the plastic work on all fold profiles.

Description – According to Figure 4.15, fold 1 started at a higher absorption rate when compared with fold 2 and fold 3 until 0.015 seconds. It shared similar energy absorption to fold 3 throughout the rest of the impact process. Fold 2 initiated with almost identical absorption curve to the fold 3 for the first 0.01 second but remained at a reduced amount of absorption rate after fold 3 gradually increased its absorption rate. While both fold 1 and fold 3 ended at similar absorption, fold 2 ended at slightly less rate.

Discussion – The above diagram summarised the effect of the energy absorption changes after increased beam curvature to 2400 mm. Fold 1 started at slightly higher absorption rate when compared with fold 2 and 3, and this represented an immediate engagement to the impact wall and started the deformation process. Lower energy absorption rate on the fold 2 and 3 suggested

multiple folds aided their initial impact behaviour. Fold 3 overtook the fold 2 after 0.015 seconds. This indicated the first fold was triggered by the impact load, and the force further increased when the first fold almost finished its compression, and the second fold started to engage the impact load. Despite it built with two additional folds than the fold 1, it only yielded slightly higher energy absorption rate when compared with fold 1. Since the curvature increases did not significantly increase the energy absorption of fold 3, it had less effect on the fold 2 where it remained reduced absorption rate throughout the impact process. This means increasing the curvature 2400 mm did not benefit the bumper beam from the energy absorption perspective.

Parameter Analysis –

Table 4.6 Curvature 2400 mm effects to the plastic work on all fold profiles.

Plastic work-Bending 2400 mm					
Profile	Weight (kg)	Total PW (kJ)	**SEA (kJ/kg)**	Avg PW (kJ)	**CFE (%)**
Fold 1	4.496	17.38	**38.653**	6.6729	**33.47**
Fold 2	5.357	14.91	**27.836**	5.1829	**32.23**
Fold 3	6.216	17.15	**27.588**	7.9181	**34.43**

Under the beam curvature of 2400 mm, all fold profiles were performed similar results, where fold 1 absorbed totally 17.38 J of impact energy which was the highest when compared with fold 2 and 3. Smooth absorption increases of the fold 1 indicated it experienced with progressive deformation without any catastrophic structural failure. Fold 1 reached to 7.00 kJ of maximum energy absorption while fold 2 and 3 yielded lower 6.30 kJ and 6.59 kJ. This suggested at a curvature radius of 2400 mm, fold 1 beam was capable of absorbing higher impact energy while fold 2 and 3 offered less. Meanwhile, it is also found the curvature of 2400 mm did not achieve positive impact in terms of energy absorption performance with multiple fold design. Fold 2 yielded 27.836 kJ/kg of SEA (specific energy absorption). And with lower total energy absorption of 14.91 kJ and average absorption rate at 5.1829 kJ, it achieved a lower crush force efficiency of 32.23 %. Despite multiple folds was available on fold 3, it achieved slightly better performance over the fold 2. It yielded 17.15 kJ of total energy absorption rate when compared with 17.38 kJ achieved by fold 1, but slightly better than fold 2. It yielded the mean load of 7.9181 kJ which was slightly higher than both fold 1 and fold 2. This aided the fold 3 and achieved higher crush force efficiency of 34.43 %.

4.9 Plastic work – curvature 3000 mm

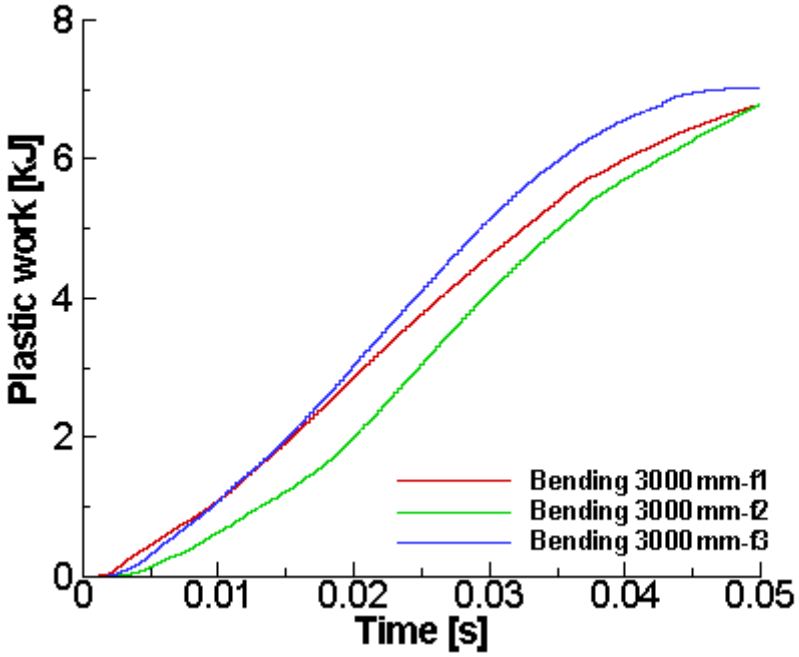

Figure 4.16 Curvature 3000 mm effects to the plastic work on all fold profiles.

Description – Fold 1 started at slightly higher absorption rate within the first 0.01 second but quickly reached by the absorption curve of fold 3. Without any fluctuations presented, it then continued at this steady increasing trend towards to the end of the simulation. After the 0.01 second, fold 3 progressed into a steady increasing trend, and gradually departed further away from the curve of fold 1 and gained higher absorption after 0.015 seconds. Fold 3 maintained this higher absorption rate towards the end of the simulation. Meanwhile, fold 2 achieved lower absorption for the first 0.01 second then both fold 1 and fold 3. It carried on at this lower absorption rate, but steadily throughout the simulation, it reached to the maximum absorption that is similar to the fold 1 and ended this process.

Discussions – Fold 1 started slightly higher absorption rate than fold 2 and 3 due to immediate engagement to the impact process. For the first 0.01 second, fold 2 appeared at less absorption rate, but fold 3 showed an increasing trend and became overlapped with the fold 1 from 0.01 and before 0.02 seconds. This indicated after the initial contact, fold 3 started absorbing the impact energy, but this absorption rate is increased towards the fold 1s' range. Fold 3 carried on climbed higher absorption after 0.02 seconds than the fold 2, this suggested the fold 3 was able to absorb more impact energy and offered more deformation This also reflected on the

absorption curve of fold 1, since it climbed steadily but remained lower than the fold 3, this was due to only one fold built into the fold 1 profile. Despite fold 2 reached the similar maximum absorption generally received lower energy absorption rate throughout the simulation although an additional fold was built in compared to the fold 1. This means fold 3 achieved overall highest energy absorption, while fold 1 came in second place, and the fold 2 was at the last. Multiple fold structure present in the beam certainly benefited and increased the energy absorption on fold 3. However, this did not appear to work on fold 2.

Parameters analysis –

Table 4.7 Curvature 3000 mm effects to the plastic work on all fold profiles.

Plastic work-Bending 3000 mm					
Profile	Weight (kg)	Total PW (kJ)	**SEA (kJ/kg)**	Avg PW (kJ)	**CFE (%)**
Fold 1	4.496	17.94	**39.906**	5.823	**32.45**
Fold 2	5.357	15.71	**29.327**	4.777	**30.41**
Fold 3	6.216	19.30	**31.043**	6.153	**31.88**

Table 4.7 showed the plastic work under the beam curvature of 3000 mm. It revealed fold 3 outperformed the fold 1. Multiple fold construction on the fold 3 improved its total plastic work as well as average plastic work. It totally absorbed 19.30 kJ of energy when compared with the 17.94 kJ yielded by fold 1. Despite this advantage, due to the fold 3 has 1.72 kg more than the fold 1, and this affects the SEA (specific energy absorption) figure. As a result, fold 3 yielded lower SEA value, which was at 31.043 kJ/kg while fold 1 achieved 39.906 kJ/kg. On the result of CFE (crush force efficiency), fold 3 have achieved very similar results to the fold 1. However, higher average energy absorption means it is capable of absorbing energy during the impact process. This indicated the fold 3 had better deformation behaviour. Although fold 2 yielded lower energy absorption curve when compared with fold 1 and 3, which were represented via both total energy absorption, which is 15.71 kJ, and average energy absorption of 4.777 kJ. This means an additional fold presented in the fold 2 did not help it to gain more energy absorption as found more effective on fold 3.

4.10 Analysis and recommendations

All the above results showed the material's effects on both reaction force and plastic work when the bumper beam material was replaced with aluminium Alloy at various curvature shapes and fold profiles.

Initial peak load – crash-box interference was reported during the analysis of the results to the structural steel made bumper beam in chapter 3. When the straight bumper beam overlapped the contact surface 100% to the rigid impact wall, the resultant significantly high force reaction was mainly caused by the crash-box interference. The initial peak existed in all profiles a regardless number of folds built to the beam. This similar observation but with marginally improved initial peak load was repeated again in this chapter after the bumper beam material was switched to aluminium alloy. This time it yielded 150 kN upon the initial contact where structural steel made beam reached over 300 kN.

Straight bumper beam also showed some negative impact on the overall force reaction. Aluminium alloy did not aid the beam to its deformation process, where fold 1 and 2 suffered from inefficiency during the deformation where either one or two folds cannot completely consume the impact load and inevitably involve the crash-box to participate the impact process and caused the force spike. This also affects the energy absorption to both fold 1 and 2, where both stopped its absorption process at 0.035 seconds. Fold 3 however received less impact from this and provided continued energy absorption after fold 1 and 2 were stopped. Despite this, a force spike still recorded 0.045 seconds indicating a certain degree of crash-box interference.

Initial peak load and overall deformation process were vastly improved after the curvature radius has been increased to 2000 mm, 2400 mm and 3000 mm each other respectively. Excepted the straight beam case, all fold profiles adapted very well, all fold profiles benefited from this and provided a gentle force upon initial contact. It is found curvature also provided a certain degree of benefits to the overall force reaction. Such examples were reflected on both curvature of 2000 mm and 2400 mm were the initial peak load remained very low, and the overall force reaction process was generally showed in gradual increases.

Further increased the curvature radius to 3000 mm maintained the initial contact force low, but did not continuously improve the overall deformation behaviour where all fold profiles experienced a different level of force steep increases. This means increased the curvature radius

to 3000 mm made all fold profiles unstable during the same impact conditions as tested in previous cases. Particularly to the deformation process after 0.03 seconds, where all fold profiles experienced some level of steep force increases reflected the bumper beam structure cannot provide a stable deformation.

Crash-box interference – When the bumper beam was made straight, all fold profiles showed a significant amount of force fluctuations towards the end of the simulation. This problem was previously showed when the bumper beam was made in structural steel and repeated again after switched the material to aluminium alloy. Both fold 1 and fold 2 showed violent force fluctuations. This indicated an insufficient number of folds available to consume the impact load completely and inevitably involved the crash-box to collide with the impact wall. Interestingly, folder 3 performed marginally better regardless of what materials when compared with fold 1 and fold 2. Similarly, to force reaction found in structural steel, aluminium alloy beam showed relatively smooth increases over the first 0.04 seconds and only registered with one force peak.

Despite the unstable deformation occurred to all fold profiles with beam curvature radius was 3000 mm, no further crash-box interference was recorded as soon as the curvature radius was increased to 2000 mm, 2400 mm or 3000 mm.

Curvature effect overall force reaction – Similar to what was discovered in the structural steel bump beam tested previously, increase the curvature radius benefited the bumper beam to yielded low initial peak load, but it also stabilised the deformation process. When compared with the straight beam as baseline performance where the violent force curves, all force curves appeared in smooth increases over the impact process under the beam curvature of 2000 mm. Increased the curvature to 2400 mm continued to benefit the fold 2 and fold 3 where the force was increased slightly after 0.03 seconds. Fold 1 also experienced the increases but at a much steeper rate. This was due to there was only one fold available and it showed a sign of unstable deformation as towards the end of the impact process.

Further increased the curvature to 3000 mm did not either maintain or improve the deformation process. All fold profiles showed gradual increases to 0.025 seconds but proceeded further differently. The force curves on fold 1 and fold 2 appeared in a flat region until further force increases were spotted after 0.045 seconds. Fold 3 showed a steep force increases from 80 kN

to almost 110 kN and also reached to a flat force region. This means the fold 1 and 2 were still at deformation process towards the end of the impact process, fold 3 lost the ability to provide further deformation due to the flat force region. Excepted fold 3, both fold 1 and 2 behaved more desirable when adapting to this beam curvature when compared with fold 3.

Fold effect overall force reaction – Replaced the bumper beam material to aluminium alloy showed similar results when compared to the structural steel used previously, although this appeared less effective on some of the curvature shapes. The benefit of the multiple fold construction was already emphasized in chapter 3. The test results in this chapter revealed this benefit retained after switched the bumper beam material to aluminium alloy.

Without any curvature radius assigned to the bumper beam, both fold 1 and fold 2 showed violent force spikes towards the end of the simulation due to the crash-box interference. This issue was largely improved when compared with fold 3. An obvious force spike still occurred at 0.045 seconds while the force curves on fold 1 and fold 2 were out of the chart limit. This indicated multiple fold construction appeared more effective to control its deformation process by induced the impact load gradually when the bumper beam is built without any curvature radius. This consumed a large portion of the impact load and reduced the crash-box interference to a minimum. The plastic work also indicated both fold 1 and fold 2 experienced a steep force abruption between 0.03 and 0.04 seconds. This means both bumper beams were fully compressed and followed with crash-box interferences. Despite the fold 3 also experienced a force spike, but recorded at the much lower spike, it continued to absorb any additional impact load, indicated by the smooth energy curve.

Multiple folds behaved well when increased the curvature to 2000 mm, where the force reaction curves to all fold profiles were maintained at steady increases throughout the impact process without any force spikes when compared with the straight beam. Both fold 2 and fold 3 performed particularly well when increased the curvature to 2400 mm. It made the force curves on both fold 2 and fold 3 increased slightly after 0.03 seconds. It is argued fold 2 also showed much steeper increases after the same time, this considered as unstable deformation due to the speed of the force increases was much faster. Fold 1 generally well curvature to 3000 mm. It showed in relatively smooth force curves excepted there was an obvious steep increase recorded by fold 2 at 0.015 seconds. Considered it performed smoothly at the same time when tested with curvature 2000 mm and 2400 mm, this is considered as unstable deformation. It

further proceeded at gradual increases indicated the overall force reaction was acceptable. Fold 3 also showed unstable deformation after 0.02 seconds, a steep force increases occurred throughout the rest of the impact process. This indicated fold 3 did not effectively control and regulate it deformation process after 0.02 seconds and behaved less desirable then fold 1 and fold 2.

Conclusion – After the analysis to the resulted displayed above, similar effects were repeated after switched the bumper beam material to aluminium alloy. Curvature can reduce the initial impact load regardless at any given radius. It can also control the deformation process in such a way that it allowed the beam to regulate its deformation gradually without causing any structural failure. However, this revealed an issue that continued to increase the curvature higher did not achieve continuous force improvement, where sudden force increases were observed to fold 1 in curvature 2400 mm and fold 3 in curvature 3000 mm.

Chapter 5. Result and Discussion (Composite)

5.1 composite Made Beam

Chapter 3 and 4 demonstrated the effect to the crashworthiness under the bumper made from either structural steel or aluminium alloy, where structural steel provided good crashworthiness performance, and aluminium alloy has achieved marginally higher energy absorption, smooth force reaction over the impact process (Stander and Craige, 2002). It is also realised that due to the stringent safety regulation each year, the vehicle manufacturer is under pressure to achieve higher safety standard, but with reduced systems' weight to retain fuel consumption. Particularly, the composite can achieve higher energy absorption at a much lower weight, if it is implemented appropriately (Avalle *et al*, 2002; Chotar and Benzeggagh, 1998).

Under this consideration of using composite, this metallic alternative replacement is extensively studied (Tanlak *et al*, 2015; Beyene *et al*, 2015; Hu *et al*, 2015; F.C. Campbell, 2004; Jimenez *et al*, 2004; Xu *et al*, 2017; Liu *et al*, 2016). An optimisation of vehicle front bumper in composite was conducted (Boria, 2017; Cheon *et al*, 1995). It mentioned the specific energy absorption represents the objective function to maximise and the geometrical parameters.

Figure 5.1 Bumper system location and cross-section profile of (a): basic and (b): modified (Boria, 2017).

Figure 5.2 Curvature shape of a): flat, b): medium, c): maximum (Boria, 2017).

Figure 5.3 effect on the force reaction with varies curvature shapes (Boria, 2017).

Figure 5.4 effect on the force reaction with the proposed cross-section profile (Boria, 2017).

Like the force showed in figure 5.3, the best behaviour at post-impact is achieved by shape b): medium. It is argued the shape a): flat gained high peak force periodically, and the initial peak force was also higher than b0: medium and c): maximum. This was caused by a large amount of contact surface between the beam and the rigid wall (Esfahlai *et al*, 2013; Farkas *et al*, 2012). Figure 5.4 displayed the effect on the force reaction with both proposed cross-section profile. It is observed compared with the basic profile, the modified profile lowered the peak force throughout the simulation through a stable deformation (Fang 2017; Fang *et al*, 2005; Fang *et al*, 2016; Gentry *et al*, 1996).

A variable cross-section for the composite made vehicle bumper beam was investigated. Two impact type was proposed with 4km/h to full front and 7km/h angular front at impact velocity. CFRP (carbon fibre reinforced plastic) was selected for the make of bumper beam (Wang *et al*, 2010; Wang and Shan, 2006).

Figure 5.5 FEA model of a composite bumper beam of (a): front impact, (b): angular impact (Zhu *et al*, 2016).

Figure 5.6 Thickness arrangement on the bumper beam (Zhu *et al*, 2016).

Figure 5.7 A material property of both high strength steel and CFRF used for the bumper beam (Zhu *et al*, 2016).

Table 5.1 Crashworthiness results between different materials (Zhu *et al*, 2016).

“Content removed due to copyright reasons”

It is displayed in table 5.1, the total amount of energy absorbed by CFRP is 320.24 J, where the bumper beam made from high-strength steel achieved 356.43 J. The composite material obviously absorbed less energy, but since the composite has the advantage of lightweight, where it weighs 3.322 kg, but the high strength steel weigh at heavier 4.891 kg. This resulted in the CFRP reached to 96.40 J/kg where high strength steel yielded at less 72.87 J/kg.

5.2 Simulation Preparation

Autodyne solver requires the geometry remained in solid if composite material is assigned, hence the bumper beam is kept as solid, but rigid impact wall and crash box were all converted to the shell state. Impact velocity, bumper system weight was all maintained the same as appeared in earlier structural steel and aluminium alloy tests as 15 km/h and 1000 kg. The material used was E-glass and carbon UD, and the properties are available in table 5.2 and 5.3. Since the density of both composites appeared in others’ investigation are relatively low of 1850 kg/m^3 and 1490 kg/m^3 when compared with both structural steel, 7850 kg/m^3 and aluminium alloy at 2700 kg/m^3, some weight difference is observed after assigned it to the bumper beam.

It is decided to make a valid comparison, the 2 mm thickness of the metallic made bumper beam is increased to 4 mm for both E-glass and carbon UD composite material. This resulted in a weight of 5.2 kg and 3.88 kg for each above mentioned composite bumper beam (Jonsen *et al*, 2009).

Table 5.2 Material properties of E-glass (Belingardi *et al*, 2014)

	ρ kg/m^3	E_{11} GPa	E_{22} GPa	G_{12} GPa	G_{23} GPa	ν_{21}	Xc MPa	Xt MPa	Yc MPa	Yt MPa	Sc MPa
E-glass	1850	31.2	9.36	5	5.5	0.29	409	483	92.2	34.9	73.3

(Change the material property to symbol)

Table 5.3 Material properties of Carbon UD (ANSYS, Inc., 2019)

	ρ kg/m^3	*E X*	*E Y*	G XY	G YZ	ν YZ	Xc MPa	Xt MPa	Yc MPa	Yt MPa	Sc MPa
Carbon UD	1490	121	8.6	4.7	3.1	0.4	1082	2231	100	29	60

5.3 Composite Made Beam – Force reaction

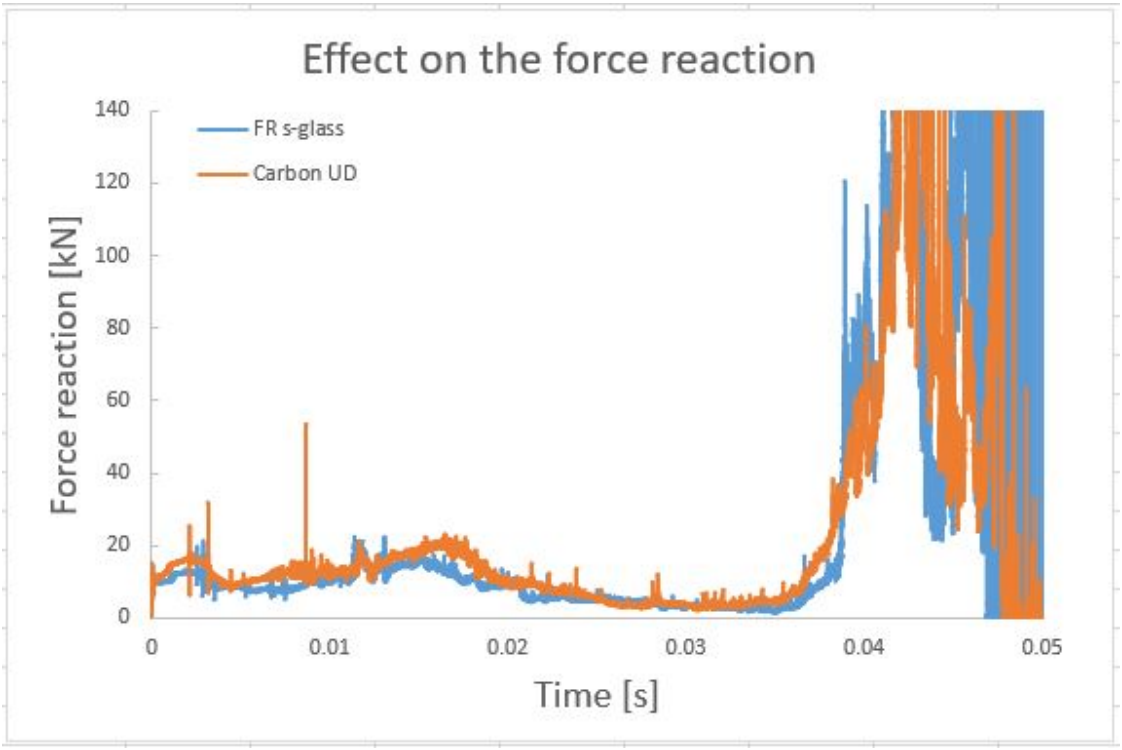

Figure 5.8 Effect to force reaction gained by E-glass and carbon UD polymer.

Figure 5.8 showed an effect on the force reaction between both types of composite material. It is observed both offered very low initial peak load upon the impact, and both proceeded towards to 0.04 seconds with considerably low force rate, but relatively smooth force trend (Gentry *et al*, 1996; Palmer *et al*, 1998). Carbon UD has registered a slightly higher force rate within this period. Both showed a heavily fluctuated force trend after 0.04 seconds. Both force trends appeared in steep increased quickly right after 0.04 seconds, and both entered into an extreme fluctuation and went off the chart limit of 160 kN. Carbon UD appeared settled down when the simulation was ended while the E-glass still violently fluctuated.

5.4 Composite Made Beam – Force reaction

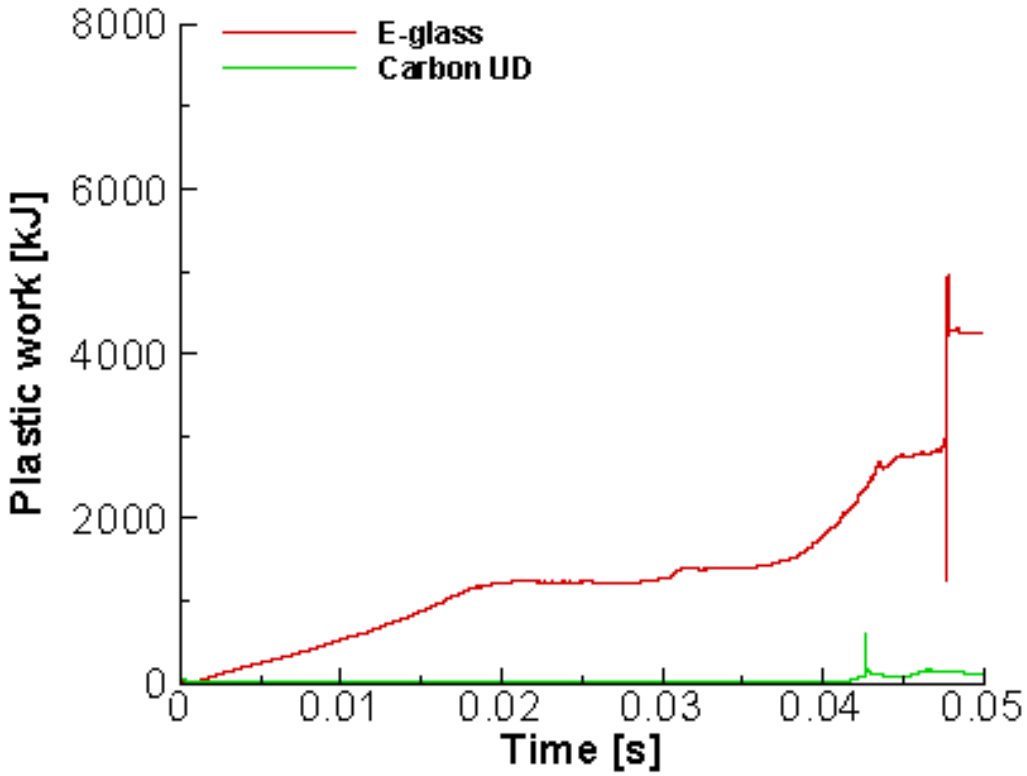

Figure 5.9 Effect to plastic work gained by E-glass and carbon UD

Figure 5.9 indicated the effect of the plastic work gained by both composite materials. It is noticed that the carbon UD showed an increasing trend throughout the simulation generally. The absorption rate for the first 0.02 seconds is at steady increases and proceeded with a slight increase until 0.04 seconds. The absorption rate further increased to 3 kJ and reached as high as just over 5 kJ at the end of the simulation. While carbon UD absorbing the impact energy, the E-glass bade beam barely registered any increasing absorption trend before 0.04 seconds. The absorption rate during this period is very low, only it started to absorb little more energy after 0.04 seconds insignificantly and carried towards the end of the simulation.

5.5 Analysis and recommendations

When compared with both composite and metallic, both metallic made beam gained much less force range which is between 0 kN to 20 kN, where its metallic counterparts have achieved between 40 kN to 120 kN. Indeed, composite made beam appeared similar smooth force curve, but due to the beam unable to process complete impact load, both force curves showed extreme fluctuations after 0.04 seconds. Low force rate registered before 0.04 seconds indicated the beam deformation did not reach to similar efficiency of which metallic made beam offered.

Where this inefficiency of deformation inevitably led to crash box interference and as a result, a heavily fluctuated force for both E-glass and carbon UD materials is observed. Despite both composite beams performed poorly, carbon UD showed some improvement then the E-glass. It yielded a slightly higher force for the first 0.04 seconds and can settle back down between 0.04 to 0.05 seconds, which E-glass failed to perform. Because of this better deformation behaviour, the energy absorption on the carbon UD is also largely improved, it increased its absorption rate until 0.02 seconds, and carried on after 0.04 seconds (Karimi *et al*, 2012; Liao *et al*, 2008; Menna *et al*, 2011).

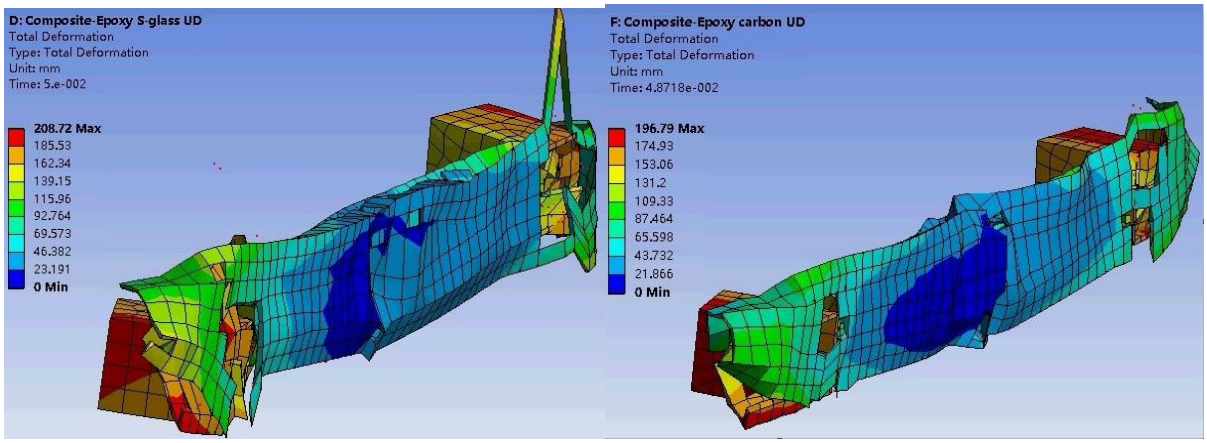

Figure 5.10 Deformation behaviour of E-glass (left) and carbon UD (right)

Figure 5.10 did not just prove the beam deformation between two composite material, but also explained the main cause of crash box interference. Despite the E-glass has a higher weight advantage, this did not help the deformation process. It is the lighter carbon UD offered slightly better control to the beam deformation, Particularly, it revealed the connection surface between the beam to the crash box was completely shattered and resulted crash box penetration directly to the rigid wall while partly connected to the beam. This phenomenon behaved much more severe on the E-glass made a beam, but less violent on the carbon UD. This also reflected both force reaction and plastic work showed earlier (Pawlus *et al*, 2011; Palmer *et al*, 1998).

Chapter 6-Filler result and discussion

This chapter focused on the results based on the effect of filling material to the empty beam. Fold 2 was selected to perform at this chapter to establish the baseline performance.

The selection of desired specifications to the bumper beam profiles was concluded after the comparison between chapter 3 and 4. Regardless of both curvature and folds increase, structural steel made beam gained some benefit on the energy absorption as well as force reaction. Both fold 1 and 3 were performed significantly inconsistent on the force reaction where only fold 2 achieved a certain degree of improvement without any significant amount of fluctuations throughout all the simulations. Fold 2 also gained very similar energy absorption cross the simulations suggested fold 2 is considered as desirable fold profile. However, due to the nature of the structural steel, it is destined that it reduced its desirability to achieve higher SEA rate as well as weight reduction of the bumper system.

Aluminium was used in chapter 4 to test if it can achieve improvement over the structural steel. Results showed fold 1 was less desirable due to the high initial peak force as well as unstable deformation behaviour. Fold 2 achieved overall good stable and regulated deformation behaviour regardless of either curvature or fold increase. The energy absorption rate is slightly lower than the fold 1 and 3 in some cases, but others were like other profiles. The results comparison of chapter 3 and 4 suggested when to consider from the main criteria such as beam curvature profiles, the shape of the fold and the material used, aluminium made fold 2 at bending curvature of 2400 mm was considered as desired beam geometry and subjected to further filling test.

While the bumper beam profile was decided, some of the existing literature was also reviewed to evaluate the effectiveness of the proposed method. Generally, it is found that with correct geometry specifications and the material, the thin-wall tube structure is very well capable to absorb significant amount of impact energy via a good stable self-regulated impact behaviour, particularly when such a structure is subjected to axial impact load scenario, where the test sample is mounted upright, and the impactor (crusher) is then travelled vertically at pre-defined velocity. However due to certain limitations presented on to such structure, such as weight or exterior characteristics. Foam filled method is considered as an alternative method without sacrificing the weight and requires a minimum amount of modification to the existing structure

and the integration process is relatively convenience (Attia *et al*, 2012; Banhart *et al*, 2001; Chen *et al*, 2002). Despite the filling method is widely investigated and very well documented on the axial impact test, some other literature was looked into the flexural impact, where the filling method was added to the transverse bumper beam or tube (Santosa *et al*, 1999; Hanssen *et al*, 2000; Rajak, *et al*, 2014; Ozer *et al*, 2016; Guo and Yu, 2011; Lan *et al*, 2014; Yu *et al*, 2012; Sha *et al*, 2011).

“Content removed due to copyright reasons”

Figure 6.1 Geometry specification of the proposed bumper beam (Xiao *et al*, 2015).

Table 6.1 Material property (Xiao *et al*, 2015).

“Content removed due to copyright reasons”

“Content removed due to copyright reasons”

Figure 6.2 True stress and strain for BL410A (Xiao *et al*, 2015).

Figure 6.3 True stress and strain of BL260LYD (Xiao *et al*, 2015).

Figure 6.4 Density of the FGF foam (Xiao *et al*, 2015).

The density of the FGF (functional graded-foam) is calculated based on Figure 6.4. It demonstrated the distance from the left to right of the bumper beam is assigned from 0.0 to 2.0 meters and the density variation is related to the normal distance. Because the constitutive of functionally graded foam is not available, the foam was defined as multiple layers and all meshed homogeneously.

“Content removed due to copyright reasons”

Figure 6.5 Proposed beam and its filler mesh (Xiao *et al*, 2015).

The assessing criteria of both functionally graded foam and uniform graded foam was tested under groups of gradient exponent *m* shown in Figure 6.4, both left and right end foam density and the wall thickness of the beam. The resulted was displayed are energy absorption *EA*, specific energy absorption *SEA*, peak force F_{max} and *CFE* (crash force efficiency).

“Content removed due to copyright reasons”

Figure 6.6 Effect to the EA and SEA at a range of gradient of foam density
(Xiao *et al*, 2015).

“Content removed due to copyright reasons”

“Content removed due to copyright reasons”

Figure 6.7 Effect to the F_{max} and CFE at a range of gradient of foam density (Xiao *et al*, 2015).

Figure 6.6 and 6.7 revealed the effect to all results with gradient foam density that range from 0 to 10.0 *m*. Figure 6.5 clearly showed decreasing energy absorption when the exponent *m* is increased. However, the SEA results on both types of filling are proportional to the exponent *m*, the specific energy absorption gained increase when the exponent *m* is increased as well. Figure 6.7 showed the peak force value, which was decreased as per exponent *m* increases. Both FGF and UF have achieved very similar maximum force rate when the exponent *m* is below 2.0 m, where the UF showed slightly improved force value that is marginally lower than the FGF when increased the exponent *m* over 2.0 m. Figure 6.6 also displayed the effect on the crash force efficiency, and it is clearly FGF achieved better efficiency when the exponent *m* was between 0.2 m to 6.0 m when compared to the UF.

6.1 Simulation preparation

During the Simulation setup mentioned in chapter 3, the “flex” command was used to generate the correct beam curvature shapes. Incorrect use of “Bend” will cause the interference problem to the connection between the beam to the crash boxes as well as retro-fitting the foam into the empty beam. It is noted in figure 6.8 where both fold 2 beam and its foam filler material were generated with “Flex” to create a perfect fit when joining the foam filler into the empty beam.

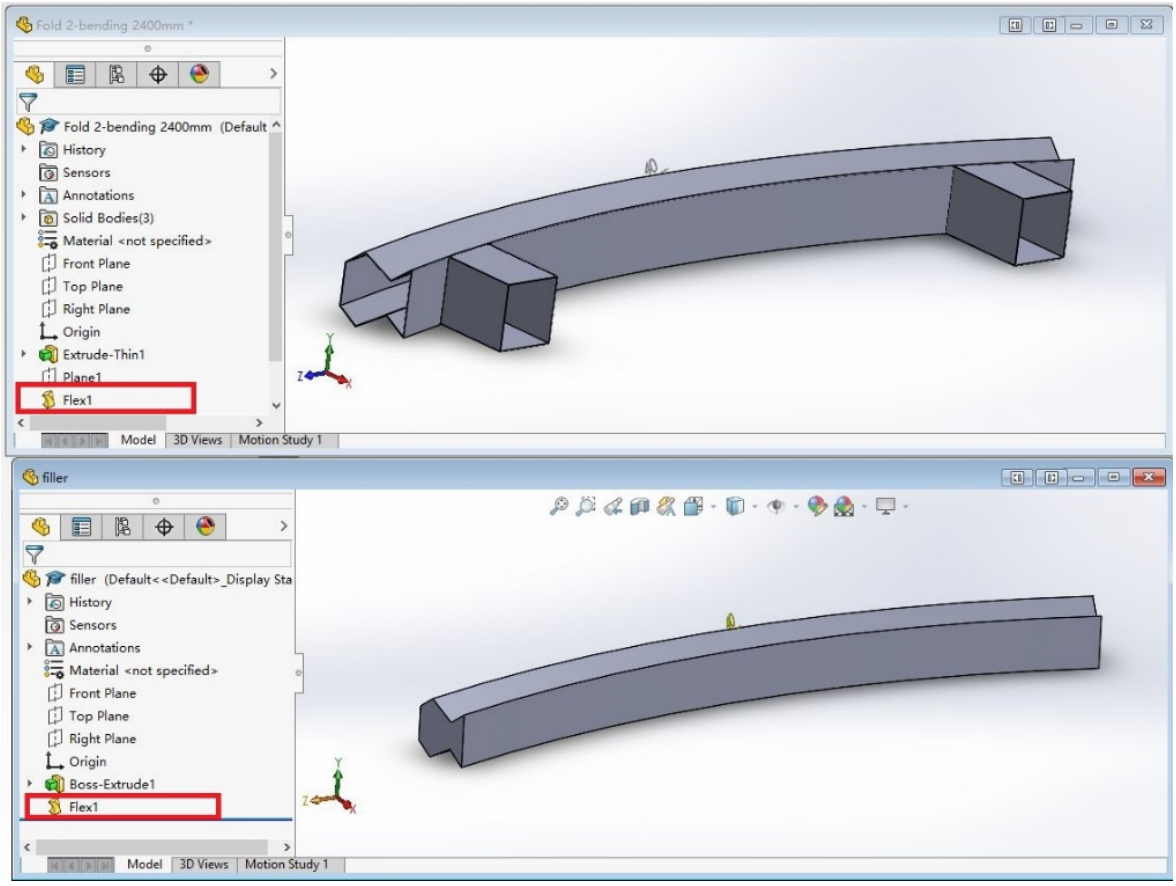

Figure 6.8 Fold 2 and its foam filler.

Figure 6.9 below demonstrated the beam cross-section after completed the procedure in figure 6.8. And Figure 6.10 below showed the filler material left as a solid element and did not subject to shell conversion to create a more realistic effect. The connection to the beam is free to move and the penalty was applied to make sure the filler does not penetrate through the beam (Craig *et al*, 2005; Duarte *et al*, 2014; Fang *et al*, 2015).

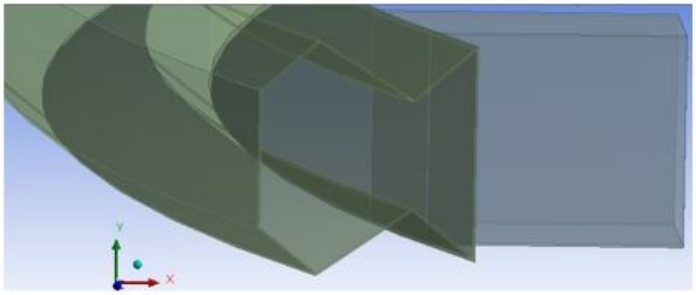

A:Empty Beam

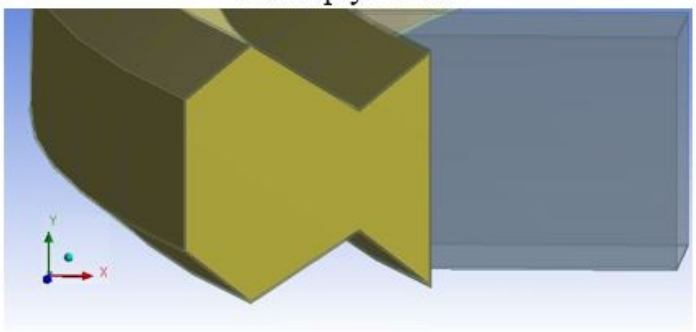

B:Full fill(3/3)

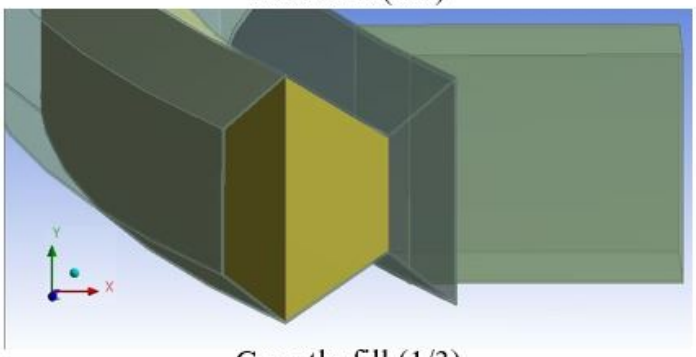

C:partly fill (1/3)

Figure 6.9 All proposed filling method.

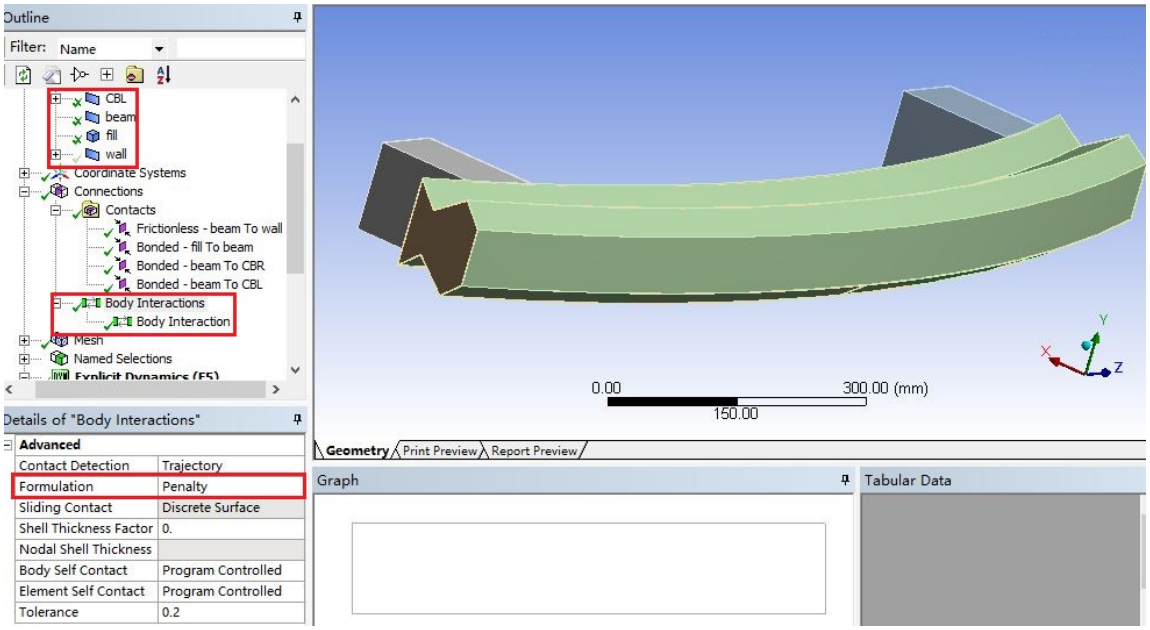

Figure 6.10 Filler material, and its contact setting

6.2 Force reaction

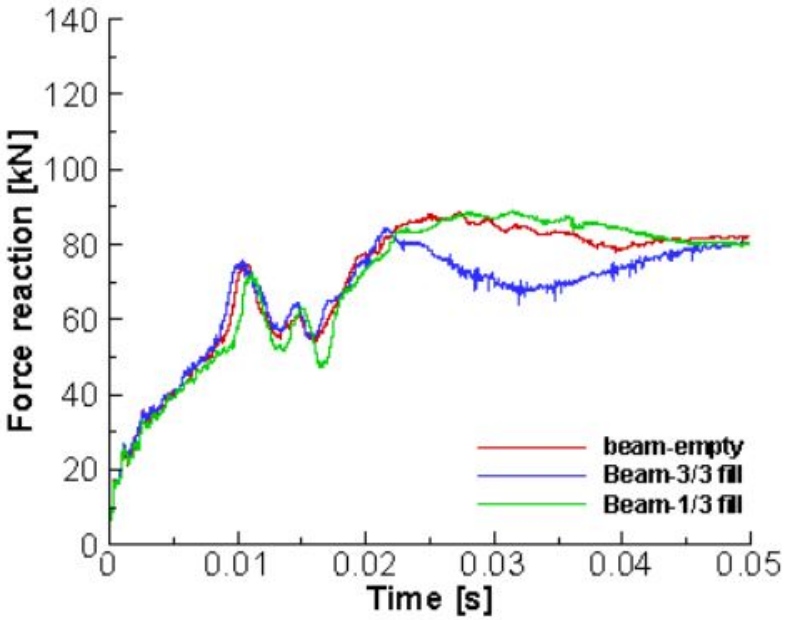

Figure 6.11 Effect on force reaction with varies filling profiles.

Description – Figure 6.11 described the effect on the force reaction and plastic work with 4 different filling method, namely: empty beam, 3/3 fill beam, 1/3 fill beam and 2/3 fill beam. To establish the baseline performance, the empty beam experienced a gradual force increases over the first 0.02 seconds with an obvious drop after 0.01 second. It quickly recovered from this drop and continued to climb slightly after and reached to the highest value of 85 kN. It then proceeded into a relatively stable trend throughout the simulation, and finally ended at 80 kN.

Other filling methods of 3/3, 1/3 and 2/3 were all generally shared similar force trend and value for the first 0.02 seconds when compared with the empty beam, but exhibited slightly different force trend after.1/3 filled beam maintained very similar force curve then the empty beam, which forces were decreasing as the simulation progressed to the end, but with slightly higher value after 0.03 seconds. Instead of remaining in the force range that is similar to both empty and 1/3 filling beams, 3/3 filling method experienced a gentle force dip where it decreased down to 70 kN until the 0.03 seconds, and force recovered and increased back towards to the end of the simulation.

Despite the different force trend in between the filling method of empty, 1/3 and 3/3, all 3 profiles were reached to a very similar force value after the simulation was ended. 2/3 was

observed at higher force curve throughout the entire simulation when compared with other 3 profiles. 2/3 filling profile started to register higher force value compared with other profiles for the first 0.02 seconds. The curve continued to increase further higher and behaved a flat force range after 0.03 seconds. This flat force range only lasted until 0.045 seconds and ended with a force dropped down to 95 kN.

Discussion – To explore and fully understand the causes of a few characteristics encountered by the force curves shown in Figure 6.9, a deformation behaviour was captured per each 0.01-second increment demonstrated in an order of 0.01s (top), 0.02s (top second), 0.03s (middle), 0.04s (lower bottom) and 0.05s (bottom) from the top to the bottom of Figure 6.10, 6.11 and 6.12. During the impact for all 3 proposed filling methods. Empty beam showed a gentle force reaction without any significant fluctuation, excepted there was a force value drop between 0.01 and 0.02 seconds.

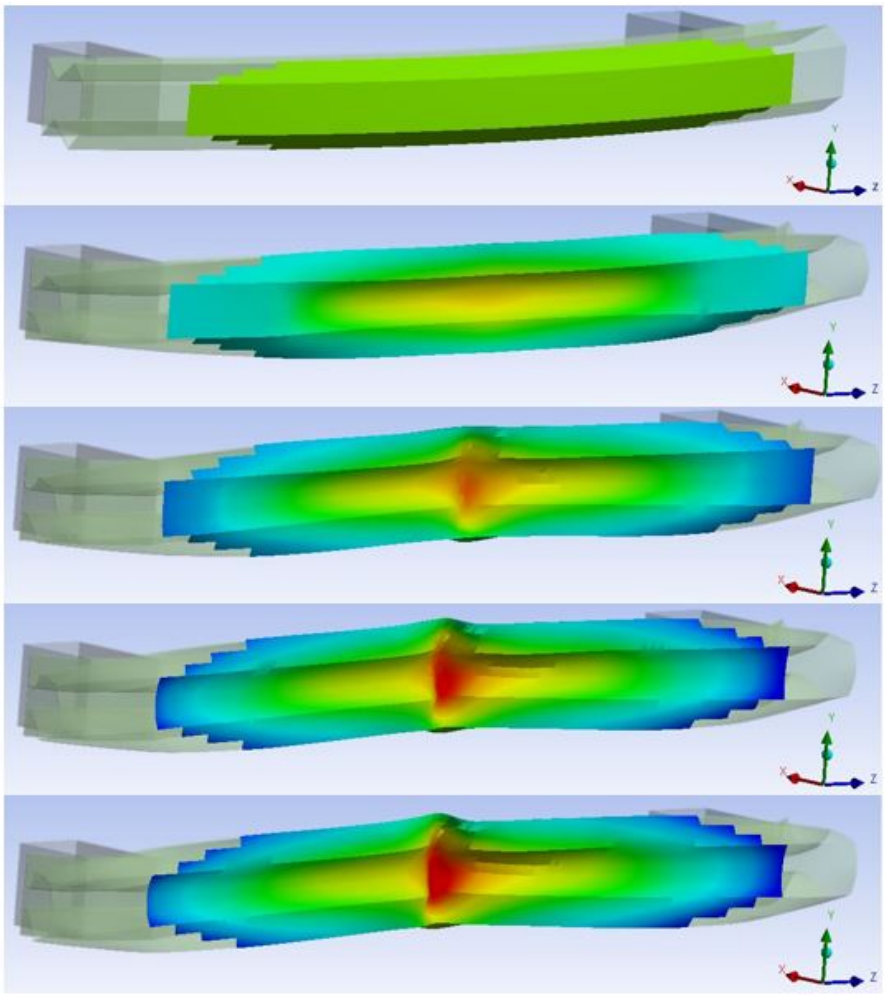

Figure 6.12 Deformation behaviour of the empty beam from 0.01s to 0.05 seconds. Top:0.00s; Top second: 0.02s; Middle: 0.03s; lower bottom: 0.04s; bottom: 0.05s

From Figure 6.12, a very clear difference is displayed at time step from 0.01 and 0.02 seconds where the beam initial contact surface was buckled inward at 0.01 second while colliding with the rigid wall. This buckling motion was completed when the time reached to 0.02 seconds and explained the force drop on the empty beam. Similar buckling behaviour was also observed throughout the force curves yielded by other profiles. The empty beam was subjected to further deformation and a vertical groove was formed at the centre of the beam when the time reached to 0.03 seconds. The gentle force drop after 0.03 seconds is represented by the groove formation that lasted until the end of the simulation. This force drop appeared stopped at 0.04 seconds and continued at a stable trend towards to the end of the simulation. This was reflected in the groove formation did not progress any deeper (Liu and Day, 2010; Raddy and Wall, 1988). A 3/3 full filled beam was added to justify the filling material was working as desired compare with the empty beam. Initially, for the first 0.02 seconds, both empty and full filled beams shared similar force reaction trend, but the filled beam gained very slightly higher force value. This showed the filling material, and full filling method to the beam profile did not affect the overall integrity of the beam, and also did not interfere with the deformation process. (Kecman, 1983).

Despite that, the initial contact area to the wall was buckled inward at 0.01 second after fully filled the empty beam showed in figure 6.11, both upper and lower edges were remained, instead of pushed inward like the initial contact surface completely which is showed in figure 6.2 during the same period. This showed the filler material helped the beam to resist the impact, hence the force value on the 3/3 filled beam was slightly higher than the empty beam performed. Interestingly, figure 5.2 and 5.3 revealed a difference of force reaction curve after 0.03 seconds, and it is observed 3/3 filled beam appeared in the dropped force curve than the empty beam (Seitzberger *et al*, 1997).

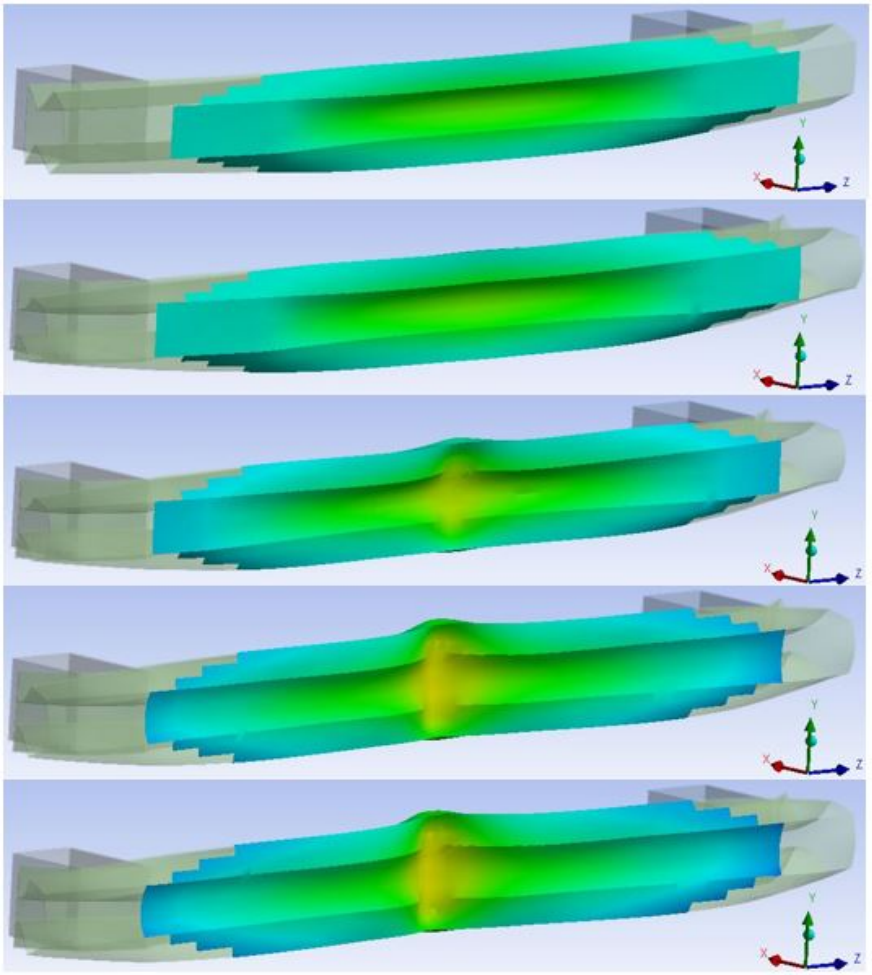

Figure 6.13 Deformation behaviour of 3/3 fill beam from 0.01 to 0.5 seconds.
Top:0.01s; Top second: 0.02s; Middle: 0.03s; lower bottom: 0.04s; bottom: 0.05s

It is understood that the filler material held the structural integrity of the beam and prolonged the contact area to the wall as the previous paragraph explained, it is expected the force value should be the same if it's not higher than the empty beam. However, upon the close inspection to the deformation behaviour showed in figure 5.2 and 5.3, it is revealed although both beam profiles experienced the same simulation conditions, and indeed groove were generated on both beam profiles, but the empty beam showed a higher concentration of deformation in near the initial contact surface, and this was highlighted in red on empty beam to represented higher deformation magnitude. Whereas less magnitude was observed on the 3/3 filled beam and therefore represented via yellow in the same region (Sun *et al*, 2010; Wierzbicki *et al*, 1994; Yang *et al*, 2005). Filler material was squeezed out of the beam was resulted in the force value drop, since it helped the beam to sustain the maximum contact surfaces during the impact, but eventually broke, and pushed out of the beam, and lost its energy absorption capability as further plastic energy has been absorbed via the beam. 1/3 filled beam, however, behaved the

most similar on bother trend and value compared to both empty and 3/3 filled beam profiles, but with slightly lower force value until 0.02 seconds. The force curve than proceeded with slightly higher value throughout the simulation, with both empty and 3/3 filled beam profiles appeared at lower force curves at the same period.

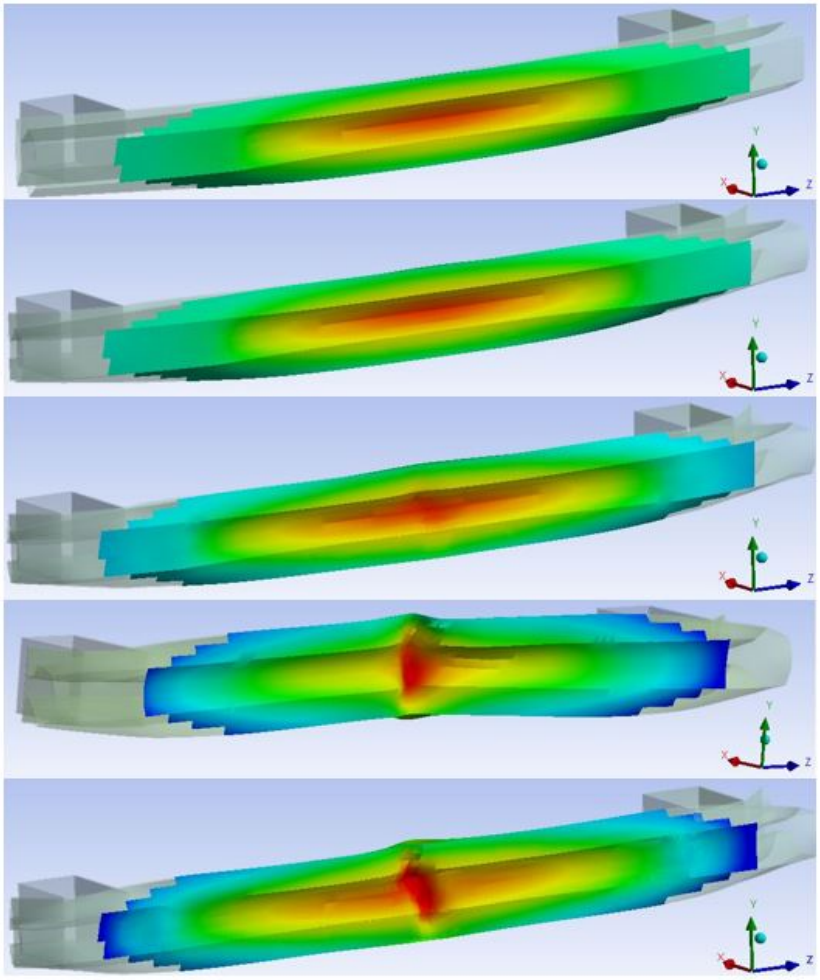

Figure 6.14 deformation behaviour of 1/3 filled beam. from 0.01 to 0.5 seconds.
Top:0.01s; Top second: 0.02s; Middle: 0.03s; lower bottom: 0.04s; bottom: 0.05s

To fully understand the reason that leads to the 1/3 filled beam to yield lower force reaction value for the first 0.02 seconds, but slightly higher after 0.03 seconds, Figure 6.12 was added to dress those questions. It revealed for the first 0.02 seconds, the force applied and concentrated horizontally at the centre of the outer surface upon the initial contact area. This force concentration did not increase further due to the filler material started to engage and resist the deformation process (Wierzbicki *et al*, 1994).

The filler material was engaged after the initial contact with the rigid wall, and the first fold became saturated because of the beam deformation. This made the filler material quickly filled

to the fold grooves cavities inside the beam. This reflected on the lower force curve for the first 0.02 seconds since the beam started to deform and did not reach to the filler material. Further deforming and displacing of the beam forced the filter material to engage with the deformation process and the relocated and redistributed into the fold grooves inside the beam. This filler material redistribution increased the stiffness of the fold. As a result, the horizontal contact surface was bent inward deeper when compared to the empty beam and 3/3 filled beam (Chen *et al*, 2002). Because of this, the deformation magnitude showed horizontal concentration as marked in red consistently over the first 0.02 seconds, subsequently, a lower force reaction was recorded. Due to the continued beam deformation, and the filler material started to fully engage the further deformation process at 0.02 seconds onwards, this could answer the question of slightly higher force reaction curve when compared to the both empty and 3/3 filled beam profile particularly between the 0.03 to 0.05 seconds (Duarte *et al*, 2014; Yu *et al*, 2008; Zarei and Kroger, 2008) This also suggested the filler material started to work with the beam together to resist the deformation. This means groove was formed and registered as 23.29 mm deep achieved by 1/3 filled beam, and 30.27 mm deep in the empty beam. This enabled the beam with more contact area with the wall and resulted in the 1/3 filled beam registered with slightly higher force reaction than empty beam after 0.03 seconds.

6.3 Plastic work

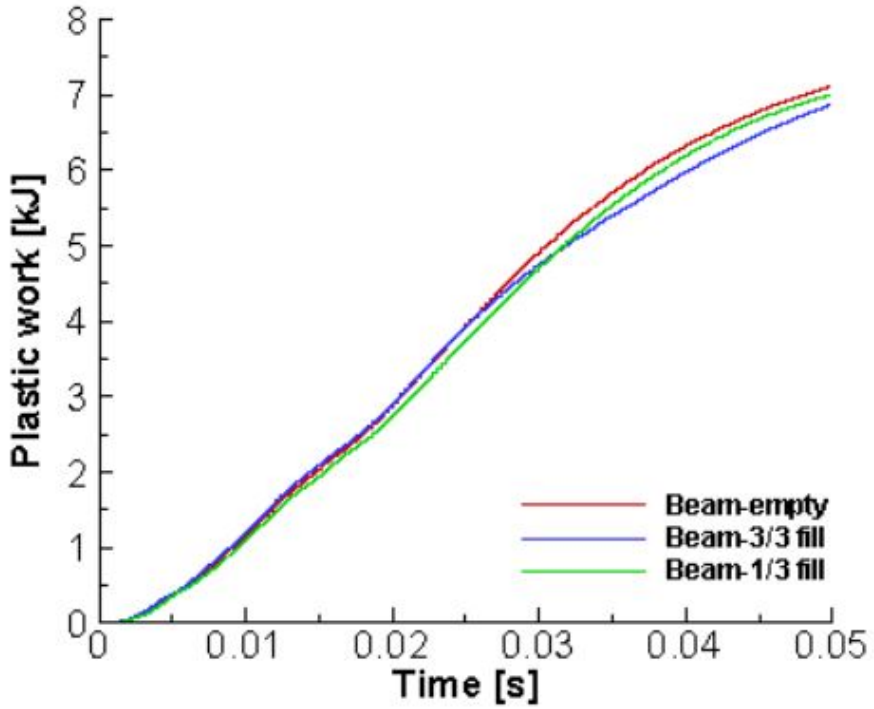

Figure 6.15 effect on the force reaction with varies filling profiles.

Description – Figure 6.13 displayed the energy absorption performed via all 4 profiles throughout the simulation. Empty beam achieved a very smooth absorption curve without any significant fluctuation. This means the deformation behaviour at consistent stages and was smooth. Both 3/3 and 1/3 filled beam profiles were also shared very similar absorption trend throughout the entire simulation but at a slightly different rate. Before the time elapsed to 0.03 seconds, 3/3 filled beam achieved slightly higher absorption rate then the empty beam yielded, this was due to the filler material started to engage the deformation process with the beam from the moment of impact. And because of this additional absorption offered by the filler material, the absorption rate was slightly higher than the empty beam. However, 3/3 filled beam did not maintain this absorption rate and proceeded at a lower absorption rate after 0.03 seconds. This was due to the filler material loses that was squeezed by the deformation of the beam, and eventually pushed out of the beam. This material loses reduced the energy absorption capability and ultimately led to reduced energy absorption showed in Figure 6.13. Although 1/3 filled beam shared very similar energy absorption trend when compared with empty and 3/3 filled beam, but with slightly less rate for the first 0.03 seconds. This was caused by the filler material was not placed near the front of the beam but was centred. It means the filler material did not engage the beam deformation upon the impact, where only the beam was absorbing the impact energy. This also reflected in the reduced absorption rate for the first 0.03 seconds shown in Figure 6.13. The energy absorption curve did not proceed appeared in the same decreasing trend gained by the 3/3 filled beam, instead, it increased its absorption rate and lasted throughout the simulation. This was due to the bumper beam was deformed and triggered the filler to engage the further deformation process after 0.03 seconds. This represented an increased absorption rate that is higher than the 3/3 fill beam profile.

2/3 filled beam exhibited slightly higher increasing rate compared to other beam profiles upon the initial contact, but it increased slightly higher rate after 0.01 second. This was due to the filler material was not available at the front section of the beam, hence the energy absorption was very similar to other profiles. The absorption rate was increased further higher after 0.01 seconds and it maintained this rate and trend almost throughout the simulation and finished at a reduced absorption rate. The increasing trend was caused by the continued beam deformation further and triggered the filler material to participate in this deformation process. However, the convex shaped absorption curve of 2/3 beam showed a concentrated absorption period until 0.045 seconds, and this was responsible the reduction of absorption took place at the end of the simulation.

6.4 **Analysis**

Empty beam was the baseline performance that yielded acceptable absorption rate which is 7.12 kJ. Despite the filler material is added into the beam, both 3/3 filled and 1/3 filled profiles achieved very close energy absorption rate, which was both 7.01 kJ when compared with the empty beam. While further analysing the effect to the energy absorption with the different filling method, it revealed full fill came slightly less absorption rate after 0.03 seconds than the empty beam.

Upon review the deformation behaviour of the 3/3 filled beam and found the internal filling material was squeezed and pushed out of the beam from 0.03 second onward, this material loses made the filler material less effective for the energy absorption purpose. On the other hand, 1/3 filled beam generally yielded lower energy absorption, but still very close to the both empty, and 3/3 filled beam for the first 0.03 seconds. This suggested the 1/3 fill filling method did not interfere with the deformation process, the plastic deformation process of the beam is similar to the empty profile. Interestingly, the absorption rate increased slightly than the 3/3 filled beam after the 0.03 seconds, and this showed the filling material aided the energy absorption together with the beam. This also suggested the losing filling material after 0.03 second on 3/3 filled beam was a correct assumption (Yin *et al*, 2013; Yin *et al*, 2014)

Considered 2/3 fill beam was only partly filled, it absorbed slightly higher energy than other proposed filling profiles. It showed a similar trend to other profiles initially for the first 0.01 second, it means the beam entered into plastic deformation and started to absorb energy upon the initial contact. As the beam further compressed and filling material begun to work, it engaged with the beam together to resist further compression due to impact, and further absorbing impact energy as the intended purpose.

Parameters analysis –

Table 6.2 Filling method effect to the plastic work on all profiles.

Plastic work-All 4 filling methods			
Profile	**FR peak (kN)**	**FR mean (kN)**	**CFE (%)**
Empty (6.96 kg)	88.44	70.39	79.60
3/3 fill (7.15 kg)	84.23	66.31	78.72
2/3 fill (6.95 kg)	117.03	100.77	86.15
1/3 fill (6.95 kg)	88.85	70.39	79.22

Based on the above results discussions to both force reaction and energy absorption, a result

concluded and displayed in Table 6.2. It showed force reaction value at peak, mean and efficiency achieved by all bumper profiles. 3/3 filled beam showed 66.31 kN of mean force reaction, which was slightly less than the empty beam, this resulted in 78.72% of crush force efficiency but without any significant difference. 1/3 filled beam yielded 88.85 kN of force reaction, a 0.41 kN higher than the empty beam. Despite it achieved 70.39 kN of mean force value, it resulted in 79.22 % of crush force efficiency with 0.38 % efficiency increases than the empty beam. 2/3 fill beam performed better than the other 2 filled beam profiles. 2/3 filling method aided the force reaction to reach to 117.0 3kN of peak value with 100.77 kN mean force value. This resulted in the crush force efficiency is higher than the other 2 filled beam profiles, and certainly better than the empty beam. From the energy absorption perspective, based on the fact that 3/3 fill beam suffered from absorption rate drop after 0.03 seconds, and 1/3 fill beam yielded generally low absorption than the empty beam, 2/3 fill beam maintained overall higher absorption rate throughout the simulation.

6.5 Recommendations – Related literature indicated the force reaction shall be as flat as possible throughout the simulation, and the mean force reaction value should be as close to the peak force as possible (Belingardi, *et al*, 2014). From energy absorption perspective, the absorption curve should be a smooth line without any significant fluctuation. The 2/3 fill beam satisfied both suggestions that indicated it is a more desirable design when compared with empty, 3/3 fill and 1/3 fill beam profiles. The importance of low initial, and peak force reaction were explained that due to this parameter is directly linked to the occupants as well as the main vehicle structure. Low initial force reaction means reduced injury risk occurred to its occupants, and overall lower force reaction will lead to low decelerations since it is a critical factor that affects the vehicle may sustain more damage to the impact surrounding area (Attia *et al*, 2012; Gupta, 2007; Wierzbicki *et al*, 1994).

Chapter 7 Connection between crash boxes and bumper beam

In most low-speed impact cases, where the impact event occurs under 8.0 km/h (~ 5.0 mph), the bumper beam and foam are going to engage the impact process and absorb impact energy. This combination is usually found very effective in processing the impact load, and contributed positive crashworthiness performance without the involvement of crash boxes. Chapters 3, 4 and 5 detailed those results between the empty and filled bumper beam under various proposed beam profiles. This chapter, however, is to investigate the effect of the crashworthiness performance after introducing the crash boxes and how the bumper beam to crash box connection method affects the crashworthiness. The bumper beam was located at very front of the bumper system while crash boxes are situated behind the bumper beam. The crash box acts as the connection between the bumper beams to further rear frame rails.

The connection – The mechanical connection existed from the bumper beam to the crash box, as well as from crash box to the frame rail. Particularly, the connection between the bumper beam to the crash boxes existed mechanically and available in many types. As per Figure 3.1 in chapter 3 demonstrated, most of the connection types are either welded or bolted.

Figure 7.1 Location of the crash box and frame rail (Costas, 2014).

Figure 7.2 longitudinal frame (EAA, 2013).

Figure 7.3 Welding connection on the Mercedes A class (EAA, 2013)

Figure 7.4 Bolt connection on the Citroen C4 Picasso (EAA, 2013)

Regardless of the types of connections, it created the load path displayed in Figure 7.1 and 7.2. It allows the crash boxes to keep consuming the additional impact load during the high-speed impact scenario, once the bumper beam alone unable to the processed complete amount of the kinetic energy into structural deformation, and the vehicle is still at forwarding motion due to additional momentum. This scenario is found particularly to the vehicle speed as high as 15km/h where the bumper beam, the crash box is considered as a sacrificial energy-absorbing structure that is to mitigate damage to main vehicle structure behind. Figure 7.2 further demonstrated the arrangement between bumper beam, crash boxes and longitudinal frame rail in the production vehicle. The main reason for this arrangement is to enhance the energy absorption characteristic, and to control the impact within the bumper system and prevent further damage to the longitudinal frame rail located behind especially the impact speed was over 8km/h, and sometimes as high as 15km/h. A poorly designed bumper system can lead to longitudinal frames to engage the deformation process inevitably, and yielded a significant amount of damage. Since the frame rail carries main drivetrain components, such as engine and gearbox, this made the frame rail very difficult to access to perform the repair (Sharpe *et al*, 2001; Noh *et al*, 2018; Tounsi *et al*, 2019; Chung *et al*, 2017; John and Nidhi, 2014; EAA, 2013; Beyene *et al*, 2014; Kim and Lee, 2017).

Legislation – Despite the bumper system can process the impact as high as 15km/h, varies legislations have a specific requirement regarding the impact velocities as well as the post-impact behaviour of the bumper system. In the case of the most North America regions scenario, the IIHS (Institute insurance of highway safety) bumper test specified when the impact velocity reaches to 8km/h for both front and rear, the bumper system must consume the impact energy and control the damage within the beam itself without effect the normal operation of any nearby safety-related components, such as headlight and indicator. The similar compulsory requirement is also available in the EU region. The E.C.E (Economic Commission for European of the United Nations) stated 4 km/h and 2.5 km/h impact test must be performed to both the front and rear of the vehicle and no safety-related equipment is affected.

Impact Speed – In general, the standalone bumper beam is very capable to process most of the impact load that happened as high as 8km/h, which is satisfied the mainstream bumper system safety requirements stated above. However, the kinetic energy generated at a higher speed when the vehicle travels over 10km/h is greater than a bumper beam can process, such as 15km/h. It than post a problem to the bumper beam, where it is less capable to absorb all,

and it will require further energy absorption structure to engage. Crash box, in this case, will engage the impact process and provide additional deformation (EAA, 2013). Figure 7.3 and 7.4 and detailed the mechanical connection exists with the bolt method. Figure 7.3 further displayed the crash box end featured a plate allows bolt connection to the frame rail. This design maximises the flexibility to the bumper system during the crash repair.

7.1 Simulation preparation

To explore the effect to the force reaction and energy absorption after including the consideration of crash boxes and spot weld connection to the bumper beam system, the fold 2 bumper beam profile with curvature shape of 2400 mm was utilised as baseline bumper beam. Moreover, the difference of beam to crash box connection affect the crashworthiness performance to the bumper system was critically analysed. The crash box is assigned with the same material as a bumper beam, and 4 welding variants were proposed (Nakayama *et al*, 2004; Henrysson, 2001; Zhang *et al*, 2018).

Method 1: Bonded, contains no spot welds.
Method 2: Weld L+R, contains 4 spot welds, at both left and right.
Method 3: Weld full, contains 8 spot welds, at left, right, top, bottom.
Method 4: Weld T+B, contains 4 spot welds, at top and bottom.

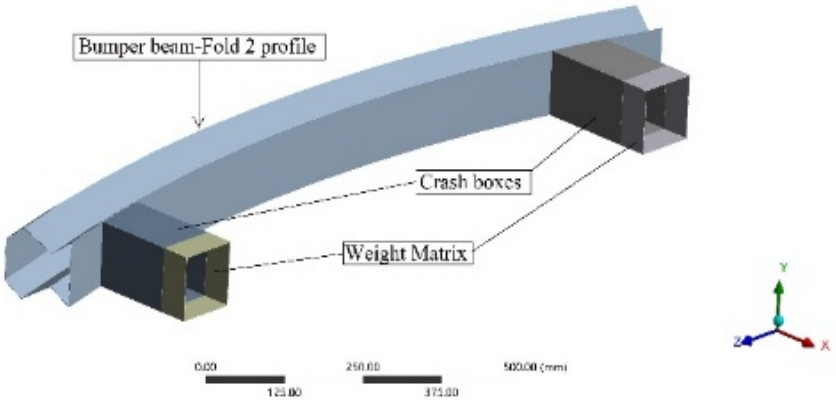

Figure 7.5 Simulation setup in explicit dynamics.

Figure 7.5 showed the bumper system set up in the FEA environment. It allowed the extraction of results to both force reaction and energy absorption generated by the beam and crash boxes. Further analysis was conducted to characterise the type of the connection method to contribute a positive effect to the crashworthiness performance. Specifically, the deformation process, the equivalent and normal stress, the equivalent strain rate at both crash box as well as the

connection surface were investigated thoroughly. Making use of the symmetry, only the left-hand side of the crash box will be displayed and analysed. The rigid impact wall, bumper beam and weight it carried were all hidden to provide a visible graph.

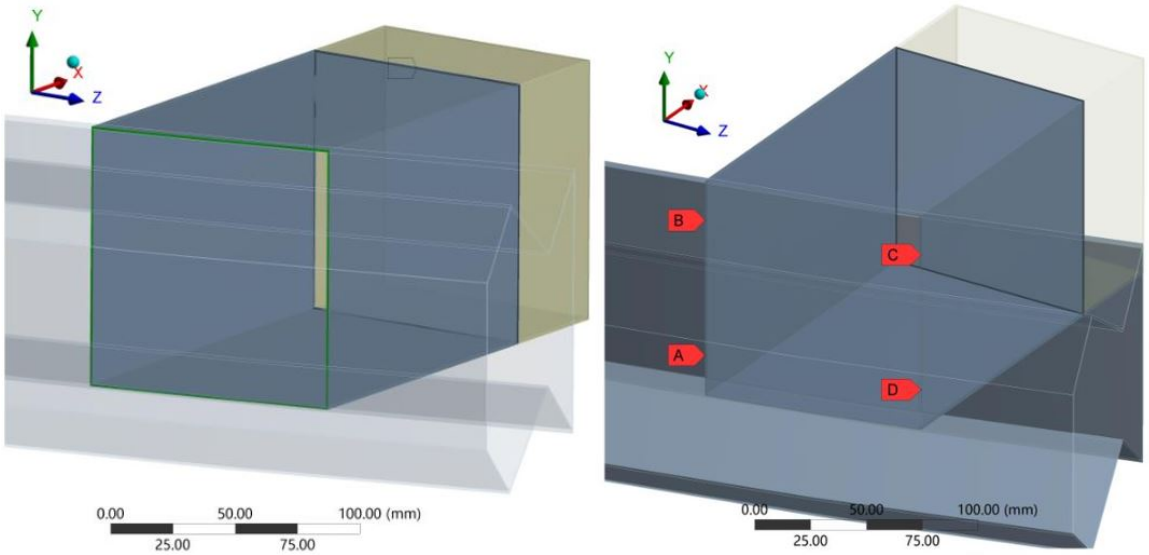

Figure 7.6 Connection method between bonded (Left) and welded L+R (Right)

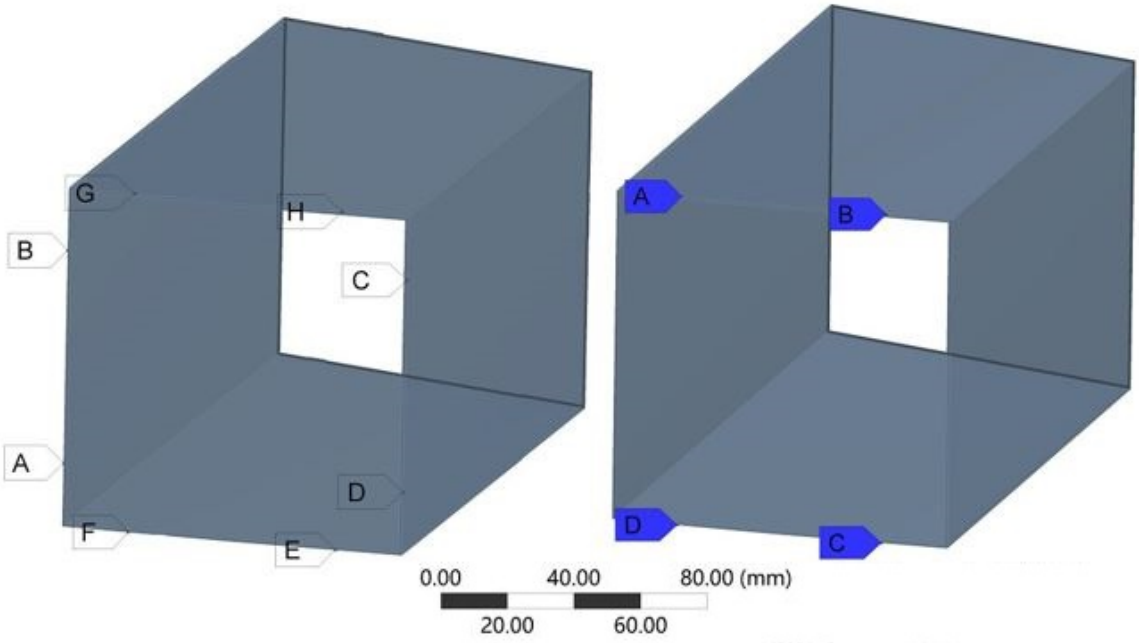

Figure 7.7 Connection method between welded full (Left) and welded T+B (Right)

Both Figures 7.6 and 7.7 demonstrated a clear difference between proposed welding variants. It is noted the bonded is still considered within this study to establish the baseline performance since most of the literature reviewed in chapter 1 either considered as integrated or ignored the details of the connection method (Wang, 2019; Liu *et al*, 2019;).

7.2 Force reaction and plastic work

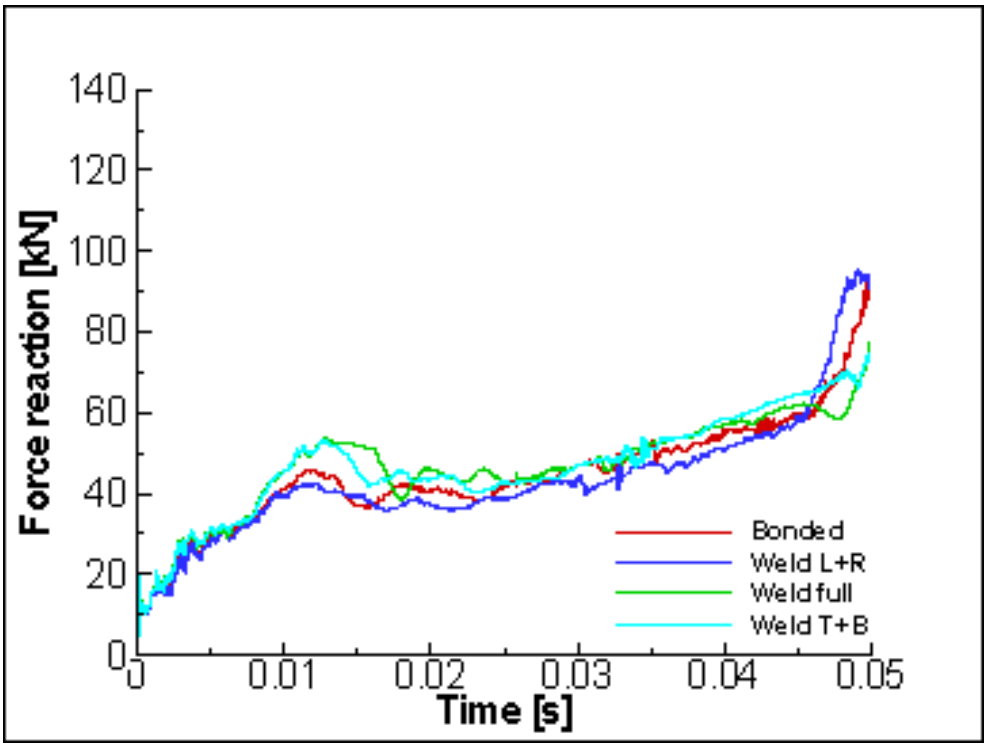

Figure 7.8 Connection effect to the Force reaction

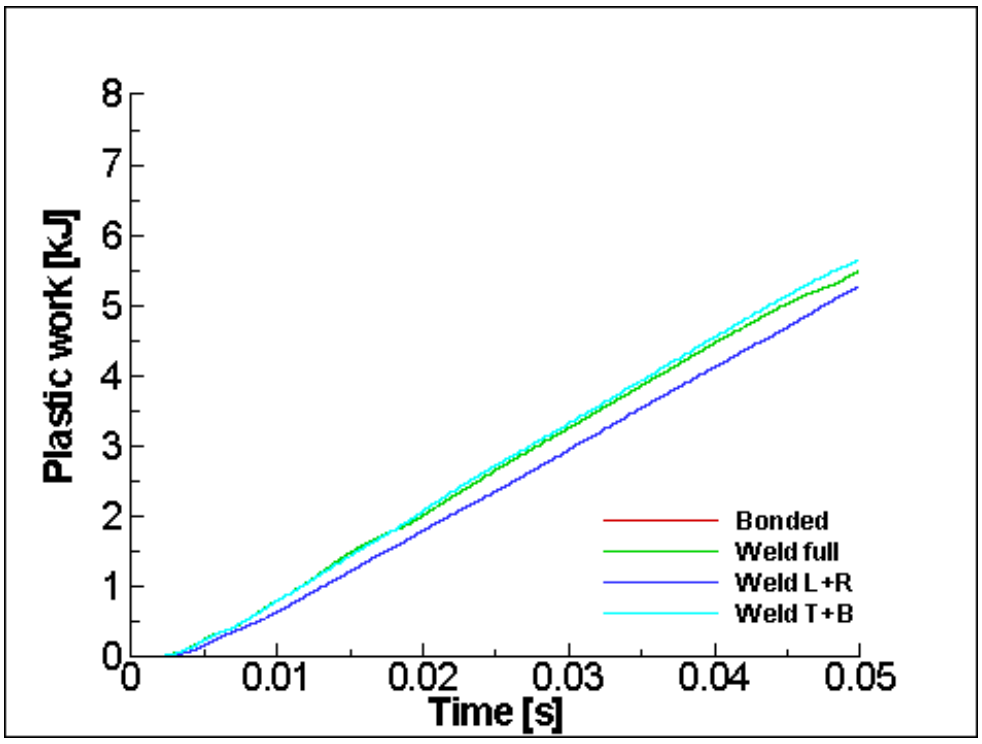

Figure 7.9 Connection effect to the Plastic work-beam

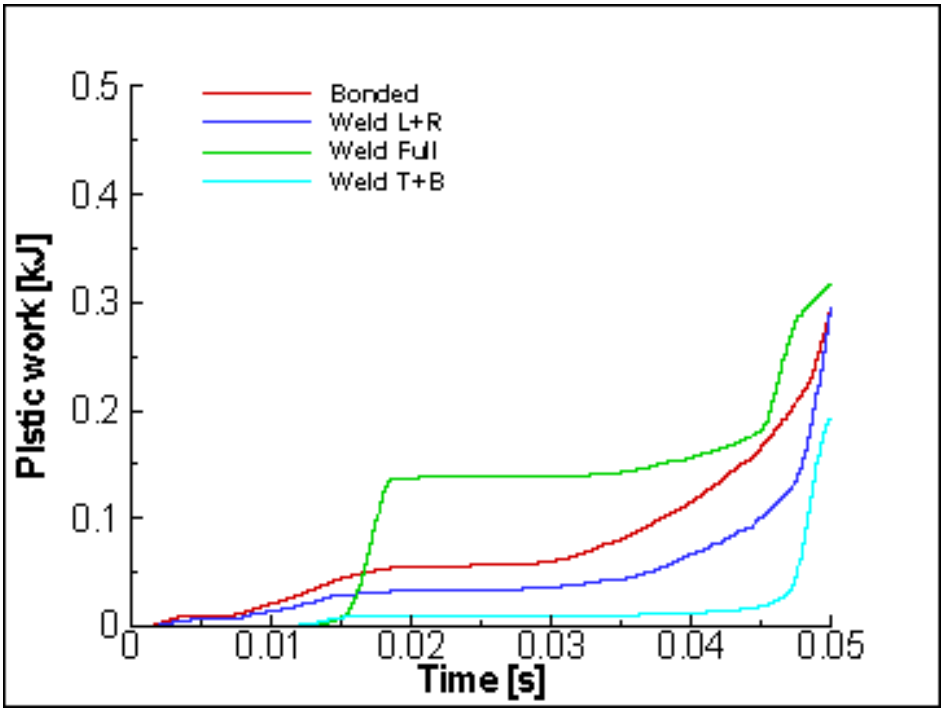

Figure 7.10 Connection effect to the plastic work-Crash box

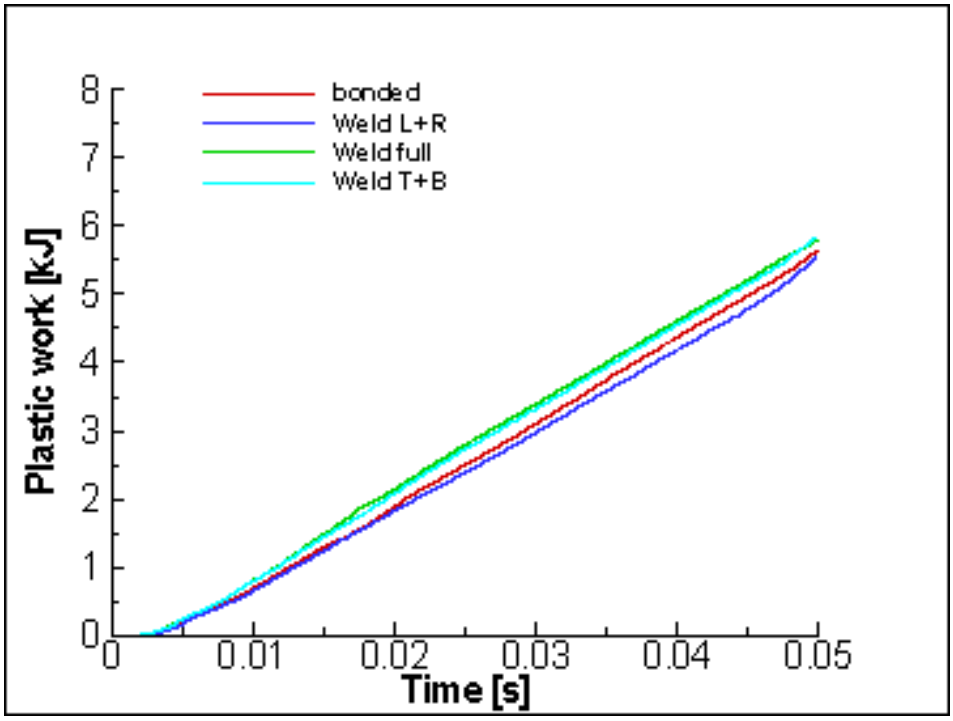

Figure 7.11 Connection method to the plastic work-Beam+CB

7.2.1 Force Reaction – Figure 7.8 showed the force reaction for all 4 connection methods. All connection methods showed relatively low initial peak force upon the impact and remained a similar increasing trend for the rest length of the simulation. Being the baseline of the performance, the bonded method showed an overall smooth force curve with an increasing trend. The welded L+R model shared an identical amount of force rate for the first 0.01 second

to the bonded model. It then carried forward with a very slight amount of decreased force rate to 0.04 seconds. It showed similar steep increases then the bonded method, but with a slightly higher rate after, and ended at the same level of bonded method. Full welded method generally exhibited an increasing force trend over most of the simulation time, with slightly higher force value for the first 0.045 seconds. It further increased its force, but not as significant as both bonded and Weld L+R cases, and ended at slightly lower force value. The welded T+B model generally maintained very similar force trend and value to the full weld method. Without any significant force fluctuation, it further increased its force value after 0.045 seconds and ended at a similar force value than the full weld method.

7.2.2 Plastic work – This chapter included the connection method effect of the crash box brought into the crashworthiness performance of a bumper system, the influence on the bumper beam was also included. The weld L+R method did not aid the bumper beam to achieve more plastic work then the bonded method has achieved for the first 0.02 seconds. But the absorption rate was lowered than the bonded case and maintained this low absorption rate throughout the simulation. While both full weld and weld T+B indeed helped the beam to yield more plastic work throughout the simulation, weld T+B appeared slightly more than the full weld method.

Figure 7.11 displayed the plastic work yielded by the crash box under 4 different connection methods. The bonded method yielded a smooth curve with a gradual increase for the first 0.04 seconds and carried further with a steep increase towards the end of the simulation. Weld L+R appeared in less absorption rate for the first 0.04 seconds. But as the crash box started to engage the deformation process after 0.04 seconds, it showed similar absorption rate compared to the bonded method and reached to the same maximum absorption value and towards to the end of the simulation. Full weld initiated with barely any absorption for the first 0.015 seconds. It then quickly increased to its energy absorption rate that was much higher than both bonded and weld L+R methods. It carried this rate steadily, and exhibited a further steep increase towards to the end of the simulation, and ended at a similar maximum absorption rate than both bonded and weld L+R. Weld T+B showed a minimum amount of energy absorption for the first 0.045 seconds which lower than any other 3 methods but also appeared in steep increase towards the end of the simulation (Trsko *et al*, 2019; Mao *et al*, 2020;).

Figure 7.11 gathered the total amount of energy absorption of the bumper system offered under 4 different connection methods. Despite weld L+R method was the basic connection method

that had 4 spot welds on the connection surface, it actually gained lower total energy absorption when compared with baseline bonded scenario. Both full weld and weld T+B were achieved generally an improvement. (Khan *et al*, 2019; Afshari *et al*, 2019;).

7.3 Equivalent stress

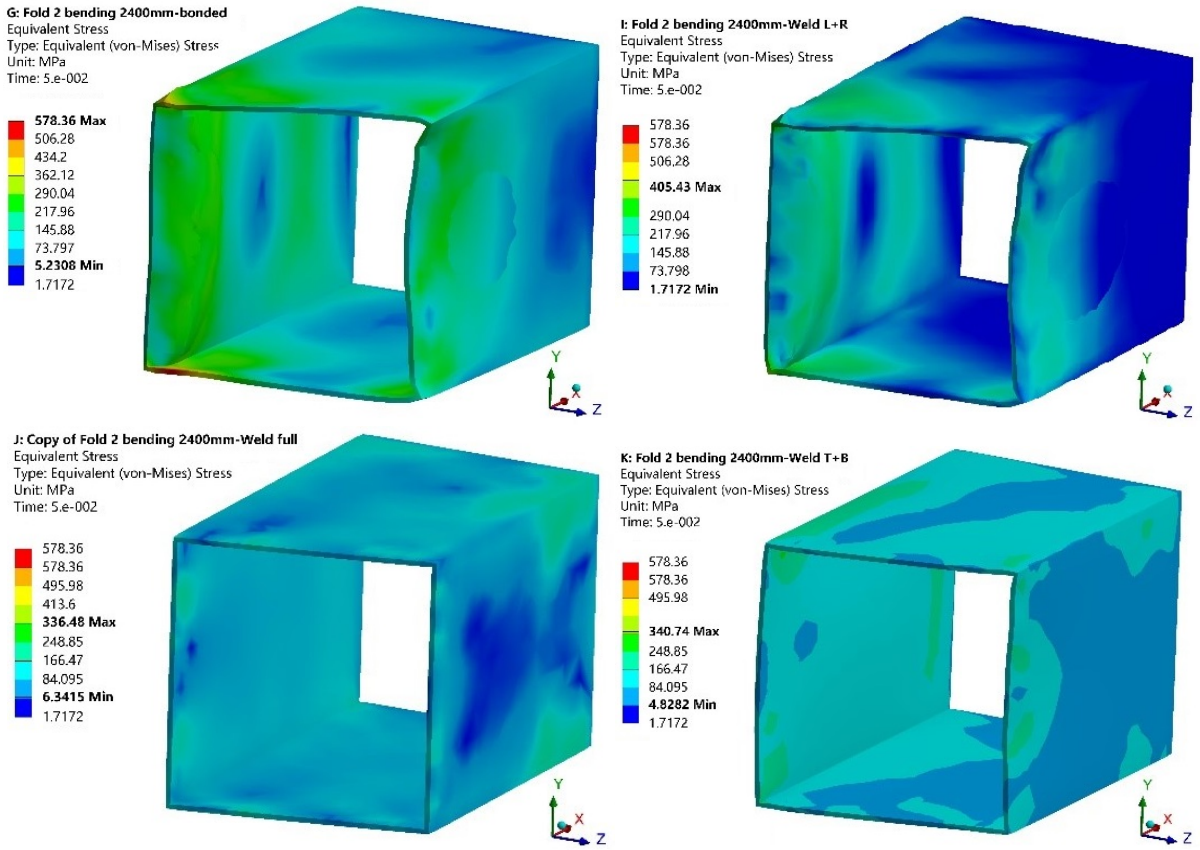

Figure7.12 Effect on to the equivalent stress of all connection method.
Top left: bonded, top right: Weld L+R, Bottom left Weld full, Bottom right: Weld T+B

Figure 7.12 revealed the equivalent stress distribution of all connection methods between the bumper beam and crash boxes. It represented structural failure criteria and displayed the stress distribution over its structure. It is noted the equivalent stress magnitude of all 4 connection methods were generally at decreasing trend. Because the connection is considered perfectly bonded without any movement, hence it sustained from the highest equivalent stress influence during the beam deformation. Particularly concentrated at the top left and bottom corner and reached to 578.36 MPa. All 4 faces on the crash box were also terribly buckled. The top right figure showed the equivalent stress distribution on the 4 spot welds method which the spot weld location was displayed at earlier Figure 7.3. It is observed adding the spot welds on both the left and right side of the crash box did not achieve a purpose of reducing its deformation as well as buckling, both left and right welding faces were still terribly buckled. This welding spot location, however, lowered the equivalent stress down to 405.43 MPa due to both top and

bottom faces were free to move without any constraints (Zeng *et al*, 2019; Cui *et al*, 2019; Zhong *et al*, 2019).

Considered the poor crashworthiness yielded by weld L+R method, a third connection method was proposed and demonstrated in the earlier figure 7.3. Adding the spot weld all around the crash box primarily resolved the problem where the equivalent stress concentration on the connection surface. Compared to bonded and weld L+R cases, the stress no longer concentrated at the connection surface but distributed more evenly on the crash box. As a result of this, both left and right crash box faces did not buckle where the deformation behaviour on the full weld case was very well regulated. And because of this, the stress level was also further lowered down to 336.48 MPa. Both bonded and weld L+R did not result in a good crashworthiness behaviour of the crash box since the crash box in both cases were started to buckle. The structural integrity of the crash box failed too early due to the buckling and will subject to catastrophic failure with reduced ability to further absorb the impact energy (Kowalski and Rozumek, 2019; Kowaski and Bohm, 2010)

Full weld crash box of been the third proposed connection Considered the deformation pattern between the cases of bonded and weld L+R, a fourth connection, where spot welds were added only to the top and bottom was proposed and tested. Immediately the overall deformation of the crash box was appropriate. Without suffering from significant buckling to the left and right side of the crash box faces, the structural integrity of the crash box was generally held well. Weld at top and bottom did not further lower the equivalent stress, where it yielded 340.74 MPa when compared to 336.48 MPa, though the difference is very little, and the equivalent stress distribution was maintained evenly.

7.4 Normal stress

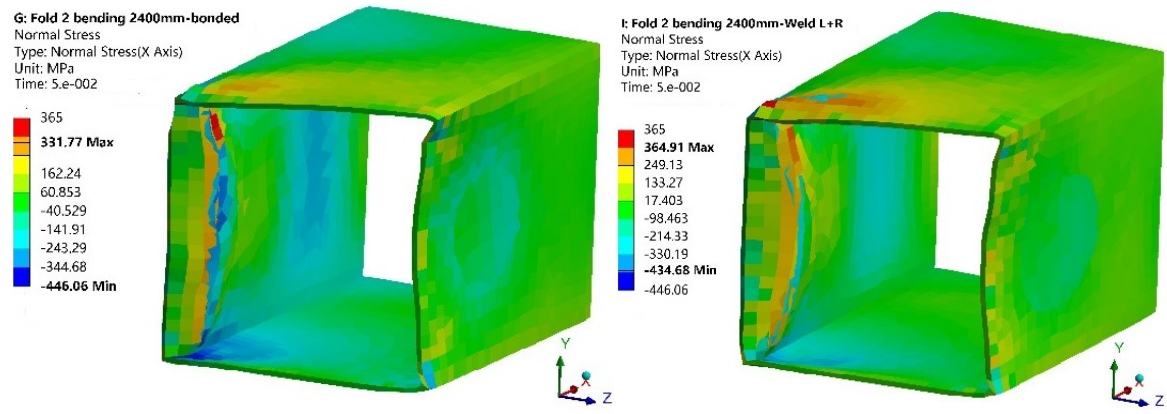

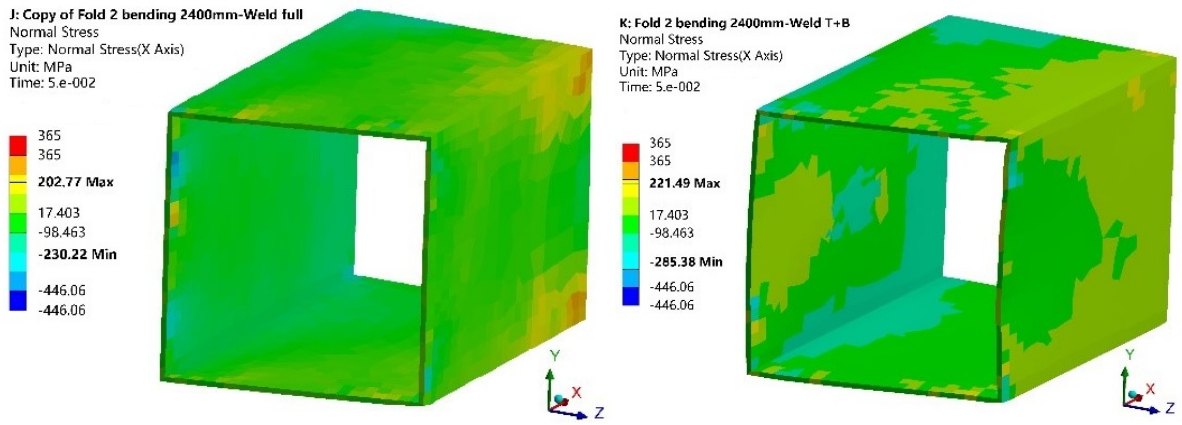

Figure 7.13 Normal stress distribution on the bonded method
Top left: bonded, top right: Weld L+R, Bottom left Weld full, Bottom right: Weld T+B

Figure 7.13 displayed the magnitude of normal stress and its distribution over the crash box in all 4 connection methods. The normal effect is calculated at the impact force occurred on the impact axis applied on the area of the surface that connected between the bumper beam and the crash box. The boned method yielded 331.77 MPa which was the highest magnitude over the other 3 methods. Because the bonded connection considered as perfect, hence the crash box also sustained the most structural deformation as well. Especially the stress was concentrated at both the left and right side of the crash box faces. A similar situation was repeated itself on the weld L+R, where the crash box was significantly damaged due to buckling effect. Fully weld yielded a maximum of 202.77 MPa over the connection surface. This value was much less than bonded and weld L+R methods by 129 MPa and 162.44 MPa each other individually.

Figure 7.13 also showed the normal stress level remained at the green colour range on the connection surface where higher magnitude was concentrated at the rear of the crash box. Both bonded and Weld L+R cases showed the normal stress was concentrated at the connection surface, particularly to both left and right faces of the crash box. Weld T+B method showed a slightly higher stress level which was 221 MPa than the full weld method, but still significantly less than the methods of bonded and weld L+R. Buckling was also appeared in both left and right faces of the crash box but found at a minimum level where the crash box integrity did not sacrifice dramatically.

7.5 Normal stress on the connection surface

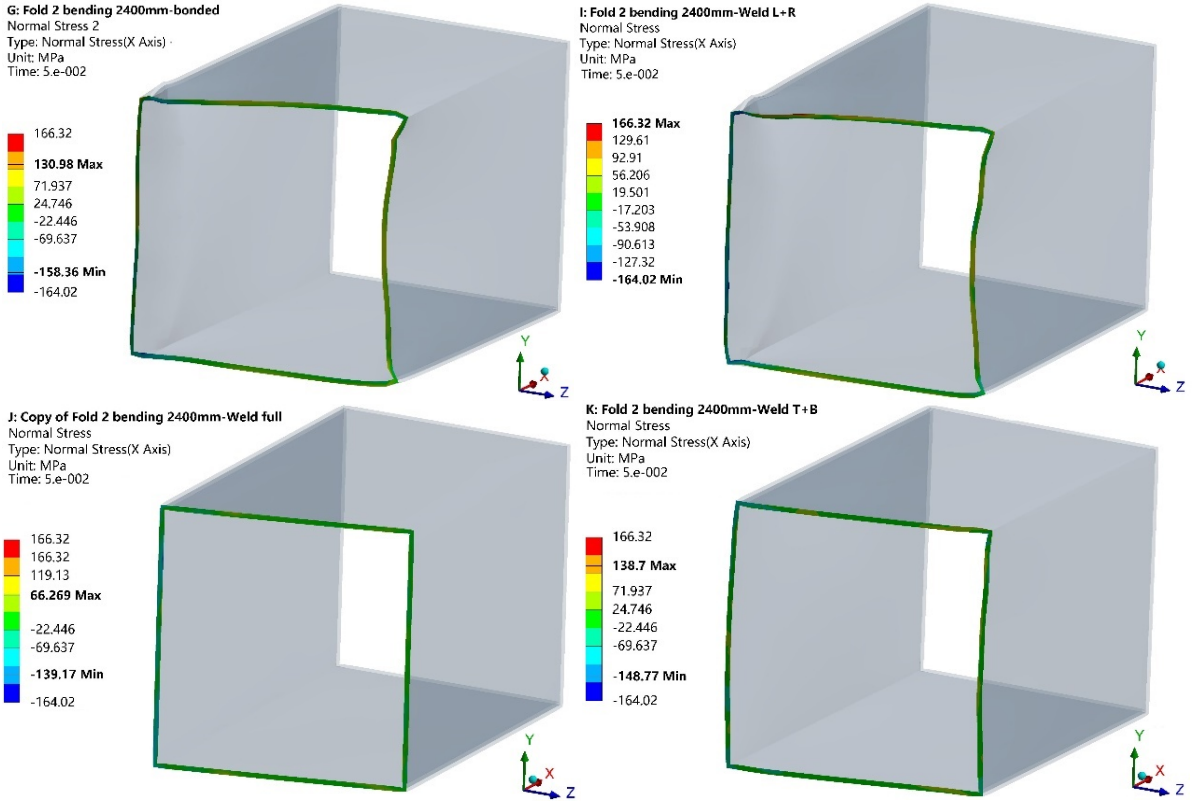

Figure 7.14 Normal stress distribution on the connection surface.

Figure 7.14 showed the normal stress distribution over the connection surface. It is clearly seen on the methods of both bonded and weld L+R, the stress level was quite high, at 130.98 MPa and 166.32 MPa each other individually. And the stress was concentrated at both top left and bottom right corners of the crash box, where left and right faces of the crash box in both cases were buckled inwards due to the influence from the bump beam deformation. The stress level and deformation on the crash box were largely improved over the full weld method, where 66 MPa of the stress level was much lower than both Bonded and weld L+R methods. Weld T+B method gained 138 MPa at its connection surface. Though its higher than both bonded and full welded methods, it's less than the weld L+R method yielded. It is clearly showed both the left and right side of the connection surface were slightly buckled than the full weld method, but once again significantly less than both bonded and weld L+R methods.

7.6 Equivalent plastic strain

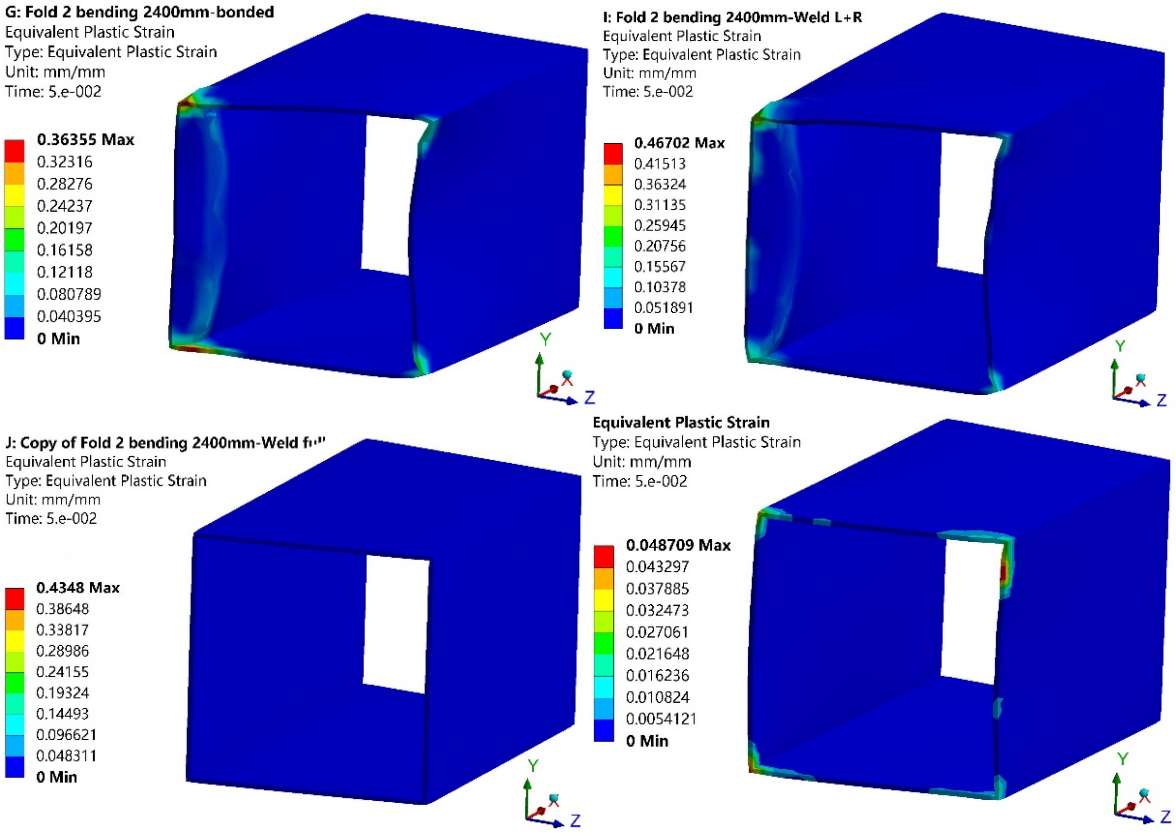

Figure 7.15 Equivalent plastic strain rate on all connection methods.

To further understand the deformation behaviour of the crash box, and also to prove its representative, an equivalent plastic strain was shown in Figure 7.15, where the strain rate of the plastic deformation experienced by the crash box was addressed in any colour except the blue. The higher of the deformation rate, the higher towards the red it represents. It is clearly showed a very similar pattern from both bonded and weld L+R methods. Most of the buckling occurred at both left and right faces, near the connection surface of the crash boxes as well as its four corners. In compared to this, full weld method achieved generally a minimum amount of deformation rate. It is worth to mention there was a certain level of plastic strain showed around all four corners of the crash box in the weld T+B method, but both left and right side faces of the crash box held at its integrity without significant buckling effect, or large plastic deformation occurred to the crash box when compared with both bonded and weld L+R methods.

7.7 Analysis and recommendations

Many works of literature were favoured of using the bonded method due to the simplified representation of connection between the bumper beam and crash box in the FEA simulation

environment. Although no use input was required for this type of boundary condition, this often led to non-representative simulation of the low-speed loading condition occurred to the bumper beam. The interaction between the bumper beam and the crash box was oversimplified. Bumper beam and crash box were considered critical during the low-speed impact. The suitable connection in between beam and crash box is equally important to their own design as discussed in earlier chapters.

The bumper beam can confidently process the impact energy up to the impact velocity of 8 km/h (EAA, 2013). While in the US scenario, the legal test requires no damage to any nearby safety-related components, and the test impact velocity is 8 km/h. A similar requirement was also emphasized in E.C.E regulation that is represented and enforced at most of the European countries, where the test speed was lowered to 4 km/h to the front, and 2.5 km/h at the rear. According to the literature review showed in chapters 1 and 2, the front bumper system impact test was conducted at various speed that is between as low as 8km/h, and as high as up to 15 km/h. Most research work not only focused on satisfying the legislations but also intended to achieve a higher standard to the overall crashworthiness performance (Milovanoivc *et al*, 2013).

Those investigations were focused on the geometrical detail of the bumper beam, the material used, but the detail to the crash box connection methods is absent. Instead, either bonded, or integrated connection type was used without any further explanation offered. It is logically assumed the results of both bumper beam and the crash box shall receive the equal attentions since both of them were included within the bumper system. Both shall be analysed and discussed, since the impact velocity of 15 km/h will certainly cause the deformation to the bumper beam, and most likely cause deformation to the crash box as well. As a matter a fact, bumper beam related results were very well explained and clarified, but the crash box related results analysis were often ignored, as well as the interaction to the crash box due to the connection in between. From this point of view, it became unclear what the outcome of those investigations was hardly convincing and less representative, especially the results displayed from 6.12 to 6.15, where the impact velocity of 15 km/h resulted in changes to the crashworthiness performance of the bumper system, and definitely some degree to the crash box. A particularly certain level of deformation to the crash box. (EAA, 2013; Hanji *et al*, 2019).

This chapter provided a more realistic level of results and revealed the interaction on the connection surface, and more importantly, illustrated the complete deformation of the crash box with the presence of spot welds. Figure 7.3 and 7.4 showed at earlier of this chapter indicated a common connection method between the bumper. But any higher speed than 8 km/h will inevitably introduce the crash box deformation in order to reduce the damage to the rest of the components.

7.7.1 Force reaction and plastic work – Figures 7.8, 7.9, 7.10 and 7.11 were represented the effect on to both force reaction and plastic work with varies proposed connection methods. It is observed adding 4 spot welds to the crash box connection did not improve the overall force reaction. The only benefit gain was increased force rate after 0.045 seconds, this means the crash box offered more deformation than the bonded method did. There was no significant difference before 0.045 seconds, where weld L+R gained lower force rate. This means the deformation of the crash box happened less. Both weld full and weld T+B have achieved slightly, but higher force rate throughout the simulation. This means, both those methods offered more deformation to the bumper system, and smooth increase curve indicated the force was registered at a constant level.

And because of this improved force reaction, weld full and weld T+B aided their bumper beam to absorb more energy than both bonded and weld L+R method can achieve. As for the plastic work of the crash box, weld full method did not just yield more energy as simulation progress further but also reached to higher maximum absorption than both bonded and weld L+R gained. Weld T+B this time showed reduced plastic work for the first 0.04 seconds, where it is started to climb higher after 0.045 seconds. Despite this fact, weld T+B aided the bumper beam to achieve higher energy absorption. This was particularly useful when the vehicle is subjected to crash repair, where there will be little deformation to the crash box, and more impact energy is consumed by the bumper beam. Once again both weld full and weld T+B achieved higher plastic work than bonded and weld L+R methods. This indicated the location of weld L+R provided did not aid either beam and crash box for more plastic work, which is no different than the bonded method. When adding totally 8 spot weld offered by Weld full method indeed aided both beam and crash box to increase their plastic work. This means more impact energy is consumed at the bumper system, and less residue energy is passed to the rest of the car.

7.7.2 Stress and strain – Equivalent stress showed both its rate and distribution over the crash box. Weld L+R that contains 4 spot welds on left and right faces did not help to prevent the deformation of the crash box, where allowed deformation occurred on the crash box, where both left and right faces were buckled. Weld L+R also gained similar stress level to the bonded method and concentrated at the bucked faces as well. This means left and right faces of the crash box are less ideal to add the spot welds. The crash box deformation was virtually eliminated when welds are presented around the crash box, where equivalent stress is reduced, and no buckling effect to the crash box. Adding the spot welds to top and bottom offered by weld T+B was found as effective as weld full. Both left and right side faces were still buckled, but better regulated than both bonded and weld L+R methods. The normal stress results also pointed the same direction, where due to the left and right face was buckled, the stress is concentrated on to those areas presented by bonded and weld L+R methods. While full weld received the lowest normal stress of 202.77 MPa, stress is concentrated at both left and right faces in weld T+B method, at much less scale and also a health low of 221.49 MPa stress yielded. Both normal stress and equivalent plastic strain were pointed to the position of the spot welds (EAA, 2013; Tounsi *et al*, 2019; Kwansoo *et al*, 2017).

Recommendations – It became clear that bonded method, as widely used in many pieces of literature actually performed badly during the test results and analysis demonstrated in the early chapters. This was often ignored by that literature and suggested the bumper system made improvements. Methods 2, 3 and 4 proved the position of the spot weld effect to force reaction and plastic work, but also the deformation of the crash box. It is ideal where the only bumper beam is subjected to deformation without further needing the crash box, this will ultimately reduce the costs during the vehicle repair, hence directly benefits both vehicle owner and its insurer. In this case, method 3, which proposed spot welds all around the crash box virtually reduced any buckling effect to the crash box. However, leave the spot welds on the top and bottom of the crash box instead of left and right incur a small degree of buckling, still, a significant improvement over either bonded or welds at left and right. This also reduced both equivalent and normal stress dramatically as well (John and Nidhi 2014; Sharpe 2001)

Chapter 8 Conclusions

8.1 Summary of findings

This thesis aimed to identify and investigate that the parameters would affect the crashworthiness of the vehicle front bumper system using numerical methods. A basic review to the current vehicle front bumper system was conducted. Some important parameters were identified which potentially can improve the crashworthiness to the bumper system. These parameters included the physical dimensions and exterior characteristics, the material used and the connection method between the bumper beam to its crash boxes.

From the post-impact results showed in chapters 3, 4 and 5, the force reaction is the parameter which reflected how well does the bumper beam engage with the rigid wall during the impact process. Specifically, the initial peak force (IPF), represents the deformation of the bumper beam upon the initial impact where this value should be as low as possible. Meanwhile, the overall force reaction throughout the simulation should the as smooth increases ideally after the IPF moment.

The plastic work represented the amount of impact energy absorbed during the impact process. Particularly both crush force efficiency (CFE) and specific energy absorption (SEA) were evaluated the effectiveness of energy absorption to the bumper beam at the given weight, cross-section profile and curvature shape. In addition to both parameters mentioned above, the connection method between the bumper beam to its crash box was also considered as a critical parameter and therefore investigated based on the location and number of the welds. Both equivalent stress and normal stress distribution informed the deformation of the crash box, and the equivalent plastic strain verifies the rate.

During the optimisation process to increase the crashworthiness to the current bumper system design, an alternative bumper beam carried the exterior characterises of cross-section profile, curvature shape, material types and thickness are created into numbers of samples and simulated accordingly. On top of this, the connection method was also addressed as a spot weld, and both numbers and locations of the spot welds were proposed at numbers of samples and simulated accordingly.

Since the possibilities of an individual component from the bumper system are subject to parameter changes, this created many potential combinations of bumper system assemblies with those components, which will need to be simulated and analysed. This research project included all the test results and analysis for all assemblies. Consequently, this incurred a significant amount of simulated data but also created a full picture and knowledge of which assemblies performed well, and other assemblies performed poorly. This gave the opportunity for this research project to determine the suitability of the specific bumper system for a specific condition.

8.2 Influence from of different parameters

1. Cross-section profile aided the impact process by providing stable deformation. It achieved smooth force reaction curves at some simulated samples via consistent beam compression to its collapse mode. This directly reflected as gradual increases in the force reaction curve. In structural steel bumper beam, cross-section profile found particularly effective to profile: fold 3 when the beam is at straight (without any curvature radius). This benefit reappeared again when later the beam material was replaced with aluminium, where multiple folds design improved the deformation process.

2. Curvature shapes found very effective to maintain a low initial peak force(IPF) on any given shapes regardless of structural steel or aluminium alloy. In the case of the straight beam (without curvature radius), it means the beam did not deform effectively and obtained IPF value as high as 300 kN in both structural steel and aluminium materials. Immediate IPF reduction was achieved as soon as the curvature radius was introduced. Where IPF decreased from almost 350 kN down to less than 90 kN. Aluminium bumper beam achieved even higher reduction, which was down to less than 50 kN.

3. Switched from structural steel to aluminium saved significant amount of weight carried on the bumper system, from 12.74 kg down to 4.49 kg with fold 1 profile, 15.18 kg down to 5.3 kg with fold 2 profile, and 17.61 kg down to 6.22 kg with fold 3 profile.

4. Both number and location of the spot welds found effective to eliminate the deformation to the crash box itself, as well as reducing the buckling effect on both the left and right face of the crash box. Weld L+R method carried 4 spot welds appeared less effective

compared to simply bonded method. Compared to this, Weld full method which featured at addition 4 more spot welds found highly effective in eliminating both deformation and buckling effect to the crash box when compared with weld L+R method. This means less equivalent stress and normal stress distributed on the crash box. As a result, the crash box will sustain little to no damage to the likelihood of the crash event. This will ultimately reduce the amount of repair work conducted on the vehicle and most likely protect more valuable nearby components.

8.3 Future work

High-speed scenario-The impact velocity used in this research work is mostly focused on low speed. Common impact velocity selected to conduct the vehicle front bumper beam test were scattered vastly, such as 2.5km/h and 4km/h used by Institute and Insurance of highway safety agency. Others than select the speed up to 10km/h (Marzbanrad *et al*, 2009; E.C.E, 1994; Hoseeinzadeh *et al*, 2005; Xiao *et al*, 2015). This research tend to agree with the argument provided by other studies (Belingardi *et al*, 2013; Belingardi *et al*, 2014; EEA, 2013; Davoodi *et al*, 2011), where the bumper beam system, particularly to the bumper beam itself should sufficiently process the impact load at a maximum impact velocity up to 15km/h. Yet this was the velocity was selected to conduct this research work was higher than the velocity appeared in most of the other literature. Nevertheless, the vehicle is repairable up to the impact velocity of 30km/h, provided both bumper beam and crash box are correctly designed and manufactured. This means the same system can be further refined to mitigate any impact velocity up to 30km/h (EEA, 2013).

Crash dummy and Passengers- The current work is carried out at step-by-step optimisation. This means each individual component contributed to the entire bumper system to achieve higher crashworthiness, but it is unknown how effective to increase the safety to its occupants as well as the interaction with any other passive safety equipment. Parameters such as the reaction of head, chest and leg injury rate to the occupants, deployment of airbag and seatbelts are all added to the complexity. It is highly desirable if the crashworthiness optimisation conducted with the consideration of how vehicle crashworthiness benefits its occupants, as well as the interaction between the occupant restraint system and occupant itself.

Costs related-This thesis covered both metallic and composite materials, despite the tested

crashworthiness results are less desirable than the metallic alternatives, composite indeed showed certain advantages, such as lightweight, specific stiffness to the name of few. However, due to the nature of the material, production technical difficulties and costs, large scale implementations and production were never made available to the vast majorities within the automotive market. The use of the composite material, particularly to carbon fibre is a symbol of luxury and therefore only appeared in the high-end market (Technologyreview, 2015). Other industrial areas have also investigated this issue, such as marine, aviation and space. The current usage of composite material is limited to high-end product, but with continuous research and development, it would be very interesting if the relationship between the cost and production of the composite material usage is further discussed and evaluated.

8.4 Caveat

This research project has achieved a certain level of improvements to the vehicle crashworthiness after the use of FEA simulations and analysis. This certainly proved the FEA simulation tool is a convenience to users. However, this research project still wanted to contribute that the FEA remained a very useful tool to test the prototype and concept product during the development process. Meanwhile, if the product development has progressed further to the mass production stage, a physical impact test shall still be performed to evaluate a real-world scenario performance since the FEA can provide the convenience but cannot completely replace the physical impact test.

References

Afshari D., Mirzaahamdi S. and Barsoum Z. (2019). Residual stresses in resistance spot welded AZ61Mg Alloy, *Computer modelling in engineering and sciences*, 118(2), 275-290. https://doi.org/10.31614/cmes.2019.03880

Attia M. S., Meguid S. A. and Nouraei H. (2012). Nonlinear finite element analysis of the crush behaviour of functional graded foam-filled columns, *Finite elements in analysis and design*, 61, 50-59. https://doi.org/10.1016/j.finel.2012.06.004

Alghamdi A. A. A. (2002). Reinversion of aluminium frusta, *Thin-wall structures*, 40(12), 1037-1049. https://doi.org/10.1016/s0263-8231(02)00041-1

Amir R.A., Ghani M.A. and Hassan M. A. (2013). Axial crush behaviour of a square column with external tapered plunger. *Journal of engineering sciences*, Assiut University, Faculty of Engineering. 41, 4

ANSYS Inc. (2016). Introduction to ANSYS explicit Dynamics, Release 17.0.

Aluminium Automotive Manual (2013). Applications-car body-Crash management systems. The aluminium automotive manual. European-aluminium. *European aluminium Association*.

Ashby M. F. and Cebon D. (1993). Material selection in mechanical design*, The 3rd European conference on advanced materials and processes,* C7-1-C7-9. https://doi.org/10.1051/jp4:1993701

Ashby M. F. (2000). Material Selection in Material Selection in Mechanical Design. Second edition, Oxford: Butterworth Heinemann, ISBN: 0-7506-4357-9

Automobile-catalog (2010). 1958 Ford Taunus 15M (Man. 3) car specifications & performance data review.
https://www.automobile-catalog.com/car/1958/899000/ford_taunus_15m.html

Banhart J. (2001). Manufacture, characterisation and application of cellular metals and metal foams. *Progress in material science*, 46(6), 559-632.
https://doi.org/10.1016/S0079-6425(00)00002-5

Barthelemy J-F. M and Haftka R. T. (1993). Approximation concepts for optimum structural design-A review, *Structural optimisation*, 5(3), 129-144.
https://doi.org/10.1007/BF01743349

Baccouche R., Mahmood H., Madasamy C. and Wagner D. (2007). Ford global technologies LLC, Lightweight bumper for automobiles, US7210717B1.

Berlingardi G., Beyene A. T. and Koricho E. G. (2013). Geometrical optimization of bumper beam profile made of pultruded composite by numerical simulation, *Composite structure*, 102: 217-225.

Belingardi G., Beyene A. T., Koricho E. G., Martorana B. (2014). Crashworthiness of integrated crash-box and beam made of die forming composite, Seville, Spain, 22-26,

Beyene A. T., Koricho E. G., Belingardi G. and Martorana B. (2014). Design and manufacturing issues in the development of lightweight solution for a vehicle frontal bumper, *Procedia Engineering*, 88: 77-84.

Belingardi G., Beyene A. T. and Martorana B. (2015). Alternative lightweight materials and component manufacturing technologies for vehicle frontal bumper beam, *Composite structures*, 120, 483-495.
https://doi.org/10.1016/j.compstruct.2014.10.007

Bezreh A. A. (1963). Helicopter versus fixed-wing crash injuries, *Aerospace medicine*, 34(1), 11-14.

Beecroft, D. (1924). Bumper Development. Automobile trade journal. Vol:29(6), 301, Chilton Company, U.S.A.
https://books.google.co.uk/books?id=gz5LAAAAMAAJ&pg=PA301&lpg=PA301&dq=Bumpers+appeared+on+cars+as+early+1904+their+function+was+chiefly+ornamental&redir_esc=y#v=onepage&q=Bumpers%20appeared%20on%20cars%20as%20early%201904%20their%20function%20was%20chiefly%20ornamental&f=false

Busch J. (2000). Composite technologies: an overview of business potentials, white working paper, IBIS Associates, Inc, Wellesley: MA.

Brain C. T. (2011). Impact speed and a pedestrian's risk of severe injury or death, *AAA foundation for traffic safety*, Washington, DC 20005.
https://nacto.org/wp-content/uploads/2012/06/Tefft-B.C.-2011.pdf

Coltman J. W., Van I. C. and Smith K. (1986). Crashworthy crewseat limit load optimisation through dynamic testing, Crashworthy design of Rotorcraft, Atlanta: Georgia Institute of technology canter of excellence for rotary-wing air-craft technology.

Carnell B. L. (1978). Crash survivability of the UH-60A helicopter, Operational helicopter aviation medicine, Neuilly-sur-seine, France: AGARD CP255, 1978,64-1 to 64-10
https://web.archive.org/web/20110927084512/http://www.combatindex.com/mil_docs/pdf/std/1200/MIL-STD-1290A.pdf

Charoenphan S, Bank L. C. and Plesha M. E. (2004). Progressive tearing failure in pultruded composite material tubes, *Composite structures*, 63:45-52

Carper C. H. (1983). Aircraft survivability, *Journal of United States military*, Revision 64, 64-74.

Chen, W., Wierzbicki, T. and Santosa, S. (2002). Bending collapse of thin-walled beams with ultralight filler: Numerical simulation and weight optimization, *Acta Mechanica*, 153(3-4), 183-206.
https://doi.org/10.1007/BF01177451

Craig K. J., Stander N., Dooge D. A. and Varadappa S. (2005). Automotive crashworthiness design using response surface-based variable screening and optimisation. *Engineering Computations*, Swansea, Wales, 22(1), 38-61

Cui X. T. Wang S. X. and Hu S. J (2008). A method for optimal design of automotive body assembly using multi-material construction, *Materials & Design*, 29(2), 381-387. https://doi.org/10.1016/j.matdes.2007.01.024

Cetin O. L. and Saitou K. (2005). Decomposition-based assembly synthesis of multiple structures for aluminium manufacturing cost, Journal of Mechanical Design, *Transaction of the ASME*, 27(4), 572-579

Carle D. and Blount G. (1999). The stability of aluminium as an alternative material for car bodies, *Materials & Design*, 20(5), 27-272. https://doi.org/10.1016/S0261-3069(99)00003-5

Costas, M., Diaz, J., Romera, L. and Hernandez, S. (2014). A Multi-Objective Surrogate-based Optimisation of the Crashworthiness of a Hybrid Impact Absorber. *International Journal of Mechanical Sciences*. 88, 46-54 https://doi.org/10.1016/j.ijmecsci.2014.07.002

Cook R. D., Mikus D. S., Plesha M. E. and Witt R. J. (2002). Concepts and applications of finite element analysis, Fourth Edition, John Wiley& Sons, Inc. ISBN:0471356050

Cheon S. S., Lee D. G. and Jeong K. S. (1997). Composite side-door impact beams for passenger cars. *Composite structures*, 38(1-4), 229-239 https://doi.org/10.1016/S0263-8223(97)00058-5

Courant R., Friedrichs K. and Levy H. (1967). On the partial differential equations of mathematical physics, *IBM Journal*, March 1967, 215-234. https://doi.org/10.1147/rd.112.0215

Charoenphan S., Bank L. C. and Plesha M. E. (2004). Progressive tearing failure in pultruded composite material. *Composites structures*, 63, 45-52 https://doi.org/10.1016/S0263-8223(03)00130-2

Cui X., Zhang H., Wang S., Zhang L. and Ko J. (2011). Design of lightweight multi-material automotive bodies using new material performance indices of thin-walled beams for the material selection with crashworthiness consideration. *Material and Design*, 32, 815-821. https://doi.org/10.1016/j.matdes.2010.07.018

Cui C., Zhang Q., Bao Y., Han S. H. and Bu Y. Z. (2019). Residual stress relaxation at innovative both side welded rib-to-deck joints under cyclic loading, 156. https://doi.org/10.1016/j.jcsr.2019.01.017

Davoodi M. M., Sapuan S. M., Ahmad D., Aidy K. A. and Jonoobi M. (2011). Concept selection of car bumper beam with developed hybrid bio-composite material, *Materials and design*,32(10), 4857-4865

Dehaven H. (1969). Beginning of crash injury research*, Proceedings of the 13th Stapp car crash conference*, Detroit: Society of automotive engineers,

Davis D. (2010). The evolution of bumpers, *The Herald palladium*, http://heraldpalladium.com/articles/2010/11/21/features/2486294.txt.

Deb K. and Jain S. (2003). Multi-based gearbox design using multi-objective evolutionary algorithms*, Journal of Mechanical Design*, Transaction of the ASME, 125(3), 609-619. https://doi.org/10.1115/1.1596242

Das S., Curless R. and Schexnayder S. (2003). Materials used in new generation vehicles: Supplies, shifts and supporting infrastructure,

Das S. (2001). The cost of automotive polymer composites: A review and assessment of DOE'S lightweight materials composites research, Energy division, *oak ridge national laboratory*, https://doi.org/10.2172/777656

Dvoodi M.M., Sapuan S.M., Ahmad D., Aidy A., Khalina A. and Jonoobi M. (2011). Concept selection of car bumper beam with developed hybrid bio-composite material. *Materials and Design*, 32, 4857-4865.
https://doi.org/10.1016/j.matdes.2011.06.011

Duarte I., Vesenjack M. and Krstulovic-Opara L. (2014). Dynamic and quasi-static bending behaviour of thin-walled aluminium tubes filled with aluminium foam, *Composites structures*, 109, 48-56.
https://doi.org/10.1016/j.compstruct.2013.10.040

EPC. (Teradyne diagnostic, 2010). Electronic part catalogue, Teradyne diagnostic, USA, Tradyne diagnostic solutions.

E.C.E. (Economic Commission for European of the United Nations). ((1980). Uniform provisions concerning the approval of vehicles with regards to their front and rear protective devices (Bumpers, etc.). *Concerning the adoption of uniform conditions of approval and reciprocal recognition of approval for motor vehicle equipment and parts. Regulation No.42. Addendum 41*, E/ECE/324, E/ECE/TRANS/505. Rev.1

E. A. A. (European Aluminium Association). (2013). Engine compartment with fully braced aluminium engine cradle. Body Components. *The Aluminium Automotive Manual*, 11.

E.C.E (1994). United Nations Agreement, Uniform provisions concerning the approval of vehicles with regards to their front and rear protective devices (bumpers, etc.), Chapter XI, road traffic B, 16.42.
https://treaties.un.org/

Evancho J. W. and Kaufman J. G. (1977). New 6XXX-series alloys for auto body sheet, *1977 international automotive engineering congress and exposition,*
https://doi.org/10.4271/770307

Feng Z. S. and Feng S. Q. (2002). Research of CA1092 automotive body lightening, *Journal of automobile technology material*, 58(62), 8-9.

Fang J. G., Gao Y. K., Sun G.Y, Zheng G. and Li Q. (2015). Dynamic crashing behaviour of new extrudable multi-cell tubes with a functionally graded thickness. *International journal of mechanical sciences*, 103, 63-73.
https://doi.org/10.1016/j.ijmecsci.2015.08.029

Farkaz L., Moens D., and Vandepitte D. and Desmet W. (2008). Application of fuzzy numerical techniques for product performance analysis in the conceptual and preliminary design stage, *computers & structures*, 86(10), 1061-1079.
https://doi.org/10.1016/j.compstruc.2007.07.012

Farkas L., Moens D., Donders S. and Vandepitte D. (2012). An optimisation study of a vehicle bumper subsystem with fuzzy parameters. *Mechanical systems and signal processing*, 32, 59-68.
https://doi.org/10.1016/j.ymssp.2011.11.014
George G. (1922). Minimum weight analysis of compression structures, *Interscience publications*, New York, NY.

Gupta N. and Ricci W. (2006). Comparison of compressive properties of layered syntactic foams having gradient in micro balloon volume fraction and wall thickness, *Materials science and Engineering*: A, 427(1-2), 331-342.
https://doi.org/10.1016/j.msea.2006.04.078

Gupta N. (2007). A functionally graded synaptic foam material for high energy absorption under compression, *Materials letters*, 61(4-5). 979-982.
https://doi.org/10.1016/j.matlet.2006.06.033

Guo L. W. and Yu J. L. (2011). Dynamic bending response of double cylindrical tubes filled with aluminium foam, *International journal of impact engineering*, 38(2-3), 85-94.
https://doi.org/10.1016/j.ijimpeng.2010.10.004

Han H. N. and Clark J. P. (1995). Lifetime costing of the body-in-white: steel VS aluminium. Journal of mechanical, 47(5), 22-8.

Hanssen A. G., Lorenzi L., Berger K. K., Hopperstad O. S. and Langseth M. (2000). A demonstrator bumper system based on aluminium foam filled crash boxes, *International journal of crashworthiness*, 5 (4), 381-392.

Hassan M. A., Amir R. A., Taha Z. and Hamdi M. A. (2013). Mechanics of energy absorption by progressive plastic deformation of a square column with an ellipsoidal bulge base, *International journal of applied mathematics& information sciences*, 9(1L), 51-58, http://dx.doi.org/10.12785/amis/091L06

Hu D. Y., Meng K. P. and Yang Z. Y. (2014). Numerical investigation of the energy absorption characteristics of a fan-shaped deployable energy absorber, *International journal of crashworthiness*, 19, 126-38.

Hu D. Y., Zhang C., Ma X. B. and Song B. (2016). Effect of fibre orientation on energy absorption characteristics of glass cloth/epoxy composite tubes under axial quasi-static and impact crushing condition, *Composite part A: Applied science and manufacturing*, 90, 489-501.

Hu D.Y., Meng, Song B, Wang D. F. and Chen Z. Y. (2016). Experiment and numerical simulation of a full-scale helicopter composite cockpit structure subject to a bird strike. *Composite Structure*, 149, 385-97.

Haley J. L. Jr. (1971). Analysis of U.S. Army helicopter accidents to define impact injury problems, Linear acceleration of the impact type, Neuilly-sur-seine, France: AGARD CP, 88-71, 9-1 to 9-12.

Haley J. L. Jr. and Hicks J. E. Jr. (1975). Crashworthiness versus cost: *A study of army rotary-wing aircraft accidents in period Jan 1970 through Dec 1971*, Aircraft crashworthiness Saczalski K., et al. (eds.), Charlottesville, VA, University Press of Virginia.

Hicks L. E., Adams B. A. and Shanahan D. F. (1982). Analysis of U. S. Army mishap patterns, Impact injury caused by linear acceleration, *Mechanism, prevention and cost*, Neuilly-sur-seine, France, AGARD CP 322, 1982, 34-1 to 34-12
https://doi.org/10.1533/cars.2000.0149

Henrysson H. F. (2001). Fatigue life predictions of spot welds using coarse FE meshes, *Fatigue & fracture of engineering materials & structures* 23(9), 737-746
https://doi.org/10.1046/j.1460-2695.2000.00338.x

Hanji T., Tateishi K., Shimizu M., Uchida D., Asano K. and Kimura R. (2019). Fatigue strength of cruciform joints and longitudinal joints with laser0arc hybrid welding, *Welding in the world*, le soudage dans le monde, 63(3), 1-12
https://doi.org/10.1007/s40194-019-00745-w

Han H. H. and Clark J. P. (1995). Lifetime costing of the body-in-white: steel VS. aluminium, *Journal of mechanical*, 47(5), 22-28.
https://doi.org/10.1007/BF03221171

Hashimoto N., Eguchi N. and Imamura Y. (2007). Trends in development of aluminium alloy extrusion products for improved vehicle energy absorption, *Kobelco technology review*,28.
https://www.kobelco.co.jp/english/ktr/pdf/ktr_28/039-043.pdf

Hirsch J. R. (1997). Aluminium Alloys for automotive application, *Materials science forum*, 242, 33-50.
https://doi.org/10.4028/www.scientific.net/MSF.242.33

Hirsch J. R. (2004). Automotive trends in Aluminium- The European perspective, *Material Forum*, 28(1), 15.

Hirsch J. R. (2011). Aluminium in innovative light-weight car design. *Materials transactions,*52(5), 818-824.
https://doi.org/10.2320/matertrans.L-MZ201132

Hu Y. F., Liu C., Zhang J. G., Ding G. P. and Wu Q. (2015). Research on carbon fibre-reinforced plastic bumper beam subjected to low-velocity frontal impact. *Advances in mechanical engineering*, 7(6), 1-15.
https://doi.org/10.1177/1687814015589458

IIHS (Insurance institute for highway safety). (2016). Status report, *Insurance institute for highway safety*, Vol:51(4).
https://www.iihs.org/api/datastoredocument/status-report/pdf/51/4

Jambo A. and Beyer M. (1997). New cars-new materials. *Material & design*, 18, Nos4/6, pp 203-209.

Jacob G. C., Fellers J. F., Simunovic S. and Starbuck J. M. (2002). Energy absorption in polymer composites for automotive crashworthiness. *Composite material*, 367-813.
https://doi.org/10.1177/0021998302036007164

Jones N., and Wierzbicki T. (1993). *Structural Crashworthiness and Failure*, Taylor& Francis Group, London and New York, 191.
ISBN: 1-85166-969-8

John A., and Nidhi M. B. (2014). Modelling and analysis of an automotive bumper used for a low passenger vehicle. *International journal of engineering trends and technology*, 15(7).
https://doi.org/10.14445/22315381/IJETT-V15P267

Kim J. S., Yoon H. J. and Shin K. B. (2010). A study on crushing behaviours of composite circular tubes with different reinforcing fibres.

Khalid K. S. and Qrimli H. A. (2016). Examine bi-metallic rectangular thin walled tube under different trigger mechanisms, *Advanced Materials Science*, 1(1), 4-8.
HTTP://doi.org/10.15761/AMS.1000102

Kindervater C. and Deletombe E. (2000). Composite helicopter structural crashworthiness: progress in Design and crash simulation Approaches.

Kecman D. (1983). Bending collapse of rectangular and Square section Tubes, *International journal of mechanical sciences*. 25(9-10), 623-636.
https://doi.org/10.1016/0020-7403(83)90072-3

Kim B. S. and Lee W. J. (2017). Analysis of crash impact of composites stay-shaped bumper using FEM method. *International journal of computing, communications instrumentation engineering (IJCCIE)*, 4(2).
ISSN: 2349-1469, EISSN: 2349-1477

Kim H. S. (2002). New extruded multi-cell aluminium profile for maximum crash energy absorption and weight efficiency, *Thin-walled structures*, 40(4), 311-327.
https://doi.org/10.1016/S0263-8231(01)00069-6

Karam s. Khalid, Haidar AI-Qrimli. (2016). Examine bi-metallic rectangular thin-walled tube under different trigger mechanisms. *Advanced material and science*, Vol: 1(1), pp: 4-8.

Koricho E. G., Belingardi G., Tekalign A. and Martorana B. (2014). 'Crashworthiness of integrated crash-box and bumper beam made by die-forming composite,' *ECCM 16-16th European conference on composite materials*, Seville, Spain, 22-26 June.

Karnhari V. M. and Chao L. X. (2003). Energy-absorbing characteristics of circular frusta, *International journal of crashworthiness*, 8(5), 471-479.
https://doi.org/10.1533/cras/8/5/471/19266

Karagiozova D. and Johns N. (2004). Dynamic buckling of elastic-plastic square tubes under axial impact- II: structural response, *International journal of impact engineering*, 30(2), 167-192.
https://doi.org/10.1016/S0734-743X(03)000620-9

Kumar C. V., Abhilash J., Anjaiah M. and Vemula A. M. (2014). FE analysis on vehicle bumper using different materials and speeds, *International journal of mechanical engineering research*, 4(2), 99-110.
Http://www.rippublication.com

Kohara S. (1994). Texture and formability of aluminium sheets, *Materials science forum*, 157-162, 1629-1634.
https://doi.org/10.4028/www.scoemtofoc.net/MSF.157-162.1629

Kelar A., Roth R. and Clark J. (2001). Automobile bodies: Can aluminium be an economical alternative to steel? *Journal of mechanical*, 53(8), 28-32.

Kwansoo C., Wooram N., Xin Y., Heung N. H. and Myoung-Gyu L. (2017). Practical failure analysis of resistance spot welded advanced high-strength steel sheets. *International journal of plasticity*, 94, 122-147.
https://doi.org/10.1016/j.ijplas.2016.10.010

Kowalski M. and Rozumek D. (2019). Numerical simulation of fatigue crack growth in steel-aluminium transition joint, *AIP conference proceedings*, 2186(1), 170020.
https://doi.org/10.1063/1/5138099

Kowaski M. and Bohm M. (2019). Numerical simulation of residual stress induced by welding of steel-aluminium transition joint, *Proceedings of the 14th International scientific conference: Computer-aided engineering,*
https://doi.org/10.1007/978-3-030-04975-1_40

Lan F. C., Zeng F. B., Zhou Y. J. and Chen J. Q. (2014). Progress on research of mechanical properties of closed-aluminium foams and its applications in automobile crashworthiness. *Journal of mechanical engineering*, 50, 22.
https://doi.org/10.3901/JME.2014.22.097

Langseth M., Hopperstad O. S. and Berstad T. (1999). Crashworthiness of aluminium extrusions: Validation of numerical simulation, the effect of mass ratio and impact velocity, *International journal of impact engineering*, 22(9).
https://doi.org/10.1016/S0734-743X(98)00070-0

Li Y. X., Lin Z. Q., Jiang A. Q. and Chen G. L. (2003). Use of high strength steel sheet for lightweight and crashworthy car body, *Materials and design*, 24(3), 177-182.
https://doi.org/10.1016/S0261-3069(03)00021-9

Liu Z., Lu J. H. and Zhu P. (2016). The lightweight design of the automotive composite bumper system using modified particle swarm optimizer. *Composite structures*, 40, 630-643.
https://doi.org/10.1016/j.compstruct.2015.12.031

Lee C. H. and Lee C. k. (1996). Low-speed impact analysis on aluminium bumper, *Proceedings PAM users conference*, Korea HAMPAM.

Liu Y. C. and Day M. L. (2010). Bending collapse of thin-walled beams with channel cross-section. *International journal of crashworthiness*, 11(3).
https://doi.org/10.1533/ijcr.2005.0408

Liu X. B., Wei Y. H., Wu H.J., Zhang T. and Liu S. L. (2019). Effect of stamping dimensional deviations on residual stresses and deformation of resistance spot welded steel sheets, *Journal of material processing technology*, 272.
https://doi.org/10.1016/j.jmatprotec.2019.04.045

Lyu N. and Saitou K. (2005). Topology optimisation of multicomponent beam structure via decomposition-based assembly synthesis, *Journal of Mechanical Design, Transaction of the ASME*, 127(2), 170-183.
https://doi.org/10.1007/10.1115/1.1814671

Marzbanrad J., Alijianpour M. and Kiasat M. S. (2009). Design and analysis of an automotive bumper beam in low-speed frontal crashes. *Thin-walled structures*, 47, 902-911.

Mao X. H., Wang H. and Deng B. J. (2020). Study of the influence of structural adhesive on the durability of a vehicle body, *Proceedings of China SAE congress 2018*.
https://doi.org/10.1007/978-981-13-9718-9_54

Noh W. R., Koh Y. W., Chung K. S., Song J. H. and Lee M. G. (2018). Influence of dynamic loading on the failure behaviour of spot-welded Automotive steel sheets. *International journal of mechanical sciences*, 144, 407-426.
https://doi.org/10.1016/j.ijmecsci.2018.06.009

Mamalis A. G., Manolakos D., Demosthenous G. and Loannidis M. B. (1997). Experimental determination of splitting in axially collapsed thick-walled fibre-reinforced composite frusta, *thin-walled structures*, 28(3), 279-296.
https://doi.org/10.1016/s0263-8231(97)00047-5

Mamalis A. G., Manolakos D., Loanidis M. B. and Hassiotis G. (2000). Finite element simulation of the axial collapse of thin-wall square frusta, *International journal of crashworthiness*, 6(2), 155-164
https://doi.org/10.1533/cras/2001.0169

Melvin J. W., King A. I. and Alem. N. M. (1985). AATD system technical characteristics, design concepts, and trauma assessment criteria, U.S Department of transportation, *national highway traffic safety administration*, Washington, DC,
https://deepblue.lib.umich.edu/handle/2027.42/1440

Melvin J. W., Baron K. J., Little W. C. Gideon T.W. (1998). Biomechanical analysis of Indy race car crashes, *SAE 1998 transactions-Journal of passenger cars-V107-6*.
https://doi.org/10.4271/983161

Milovanoivc V., Dunic V., Rakic D. M. and Zivkovic M. (2013). Identification cause of cracking on the underframe of a wagon for containers transportation – fatigue strength assessment of wagon welded joints, *Engineering failure analysis*, 31, 118-131.
https://doi.org/10.1016/j.engfailanal.2013.01.039

Technology Review. (2015). Where's the affordable carbon fibre automobile? A test drive of the alfa Romeo 4C reveals what a difference carbon fibre can make in a car, *Climate change, MIT technology Review,*
https://www.technologyreview.com/s/539971/wheres-the-affordable-carbon-fiber-automobile/

Nagel G. M. and Thambiratnam D. P. (2005). Computer simulation and energy absorption of tapered thin-walled rectangular tubes, *Thin-walled structures*, 43, 1225-1242. https://doi.org/10.1016/j.tws.2005.03.008.

NHSTSA. (2000). FE model of body-in-white of four door sedan. *US national highway traffic safety administration*,

Ozer H., Can Y., Guclu H., Karen I. and Yazici M. (2016). Development of lightweight bumper beam and crash box with thermoplastic composite and syntactic foam-based sandwich materials. 8. *Automotive technologies congress 23-24*, Bursa.

Patton R. D., Micael E. and Li F. (2004). Causes of weight reduction effects of material substitution on constant stiffness components. *Think-walled structures*, 42 (4), 613-637. https://doi.org/10.1016/j.tws.2003.08.001

Palmer D. W., Bank L. C. and Gentry T. R. (1998). Progressive tearing failure of pultruded composite box beams: experiment and simulation. *Composites science and technology*, 58, 1353-1359. https://doi.org/10.1016/S0266-3538(98)00005-0

Pilkey W. D. and Pikley D. F. (2008). *Stress concentration factors*. 3rd edition, John wiley&sons, New Jersey. ISBN: 978-0-470-04824-5

Przybylski W. (2012). European enhanced vehicle-safety Committee (EEVC)-the results of 42 years of activity. Motor transport institute, Deputy Director for technology and international cooperation, *Journal of Kones powertrain and transport*, 19, 4.

Rajak D. K., Kumaraswamidhas L. A. K and Das S. (2014). An energy absorption behaviour of foam filled structures. *International conference on advances in manufacturing and materials engineering,* AMME. https://doi.org/10.1016/j.mspro.2014.07.254

Reid S. R. and Reddy T. Y. (1986). Static and dynamic crushing of tapered sheet metal tubes of rectangular cross-section, International journal of mechanical sciences, *International journal of mechanical sciences*, 28(9), 623-637. https://doi.org/10.1016/0020-7403(86)90077-9

Reddy T. Y. and Wall R. J. (1988). Axial compression of foam-filled thin-walled circular tubes, *International journal of impact engineerin*g, 7(2), 151-166. https://doi.org/10.1016/0734-743X(88)90023-1

Roopesh E. S. and Rao L. B. (2015). Design and analysis of an automotive frontal bumper beam for low-speed crashes*, Journal of multidisciplinary engineering science and technology*, 2(5).
ISSN:3159-0040

Rimy M. M. and Faieza A. A. (2010). Simulation of car bumper material using finite element analysis, *Journal of software engineering*, 4(3), 257-264.
Https://doi.org/10.3923/jse.2010.257.264

Shanahan D. F.(1989a). Kinematics of U.S. Army Helicopter crashes 1980-1985, aviation, space and environmental Medicine, 60:112-121.

Shanahan D. F.(1989b). Injury in U.S. Army helicopter crashes October 1979-September 1985, *Journal of trauma*, 29(4), 415-423.

Shanahan D. F. (1993). Basic principles of helicopter crashworthiness, Impact, Tolerance, and protection Division, *USAARL report* No.93-15.

Shanahan D. F. (1991). Black hawk crew seats: A comparison of two designs, Fort Rucker, AL: *U. S. Army aeromedical research laboratory*, LR, 92-1-4-1.
Singley G. T. (1981). Aircraft occupant crash-impact protection, *Army Research and development association*, 22(4), 10-12.

Sharpe N., Vendrig R. and Houtzager k. (2001). 'Improved design for frontal protection,' *International technical conference on the enhanced safety of vehicles*, 329

Sha J. B., Yip T. H. and Teo M. H. (2011). FEM modelling of single-core sandwich and 2-core multiplayer beams containing foam aluminium core and metallic face sheets under monolithic bending. *Progress in natural science: Materials international*, 21, 127-138.
https://doi.org/10.1016/S1002-0071(12)60046-X

Stewart R. L., Osterman A. J. and Jalbert A. D. (1991). Chrysler Crop and Shape Crop. Vehicle bumper beam. US5080410A.

Santosa S. P., Wierzbicki T., Hanssen A. G. and Langseth M. (1999). Experimental and Numerical Studies of foam-filled sections. *International Journal of impact engineering*, 24, 509-534.
Https://doi.org/10.1016/S0734-743X(99)00036-6

Sha J. B., Yip T. H. and Teo M. H. (2011). FEM modelling of single-core sandwich and 2-core multiplayer beams containing foam aluminium core and metallic face sheets under monolithic bending. *Progress in natural science: Materials international*, 21, 127-138.
https://doi.org/10.1016/S1002-0071(12)60046-X

Song J., Chen Y. and Lu G.X. (2012). Axial crushing of internally braced Tubes. *School of mechanical and aerospace engineering*, Nanyang Technological University, Singapore.
Stewart R. L., Osterman A. J. and Jalbert A. D. (1991). Chrysler Corp. Vehicle and bumper beam combination, US5080412A.

Saxena A. (2005). Topology design of large-displacement compliant mechanisms with multiple materials and multiple output ports, *Structural and multidisciplinary optimisation*, 30(6), 477-490.
https://doi.org/10.1007/s00158-005-0535-z

Shanley E. R. (1960). *Weight-strength analysis of aircraft structures*, 2nd edition, Dover publications, New York, NY, 13-65

Seitzberger M., Rammerstorfer F. G., Degischer H. P. and Gradinger R. (1997). Crushing of axially compressed steel tubes filled with aluminium foam, *Acta Mechanica*, 125(1-4), 93-105
https://doi.org/10.1007/BF01177301

Sun G. Y., Li G. Y., Hou S. J., Zhou S. W., L W. and Li Q. (2010). Crashworthiness design for functionally graded foam-filled thin-wall structures, *Materials science and engineering*: A, 527(7-8), 1911-1919
https://doi.org/10.1016/j.msea.2009.11.022

Timothy Z. (2016). Chrome Bumpers: *The good old days when bumper was metal*. https://www.carid.com/articles/chrome-bumpers-good-old-days-when-bumpers-were-metal.html

Tehrani P. H. and Nikahd M. (2006). Two materials S-Frame representation for improving crashworthiness and lightening*, Thin-walled structures*, 44, 407-414.

Tounsi R., Haugou G., Chaari F., Leconte N., Markiewicz E. (2019). Experimental characterization of the mechanical behaviour and the failure of multi-sheet and multi-material spot-welded assembly. *International journal of impact engineering*, 130, 226-238. https://doi.org/10.1016/j.ijimpeng.2019.04.017

Wan X. M., Zhi X., Zhao Q. J., Wang G. Y. and Xu X. F. (2013). Concept analysis of automotive aluminium alloy bumper, *Proceedings of the FISTA 2012 world automotive congress*, January. https://doi.org/10.1007/978-3-642-33738-3_13

Wang C.Y., Wang W.W., Zhao W. Z., Wang Y. L. and Zhou G. (2018). Structure design and multi-objective optimization of a novel NPR bumper system, *Composite Engineering Part B*, 153, 78-96. https://doi.org/10.1016/j.compositesb.2018.07.024

Wierzbicki T., Reche L., Abramowicz W., Gholami T. and Huang J. (1994). Stress profiles in thin-walled prismatic columns subjected to crush loading-II. Bending, *Computers & structures*, 51(6), 625-641. https://doi.org/10.1016/S0045-7949(05)80002-1

WHO (World health organisation). (2015). Who's 2015 global status report: Underestimating need for pedestrian safety? Violence and injury prevention in global status report on road safety 2015. https://www.who.int/violence_injury_prevention/road_safety_status/2015/en/

Xiao Z., Fang J. G., Sun G. Y. and Li Q. (2015). Crashworthiness design for a functionally graded foam-filled bumper beam. *Advances in engineering software*, 85, 81-95. https://doi.org/10.1016/j.advengsoft.2015.03.005

Yang Y. X. (2009). The analysis of crashworthiness to car bumper beam system subject to low speed impact, *Harbin engineering university*, China, 150001,

Yu Y. H, Wu X. N. and Lang G. J. (2012). Simulation analysis of automobile collision energy-absorber. *World science and technology research and development*, 34(2), 184-187

Yang R. J., Wang N., Tho C. H. and Bobineau J. P. (2005). Metamodeling development for vehicle frontal impact simulation, *Journal of Mechanical Design, Transactions of the ASME*, 127(5), 1014-1020. https://doi.org/10.1115/1.1906264

Yu J. L., Wang E. H., Li J. R. and Zheng Z. J. (2008). Static and low-Velocity impact behaviour of sandwich beams with closed-cell aluminium-foam core in three-point bending, *International journal of impact Engineering*, 35(8), 885-894. https://doi.org/10.1016/j.ijimpeng.2008.01.006

Yin H. F., Wen G. L., Hou S. J. and Qing Q. X. (2013). Multi-objective crashworthiness optimisation of functionally lateral graded foam-filled tubes, *Materials& Design*, 44, 414-428. https://doi.org/10.1016/j.matdes.2012.08.033

Yin H. F., Wen. G. L., Fang H. B., Qing Q. X., Kong X. K., Xiao J. R. and Liu X. B. (2014). The multiobjective crashworthiness optimisation design of functionally graded foam-filled tapered tube based on dynamic ensemble metamodel, *Material and design*, 55, 747-757. https://doi.org/10.1016/j.matdes.2013.10.054

Yamane K. and Furuhama S. (1998). A study on the effect of the total weight of fuel and fuel tank on the driving performances of cars. *International Journal of Hydrogen Energy*, 23(9), 825-831 https: doi.org/10.1016/s0360-3199(97)00125-0

Zhong W., Ding Y. L., Song Y.S. and Geng F. F. (2019). Relaxation behaviour of residual stress on deck-to-rib welded joints by fatigue loading in an orthotropic bridge deck, *Periodica polytechinica civil engineering*,
https://doi.org/10.3311/PPci.14250

Zhang W. C., Zhu M. L., Wang K. and Xuan F. Z. (2018). Failure mechanisms and design of dissimilar welds of 9% Cr and CrMoV steels up to very high cycle fatigue regime, *International Journal of fatigue*, 113
https://doi.org/10.1016/j.iifatigue.2018.04.032

Zhang Y., Zhu P. and Chen G. L. (2007). The lightweight design of automotive front side rail based on robust optimisation. *Thin-walled structures*, 45(7-8), 670-676.
https://doi.org/10.1016/j.tws.2007.05.007
Zarei H. R. and Kroger M. (2008). Bending behaviour of empty and foam-filled beams: Structural optimization, *International Journal of Impact Engineering*, 35(6), 521-529.
https://doi.org/10.1016/j.ijimpeng.2007.05.003

Z. L. (2019). Finite element analysis of residual stress in welded joints of T91 steel, *IOP conference series materials science and engineering* 637:012013.
https://doi.org/10.1088/1757-899X/637/1/012013

Zeng C., Tian W., Liu X. Y. and Xue Y. T. (2019). Experimental and numerical studies of stress/strain characteristics in riveted aircraft lap joints, *Journal of mechanical science and technology*, 33(1),
https://doi.rog/10.1007/s122206-019-0620-7

This is the end of the thesis